UNIVERSITY OF OKLAHOMA

GRADUATE COLLEGE

# THE DEVELOPMENT OF FERROCENE-MODIFIED LINEAR POLY(ETHYLENIMINE) REDOX POLYMERS AND THEIR APPLICATION IN AMPEROMETRIC GLUCOSE BIOSENSORS AND COMPARTMENT-LESS BIOFUEL CELLS

A DISSERTATION

SUBMITTED TO THE GRADUATE FACULTY

in partial fulfillment of the requirements for the

Degree of

DOCTOR OF PHILOSOPHY

By

MATTHEW MEREDITH
Norman, Oklahoma
2010

Downloaded from SHAREOK. Persistent Handle URL: https://hdl.handle.net/11244/318857

# THE DEVELOPMENT OF FERROCENE-MODIFIED LINEAR POLY(ETHYLENIMINE) REDOX POLYMERS AND THEIR APPLICATION IN AMPEROMETRIC GLUCOSE BIOSENSORS AND COMPARTMENT-LESS BIOFUEL CELLS

A DISSERTATION APPROVED FOR THE
DEPARTMENT OF CHEMISTRY AND BIOCHEMISTRY

BY

_____
Dr. Daniel Glatzhofer

_____
Dr. David Schmidtke

_____
Dr. Robert Cichewicz

_____
Dr. Roger Frech

_____
Dr. Charles Rice

© Copyright by MATTHEW MEREDITH 2010
All Rights Reserved.

**ACKNOWLEDGEMENTS**

I would like to take this opportunity to thank all of the people who have inspired or supported me in this endeavor. First, I want to thank my wonderful wife Shannon, who has always supported my graduate work at OU and kept me focused on the important things in life. I would also like to thank my parents, who have always inspired me to learn, be a better student, and to work hard at whatever I do.

I would like to thank my high school chemistry teacher, Meg Young, who really stimulated my interest in chemistry and provided a solid scientific foundation for me to grow from. Her passion and enthusiasm for teaching chemistry is incredible!

I would like to thank the members of my committee: Dr. Glatzhofer, Dr. Schmidtke, Dr. Cichewicz, Dr. Rice, and Dr. Frech. I especially want to thank my advisor, Dr. Glatzhofer for giving me the opportunity to work on these projects and for letting me unabatedly explore so many different side-projects at the same time. Also, I would like to thank Dr. Schmidtke for all of his valuable advice and collaborative efforts over the past 3 years. I would also like to thank everyone I have worked with in the Glatzhofer, Frech, and Schmidtke labs: Dr. Richard Hu, Dr. Frank Yepez Castillo, Dr. Zhe Jiang, Dr. Rachel Mason, Dr. Gwen Giffin, Rahul Kadam, Sachin Chavan, Farid Ismail, David Hickey, Dr. Steve Merchant, Andrea Tran, and Der-You Kao. I have really enjoyed my time working and learning with you at OU.

**TABLE OF CONTENTS**

List of Tables.....xi

List of Figures.....xii

Abstract.....xvii

**Chapter 1: Introduction and Background**.…….....1

General Introduction to Biosensors and Biofuel Cells…...……..1

In-depth background of Amperometric Biosensors……..3

First Generation Biosensors

Second Generation Biosensors

Third Generation Biosensors

Conclusions

Theory and Background of Enzymatic Biofuel Cells……..12

Introduction

Enzymes Used in Biofuel Cells

Operating Principles

Mediator Choice: Determination of Maximum Operating Voltage

Mediator Choice: How Overpotential Affects Biofuel Cell Performance

Applications of Biofuel Cells

Conclusions

Project Background…….25

Purpose of the Work and Summary of Chapters…….29

References……...…32

**Chapter 2: Electro-oxidative Stability of Aliphatic Amines**……..37

Introduction……...…….37

Experimental……42

Results and Discussion...…….....43

Cyclic Voltammetry and Time-based Constant Potential Amperometry of Monoamines

Cyclic Voltammetry and Time-based Constant Potential Amperometry of Diamines

Constant Potential Amperometry of Tri- and Tetra-amines

Constant Potential Amperometry of Polyamines

Aqueous Electrochemistry of Imidazole Relative to PMEI and LPEI

Conclusions…….69

References……..……..71

**Chapter 3: Effect of Substitution Percentage on the Electrochemical Properties of Ferrocene-Modified Linear Poly(ethylenimine)**……..74

Introduction……74

Results and Discussion……77

Development of the Synthetic Method

NMR Characterization of Fc-$C_1$-LPEI

Solution Electrochemistry of Fc-$C_1$-LPEI and its Model Compound

Cyclic Voltammetry of Cross-linked films of Fc-$C_1$-LPEI(x%)

Effect of Ferrocene Substitution Percentage on Enzymatic Biosensor Performance

Conclusions…….95

Experimental……97

Chemicals and Solutions

Synthesis of Fc-$C_1$-LPEI(x%)

$^1$H-NMR Characterization of the Polymers

Methods

Electrochemical Measurements

References……101

**Chapter 4: Effect of Mediator Spacing on Electrochemical and Enzymatic Response of Ferrocene Redox Polymers**…….....103

Introduction……...103

Results and Discussion……...…….....106

Electrochemistry of Cross-linked Films in PBS

Electrochemical Stability CV Experiments

Film Swelling

Wired GOx Glucose Sensors

Electron Transport in Crosslinked Films of Fc-$C_3$-LPEI and Fc-$C_6$-LPEI

Long Term Stability of Wired GOx Sensors

Conclusions.....122

Experimental.....123

Chemicals and Solutions

Redox Polymer Synthesis

$^1$H NMR Characterization of the Polymers

Enzyme Sensor Construction

Electrochemical Measurements

XPS Measurements

Swelling and Film Thickness Measurements

References.....129

**Chapter 5: High Current Density Ferrocene-Modified Linear Poly(ethylenimine) Bioanodes and their use in Biofuel Cells**.....132

Introduction.....132

Results and Discussion.....135

Effect of Ferrocenyl Moiety Methylation on Redox Potential and Electrochemical Stability

Effect of Ferrocenyl Moiety Methylation on Electron Transport

Anodic Response to Glucose

Cathode Development

Glucose/$O_2$ Biofuel Cell

Conclusions.....157

Experimental.....160

Chemicals and Solutions

Notes on Synthesis and NMR Characterization

Redox Polymer Synthesis

Enzyme Electrode Construction

Electrochemical Measurements

References.....167

**Chapter 6: Synthesis of Tetramethylferrocene-Modified Linear Poly(ethylenimine) and its Use as an Anodic Redox Polymer in Biosensors and Biofuel Cells**.....171

Introduction.....171

Results and Discussion.....174

Synthesis of Tetramethylferrocene

Modification of Tetramethylferrocenes (**1**) with a Three-Carbon Tether

Characteristics of Enzyme Electrodes Made with $FcMe_4$-$C_3$-LPEI

Electron Diffusion in $FcMe_4$-$C_3$-LPEI Films

Glucose Biosensors with $FcMe_4$-$C_3$-LPEI

Ascorbate Interference

Performance of $FcMe_4$-$C_3$-LPEI Anodes in a Biofuel Cell

Biofuel cell with $FcMe_4$-$C_3$-LPEI/GOx Anode and Rotating PVPOs/laccase Cathode

Levich Analysis of the Biofuel Cells

Conclusions.....200

Experimental.....202

Chemicals and Solutions

Notes on Synthesis and NMR Characterization

References.....212

**Chapter 7: Conclusions and Recommendations for Future Work**.....216

Conclusions.....216

Future Studies.....218

**Appendix A: $^{1}$H NMR Spectra**.....222

**LIST OF TABLES**

Table 3.01: Chemical shifts and calculated ferrocene substitution amounts (using equation 1) for each polymer.....99

Table 4.01: Effects of Redox Polymer Type on Biosensor Response.....118

Table 5.01: Effect of Redox Polymer Type on Electrochemical and Biocatalytic Properties.....142

Table 5.02: Summary of Biofuel cells with Stationary or Rotating Biocathodes at 25$^{o}$ and 37$^{o}$ C.....155

Table 6.01: Effect of Redox Polymer Type on Electrochemical and Biocatalytic Properties.....188

Table 6.02: Effect of Ascorbate on Catalytic Current Density.....190

Table 6.03: Summary of Biofuel Cells with Stationary or Rotating Biocathodes at 25 and 37$^{o}$ C.....194

## LIST OF FIGURES

**Figure 1.01:** Schematic of the transduction steps involved in the bioelectrocatalytic oxidation of the substrate in a cross-linked redox polymer-enzyme-coated electrode.....5

**Figure 1.02:** Enzymes (E), mediators (M), and polymer backbone (black line) immobilized on an electrode surface.....7

**Figure 1.03:** Low Potential Redox Polymer with no Tether (from ref. 28).....8

**Figure 1.04:** Low Potential Redox Polymer with long Tether (from ref. 24).....8

**Figure 1.05**: crystal structure of laccase showing type 1 and type 2/3 copper centers (from ref. 64).....15

**Figure 1.06:** Schematic of the processes occurring in a mediated biofuel cell utilizing GOx and laccase.....17

**Figure 1.07:** Schematic of a biofuel cell utilizing an enzyme cascade inspired by the Krebs cycle (from ref. 58).....24

**Figure 1.08:** Structures of BPEI (left) and LPEI (right).....26

**Figure 1.09:** Schematic for constructing a biosensor using Fc-$C_1$-LPEI, ethylene glycol diglycidyl ether (EGDGE), and glucose oxidase (GOx).....28

**Figure 2.01**: Schematic of possible degradation pathways for aliphatic amines after electrochemical oxidation. (from ref. #9).....38

**Figure 2.02:** Cyclic voltammograms of aliphatic monoamines at pH 11 in 0.1 M triflate, 100 mV/s.....44

**Figure 2.03:** Cyclic voltammograms of aliphatic monoamines at pH 1.8 in 0.1M triflic acid, 100 mV/s.....45

**Figure 2.04:** pH vs. current plots for aliphatic monoamines at 1.0 V vs. SCE, 0.1M triflic acid, stirring.....46

**Figure 2.05:** pH vs. current plots for aliphatic monoamines showing the low and intermediate pH regions.....47

**Figure 2.06:** Three possible protonation states of a symmetrical ethylenediamine.....49

**Figure 2.07:** Protonation distribution for N,N'-DMEDA.....50

**Figure 2.08:** Cyclic voltammograms of N,N'-DMEDA in 0.1M triflic acid at various pH values. Scan rate = 100 mV/s.....50

**Figure 2.09:** pH vs. current plots for DEA and N,N'-DMEDA at 1.0 V vs. SCE, 0.1M triflic acid, stirring.....53

**Figure 2.10:** pH vs. current plots for TEA and TMEDA at 1.0 V vs. SCE, 0.1M triflic acid, stirring.....55

**Figure 2.11:** Possible Eschweiler Clarke methylation products of diethylenetriamine.....57

**Figure 2.12:** Structures, names and $pK_a$'s of tri- and tetra-amines used in this study.....58

**Figure 2.13:** pH vs. current plots for tertiary amines at 1.0 V vs. SCE, 0.1M triflic acid, stirring.....58

**Figure 2.14:** Deactivating effects of a single protonation for monoamines, diamines, and triamines.....60

**Figure 2.15:** pH vs. current plots for PMDTA and HMTTA.....61

**Figure 2.16:** Protonation distribution for PMDTA.....61

**Figure 2.17:** Protonation distribution for HMTTA.....61

**Figure 2.18:** pH vs. current plots for PMDTA, HMTTA, and PMEI at 1.0 V vs. SCE, 0.1M triflic acid, with stirring.....63

**Figure 2.19:** pH vs. current plots for the polymeric amines LPEI and PMEI.....64

**Figure 2.20:** pH vs. current plots for LPEI, PMEI, and imidazole at 1.0 V vs. SCE, 0.1M triflic acid, stirring.....67

**Figure 2.21:** Low pH region of Figure 2.19 showing pH vs. current plots for LPEI, PMEI, and imidazole at 1.0 V vs. SCE, 0.1M triflic acid, stirring.....69

**Figure 3.01**: Structure of the polymer Fc-$C_1$-LPEI(x%).....75

**Figure 3.02**: Original synthesis of Fc-$C_1$-LPEI.....77

**Figure 3.03**: Nucleophilic addition method to synthesize Fc-$C_1$-LPEI.....78

**Figure 3.04:** NMR spectra of Fc-$C_1$-LPEI(5%-100%) in $CD_3OD$ (except 100%, which was in $CDCl_3$).....79

**Figure 3.05:** Structure of dimethylaminomethylferrocene, a model compound for Fc-$C_1$-LPEI.....80

**Figure 3.06:** Cyclic voltammograms of 0.01 M DMAMFc in water with added HCl or NaOH. Scan rate = 100 mV/s.....81

**Figure 3.07:** Cyclic voltammetry of 2 mg/mL Fc-$C_1$-LPEI(25%) under acidic and basic conditions with HCl and/or NaOH.....82

**Figure 3.08:** Snapshot of poly-protonated Fc-$C_1$-LPEI showing various phenomena that could affect the solution electrochemistry of the polymer.....83

**Figure 3.09**: Model compounds of Fc-$C_1$-LPEI.....84

**Figure 3.10:** Cyclic voltammetry of 2 mg/mL Fc-$C_1$-LPEI(x%) at pH 2. Scan rate 100 mV/s.....86

**Figure 3.11:** % tertiary amine protonation as calculated from the ratio of $ip_{a(high)}$ to $ip_{a(low)}$.....86

**Figure 3.12:** Percent tertiary amine protonation, as estimated from cyclic voltammetry (closed squares) and DMA/TMA model system calculations.....88

**Figure 3.13:** Cyclic voltammetry of Fc-$C_1$-LPEI(30%) crosslinked with EGDGE on a 3 mm GC electrode in PBS buffer.....90

**Figure 3.14:** Cyclic voltammetry of Fc-$C_1$-LPEI(x%) crosslinked with EGDGE on a 3 mm GC electrode in PBS buffer.....91

**Figure 3.15:** Calibration curve for Fc-$C_1$-LPEI(20%). PBS, pH 7.4, 25$^o$ C, stirring, E = 0.4 V vs. SCE.....93

**Figure 3.16:** Plot of $j_{max}$ vs. substitution percentage for Fc-$C_1$-LPEI(x%) in PBS buffer, pH 7.4, 25$^o$ C, stirring.....94

**Figure 4.01:** Summary of synthetic routes and structures of Fc-$C_1$-LPEI, Fc-$C_3$-LPEI, and Fc-$C_6$-LPEI redox polymers.....105

**Figure 4.02:** Cyclic voltammograms of crosslinked Fc-$C_1$-LPEI films in PBS at (A) pH 3, (B) pH 7, and (C) pH 11.....107

**Figure 4.03:** Cyclic voltammograms of crosslinked films of Fc-$C_3$-LPEI (A) and Fc-$C_6$-LPEI (B) in PBS as a function of pH.....108

**Figure 4.04.** Effect of electrochemical cycling on phosphate incorporation.....111

**Figure 4.05:** Plot of the changes in the area of integrated voltammetric waves for cross-linked films of Fc-$C_1$-LPEI, Fc-$C_3$-LPEI, Fc-$C_6$-LPEI.....112

**Figure 4.06:** Dry film thickness profiles. Profilometry traces for cross-linked films of Fc-$C_1$-LPEI, Fc-$C_3$-LPEI, and Fc-$C_6$-LPEI.....114

**Figure 4.07:** Effect of polymer type on film swelling.....114

**Figure 4.08:** Biocatalytic Response of Redox Polymer-Enzyme Modified Electrodes to Glucose.....116

**Figure 4.09:** Glucose calibration curves of electrodes modified with crosslinked films of Fc-$C_1$-LPEI, Fc-$C_3$-LPEI and Fc-$C_6$-LPEI containing glucose oxidase.....117

**Figure 4.10:** Effect of tether length on electron transport.....119

**Figure 4.11**: Effect of tether length on the operational enzymatic stability of glucose biosensors.....121

**Figure 5.01:** Structures of Polymers Discussed or Used in this Study.....133

**Figure 5.02:** Electrochemistry of Anodic Redox Polymers.....136

**Figure 5.03:** Electrochemical Stability of Cathodic and Anodic Films.....137

**Figure 5.04:** Steady-State Enzymatic Response to Glucose.....141

**Figure 5.05:** Effect of Methylation on Stability of Steady-State Response to Glucose.....142

**Figure 5.06:** Polarization (A) and Power Density (B) curves for biofuel cell constructed with $FcMe_2$-$C_3$-LPEI and an E-TEK GDE.....143

**Figure 5.07:** Biofuel Cell With PVPOs/BOD Cathode. Polarization (A) and Power Density (B) curves for a $FcMe_2$-$C_3$-LPEI/GOx anode coupled with a PVPOs/BOD cathode.....146

**Figure 5.08**: Effect of laccase weight percent on biocathode current output.....148

**Figure 5.09:** pH Analysis of Anode and Cathode. Steady-state measurements of current density for a $FcMe_2$-$C_3$-LPEI/GOx anode and PVPOs/laccase cathode at different pH values.....150

**Figure 5.10:** Polarization of the Fc-$C_3$-LPEI anode, $FcMe_2$-$C_3$-LPEI anode, and PVPOs/laccase cathode.....151

**Figure 5.11:** Effect of Temperature and Polymer Type on Biofuel Cell Performance.....153

**Figure 5.12:** Biofuel Cell Performance with RDE cathodes.....154

**Figure 5.13:** Biofuel Cell Stability.....156

**Figure 6.01:** Outline of possible synthetic routes to di-substituted dimethylferrocene products.....175

**Figure 6.02**: Reaction Sequences to Synthesize Tetramethylferrocene.....177

**Figure 6.03:** Reaction Scheme for Failed Acylation/Reductive Deoxygenation of **1**.....178

**Figure 6.04:** Synthetic Route for Attachment of Three-carbon Tether to **1**.....180

**Figure 6.05**: Cyclic Voltammetry of $FcMe_4$-$C_3$-LPEI/GOx Films.....183

**Figure 6.06:** Cyclic Voltammetry of $FcMe_4$-$C_3$-LPEI/GOx Films.....184

**Figure 6.07:** Electrochemical Stability of Anodic Films.....185

**Figure 6.08:** Calibration curves for $FcMe_4$-$C_3$-LPEI under different curing pH conditions and at 37$^o$ C.....189

**Figure 6.09:** Polarization Curves of the Electrodes.....192

**Figure 6.10:** Effect of Temperature and Polymer Type on Biofuel Cell Performance.....193

**Figure 6.11:** Biofuel Cell Performance with RDE cathodes.....195

**Figure 6.12:** Effect of Rotation Rate on $FcMe_2$-$C_3$-LPEI Biofuel Cell Performance.....198

**Figure 6.13:** Effect of Rotation Rate on $FcMe_4$-$C_3$-LPEI Biofuel Cell Performance.....199

**ABSTRACT**

A series of redox polymers was synthesized by attaching various ferrocene derivatives to linear poly(ethylenimine) (LPEI). These polymers displayed a remarkable ability to shuttle electrons from the active site of the enzyme glucose oxidase (GOx) to the surface of an electrode.

The first type of polymer which was studied consisted of LPEI modified with a ferrocenylmethyl group (Fc-$C_1$-LPEI). A new, versatile method was developed for the synthesis of this polymer at any substitution percentage (between 1% and 100%). The electrochemistry of these polymers in solution was unique and they displayed a double-wave behavior under acidic conditions which could be used to estimate the degree of protonation on the polymer backbone. As biosensors, it was found that polymers with 20% substitution performed the best, but that between 10% and 25%, the performance did not vary much.

Because the polymer designated as Fc-$C_1$-LPEI was believed to be unstable under physiological conditions due to its proximity to the LPEI backbone, polymers with different spacer lengths between the ferrocene and the polymer backbone were synthesized (Fc-$C_6$-LPEI and Fc-$C_3$-LPEI). Increasing the distance between the ferrocene and the backbone was shown to increase the lifetime of biosensors made with Fc-$C_6$-LPEI and Fc-$C_3$-LPEI 10-fold over that of Fc-$C_1$-LPEI. Sensors made with Fc-$C_6$-LPEI had lower maximum current densities than those made with Fc-$C_3$-LPEI, and it was determined that three carbons was the optimal spacer length for these redox polymers.

Once the optimal spacer length was determined, a new polymer, $FcMe_2$-$C_3$-LPEI was synthesized using dimethylferrocene instead of ferrocene. It was shown that the added methyl groups on the ferrocene resulted in biosensors with increased electrochemical and operational stability. This polymer (along with Fc-$C_3$-LPEI) was shown to produce current densities of ~ 2 mA/cm$^2$ at 37$^o$ C, which made it an attractive candidate for use in a biofuel cell. Biofuel cells using Fc-$C_3$-LPEI and $FcMe_2$-$C_3$-LPEI as anodic mediators were constructed and produced power densities of up to 56 μW/cm$^2$ in a stationary mode and 146 μW/cm$^2$ when a rotating biocathode was used. $FcMe_2$-$C_3$-LPEI was shown to be a superior bioanode material for biofuel cells due to its lower redox potential and higher stability.

In order to increase the biofuel cell power density further (as well as make a more effective glucose biosensor), tetramethylferrocene-modified LPEI ($FcMe_4$-$C_3$-LPEI) was synthesized in order to create a redox polymer with more stability and a lower redox potential. The desired effect of lowering the redox potential was achieved, and stationary biofuel cells using $FcMe_4$-$C_3$-LPEI produced power densities of up to 70 μW/cm$^2$. However, when a rotating cathode was used, the performance of biofuel cells using $FcMe_4$-$C_3$-LPEI was not significantly better than that of biofuel cells using $FcMe_2$-$C_3$-LPEI. This was due to the lower limiting current densities produced by the $FcMe_4$-$C_3$-LPEI bioanodes.

# CHAPTER 1: INTRODUCTION

*General Introduction to Biosensors and Biofuel Cells*

According to the International Union of Pure and Applied Chemistry (IUPAC), a biosensor is "a device that uses specific biochemical reactions mediated by isolated enzymes, immunosystems, tissues, organelles or whole cells to detect chemical compounds usually by electrical, thermal or optical signals.[1"] The applications of biosensors are wide-ranging and have found a place in medicine, industry, the military and environmental regulation. Because of the large variety of sectors where biosensor technology can be used, there has been a large demand for the development of new and improved biosensing systems which are able to detect targeted, specific analytes in different environments. These new materials should be robust and should exhibit high sensitivity, selectivity and signal output when their targeted substrate comes into contact with the biosensor.

More specifically, it is estimated that 85% of the overall biosensor market is focused on the development of glucose biosensors.[2] Glucose biosensors are extremely important because of their use in the monitoring of blood-glucose concentration in diabetic patients. The CDC estimated that as of 2008, 24 million Americans, or 8.0% of the population, had diabetes.[3] Another 57 million were estimated to have "pre-diabetes," or at high risk for developing the disease.[3] An important part of regulating and controlling this disease is through careful monitoring of blood-glucose levels, and one important goal of glucose biosensor research is to develop an inexpensive, permanent, non-toxic, highly accurate, and minimally invasive implantable glucose

biosensor that can detect blood-glucose concentrations in real time. This way, a biosensor could be coupled to an insulin pump to instantaneously provide insulin whenever blood-glucose levels dip too low. While many advances have been made in this field in the past, improvements must be made in each category listed above.

Also, the development of fuel cells that can run off of biological and renewable fuels has gained much attention as of late. While conventional $H_2$ and direct methanol fuel cells have garnered much attention with respect to "green" energy production, biofuel cell development - which is still in its infancy – will play an important role in "green" energy production as well. The allure of biofuel cells is that they typically use fuels, such as sugar, which are cheap and easy to handle. They also use renewable catalysts in the form of microbes or enzymes. This sets them apart from the expensive and non-renewable precious metal catalysts of conventional fuel cells. The power that is generated from these biofuel cells normally ranges in the 10's of μWatts to the 100's of μWatts, and will never be enough to solve the world's energy problems. However, biofuel cells could have some useful applications including power sources for portable electronic devices, clean power sources during space travel, and implantable power sources that could greatly simplify many medical devices. Because of the potential of their many applications and the mild conditions under which they operate, the drive to create new and better materials for use in biofuel cells is constantly increasing.

**In-depth background of Amperometric Biosensors**

*First Generation Biosensors*

The demand for a way to detect glucose in human blood samples has existed as long as diabetes has been a known condition. Early in the investigation of these techniques, chemical reaction-based methods to detect glucose were the primary choice of scientists. However, Benedicts test, Fehlings test, along with others that utilize the general reducing properties of glucose were inconsistent[4] and better methods were necessary. In 1962, Clark and Lyons developed the first glucose sensing device based on the oxidation of glucose by the enzyme glucose oxidase.[5] Glucose oxidase (GOx) falls into a class of oxidoreductases, which are enzymes that, in broad terms, catalyze the transfer of electrons from one molecule to another. More specifically, in its natural setting GOx removes two electrons from glucose (oxidizing) and uses those electrons to reduce oxygen to hydrogen peroxide. It performs these reactions with the aid of a cofactor, flavin adenine dinucleotide (FAD), which is a common part of many biological redox reactions. Clark and Lyons were able to take advantage of the specificity of GOx for glucose and used Clark's oxygen electrode to amperometrically determine the amount of molecular oxygen that was consumed in the following reaction:

$$\text{glucose} + O_2 \xrightarrow{\text{glusoce oxidase}} \text{gluconic acid} + H_2O_2$$

Depending on how much glucose was in the test solution, a certain amount of oxygen would be consumed, thereby decreasing the concentration of oxygen in the sample and

lowering the current. This development led to many other advances which involved measuring the concentration of a specific reactant or product in an enzymatic reaction. A good example of this is the work that has been done that amperometrically detects the hydrogen peroxide produced in reaction 1.[6-8] These types of sensors are known as "1st generation" biosensors. While effective in certain applications, these glucose sensors either depend on the detection of a gas ($O_2$) or are held at high potentials(for the oxidation of $H_2O_2$)[2, 8, 9] (ex: 0.6 V vs. Ag/AgCl to detect $H_2O_2$). Oxygen-based biosensors are easily compromised by fluctuating $O_2$ levels and $H_2O_2$ sensors can give inaccurate readings due to interferences which are oxidized at 0.6 V (ascorbic acid, uric acid, and acetaminophen). Some of these interfering molecules can be prevented from reaching the electrode by electropolymerizing a conducting polymer around glucose oxidase[10, 11] or using membranes[12] to keep interfering molecules away from the electrode, but further improvements were still needed to make a simple, effective biosensor. To know what those improvements should be, one must examine the important properties of an effective electrochemical glucose biosensor. They are: high current response to glucose, high sensitivity (to detect small changes in glucose concentration), low operating potential (to minimize power consumption and interferants such as ascorbate and acetaminophen), high stability, biocompatibility, and reproducibility.

*Second Generation of Biosensors*

The "second generation" of biosensors attempts to satisfy all of the requirements of an effective biosensor by using mediators which allow the enzyme to communicate

with an electrode. This way, instead of monitoring the production or consumption of a specific substance (i.e. oxygen or $H_2O_2$), some or all of the electrons collected by glucose oxidase can be transferred to an electrode and detected as current. Mediators in general should have low oxidation potentials in order to lower the working potential of the sensor, minimize overpotential, and minimize interfering species. Mediators used in second generation biosensors are normally conjugated polymers (discussed later), redox polymers, or small organic/organometallic molecules which can have multiple oxidation states. Some of the first mediators developed for second generation biosensors were hexacyanoferrate, benzoquinone, methylene blue, and ferrocene derivatives.[13, 14] Sensors made with these early mediators actually depended on the diffusion of the mediator (which was dissolved in solution) to the electrode where glucose oxidase was immobilized.[13] While these sensors could alleviate the problem of high-potential hydrogen peroxide detection, dissolved oxygen still competed with the mediators as the electron acceptor from glucose oxidase.[2]

In 1989, Heller's group at the University of Texas introduced a new, improved form of second generation biosensor by trapping the mediator (an osmium organometallic complex) and enzyme together on top of an electrode inside of a cross-linked redox polymer hydrogel.[15] This effectively "wired" the enzyme to the electrode and introduced a whole new methodology for biosensors.[16] A schematic of the proposed steps in redox polymer "wired" electron transfer is shown in Figure 1.01.[17] While there are five potentially rate-limiting steps in the complete mediated electron transfer cycle, steps 3 or 4 are normally considered to be rate-determining.[18-20]

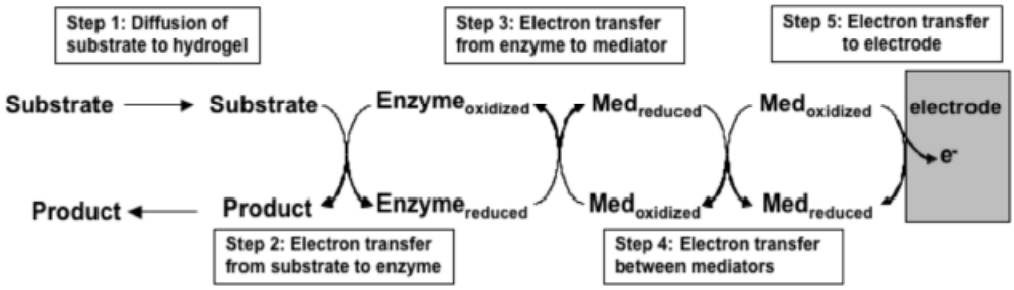


**Figure 1.01:** Schematic of the transduction steps involved in the bioelectrocatalytic oxidation of the substrate in a cross-linked redox polymer-enzyme-coated electrode. (Figure from ref. 13)

In step 3, electron transfer from the enzyme to the mediator has been shown to be improved when an electrostatic complex is formed between the polymer and the enzyme.[18, 21] For example, an enzyme like glucose oxidase has an overall negative charge[22] so a highly protonated or quaternized polyamine should easily form a charged complex with the enzyme. If redox mediators are attached to the polymer, this brings them closer to the enzyme active site than if they were attached to a neutral polymer. Step 4 depends on the rate of charge transport within the polymer film. The rate of this charge propagation can depend on the electrical conductivity of the film, the frequency/ease of collisions between oxidized and reduced mediators, self exchange of electrons between identical redox centers, or ion movement.[23]

After the first report on redox polymers, the majority of glucose biosensors that have been developed use some form of enzyme/mediator immobilization technique on the surface of an electrode. The redox polymer hydrogel "wiring" method is attractive for several reasons: redox polymer hydrogels are permeable to water, glucose, gluconolactone, water-soluble ions, and many other potential analytes, while also being electronically conducting. This makes them very unique in the field of chemistry as one of the only materials to have both of those properties. Also, because all of the

components of the sensor are trapped on the electrode, leaching of mediators or enzymes is not an issue. Finally, because the hydrogels are wrapped around the enzymes, the spatial orientation of the enzymes is not an issue and enzymes near to and far away from the electrode surface can be utilized. A simplified version of what these hydrogels look like when coated on top of an electrode is presented in Figure 1.02.

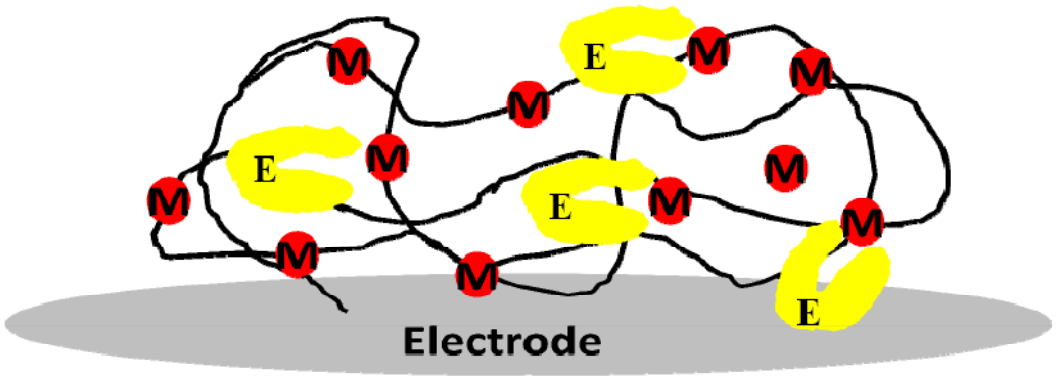


**Figure 1.02:** Enzymes (E), mediators (M), and polymer backbone (black line) immobilized on an electrode surface

The many favorable properties that resulted from entrapping enzymes within redox polymer hydrogels has lead to the development of biosensors with current densities on smooth electrodes that exceed 1 mA/cm$^2$.[17, 24]

Throughout the past 20 years, much progress has been made in this area of biosensor technology by Heller's group and by others.[2, 9] This technology has even made it into the glucose-monitoring marketplace in the form of blood glucose testing strips and continuous glucose monitoring system.[9, 25] Because the main types of biosensors that will be discussed in this work are based on redox polymer hydrogels, they will be discussed in more depth and the general progression of advances in the area will be shown. The original redox polymers created by Heller's group involved an osmium-based redox mediator directly attached to a polymer.[26, 27] Synthetically, direct

polymer backbone attachment was the easiest way to attach an osmium center to a polymer backbone, and the films were very effective at measuring glucose concentrations. One of the benefits of using osmium is that the redox potential of the metal can be tuned by attaching different ligands to it. Using this property, major improvements in lowering the redox potential of the polymers were made by modifying these ligands, as shown in Figure 1.03.[28]

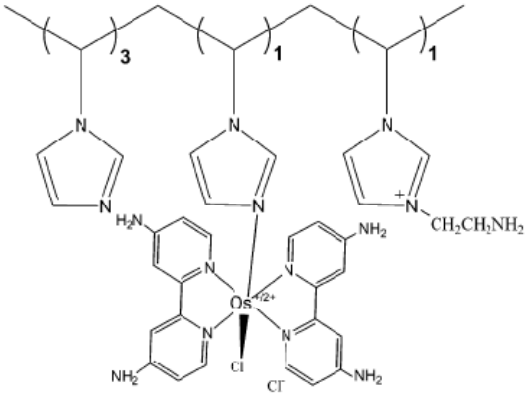

**Figure 1.03:** Low Potential Redox Polymer with no Tether (from ref. 28)

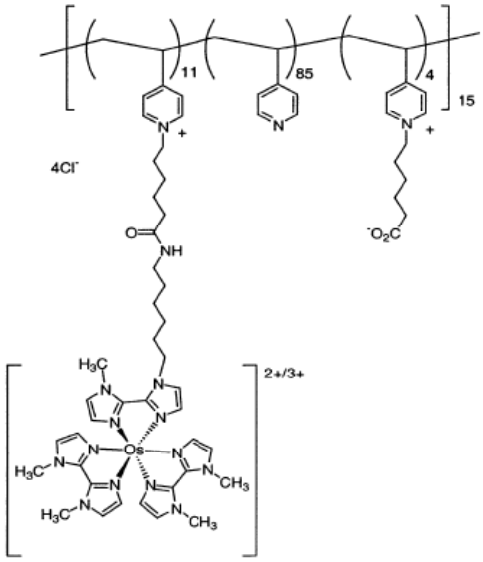

**Figure 1.04:** Low Potential Redox Polymer with long Tether (from ref. 24)

More electron-donating ligands led to very low redox potentials (-0.160 V vs. Ag/AgCl for Figure 1.03). This allowed the sensor to operate at a potential that would not interfere with any other blood-borne components. Also, improvements in electron diffusion and current response were made by Heller's group when the redox center was moved further away from the polymer backbone.[24] This type of polymer (Figure 1.04), which has a 13-atom tether between the osmium and the pyridine backbone, is one of the primary benchmarks for redox polymer hydrogel biosensors. At 37$^{o}$ C under physiological conditions, adding the spacer between the polymer backbone and the

redox center increased the maximum current density ($j_{max}$) from 150 uA/cm$^2$ to 1100 uA/cm$^2$ and increased the electron diffusion coefficient ($D_{app}$) 1700 fold.[24] Sensors made with this polymer constitute the best overall performance obtained with a mediated redox polymer hydrogel. According to Heller, the increases in $D_{app}$, and $j_{max}$, were due to an increase in the segmental mobility of the tethered redox center with respect to a non-tethered center. When the gel swells up in water, the increased range of motion makes it easier for redox centers to collide and undergo electron hopping. The idea that longer tethers to redox centers lead to better electron diffusion and performance in redox hydrogels is a generally accepted theory in the literature.

This constitutes a brief summation of the advances in second generation biosensors based on redox polymer hydrogels. Progress continues to be made in this area and a lot of the focus has shifted towards improving biosensor performance by incorporating other "enhancers" like nanowires, carbon nanotubes and other nanomaterials.[7, 29-33]

Conjugated polymers comprise another well-studied system that has been developed for second generation biosensors.[34] The most popular conjugated polymers that have been used for biosensor applications are polypyrrole,[35-37] polythiophene,[38, 39] and polyaniline.[32] These sensors provide an alternative to the redox polymer sensors in that the electrons actually conduct through the polymer backbone instead of hopping from one redox center to another. Conjugated polymer films typically have high electron diffusion coefficients and higher conductivities than redox polymer hydrogels, indicating that electron conduction should be fast once transfer from the enzyme occurs. However, they have quite a few disadvantages when compared to redox polymer

hydrogels. Although electrostatic enzyme complexation with cationic polypyrrole has been suggested due to enzyme incorporation during electropolymerization,[40, 41] sensors made with conjugated polymers generally suffer from low current densities. This is believed to be due to an inefficient transfer of electrons from the enzyme to the polymer and is evidenced by $H_2O_2$ production in the sensor.[42] Also, it can be speculated that incorporation of large hydrated enzymes within a conjugated polymer matrix would be expected to lower the conductivity of the films. Finally, because of their high redox potentials, the operating potentials of these sensors are quite high.[36, 41] One interesting method which tries to overcome the enzyme/polymer electron transfer problem is the fabrication of conjugated polymers with redox centers like ferrocene and osmium attached. [35, 43, 44] The idea behind this type of sensor is that glucose oxidase or another enzyme can oxidize the organometallic redox center, and that "hole" can then be transferred from the redox center to the polymer backbone, achieving electron transport that way. Overall, while some favorable results have been achieved with conjugated polymer biosensors, the high current responses seen with "wired" redox hydrogels have not been realized.

*Third Generation Biosensors*

Third generation biosensors are sensors which require no mediator and operate through direct electron transfer between the enzyme and the electrode. The full scope of this generation of biosensors has not been realized yet because of the difficulty of engineering an enzyme to directly communicate with a surface. It is believed that electrons must tunnel from the enzyme active site to an electron acceptor, and the rate

of electron tunneling decays rapidly at distances greater than 3 A.[16] The active site of glucose oxidase is 13 A deep into the enzyme[45] so positioning it on top of an electrode where the distance between the a active site and the electrode surface is 3 A or less is exceedingly difficult. Single walled and multi-walled carbon nanotubes have been used to facilitate DET to an electrode,[46] but this technology is still in its infancy and only time will tell whether it will be a viable option for glucose biosensors or not.

*Conclusions*

Glucose biosensor development has progressed rapidly over the past twenty years. The most progress in the area has been made in the development of second generation glucose biosensors, which have evolved into materials advanced enough to be used in the diabetes management industry. Specifically, mediated glucose biosensors made using redox polymer hydrogels seem to be the most promising area for further development, as they can provide high current response to glucose, high sensitivity to small changes in glucose concentration, low mediator redox potential, high mediator stability, biocompatibility, and reproducibility. These favorable factors have also led to the use of glucose biosensing electrodes as the anodes of biofuel cells. A biofuel cell basically consists of two sensors connected to each other: a glucose sensor on one side, operating at a low potential, and an oxygen sensor on the other side, operating at a high potential. The voltage between these electrodes drives the production of current and produces power. These biofuel cells will be discussed in depth in the following section.

## Theory and Background of enzymatic biofuel cells

*Introduction*

First, a bit of nomenclature clarification: The term "biofuel cell" can refer to a fuel cell which uses either living bacteria or enzymes to generate electricity. For the purposes of this discussion, the term "biofuel cell" will henceforth refer to enzymatic biofuel cells.

The potential for using enzymes to generate power has been known since the 1960's.[47] However, the lack of a need to develop alternative energy sources prevented any extensive investigation into biofuel cell development until recently. Now, as traditional fuel cells are predicted to be part of our energy future, interest in biofuel cells has risen steadily as well. This recent interest stems from some of the intrinsic properties of enzymatic biofuel cells which make them more attractive than traditional fuel cells for certain applications. Biofuel cells typically undergo very mild oxidation/reduction catalysis at room temperature and neutral, physiological pH, whereas traditional fuel cells normally require high temperatures and acidic conditions for optimum performance. Also, because of the use of enzymes in biofuel cells, the cathode and anode materials are much more selective for the required substrates and can perform in the presence of many interfering species, as enzymes are known for their great chemoselectivity. In fact, many biofuel cells that have been constructed do not need any separator between the cathode and anode.[48-50] Conversely, in traditional fuel cells, leaching of fuel from the anode to the cathode can be a problem (as in direct methanol FC's). Fuels crossing over the polymer membrane can come in contact with and react with the cathodic catalyst, lowering fuel cell performance. Lastly, the fuels

required for biofuel cells (sugars) are safer and more easily handled than the fuels for typical fuel cells (hydrogen, methanol). A solution of glucose or another sugar is much less toxic than methanol, and is easier to handle than compressed hydrogen.

Another factor driving the development of biofuel cells has been the development of biosensors which was discussed in the first section. This is due to a large convergence between biofuel cell and biosensor technology. In many aspects, factors which lead to better performance in a biosensor also lead to better performance in a biofuel cell. For example, lowering the redox potential of a mediator in a glucose biosensor consumes less power and allows for less interference during operation, while it also increases the cell voltage in a biofuel cell. Also, optimizing electron transport from enzyme to electrode is still one of the most important factors in each area, as well as stability, cost, and ease of fabrication. Where the two technologies differ is the fact that biosensors consume energy and biofuel cells produce energy. Biosensors operate by applying energy from an external power source, and their goal is to monitor changes in the amounts of a substance while consuming the least amount of power. Conversely, biofuel cells (and fuel cells in general) generate their own power by coupling two redox reactions together in order to generate maximum power.

*Enzymes Used in Biofuel Cells*

Before discussing the inner workings of biofuel cells any further, the choice of enzymes should be discussed. In the previous glucose biosensor discussion, the choice of enzyme was obvious as it needed to be an enzyme that was specific for the oxidation of glucose. In the case of biofuel cells, there are more options because the requirements

of the enzymes are less specific. The enzymes used in an enzymatic biofuel are almost always oxidoreductases, meaning that they catalyze the transfer of electrons from one molecule to another. For the anode side, where oxidation of a fuel occurs, there are many choices of enzymes. Some of the enzymes used for biofuel cell anodes are glucose oxidase,[28, 51-53] glucose dehydrogenase,[54, 55] cellbiose dehydrogenase,[56] and alcohol dehydrogenase.[57] Of these enzymes, glucose oxidase is the most common and most studied, primarily because of its extensive use in glucose biosensors. It has been suggested, however, that because glucose oxidase only partially oxidizes glucose, (removing two electrons) it is an inefficient catalyst for biofuel cells as it leaves a lot of energy tied up in the molecule.[58, 59] To overcome the "waste" of energy problem that glucose oxidase has, systems have been developed to completely oxidize certain fuels like ethanol or pyruvate all the way to $CO_2$.[57-59] These type of enzyme electrodes are efficient in terms of complete fuel oxidation, but may be difficult to optimize due to multiple enzymatic components. Also, glucose oxidase is very specific for the oxidation of glucose and it does not catalyze the oxidation of other sugars with much efficiency. This has lead to the investigation of other enzymes such as cellbiose dehydrogenase,[55, 56] which has the ability to oxidize multiple fuels, thereby making it a more robust enzyme for biofuel cells in terms of the variety of fuels it may oxidize.

The choice of the cathodic enzyme is a little more straightforward. The two enzymes that are commonly used for the enzymatic cathode are bilirubin oxidase (BOD) and laccase. Both of these enzymes fall in the category of "blue" multicopper oxidases, as they use different copper centers to catalyze the reduction of molecular oxygen to water. The three different types of copper in the enzymes are classified as

T1, or blue copper, T2, and T3. A crystal structure of laccase can be seen in Figure 1.05. T1 copper is close to the surface of the enzymes and is coordinated to two histidine residues and the sulfur from a cysteine residue. It is called blue copper because it has an absorption band at about 600 nm which arises from a charge transfer between the cysteine sulfur atom and the copper atom.[60] T2 is known as "normal" copper and is typically coordinated by histidine residues.[60] T3 copper is actually a bi-nuclear copper center with a hydroxide bridging ligand between the two copper atoms.[60] The T2 and T3 copper sites form a trinuclear cluster where oxygen is reduced to water. The general mechanism by which these enzymes reduce oxygen is quite complex and will not be covered here in full, but a general mechanism involves the T1 copper site accepting electrons from organic substrates which act as electron donors and passing those electrons on to the T2/T3 tricopper cluster, where $O_2$ is coordinated and reduced by four electrons. The redox potential of the T1 site in the enzyme determines the maximum potential of the enzymatic cathode, and this redox potential differs greatly depending on the source of the enzyme (different fungi and bacteria).[61] The enzymes differ slightly in their properties: Laccase is more thoroughly studied and has a higher redox potential than BOD.[61, 62] It is also possible to purify laccase to a higher activity than BOD, meaning that in theory, laccase in its purest form

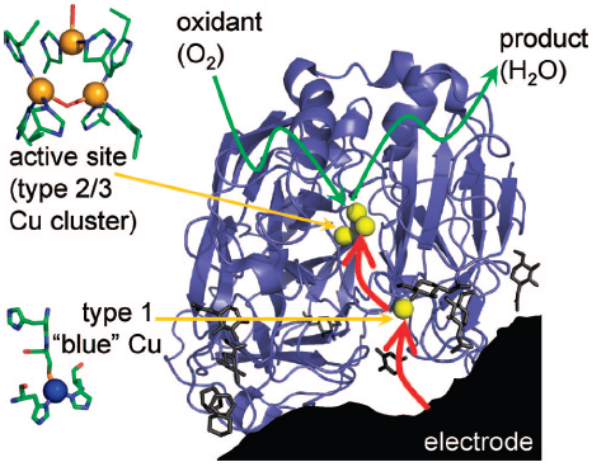


**Figure 1.05**: crystal structure of laccase showing type 1 and type 2/3 copper centers (from ref. 64)

can perform more effectively than BOD in its purest form. Laccase, however, reacts optimally at pH 5 and can be inhibited by halide ions, especially F- and Cl-.[63] BOD, on the other hand, operates optimally at pH 7 and is not inhibited by halide ions, which makes it more promising for implantable biofuel cells.[62, 64] Both enzymes have been used in biofuel cells, and the choice between the two depends on the mediators being used and the exact conditions and goals of the experiments being performed.

*Operating principles*

An enzymatic biofuel cell operates on the same principles as any traditional fuel cell: A fuel (hydrogen, methanol, glucose, etc.) comes in contact with a catalyst, where it is oxidized. The electrons from this oxidation travel through a circuit and are available to do electrical work. The electrons then travel to the cathode, where they can recombine with the oxidized fuel from the first step. In almost all cases, the cathode of a fuel cell takes electrons from the anode and uses them to form water from oxygen (in the air or in solution) and protons. The high redox potential of this reaction (1.23 V vs. NHE, catalyzed on platinum) drives the overall generation of current. In a hydrogen fuel cell, the important reactions can be seen below:

| **Anode** | **Cathode** |
|---|---|
| $H_2 \rightarrow 2H^+ + 2e^-$ (E = 0 vs. NHE) | $4H^+ + 4e^- + O_2 \rightarrow 2H_2O$ (E = 1.23 V vs. NHE) |

**Scheme 1.01:** Redox reactions that take place in a $H_2/O_2$ fuel cell

A biofuel cell usually diverges from these reactions at the anodic side and in the catalysts used at each electrode. For the bioanode, a common example of the process that takes place is the oxidation of glucose using glucose oxidase as the catalyst:

glucose + GOx → gluconolactone + $2H^+$ + 2e- (E = -0.12 V vs. NHE)[65]

For the biocathode, although the overall reaction does not change for an enzymatic biofuel cell, the catalyst which reduces oxygen to water can be much different. A typical fuel cell would use platinum for this process, whereas a biofuel cell frequently uses one of the two "blue multi-copper oxidase" enzymes: laccase or bilirubin oxidase. Biofuel cells can be constructed to utilize electron mediators or direct electron transfer (DET), just like biosensors. A mediated biofuel cell using glucose oxidase at the anode and laccase at the cathode can be seen in Figure 1.06 .

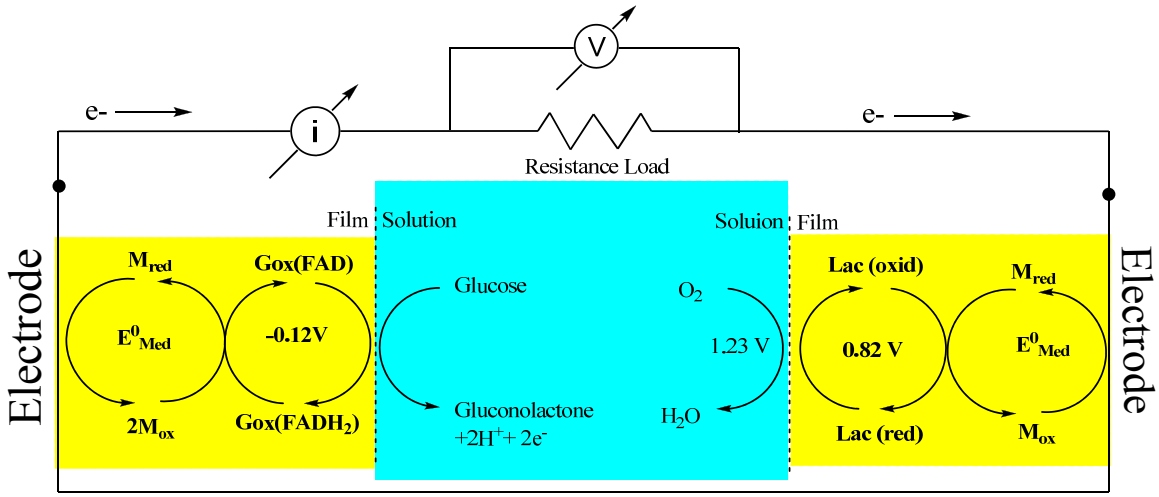


**Figure 1.06:** Schematic of the processes occurring in a mediated biofuel cell utilizing GOx and laccase

The anode of the biofuel cell in Figure 1.06 is essentially the same as a glucose biosensor – the only difference being that the current travels to another enzymatic electrode instead of a potentiostat. Starting from the glucose in solution, the sequence of steps that lead to the generation of electricity is as follows: **1**. Glucose diffuses into the film from the solution phase and comes in contact with the active site of glucose oxidase, which oxidizes the glucose into gluconolactone. **2**. The electrons removed

from glucose are passed from the active site in GOx to oxidized mediators, which reduce the enzyme. **3**. The reduced form of the mediator comes close enough to an oxidized mediator to pass an electron to it, and this cascade continues until the electron reaches the electrode. **4**. The electron travels through the circuit to the surface of the cathode, where it reduces a different mediator which is immobilized in the cathodic film. **5**. This starts a cascade of electron transfers to oxidized mediators on the cathode until a reduced mediator is oxidized by the cathodic enzyme. **6**. Once the cathodic enzyme (laccase in this case) is in its reduced state, it uses the electrons to reduce oxygen to water, completing the cycle.

Apart from the aspects of enzymatic biofuel cell development which overlap with biosensor development, (i.e. efficient enzyme/mediator communication, fast electron transfer, highly hydrated films), three major factors must be considered when designing a mediated biofuel cell, and those factors are: difference in redox potential between anode mediator and cathode mediator, difference in the potentials of the redox mediators and the enzymes, and stability of the enzyme/mediators for long-term use.

*Mediator Choice: Determination of Maximum Operating Voltage*

In a conventional hydrogen fuel cell, the maximum operating voltage is the difference between the two redox reactions at each electrode. In the case of a hydrogen/oxygen fuel cell, that difference comes out to 1.23 V as seen from the redox potentials in Scheme 1.01. However, voltages this high during fuel cell operation are rarely seen due to activation loss, ohmic loss, and mass transport loss.[66] In a mediated biofuel cell, determining the maximum operating voltage it is slightly more

complicated, but the principle is the same. By definition, the anode and cathode of a mediated biofuel cell have more than one redox reaction occurring at each electrode due to the enzyme and the mediators each having their own redox potentials. While the enzymes are the driving force behind each electrode reaction, the mediators greatly outnumber them and are responsible for passing electrons directly to the electrode. This means that the mediators actually control the overall electrode potential and that the maximum voltage at peak current depends mostly on the difference in redox potential of the mediators at each electrode.[67] This puts mediated biofuel cells at a slight disadvantage in that there is an inherent "activation loss" any time mediators are coupled with an enzyme. The true potentials of the enzymes used cannot be completely harnessed and is one reason direct electron transfer biofuel cells are being studied as an alternative.[46, 68, 69] Because of the factors discussed above, the optimization of cathodic and anodic mediators is very important in maximizing fuel cell power output.

*Mediator Choice: How Overpotential Affects Biofuel Cell Performance*

Based on the discussion above, one might speculate that biofuel cell mediators with potentials identical to the different enzymes should be chosen to maximize cell voltage and minimize the activation loss. However, another important factor must be considered when choosing a mediator: overpotential. In general electrochemistry terms, overpotential is the excess voltage that must be applied to a half-cell in order to actually observe the redox event and produce current. For example, while the $O_2/H_2O$ half cell has a thermodynamic potential of 1.23 V vs. NHE, in order to reduce oxygen, a voltage more reducing than 1.23 V must be applied in order to drive the reaction forward and

produce a steady-state current.[49] For a fuel cell catalyst, large overpotentials lead to large voltage losses, so materials which require a small overpotential are desirable. When applying this concept to mediated biofuel cells, the difference between the redox potential of the enzymes and their respective mediators is called mediator/enzyme overpotential. It is useful to find the smallest necessary overpotential between a mediator and an enzyme in order to maximize biofuel cell voltage.

Changing mediator redox potential can greatly affect the efficiency of electron transfer to or from an enzyme. The redox potentials of glucose oxidase and laccase (from *trametes versicolor*). are -0.12 V[65] and 0.82 V[70] vs. NHE, respectively. Based on these values, mediators should be developed for each electrode with potentials as close to the enzymatic redox potentials as possible in order to maximize the biofuel cell voltage. For glucose oxidase, Heller's group has shown that a mediator with a redox potential as low as 0.045 V vs. NHE is extremely effective at mediating electron transfer between glucose oxidase and an electrode.[24] It may be possible to come even closer to the GOx redox potential, but it is likely that going much closer will start to cause a drop in the performance of the electrode due to a lack of thermodynamic driving force for electron transfer between enzyme and mediator. Because of this, mediators should be designed to come as close to 0.045 V vs. NHE in order to maximize the biofuel cell voltage from the anode side. In addition, study by Barton et al. recently examined a series of osmium-based mediators of different potentials and showed that the optimal redox potential for the cathode (using laccase from *tram. vers*.) is 0.66 V vs. NHE, which was 0.16 V less than the T1 copper site in the enzyme.[70] When the redox potential of the mediator was any closer to that of laccase, the potential difference of the

enzyme/mediator couple was too small to effectively drive electron transfer forward, resulting in a decrease in current. When the mediator potential was further from that of laccase, (< 0.66 V) the current output remained high, but the overall maximum fuel cell power decreased because of the lower voltage mediator. This suggests that when developing a cathodic mediator for a laccase electrode, the potential should be as close to 0.66 V vs. NHE as possible. Of course, it remains to be seen if this 0.16 V difference is optimal for all cathodic enzymes, but it is a good starting point for mediator development. From these studies, one can conclude that the maximum operating voltage that can be achieved by an enzymatic biofuel cell is around 0.7 V, although some exceptions to this have been found in cases where electron transfer from enzyme to mediator to electrode is extremely efficient.[49, 71]

*Applications of Biofuel Cells*

For the most part, the possible applications for biofuel cells differ greatly from those of conventional fuel cells due to their different properties and power outputs. There are three major applications that have been envisioned for biofuel cells, the first being implantable power sources. If a biofuel cell is developed that can generate a significant amount of power from sugars in human or animal blood, many small electronic devices could be powered with no external batteries or fuels. Devices that could be powered with implantable biofuel cells include pacemakers, artificial limbs, and hearing aids. From a compatibility standpoint, biofuel cells could be ideal for use in the body because the enzymes utilized in them have evolved to work in complex environments and are very selective as to the fuels that they utilize. However, there are

still major stability issues that will have to be overcome before these goals are realized, as most enzymatic biofuel cells cannot operate continuously for more than a week. Also, glucose oxidase can oxidize a number of other compounds in the body such as ascorbate and urate and the most common cathodic enzyme, laccase, does not work very well at physiological pH or in the presence of chloride ions.[63] Another factor which must be considered for implantable biofuel cells is the physical act of implanting the devices. As with implantable biosensors, this can cause clotting and other immune responses which could render the biofuel cells useless and cause harm to the subject.

The second primary application for biofuel cells is that of alternative, "green," power sources for small electronic devices. A portable electronic device which uses only glucose or another sugar source (ex: fruit juices) and produces water would be preferred over conventional batteries or fuel cells provided that the performance is comparable. The main issue with this application is long-term stability. Not only would the biofuel cell need to have a long room-temperature shelf life, but it would need to provide the necessary power for weeks or months without a large loss in performance. This problem with the biofuel cell enzymes is currently being solved by genetic modification of enzymes and isolating/trapping the enzymes inside of hydrophilic materials such as silica gel, which can limit vibrational motion and thereby prevent (or slow down) the disruption of their three-dimensional structure of the enzymes.[72]

The third application where biofuel cells could be a promising technology is the combination of traditional fuel cells with bio-electrodes. This type of system would involve replacing one electrode of a conventional $H_2$ or DMFC with a bio-electrode.

The resulting "hybrid" biofuel cells would need to compete with traditional fuel cells, and as far as power output or current density, the performance of hybrid biofuel cells has not come close to the performance of traditional fuel cells. Where they can make up for some of their power output shortcomings is in the areas of low temperature, neutral pH operation, chemical selectivity, and manufacturing cost. The benefits of low temperature and neutral pH conditions at which enzymatic electrodes can operate are self explanatory and need no further discussion. The chemical selectivity of enzymatic electrodes can be utilized in hybrid biofuel cells by replacing either the anode or cathode with a bioelectrode. The replacement of a traditional platinum cathode in a direct methanol fuel cell with a chemoselective oxygen-reducing enzyme could be a viable alternative for DMFC's and could help solve the problem of methanol crossover, which lowers the power output and lifetimes of DMFC's. Barton et. al. have shown that biocathodes based on laccase and an osmium redox polymers can operate under concentrations of methanol which would poison a normal platinum-based cathode.[73] The downside to these types of DMFC's is that they require the presence of water at the cathode and gas-phase delivery of oxygen is not very effective. This is currently being investigated.[74] If this problem as well as long-term enzyme stability is improved, these biocathodes could be viable alternatives to precious metal-based DMFC cathodes.

The other alternative in hybrid biofuel cells is to replace the anode with an enzyme electrode and leave the cathode as platinum. This technique allows for the use of green, natural fuels while still utilizing well-characterized platinum as the cathode material.

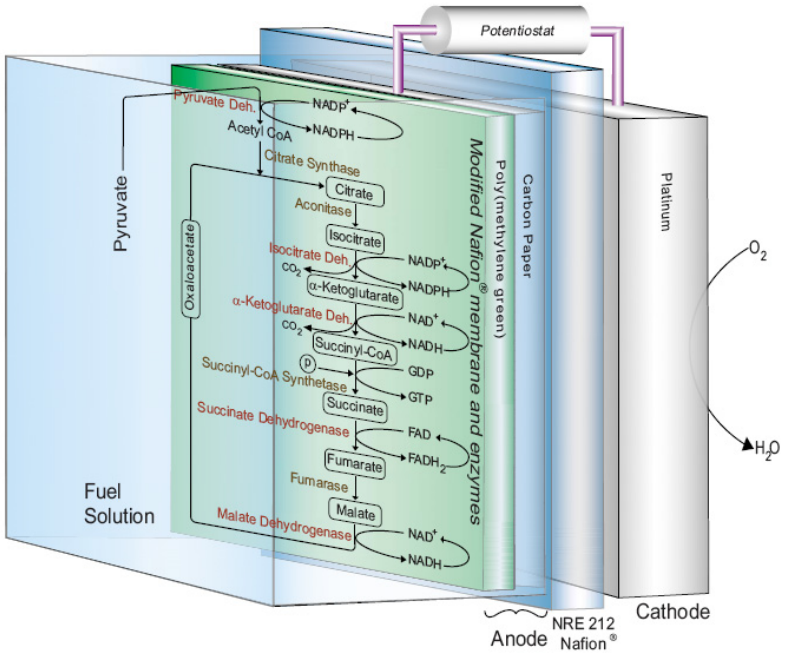


**Figure 1.07:** Schematic of a biofuel cell utilizing an enzyme cascade inspired by the Krebs cycle (from ref. 58 )

Minteer et. al. have developed many different hybrid biofuel cells based on this idea like the one pictured in Figure 1.07 which utilizes a platinum cathode and an immobilized enzyme cascade to oxidize pyruvate all the way to $CO_2$.[58] This type of design holds a lot of promise due to its high power outputs (almost 1 mW/cm$^2$).

*Conclusions*

Biofuel cell development has progressed rapidly over the past ten years and the advances made in this area may soon lead to various commercial applications. However, to this date biofuel cells are only being used in a few "real-world" settings.[75] From a review of the current literature, it seems that the most real-world ready application may be the use of mediated laccase biocathodes as replacements for

platinum cathodes in direct methanol fuel cells as they have been shown to be more tolerant of methanol crossover than platinum.[73] The most desired and potentially most useful application would be the use of biofuel cells in implantable electronic devices. However, *in vivo* testing is not reasonable at this time due to enzyme and mediator instability. Also, before biofuel cells can be relied on as power sources, higher energy densities are necessary in order to avoid the need for complex multi-celled devices and new materials must be developed to meet this goal. Overall, biofuel cells are in their infancy as a viable energy-producing technology. The investigation into new materials and methods for biofuel cell development is important to expand the knowledge base and improve all aspects of biofuel cell performance.

**Project Background**

Based on the previously discussed background material, our group hypothesized that a new redox polymer could be synthesized from linear poly(ethylenimine) (LPEI) and ferrocene that could act as an effective mediator of electrons between glucose oxidase and an electrode. LPEI is less common in the literature than the commercially available branched poly(ethylenimine) (BPEI) because it must be synthesized from other polymers and is not soluble in neutral water like BPEI.

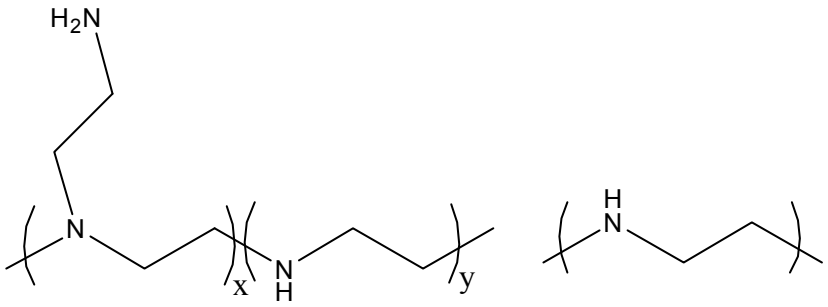


**Figure 1.08:** Structures of BPEI (left) and LPEI (right)

Branched and linear PEI (seen in Figure 1.08) have very different properties, and the full scope of their possible applications has yet to be realized. In particular, our group has a lot of experience with synthesizing LPEI and has shown that it can be a robust polymer for a variety of applications, including polymer electrolyte membranes for fuel cells and ionic conductors for solid state lithium ion batteries.[76-79]

The motivation behind using LPEI as a redox polymer was due to the favorable properties it has for enzyme interaction and mediated electron transfer. LPEI has a low glass transition temperature (-35$^{o}$ C),[80] which suggests that at room temperature it should have a high flexibility/segmental mobility. Also, every third atom is a reactive nitrogen, meaning that there is a high density of sites which can be functionalized or cross-linked. These sites are located along the polymer backbone. This is a unique feature in that most other redox polymers (PVP, PVI, Poly(allylamine)) have reactive sites which are "tethered" to a hydrocarbon backbone. Finally, cross-linked films of LPEI have the ability to hydrate and take up water,[81] which is necessary in order to allow molecules to diffuse in and out of the polymer film.

Other studies which showed that BPEI could interact with enzymes also lead us to investigate LPEI as a redox polymer. A few efforts have been made to use branched poly(ethylenimine) (BPEI) as a polymer in mediated biosensors, and those efforts yielded successful biosensors.[29, 82-84] BPEI has also been shown to enhance the stability and sensitivity of enzymatic biosensors when used as an additive.[83, 85, 86] From a light scattering study, BPEI has been shown to favorably interact with enzymes due to its poly-cationic nature when hydrated or dissolved in water.[87] Enzymes which have an

overall negative charge can interact electrostatically with the large number of protonated nitrogens in the BPEI backbone. Overall, BPEI has only been used as a redox polymer with glucose oxidase in two studies, and has been used as a stabilizer in many studies. When it was used as a redox polymer, marginal current densities were obtained (~500 uA/cm$^2$)[82] and a systematic study of pH or cross-linking effects was not carried out. The body of research involving the interaction of BPEI with enzymes suggested that the potential of aliphatic polyamines as redox polymers had not been fully realized and that cross-linked films of these polyamines with tethered redox centers should be fully characterized and investigated. In addition, the use of LPEI as a redox polymer is non-existent. These factors studies encouraged us to employ LPEI as a biosensing redox polymer to determine if the performance of BPEI could be matched or enhanced.

Ferrocene was chosen as the initial mediator because it is well studied, cheap, easy to handle and can easily be modified synthetically for attachment. It is also well-known that ferrocene derivatives are used in commercial glucose meters[88] and that ferrocene fits into the active site of glucose oxidase.[89]

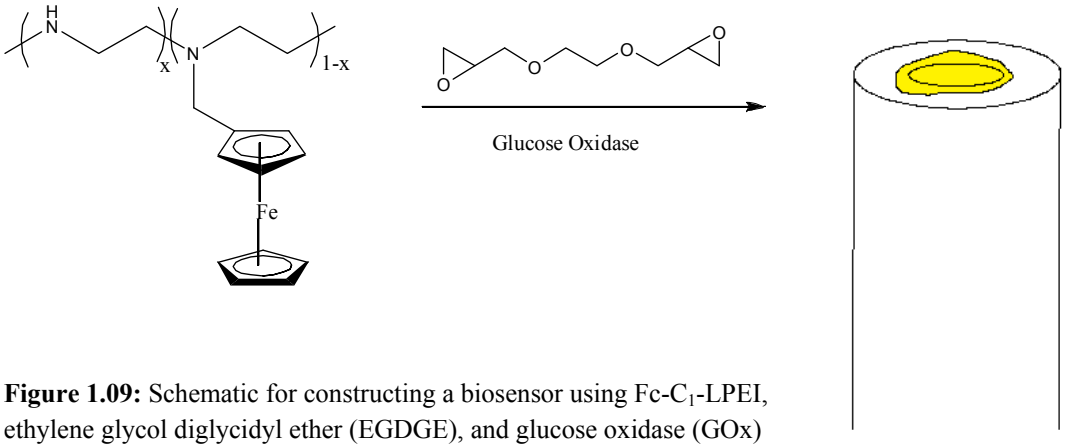


**Figure 1.09:** Schematic for constructing a biosensor using Fc-$C_1$-LPEI, ethylene glycol diglycidyl ether (EGDGE), and glucose oxidase (GOx)

The initial redox polymer hydrogels which were synthesized from ferrocene tethered to LPEI (Figure 1.09) or BPEI (not shown) were able to be utilized as glucose sensors which responded electrocatalytically to the addition of glucose. Films made with Fc-$C_1$-BPEI gave results similar to what was seen in the literature, but surprisingly, cross-linked films of Fc-$C_1$-LPEI displayed maximum catalytic current densities in the range of 1.2 mA/cm$^2$.[17] These current densities were approximately four times higher than other ferrocene-based redox polymers and were similar to the highest reported values for the osmium-based redox polymers with GOx.[24] It should be noted that the ~1 mA/cm$^2$ current densities obtained with Heller's osmium polymers were obtained at 37$^o$ C while ours were at room temperature. It was thought that the high current densities obtained must have been due to fast electron diffusion through the films. However, determination of the apparent electron diffusion coefficient ($cD_e$) using impedance spectroscopy showed that electron diffusion was 2 orders of magnitude slower than that of the best Os-based redox polymers.[24, 80] This led us to the hypothesis that the high current densities might be due to another factor – perhaps an enhanced interaction between LPEI and glucose oxidase resulting from a very close coordination of the LPEI backbone to the enzyme, thereby bringing the ferrocene moieties very close to the GOx active site.

Also, it should be noted that peroxide sensors were also made by cross-linking Fc-$C_1$-LPEI in the presence of horseradish peroxidase,[17] showing that redox polymers based on LPEI and ferrocene could be used to communicate with a variety of enzymes.

**Purpose of the Work and Summary of Chapters**

The intention of this work is to continue the investigation of redox polymers based on LPEI and ferrocene. While the initial results were very promising as highlighted above, there are many aspects of the system which need improvement and/or optimization. Also, there are many fundamental properties of these unique materials that remain un-investigated. As such, the following chapters will document research based on the following topics:

*Ch. 2: Electro-oxidative Stability of Aliphatic Amines*

Biosensors and biofuel cells utilizing ferrocene-modified LPEI are subjected to constant oxidizing conditions. Therefore, the electro-oxidative stability of the LPEI backbone should be verified in order to rule out any backbone degradation as a source of instability. Also, LPEI has been used to make membranes for conventional $H_2$ fuel cells and this study will help determine whether electro-oxidative cleavage of LPEI should be considered as a degradation mechanism. A systematic electrochemical study of small molecule aliphatic amines, oligo-amines, and polyamines will be performed in order to investigate the susceptibility of LPEI to electrochemical oxidation.

*Ch. 3: Effect of Substitution Percentage on the Electrochemical Properties of Ferrocene-Modified Linear Poly(ethylenimine*

This study will describe a more versatile synthetic method for making Fc-$C_1$-LPEI (than the one previously reported) and use that method to synthesize a series of polymers with different ferrocene substitution amounts. The solution electrochemistry

of these polymers (which is of fundamental interest) will be studied as well as their performance as redox polymers for glucose biosensors.

*Ch. 4: Effect of Mediator Spacing on Electrochemical and Enzymatic Response of Ferrocene Redox Polymers*

While the maximum current density obtained with sensors made with Fc-$C_1$-LPEI/GOX/EGDGE was exceptional relative to current literature, the stability of this current was fairly poor, having a half life of about 3 hours. The reasons for this instability have been speculated upon, but are not clear. Taking a cue from some past literature, a study will be carried out which attempts to improve the stability of the sensors and evaluates the effect of changing the tether length between the ferrocene moieties and the polymer backbone.

*Ch. 5: High Current Density Ferrocene-Modified Linear Poly(ethylenimine) Bioanodes and their use in Biofuel Cells*

Methylation of ferrocene has been shown in the literature to lower the redox potential of ferrocene and increase its stability.[90-92] This occurs because methyl groups attached to the Cp ring serve as weak electron donors and stabilize the ferrocenium ion. They also provide steric hindrance around the iron center, making it less susceptible to nucleophilic attack. Therefore, it is logical to use methylated ferrocenes to attempt to improve biosensor performance by lowering the working potential of the sensor and increasing the stability the ferrocenium species in the hydrogel. In this chapter, 1,1'-dimethylferrocene will be modified for attachment to LPEI and the resulting redox

polymer will be evaluated as a glucose biosensor and as a bioanode in a compartment-less biofuel cells.

*Ch. 6: Synthesis of Tetramethylferrocene-Modified Linear Poly(ethylenimine) and its Use as an Anodic Redox Polymer in Biosensors and Biofuel Cells*

In this chapter, the synthesis of tetramethylferrocene will be presented, as well as the synthetic steps required to attach it to LPEI with a three-carbon tether. This polymer will be evaluated as a glucose biosensor and biofuel cell anode and its properties and performance will be compared to the polymers discussed in the previous chapter.

*Chapter 7: Conclusions and Recommendations for Future Work*

Chapter 7 includes a summary of the conclusions reached during the course of this work and provides some suggestions for future studies.

## References


1. Nagel, B.; Dellweg, H.; Gierasch, L. M., *Pure Appl. Chem.* **1992,** *64*, 143-168.

2. Wang, J., *Chem. Rev. (Washington, DC, U. S.)* **2008,** *108* (2), 814-825.

3. National Diabetes Fact Sheet. Prevention, C. f. D. C. a., Ed. Atlanta, GA, 2007.

4. Giampietro, O., *Clinical Chemistry* **1982,** *28* (12), 2405-2407.

5. Clark, L. J.; Lyons, C., *Ann. NY Acad. Sci.* **1962,** *102*, 29.

6. Guilbaul.Gg; Lubrano, G. J., *Anal. Chim. Acta* **1973,** *64* (3), 439-455.

7. Zhang, X. J.; Wang, G. F.; Zhang, W.; Hu, N. J.; Wu, H. Q.; Fang, B., *J. Phys. Chem. C* **2008,** *112* (24), 8856-8862.

8. Vanos, P. J. H. J.; Bult, A.; Vanbennekom, W. P., *Anal. Chim. Acta* **1995,** *305* (1-3), 18-25.

9. Heller, A.; Feldman, B., *Chem. Rev. (Washington, DC, U. S.)* **2008,** *108* (7), 2482-2505.

10. Sasso, S. V.; Pierce, R. J.; Walla, R.; Yacynych, A. M., *Anal. Chem.* **1990,** *62* (11), 1111-1117.

11. Malitesta, C.; Palmisano, F.; Torsi, L.; Zambonin, P. G., *Anal. Chem.* **1990,** *62* (24), 2735-2740.

12. Moussy, F.; Jakeway, S.; Harrison, D. J.; Rajotte, R. V., *Anal. Chem.* **1994,** *66* (22), 3882-3888.

13. Schlapfe.P; Mindt, W.; Racine, P., *Clin. Chim. Acta* **1974,** *57* (3), 283-289.

14. Cass, A. E. G.; Davis, G.; Francis, G. D.; Hill, H. A. O.; Aston, W. J.; Higgins, I. J.; Plotkin, E. V.; Scott, L. D. L.; Turner, A. P. F., *Anal. Chem.* **1984,** *56* (4), 667-671.

15. Degani, Y.; Heller, A., *J. Am. Chem. Soc.* **1989,** *111*, 2357-2358.

16. Heller, A., *Acc. Chem. Res.* **1990,** *23* (5), 128-134.

17. Merchant, S.; Tran, T. O.; Meredith, M. T.; Cline, T. C.; Glatzhofer, D. T.; Schmidtke, D. W., *Langmuir* **2009,** *25* (13), 7736-7742.

18. Rajagopalan, R.; Aoki, A.; Heller, A., *J. Phys. Chem.* **1996,** *100*, 3719-3727.

19. Aoki, A.; Rajagopalan, R.; Heller, A., *J. Phys. Chem.* **1995,** *99*, 5102-5110.

20. Aoki, A.; Heller, A., *J. Phys. Chem.* **1993,** *97*, 11014-11019.

21. Katakis, I.; Ye, L.; Heller, A., *J. Am. Chem. Soc.* **1994,** *116*, 3617-3618.

22. Voet, J. G.; Coe, J.; Epstein, J.; Matossian, V.; Shipley, T., *Biochemistry* **1981,** *20* (25), 7182-7185.

23. Rusling, J.; Forster, R. J., *J. Colloid Interf. Sci.* **2003,** *262*, 1-15.

24. Mao, F.; Mano, N.; Heller, A., *J. Am. Chem. Soc.* **2003,** *125* (16), 4951-4957.

25. Heller, A., *Curr. Opin. Chem. Biol.* **2006,** *10* (6), 664-672.

26. Heller, A., *J. Phys. Chem.* **1992,** *96*.

27. Ohara, T. J.; Rajagopalan, R.; Heller, A., *Anal. Chem.* **1994,** *66* (15), 2451-2457.

28. Kim, H. H.; Mano, N.; Zhang, X. C.; Heller, A., *J. Electrochem. Soc.* **2003,** *150* (2), A209-A213.

29. Yan, Y. M.; Baravik, I.; Yehezkeli, O.; Willner, I., *J. Phys. Chem. C* **2008,** *112* (46), 17883-17888.

30. Sulak, M. T.; Gokdogan, O.; Gulce, A.; Gulce, H., *Biosens. Bioelectron.* **2006,** *21* (9), 1719-1726.

31. Joshi, P. P.; Merchant, S. A.; Wang, Y.; Schmidtke, D. W., *Anal. Chem.* **2005,** *77*, 3183-3188.

32. Liu, Y. G.; Feng, X. M.; Shen, J. M.; Zhu, J. J.; Hou, W. H., *J. Phys. Chem. B* **2008,** *112* (30), 9237-9242.

33. Yehezkeli, O.; Yan, Y. M.; Baravik, I.; Tel-Vered, R.; Willner, I., *Chem. Eur. Jour.* **2009,** *15* (11), 2674-2679.

34. Rahman, M. A.; Kumar, P.; Park, D. S.; Shim, Y. B., *Sensors* **2008,** *8* (1), 118-141.

35. Foulds, N. C.; Lowe, C. R., *Anal. Chem.* **1988,** *60*, 2473-2478.

36. Cache-GuCrente, L.; Deronzier, A.; Mailley, P.; Moutet, J.-C., *Anal. Chim. Acta* **1994,** *289*, 143-153.

37. Ekanayake, E. M. I. M.; Preethichandra, D. M. G.; Kaneto, K., *IEEE Transactions on Instrumentation and Measurement* **2008,** *57* (8), 1621-1626.

38. Hiller, M.; Kranz, C.; Huber, J.; Bauerle, P.; Schuhmann, W., *Adv. Mater. (Weinheim, Ger.)* **1996,** *8* (3), 219.

39. Rockel, H.; Huber, J.; Gleiter, R.; Schuhmann, W., *Adv. Mater. (Weinheim, Ger.)* **1994,** *6* (7-8), 568-571.

40. Kajiya, Y.; Sugai, H.; Iwakura, C.; Yoneyama, H., *Anal. Chem.* **1991,** *53*, 49-54.

41. Os, P. J. H. J. v.; Bult, A.; Bennekom, W. P. v., *Anal. Chim. Acta* **1995,** *305*, 18-25.

42. Bult, P. J. H. J. v. O. A.; Koopal, C. G. J.; Bennekom, W. P. v., *Anal. Chim. Acta* **1996,** *335*, 209.

43. Gajovic, N.; Habermuller, K.; Warsinke, A.; Schuhmann, W.; Scheller, F. W., *Electroanalysis* **1999,** *11* (18), 1377-1383.

44. Zotti, G.; Zecchin, S.; Schiavon, G., *Chem. Mater.* **1995,** *7*, 2309-2315.

45. Hecht, H. J.; Kalisz, H. M.; Hendle, J.; Schmid, R. D.; Schomburg, D., *J. Mol. Biol.* **1993,** *229* (1), 153-172.

46. Ivnitski, D.; Artyushkova, K.; Rincon, R. A.; Atanassov, P.; Luckarift, H. R.; Johnson, G. R., *Small* **2008,** *4* (3), 357-364.

47. Yahiro, A. T.; Lee, S. M.; Kimble, D. O., *Biochim. Biophys. Acta* **1964,** *88* (2), 375

48. Mano, N.; Mao, F.; Heller, A., *ChemBioChem* **2004,** *5*, 1703-1705.

49. Heller, A., *J. Am. Chem. Soc.* **2004,** *126*.

50. Mano, N.; Mao, F.; Heller, A., *J. Am. Chem. Soc.* **2003,** *125*, 6588-6594.

51. Mano, N.; Mao, F.; Heller, A., *J. Am. Chem. Soc.* **2002,** *124*, 12962-12963.

52. Kim, J., *Electroanalysis* **2006,** *18*, 2016-2022.

53. Lim, J.; Malati, P.; Bonet, F.; Dunn, B., *J. Electrochem. Soc.* **2007,** *154* (2), A140-A145.

54. Sakai, H.; Nakagawa, T.; Tokita, Y.; Hatazawa, T.; Ikeda, T.; Tsujimura, S.; Kano, K., *Energy Environ. Sci.* **2009,** *2* (1), 133-138.

55. Stoica, L.; Dimcheva, N.; Ackermann, Y.; Karnicka, K.; Guschin, D. A.; Kulesza, P. J.; Rogalski, J.; Haltrich, D.; Ludwig, R.; Gorton, L.; Schuhmann, W., *Fuel Cells* **2009,** *9* (1), 53-62.

56. Tasca, F.; Gorton, L.; Harreither, W.; Haltrich, D.; Ludwig, R.; Noll, G., *J. Phys. Chem. C* **2008,** *112* (35), 13668-13673.

57. Akers, N. L.; Moore, C. M.; Minteer, S. D., *Electrochim. Acta* **2005,** *50*, 2521-2525.

58. Sokic-Lazic, D.; Minteer, S. D., *Electrochem. Solid St.* **2009,** *12* (9), F26-F28.

59. Sokic-Lazic, D.; Minteer, S. D., *Biosens. Bioelectron.* **2008,** *24* (4), 939-944.

60. Solomon, E. I.; Sundaram, U. M.; Machonkin, T. E., *Chem. Rev. (Washington, DC, U. S.)* **1996,** *96*, 2563-2605.

61. Xu, F.; Shin, W.; Brown, S. H.; Wahleithner, J. A.; Sundaram, U. M.; Solomon, E. I., *Biochem. Biophys. Acta* **1996,** *1292*, 303-311.

62. Christenson, A.; Shleev, S.; Mano, N.; Heller, A.; Gorton, L., *Biochem. Biophys. Acta* **2006,** *1757*, 1634-1641.

63. Xu, F., *Biochemistry* **1996,** *35*, 7608-7614.

64. Cracknell, J. A.; Vincent, K. A.; Armstrong, F. A., *Chem. Rev.* **2008,** *108* (7), 2439-2461.

65. Stankovich, M. T.; Schopfer, L. M.; Massey, V., *J. Biol. Chem.* **1978,** *253* (14), 4971-4979.

66. Larminie, J.; Dicks, A., *Fuel Cell Systems Explained*. 2 ed.; John Wiley & Sons: 2003.

67. Barton, S. C.; Gallaway, J.; Atanassov, P., *Chem. Rev. (Washington, DC, U. S.)* **2004,** *104* (10), 4867-4886.

68. Ivnitski, D.; Atanassov, P., *Electroanalysis* **2007,** *19* (22), 2307-2313.

69. Ivnitski, D.; Branch, B.; Atanassov, P.; Apblett, C., *Electrochem. Commun.* **2006,** *8* (8), 1204-1210.

70. Galloway, J. W.; Barton, S. C., *J. Am. Chem. Soc.* **2008,** *130*, 8527.

71. Mano, N.; Mao, F.; Shin, W.; Chena, T.; Heller, A., *Chem. Commun. (Cambridge, U. K.)* **2003**, 518-519.

72. Gill, I., *Chem. Mater.* **2001,** *13* (10), 3404-3421.

73. Barton, S. C., *J. Electrochem. Soc.* **2005,** *152* (5), A876-A881.

74. Hudak, N. S.; Gallaway, J. W.; Barton, S. C., *J. Electrochem. Soc.* **2009,** *156* (1), B9-B15.

75. Bullen, R. A.; Arnot, T. C.; Lakeman, J. B.; Walsh, F. C., *Biosens. Bioelectron.* **2006,** *21* (11), 2015-2045.

76. Glatzhofer, D. T.; Erickson, M. J.; Frech, R.; Yepez, F.; Furneaux, J. E., *Solid State Ionics* **2005,** *176*, 2861-2865.

77. Giffin, G. A.; Castillo, F. Y.; Frech, R.; Glatzhofer, D. T.; Burba, C. M., *Polymer* **2009,** *50*, 171-176.

78. Sanders, R. A.; Snow, A. G.; Frech, R.; Glatzhofer, D. T., *Electrochemica Acta* **2003,** *48*, 2247-2253.

79. Snow, A. G.; Sanders, R. A.; Frech, R.; Glatzhofer, D. T., *Electrochemica Acta* **2003,** *48*, 2065-2069.

80. Merchant, S.; Glatzhofer, D. T.; Schmidtke, D. W., *Langmuir* **2007,** *23*, 11295.

81. Watanabe, M.; Ikezawa, R.; Sanui, K.; Ogata, N., *Macromolecules* **1987,** *20* (5), 968-973.

82. Chuang, C. L.; Wang, Y. J.; Lan, H. L., *Anal. Chim. Acta* **1997,** *353* (1), 37-44.

83. Jezkova, J.; Iwuoha, E. I.; Smyth, M. R.; Vytras, a. K., *Electroanalysis* **1997,** *9* (13), 978-984.

84. Huan, Z. W.; Persson, B.; Gorton, L.; Sahni, S.; Skotheim, T.; Bartlett, P., *Electroanalysis* **1996,** *8* (6), 575-581.

85. McMahona, C. P.; Rocchitta, G.; Kirwan, S. M.; Killoran, S. J.; Serra, P. A.; Lowryb, J. P.; O'Neill, R. D., *Biosens. Bioelectron.* **2007,** *22*, 1466-1473.

86. Wang, J.; Llu, J.; Chen, L.; Lu, F., *Anal. Chem.* **1994,** *66*, 3600-3603.

87. Andersson, M. M.; Hatti-Kaul, R., *J. Phys. Chem. B* **2000,** *104*, 3660-3667.

88. Forrow, N. J.; Sanghera, G. S.; Walters, S. J., *J. Chem. Soc. Dalton Trans.* **2002,** (16), 3187-3194.

89. Alvarez-lcaza, M.; Kalisz, H. M.; Hecht, H. J.; Aumann, K.-D.; Schomburg, D.; Schmid, R. D., *Biosens. Bioelectron.* **1995,** *10*, 735-742.

90. Hradsky, A.; Bildstein, B.; Schuler, N.; Schottenberger, H.; Jaitner, P.; Ongania, K. H.; Wurst, K.; Launay, J. P., *Organometallics* **1997,** *16* (3), 392-402.

91. Shubina, E. S.; Krylov, A. N.; Kreindlin, A. Z.; Rybinskaya, M. I.; Epstein, L. M., *J. Mol. Struct.* **1993,** *301*, 1-5.

92. Bashkin, J. K.; Kinlen, P. J., *Inorg. Chem.* **1990,** *29* (22), 4507-4509.

# CHAPTER 2: ELECTRO-OXIDATIVE STABILITY OF ALIPHATIC AMINES

## Introduction

Hydrogen or methanol-fueled polymer electrolyte membrane fuel cells (PEMFC's) represent a large segment of energy research and PEMFC technology has been proposed as a replacement for non-renewable energy sources such as fossil fuels and batteries. Two large obstacles which lie in the way of realizing this goal are the need for precious metal catalysts (i.e. platinum), and the need for a chemically, mechanically, and thermally stable proton conducting material. This lack of an ideal proton-conducting material for use in PEFC's is a significant factor in why the full potential of hydrogen and/or direct methanol fuel cells has not been met to date. The most common materials used in commercial fuel cells to conduct protons are polysulfonated aromatics and DuPont's Nafion polymer. Nafion is the industry standard for polymer electrolyte fuel cell membranes and has been studied in great detail to gain insight into how to improve on its properties.[1-6] While Nafion has many favorable properties, it can be degraded both chemically[3, 6] and mechanically[4, 7] and it is not an effective proton conductor under high temperature, dehydrated conditions. There is a need for new membrane materials which are stable under high temperature, acidic, reductive, and oxidative conditions. Polysulfonated aromatic polymers conduct protons effectively under hydrated conditions, but once water is removed from the system they also do not provide the required conductivities for fuel cell operation.[8] The possibility of de-sulfonation also exists under acidic conditions, which leads to chemical breakdown in these polymers.[8]

Aliphatic amines constitute a large class of organic materials which are not normally thought of for fuel cell applications because of the ease with which they can be oxidized. The lone pair of electrons on an amine nitrogen can be oxidized at potentials around +1.0 V or higher, depending on the amine.[9-13] Numerous studies by Mann have investigated the series of chemical transformations that follow this oxidation[10, 11, 14] (Figure 2.01) and some studies even use this

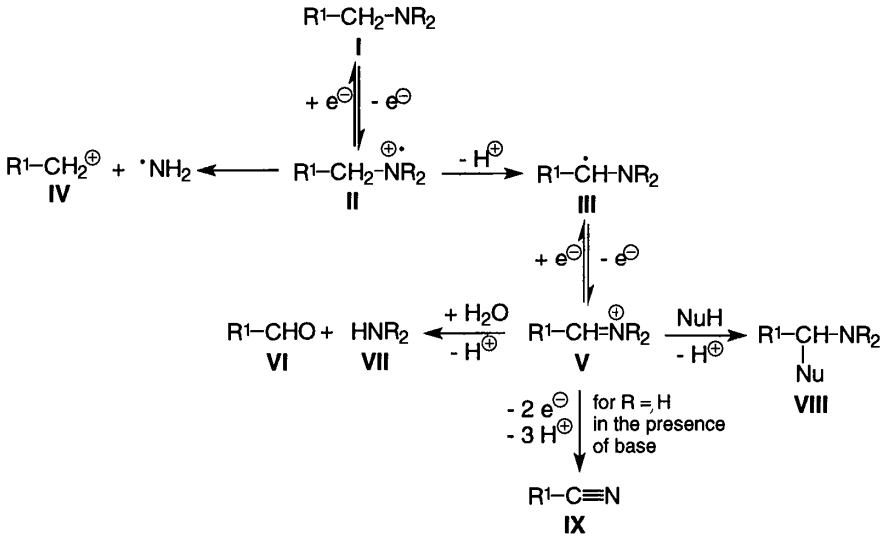


**Figure 2.01:** Schematic of possible degradation pathways for aliphatic amines after electrochemical oxidation. (from ref. #9)

oxidation to carry out controlled chemical reactions on a preparative scale.[9, 15] In general, when one of the two lone pair electrons on nitrogen is removed, a series of reactions follows which result in cleavage of the molecule, leading to a variety of aldehyde and amine products. One aspect which permeates these studies is the use of organic solvents to investigate the reactions. Only one study uses an aqueous solvent but the oxidations in that case are carried out under basic conditions.[12] Different reaction pathways exist for cleavage of the amines depending on how much water is

present,[16] but it is clear that once an aliphatic nitrogen has been electrochemically oxidized, it is very reactive and reacts with itself, the solvent, or other amines.

There are no studies which investigate the oxidation of aliphatic amines under neutral aqueous or acidic aqueous conditions. This might be due to the fact that in an aqueous environment, amine compounds become protonated and do not have a free lone pair of electrons. These compounds are known as ammonium salts and have a positive charge on the nitrogen. One study actually investigates the use of quaternary ammonium salts as materials for capacitors.[17] The only oxidation they observed was the oxidation of the *anion* of the ammonium salt, and this only occurred at potentials greater than +2.0 V. Because the nitrogen has no available electrons, it should not be able to be oxidized and should be stable when subjected to positive electric potentials. It should be noted that the protonation of amines could lead to a species which is easier to reduce than the neutral amine, thereby making the amine less electrochemically stable in the opposite direction. However, at least one study has shown that the reduction of alkyl ammonium salts (in organic media) requires high voltages (> -1.5 V vs. NHE) and produces only hydrogen and the neutral amine.[18]

Linear poly(ethylenimine) (LPEI) is a linear aliphatic polyamine which can conduct both protons and ions like lithium. Our group has utilized these properties to demonstrate its use as a potential material for polymer electrolyte membrane fuel cells (PEMFC's) or solid state lithium ion batteries.[19-22] For proton conducting fuel cell membranes, cross-linked membranes of LPEI mixed with hydrochloric acid and phosphoric acid have been shown to exhibit conductivities which are high enough to warrant consideration as membranes for fuel cells.[21] These films also have acceptable

mechanical and thermal stability, which are required for high temperature fuel cell applications. The use of LPEI in fuel cells would be advantageous as it is cheap to synthesize and is easier to process than sulfonated polyaromatics and nafion. However, fuel cells normally operate at potentials around 1.0 volt, which is enough potential to oxidize some aliphatic amines. This fact raises some concerns about the stability of LPEI under electrochemically oxidizing conditions.

Another application for LPEI which requires operation under oxidizing conditions is as a scaffold for mediated glucose biosensors.[23-25] For this application, cross-linked films of ferrocene-modified LPEI are coated onto an electrode in the presence of glucose oxidase and held at constant potentials as high as 0.642 V (vs. NHE). These sensors exhibit high sensitivity and current response to glucose and further development may lead to in-vivo applications of these sensors. However, because these sensors operate optimally around neutral pH, there is a chance that many of the nitrogens on the LPEI backbone will be deprotonated and vulnerable to oxidative cleavage. An investigation into the electro-oxidative stability of LPEI would help determine the range of utility of these materials for biosensors and biofuel cells.

Because LPEI is a polyamine, it exhibits different acid/base characteristics than a normal amine. For instance, under acidic conditions (ex: pH = 4.1), almost 100% of a normal aliphatic amine like diethylamine is in the protonated form. In contrast, LPEI has been reported to only be 70% protonated under these conditions.[26] This means that even at low pH values, up to 30% of the nitrogens on the polymer backbone could be neutral and potentially available to be oxidized at a high enough potential. This incomplete protonation is believed to be due to a well-studied neighboring ion effect

which causes neutral nitrogens to be less basic than normal because of their proximity to neighboring protonated nitrogens.[27, 28] LPEI contains only two methylene groups between each nitrogen, which means that a strong electrostatic repulsion effect occurs when two neighboring nitrogens are protonated.[28] Furthermore, each protonated nitrogen leads to a positive charge on the polymer chain and the chain becomes "saturated" with positive charges, preventing complete protonation of the polymer. Another way to look at this phenomenon would be in terms of local $pK_a$ effects (the pKa values of the amines discussed in this work will all correspond to the acid dissociation constant of the protonated amine). As the polymer chain becomes more saturated with positive charges, the $pK_a$ of any random protonated nitrogen gets lower and lower (more acidic) and the $pK_b$ of any random free nitrogen increases (less basic) as it becomes surrounded by positive charges. Because the $pK_a$ of LPEI changes with respect to pH, it is difficult to predict how changes in pH will affect the oxidative stability of the polymer. However, we hypothesize that the neighboring ion effect described above will have an electrochemical effect similar to the established protonation effect. The oxidation potential ($E_{ox}$) of a non-protonated nitrogen should increase if it is adjacent to one or two protonated nitrogens, and, if sufficient numbers of nitrogens are protonated on the polymer backbone, the electrochemical stability of the remaining neutral nitrogens should be high enough to prevent electro-oxidative degradation.

This study will investigate whether oxidative degradation of LPEI should be a concern when using LPEI for fuel cell and biosensor/biofuel cell applications, and whether neighboring ion effects on LPEI will cause neutral nitrogens to be harder to oxidize than if they were isolated small molecules. The oxidation of a series of

monoamines, diamines, oligoamines, and polyamines amines was carried out with respect to pH to determine if increasing the number of neighboring nitrogens on the molecule causes a relative decrease in the ease of oxidation. The goal of this chapter is not to provide a quantitative analysis of exactly how much LPEI should degrade in a fuel cell or biosensor. Rather, it is to show the general qualitative stability (or instability) of amines and polyamines under electro-oxidative conditions.

**Experimental**

All amines were purchased from Aldrich except for LPEI, which was synthesized by acidic hydrolysis of poly(2-ethyl-2-oxazoline) (Aldrich, $M_n$ = 200,000).[29, 30] A conventional three-electrode setup was used for all electrochemical procedures. The working electrode was a 1 mm platinum disc, the counter electrode was a platinum wire, and a standard calomel electrode was used for the reference. A general experiment was carried out as follows: 30 mL of a 0.1 M solution of triflic acid was added to a closed cell and the cell was placed in a temperature bath at 25$^o$ C. Cyclic voltammetry was carried out in the oxidative and reductive directions, and a time-based constant potential experiment was carried out at 1.0 V (vs. SCE) for 300 seconds with stirring. Then, enough amine was added to change the pH of the solution to the desired value. After adding the amine and letting the temperature equilibrate, the cyclic voltammetry and time-based constant potential experiments were repeated. The average current of the last 50 seconds of the constant potential experiment was used for analysis. After this, more amine was added to gradually increase the pH and the procedure was repeated. This method was chosen in order to avoid changing the ionic

strength of the solution by adding extra acids or bases. By mixing only amine and acid, the overall system is simple and acid-base calculations were fairly straightforward for monoamines. The potential of 1.0 V vs. SCE was chosen because of its relative proximity to the highest theoretical open circuit voltage of a fuel cell, which would be 1.23 V (vs. NHE). 1.0 V vs. SCE is equivalent to 1.242 V vs. NHE, so any species which is electro-oxidatively stable at this voltage should be stable under PEM fuel cell or biosensor operating conditions. All concentration calculations and protonation distribution predictions based on the pH of the solutions were made using CurTiPot acid-base titration simulation software.

**Results and Discussion**

The results and discussion will be presented in a stepwise fashion, with the mono-amine electrochemistry serving as a starting point for the more complex di-, tri-, oligo-, and poly-amines. An exclusive investigation of the electrochemical stability of polyamines would have constituted an incomplete set of data because experiments of this type have not been carried out on well-known aliphatic amines. An examination of polyamine electrochemical stability might show a promising result, but it is advantageous to show this stability as a trend starting with smaller molecules (i.e. model compounds) and building up to polymers.

*Cyclic Voltammetry and Time-based Constant Potential Amperometry of Monoamines*

It is known that the ease of aliphatic amine oxidation follows a general trend of tertiary>secondary>primary.[9] This trend is due to the slight electron donating nature of

the carbon atoms attached to the nitrogen and their ability to stabilize a positive charge. Therefore, it would be expected that under basic pH conditions, triethylamine would have an oxidation onset voltage lower than that of diethylamine, which would have a lower onset voltage than of propylamine. These predictions can be investigated by using cyclic voltammetry, as seen in Figure 2.02. As predicted, the onset voltage for the oxidation of amines at pH 11.0 seems to get lower with each added alkyl group. Also, at similar potentials, much more of the tertiary amine is oxidized than the secondary or primary amines, as represented by its much higher anodic peak current ($i_{pa}$).

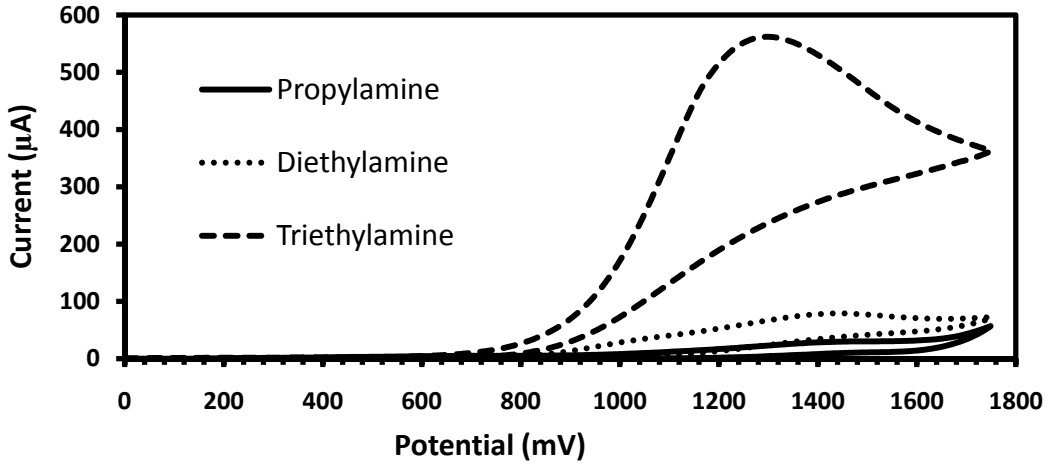


**Figure 2.02:** Cyclic voltammograms of aliphatic monoamines at pH 11 in 0.1 M triflate, 100 mV/s

This suggests that the effect of each alkyl group is greater than additive and that tertiary amines could cause more problems when used under electro-oxidative conditions. The cyclic voltammograms in Figure 2.02 all show irreversible redox behavior. This fits well with the degradation mechanisms described in the literature and shows that once the lone pair of electrons on an amine *has* been oxidized, the radical cation reacts quickly.

When the same cyclic voltammetry experiments were carried out at low pH, different results were obtained (Figure 2.03). At pH 1.8, none of the amines were oxidized as they were under basic conditions, and the only oxidative current seems to arise from the solvent oxidation (water) at very high potentials. This is expected because as at this pH, it can be calculated that only 1 out of every 1.4 x $10^9$ amines in solution is deprotonated, meaning that almost every nitrogen atom should be protonated and therefore virtually impossible to oxidize.

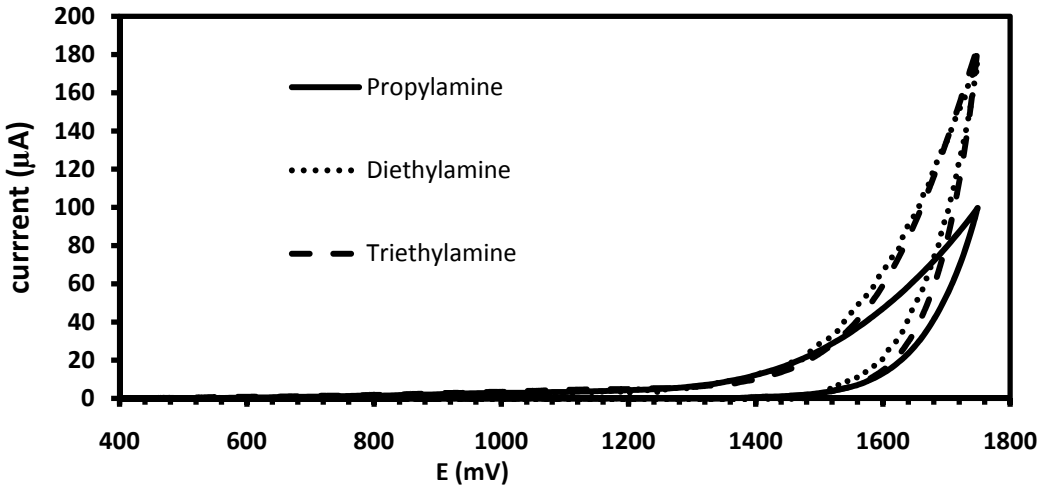


**Figure 2.03:** Cyclic voltammograms of aliphatic monoamines at pH 1.8 in 0.1M triflic acid, 100 mV/s

At low and intermediate pH values, there was no appreciable change between the background current and oxidative current, so a constant potential experiment was carried out rather than a scanning experiment to better determine how much oxidation was occurring across the whole pH range. Constant potential experiments allowed for the acquisition of the steady state current resulting from any oxidation of the amine that may have been occurring. When the current obtained at 1.0 V (vs. SCE) was plotted vs. pH, graphs were obtained which showed a lot of oxidation at higher pH, and very small

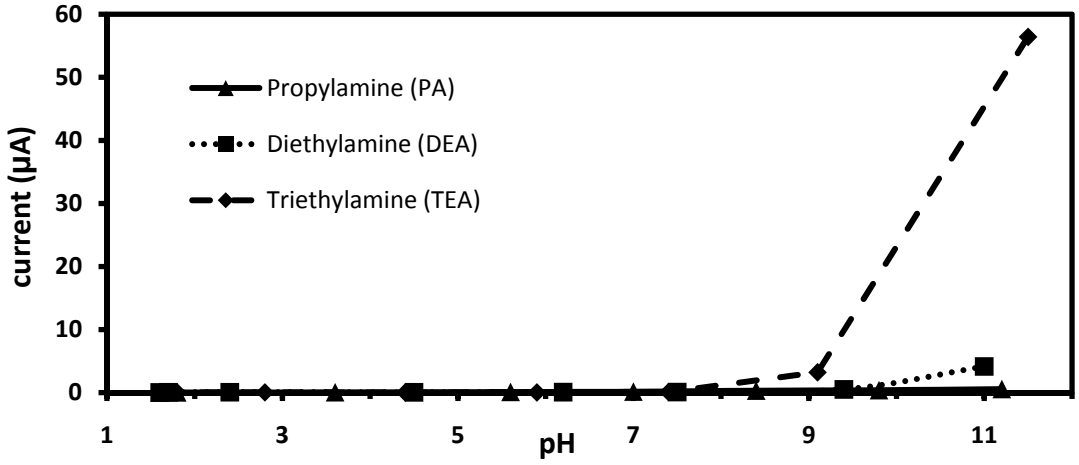


**Figure 2.04:** pH vs. current plots for aliphatic monoamines at 1.0 V vs. SCE, 0.1M triflic acid, stirring.

amounts of oxidation at lower pH's (Figure 2.04). The most significant increase in current on the graph lies between pH's 9.0 and 11.0. This behavior of the mono-amines corresponds directly to their $pK_a$ values, which all lie between 10.54 and 10.84,[31] and the reason for the sudden increase in current around pH 9 is evident when it is calculated (i.e. for DEA) that between pH 9.0 and 11.0, the amount of free amine in solution changes from 1.1 mM to 110.7 mM, or relatively, from 1.1% of the total amine present to 52% of the total amine present. This large increase in the concentration of free amine leads to the sudden increase in current.

The scale of the graph in Figure 2.04 is dictated by the high current resulting from the oxidation of triethylamine at high pH. This reinforces the idea that tertiary amines are much easier to oxidize than secondary or primary amines once they are deprotonated. To get a better look at the behavior of these amines when they are mostly protonated, up the low/intermediate pH region of the graph can be enlarged (Figure 2.05).

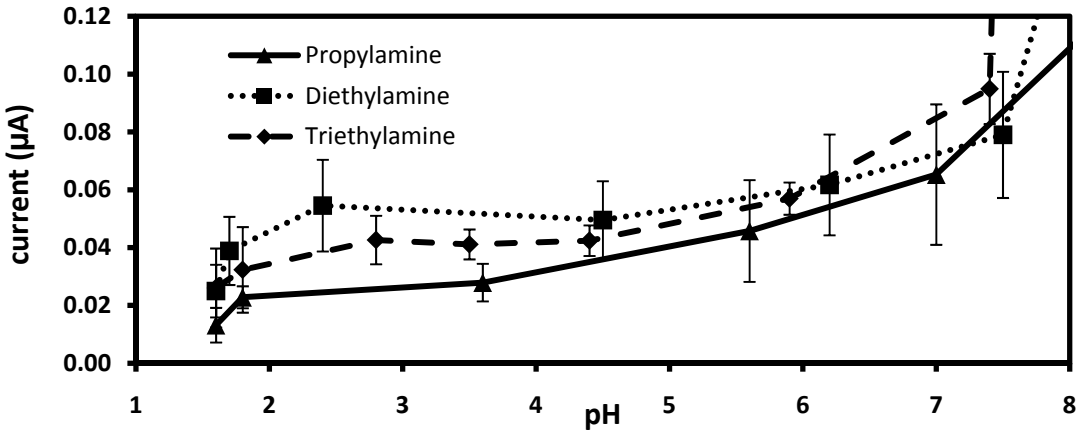


**Figure 2.05:** pH vs. current plots for aliphatic monoamines showing the low and intermediate pH regions. First point of each series is 0.1 M triflic acid, and each additional point is with added amine. Error bars are based on standard error of the mean.

One immediate observation from Figure 2.05 which shows the stability of ammonium ions is the similarity of all three amines. As previously shown, the amines with more alkyl groups are oxidized at a much faster rate under basic conditions. However, at these low and intermediate pH values, all three amines behave similarly and there is no significant difference between the three. While there appears to be a small increase in current after the first addition of each amine, this change is statistically insignificant. The amount of free amine that is present at this point is in the picomolar range and therefore cannot be detected by the instrument. Also, very little increase in overall current occurs between pH 1.8 and 7.5. The changes in current at these low and intermediate pH's are extremely minimal and show that protonated monoamines undergo very little electrochemical oxidation at 1.0 V vs. SCE.

Because the concentration of the acid and the pKa's of the three amines are known, it can be determined that up to pH 5.8 – 6.0 (exact value depends on the amine), almost 100% of the amines that are present in the solution exists as ammonium ions. After pH 5.8 – 6.0, free amine concentration begins to increase and the result of this is a

sudden increase in current. The drastic increase in current which occurs after pH 7.5 can be explained by the fact that the concentration of free amine in solution increases by 33-fold between pH 7.5 and pH 9.0. (for example: at pH 7.5, [free DEA] = 0.036 mM and at pH 9, [free DEA] = 1.18 mM).

It can be concluded from this section that monoamines do not undergo any significant, detectable oxidation at 1.0 V vs. SCE under acidic conditions due to their existence as ammonium ions. However, once the monoamines are deprotonated, they oxidize at 1.0 V vs. SCE. Also, the ease of oxidation follows the trend of tertiary >>> secondary > primary.

*Cyclic Voltammetry and Time-based Constant Potential Amperometry of Diamines*

When a second amine functional group is added to the molecule (as in ethylenediamine and its alkylated derivatives), different electrochemical results were expected due to interactions from the neighboring nitrogen. Figure 2.06 shows three distinct species that an aliphatic diamine can assume under aqueous, acidic conditions. In species I, both nitrogens are neutral and available to be oxidized. In species II, one nitrogen is protonated and three different equilibrium structures can be drawn. This species shows an example of a neighboring ion effect and the consequences of this effect can be seen in the known pKa's for diamines.

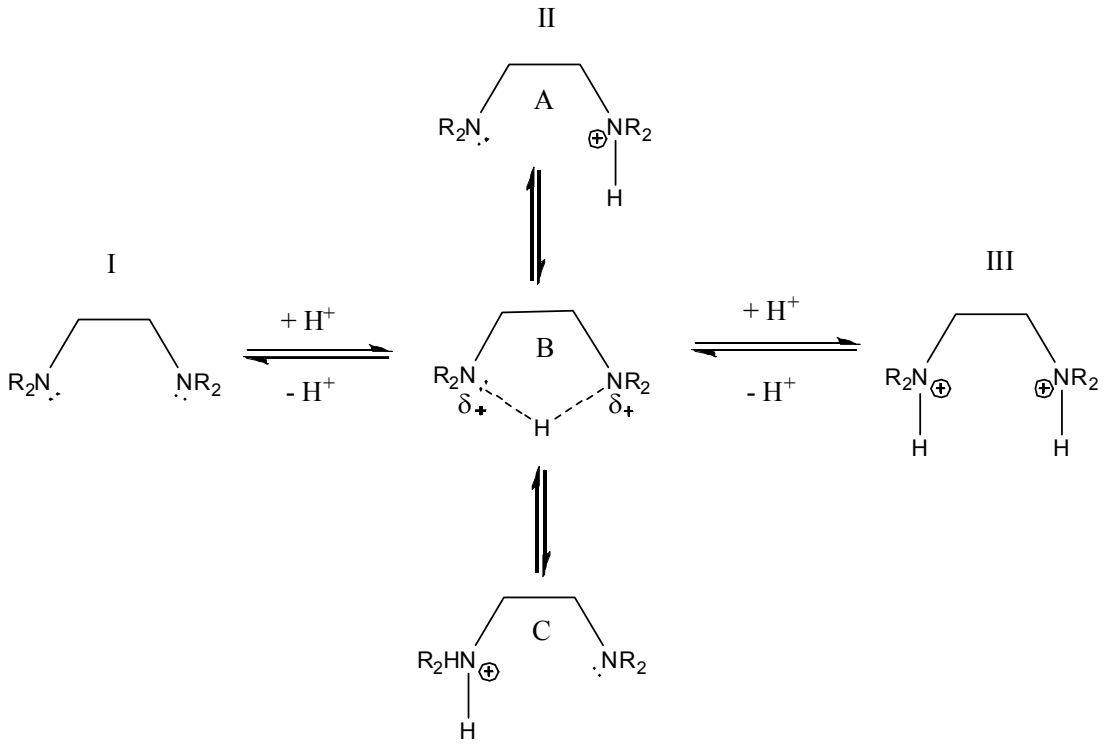


**Figure 2.06:** Three possible protonation states of a symmetrical ethylenediamine

An example would be N,N'-dimethylethylenediamine (N,N'-DMEDA) ($pKa_1$ = 10.16, $pKa_2$ = 7.40).[32] The neighboring ion effect makes it more difficult to protonate the second nitrogen for two possible reasons: 1. The additional charge on the molecule creates a "proximity effect" where a second protonation of the molecule makes it more unstable due to the proximity and charge repulsion of the two positive charges. 2. The lone pair of electrons on the free nitrogen is less "available" for protonation because they could be involved in an intramolecular hydrogen bond with a proton on the charged nitrogen (as seen in equilibrium structure II-B).

It was hypothesized that both of these factors should also contribute to an increase in the oxidation potential of the neutral nitrogen in species II relative to the oxidation potential of the free amine (Species III). Ideally, this change would be

evident in a cyclic voltammetry experiment by analyzing a diamine at different pH values.

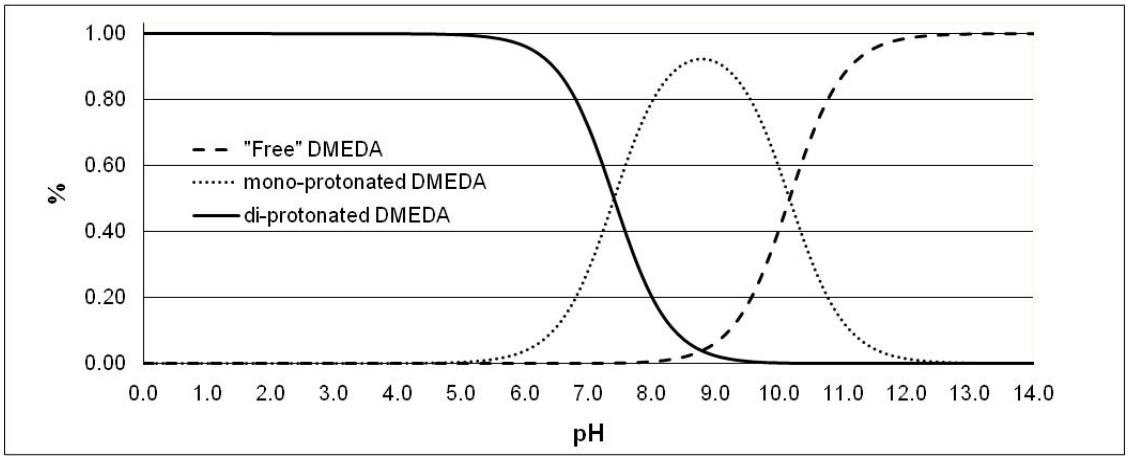


**Figure 2.07:** Protonation distribution for N,N'-DMEDA

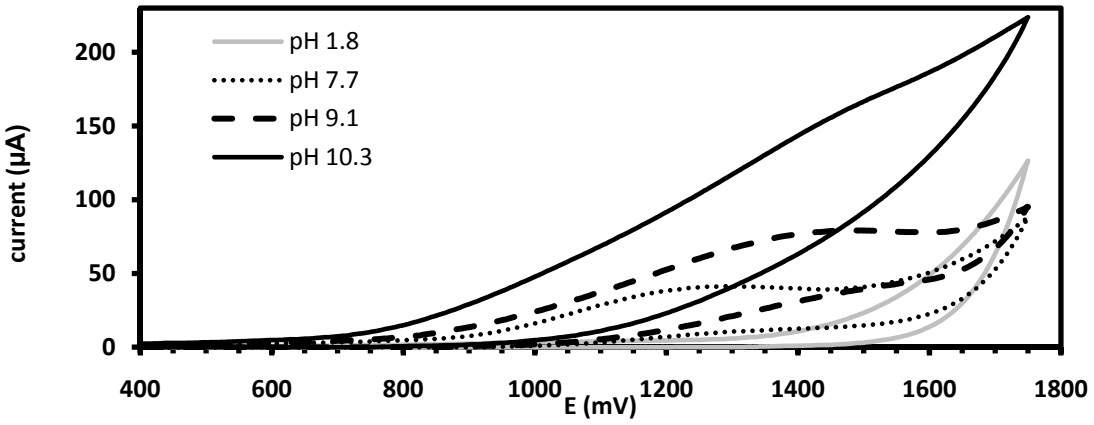


**Figure 2.08:** Cyclic voltammograms of N,N'-DMEDA in 0.1M triflic acid at various pH values. Scan rate = 100 mV/s

Figure 2.07 shows the protonation distribution for N,N'-DMEDA across the whole pH spectrum. Figure 2.08 shows cyclic voltammograms of N,N'-DMEDA at various pH values, each corresponding to a different protonation state of the molecule. At pH 1.8, all of the amine in solution is di-protonated, so no oxidation takes place until the solvent

oxidation at very high potential. The next pH examined is 7.7, which corresponds to the ~50% of the diamines being protonated (Figure 2.07). Significant oxidation in this solution takes place, with the onset of oxidation at ~880 mV and an $E_{pa}$ of 1275 mV. When the pH increases to 9.1, the solution is almost completely comprised of monoprotonated species (Figure 2.07). Not surprisingly, the $i_{pa}$ (peak anodic current) increases from ~40 to 80 μA due to a large increase in the concentration of oxidizable nitrogens. What is surprising is that the $E_{pa}$ (potential at peak anodic current) shifts anodically to 1480 mV even though the protonation state of the amine should not change. While an anodic shift in the $E_{pa}$ of a molecule normally indicates an increase in the difficulty of oxidation, that is unlikely in this case and this shift may be due to a concentration effect or an unknown phenomenon. When the pH increases further to 10.3, a large increase in $i_{pa}$ occurs. There is no clear "peak" to label with a specific value as the amine oxidation merges directly into the background solvent oxidation, but it can be estimated at ~175 μA. Unfortunately, without a clear $E_{pa}$ at this pH, it is impossible to give the free amine a specific oxidation potential. What can be done, however, is to note the significant shift of the oxidation onset voltage in the cathodic direction to ~650 mV, which is 230 mV lower than at pH 7.7. This phenomenon could be due to a concentration effect, or it could suggest an increase in the ease of oxidation of the free amine relative to the monoprotonated amine. These experiments were informative, but in order to observe how the oxidative stability of diamines changes with respect to mono-amines, time-based constant potential experiments are appropriate.

The monoamine/diamine comparisons which will be discussed in this section are DEA vs. N,N'-DMEDA and TEA vs. tetramethylethylenediamine (TMEDA). The comparison between propylamine (PA) and ethylenediamine (EDA) could not be made due to unusual electrochemical behavior from ethylenediamine. A "crossover" was observed in the cyclic voltammetry of EDA, indicating formation of a substance on the surface of the platinum electrode. Past studies have shown that EDA can be electrochemically polymerized into some form of poly(ethylenimine)[33, 34] and this was most likely occurring here as well.

The pH vs. current plots for DEA and N,N'-DMEDA in Figure 2.09 show that at low pH values, neither amine is significantly oxidized. This is due to complete protonation of each amine. However, this figure reveals two interesting phenomena resulting from the neighboring ion effect: N,N'-DMEDA begins to oxidize at a lower pH than DEA, and the maximum current achieved at pH 10.3 for N,N'-DMEDA was roughly equal to the current for DEA at the same pH (estimated with the plot). The lower pH onset of oxidation for N,N'-DMEDA is most likely due to the monoprotonated N,N'-DMEDA species (Figure 2.06, Species II) appearing at a lower pH than free DEA due to the increased acidity of di-protonated N,N'-DMEDA. The electrons on monoprotonated N,N'-DMEDA are available at pH 6-10, while DEA remains mostly protonated at those pH values. However, even though the electrons are seemingly "free," the neighboring ion effect prevents this lone pair from being oxidized as easily as a free lone pair on a secondary mono-amine, which is why the current does not increase as drastically as seen in the DEA plot.

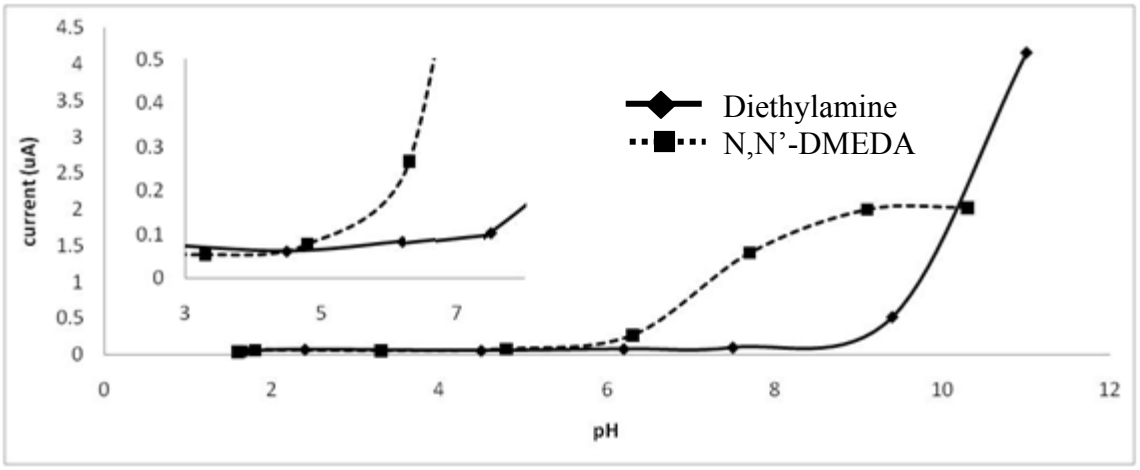


**Figure 2.09:** pH vs. current plots for DEA and N,N'-DMEDA at 1.0 V vs. SCE, 0.1M triflic acid, stirring

As the pH increases, the current for N,N'-DMEDA continues to rise until it reaches a maximum around pH 9. At pH values higher than 9.0, the current from N,N'-DMEDA oxidation seems to reach a plateau. It may seem contradictory to our hypothesis that N,N'-DMEDA has an onset of oxidation at a lower pH than DEA, but a closer look at the speciation that is occurring at these intermediate pH values suggests otherwise.

The protonation distribution of N,N'-DMEDA is again useful (Figure 2.07). This figure justifies the previous statement that N,N'-DMEDA has a lower oxidation onset voltage due to the formation of the monoprotonated amine around pH 6.0. It also shows that at pH 9.0, the vast majority of diamine in the solution is in the mono-protonated form. At pH 10.3, which corresponds to the highest point on the pH vs. current plot for N,N'-DMEDA, the protonation graph reveals that there should be a roughly 50/50 mixture of mono-protonated and free amine in the solution. Curiously, this large increase in free amine concentration does not lead to an increase in current.

According to the current vs. pH plot in Figure 2.09, the currents for each of these amines are about equal at pH 10.3 (although there is no exact point on the DEA plot for this pH). To determine if the neighboring ion effect is having any effect, the

$pK_a$ values of each amine can be used to calculate concentrations of N,N'-DMEDA and DEA at pH 10.3. Similar currents *should* indicate similar concentrations of oxidizable nitrogens if all experimental conditions are the same for each amine. At pH 10.3, DEA has a calculated concentration of 0.123 M, with 0.0218 M in the free amine form. N,N'-DMEDA has a calculated concentration of 0.209 M, with 0.0997 M in the mono-protonated form and 0.109 M in the free amine form. This means that the concentration of "totally free" nitrogens (Species I from Figure 2.06) in the N,N'-DMEDA solution is 10 times higher than in the DEA solution. Going a step further, if we include the monoprotonated N,N'-DMEDA molecules as having one free nitrogen, the concentration of free nitrogens in the N,N'-DMEDA solution is almost 15 times higher than in the DEA solution. This 15-fold difference does not translate to any significant difference in current, indicating that free N,N'-DMEDA nitrogens are more difficult to oxidize than free DEA nitrogens.

It has been shown that a significant neighboring ion effect inhibits oxidation of the N,N'-DMEDA under acidic, neutral, and basic conditions. At low pH, N,N'-DMEDA is di-protonated and therefore cannot be oxidized. At neutral pH (6-8), a significant amount of mono-protonated diamine is present, however the current is not equivalent to that of an equal concentration of free DEA. At the higher pH values, a significant increase in the concentration of oxidizable nitrogens does not lead to an increase in current, meaning that these nitrogens must still be deactivated somehow. This inhibition could be due to hydrogen bonding with the solvent causing a deactivation of one or both nitrogens. Also, treating the two neutral nitrogens on each free N,N'-DMEDA molecule as equally oxidizable is likely inaccurate. It is likely that

once one of the nitrogens is oxidized, the other cannot be, and this could be caused by two factors: 1. The monocation generated from one oxidation is so unstable that it cleaves before a second oxidation can take place. 2. The molecule simply does not have enough electron donors (alkyl groups) on each nitrogen to be able to stabilize two positive charges.

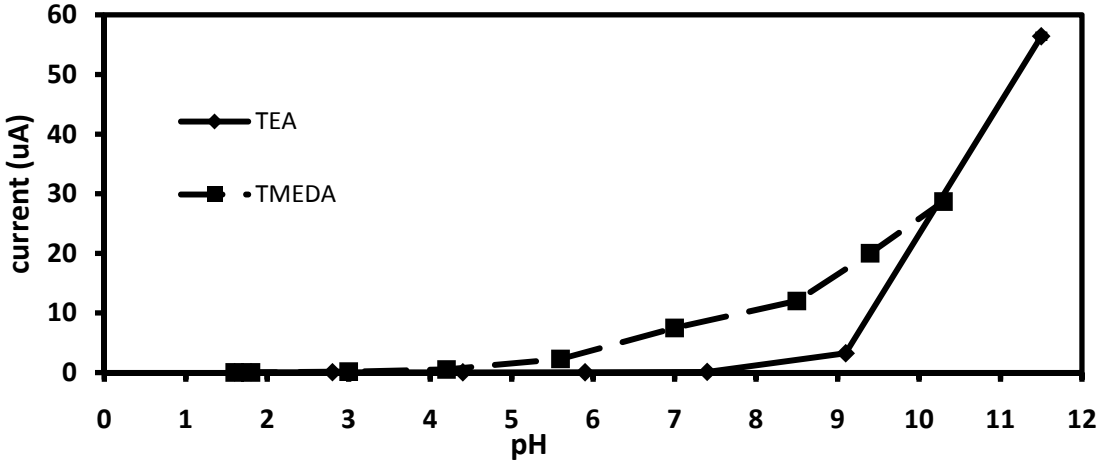


**Figure 2.10:** pH vs. current plots for TEA and TMEDA at 1.0 V vs. SCE, 0.1M triflic acid, stirring

The electrochemistry of TMEDA when compared to TEA also reinforces the concept of the neighboring ion effect. (Figure 2.10) Like N,N'-DMEDA, TMEDA shows very little oxidation at low pH values and has a lower onset of oxidation than it's monoamine counterpart, which is due to the emergence of Species II around a pH of 6.0. Again, there is a free nitrogen, but it is deactivated by the neighboring positive charge through charge saturation and hydrogen boding. This makes it only partially available to be oxidized. Where TMEDA differs from N,N'-DMEDA is that it does not show a plateau at higher pH values. Instead, the oxidative current for TMEDA continues to increase with pH. At a glance, this could seem to indicate that the neighboring ion effect does not apply in the TMEDA system. However, it is most

likely that the effect is lessened because of the large increase in the ease of oxidation of tertiary amines relative to secondary amines. Also, some of the completely deprotonated TMEDA molecules could be oxidized twice because of the additional methyl groups, leading to the higher currents.

If we apply the same $pK_a$/concentration analysis to the TMEDA/TEA comparisons as was done with the secondary amines, it is evident that a neighboring ion effect still occurs: Because of their similar $pK_a$ values, the protonation distribution plot for TMEDA is essentially identical to the one for N,N'-DMEDA (Figure 2.07) and shows that between pH 1.0 and 6.0, the solution is comprised of the diprotonated species. After that, the concentration of the monoprotonated form begins to increase and reaches a maximum at pH 9.2. Finally, at pH 10.4, the monoprotonated and free amine forms are equal in concentration.

At pH 9.4, TMEDA oxidation yields a current of 20.0 uA (Figure 2.10). At this pH, it can be calculated that the monoprotonated form dominates the solution and has a concentration of 0.0763 M. On the plot for TEA at pH 9.4, the oxidative current is fairly low due to the low concentration of free amine (0.0036 M). However, moving to the next point on the TMEDA plot (the intersection of these two amines at pH 10.3), the currents for each amine are roughly equal (there is no exact point at pH 10.3 for TEA). At this pH, the concentrations of free and monoprotonated TMEDA are 0.0596 M and 0.0965, respectively. For TEA, the concentration of free amine is 0.0277 M. This shows that the concentration of totally free nitrogens on TMEDA is 4.3 times higher than the conc. of free nitrogens on TEA. If the monoprotonated TMEDA molecules are included in this comparison, the ratio of oxidizable nitrogens rises to 7.8:1 (TMEDA:

TEA). This clearly shows that while the effect is not as drastic as for the secondary amine systems, the neighboring ion effect does inhibit the oxidation of TMEDA.

*Constant Potential Amperometry of Tri- and Tetra-amines*

The next logical step in the progression of this series was to carry out similar pH/current experiments using amines with increasing numbers of nitrogens per molecule. With LPEI being the polymer of interest for this study, a series of secondary amines was sought to study. However, secondary tri- and tetra- amines are not commercially available and are difficult to synthesize from amines like diethylenetriamine (Figure 2.11), as methylation reactions are not selective enough to yield only secondary amines.

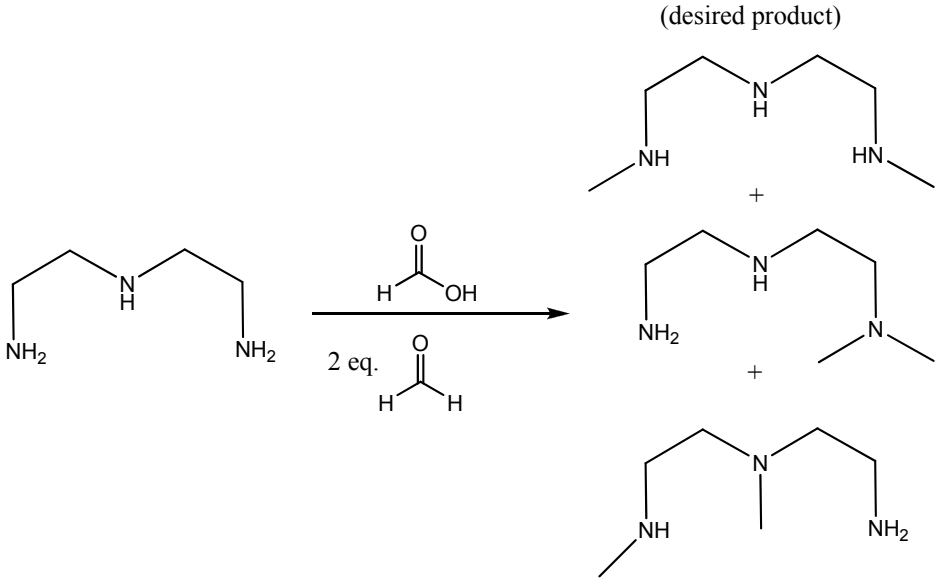


**Figure 2.11:** Possible Eschweiler Clarke methylation products of diethylenetriamine

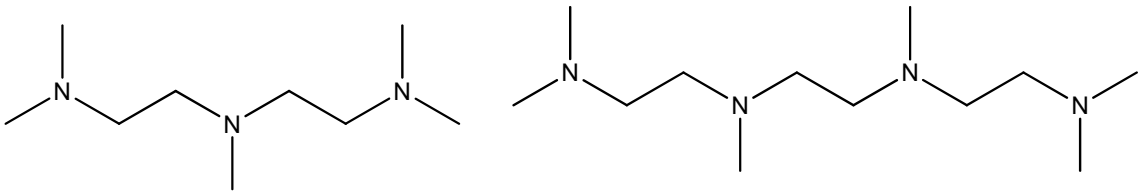

N,N,N',N'',N''-Pentamethyldiethylenetriamine (PMDTA)

$pK_a$'s = 2.4, 8.4, 9.4

N,N,N',N'',N''',N'''-Hexamethyltriethylenetetramine (HMTTA)

$pK_a$'s = 1.5, 4.8, 8.2, 9.2

**Figure 2.12:** Structures, names and $pK_a$'s of tri- and tetramines used in this study[35]

Therefore, it was necessary to use a series of tertiary amines to complete the study. Tertiary triamines and tetramines are commercially available, and Figure 2.12 depicts the tertiary amines used in this series. Experimentally, these amines were added to the triflic acid solution in the same manner as before, and Figure 2.13 shows the pH/current response for PMDTA and HMTTA on top of the previously discussed TEA and TMEDA.

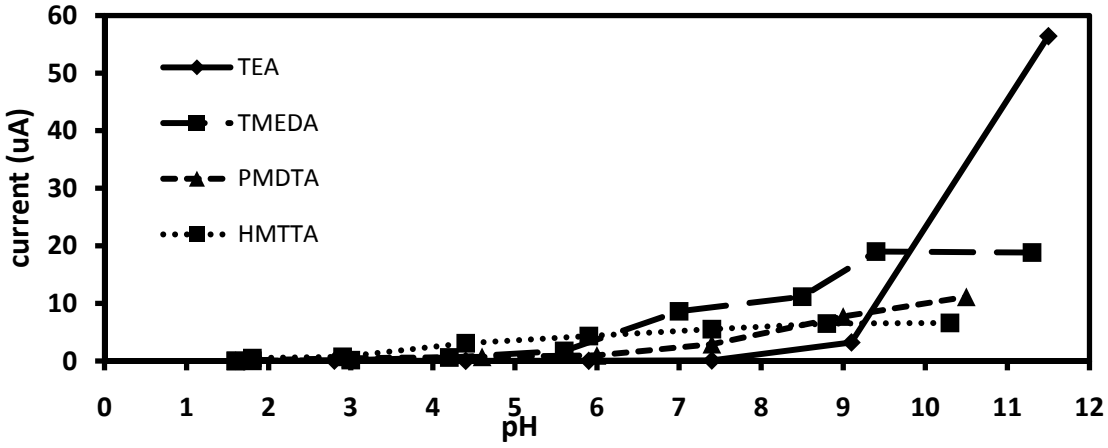


**Figure 2.13:** pH vs. current plots for tertiary amines at 1.0 V vs. SCE, 0.1M triflic acid, stirring

The highest pH values obtained by the addition of PMDTA and HMTTA are both lower than the maximum pH values from TEA and TMEDA. This indicates an overall lower basicity of triamines and tetramines (as reflected in their $pK_a$ values[35]) and shows in a general sense that more nitrogens on the molecule leads to a more "buffered" system where the $pK_a$'s of individual nitrogens change drastically under different conditions. Also, at the highest pH values for each amine, the current follows the trend of monoamine> diamine> triamine> tetramine. Most likely this is due one or two protonated nitrogens on PMDTA and HMTTA greatly inhibiting oxidation of the rest of the molecule. This phenomenon fits the hypothesis that more nitrogens leads to less amine oxidation and be explained further by a hypothetical statistics argument.

Assuming that at a certain pH, one out of every three nitrogens in an aqueous amine solution is protonated (Figure 2.14). For TEA, one protonation deactivates one amine but leaves two completely "free" amines which can be oxidized. For TMEDA, one protonation completely deactivates one nitrogen, moderately deactivates another nitrogen, and leaves one "free" nitrogen on a separate molecule. For PMDTA, one protonation completely deactivates one nitrogen and moderately deactivates two nitrogens (Figure 2.14). This type of analysis is by no means meant to be an exact prediction of how these amines behave, but it does reveal how protonation begins to affect more than just one nitrogen on a poly-amine.

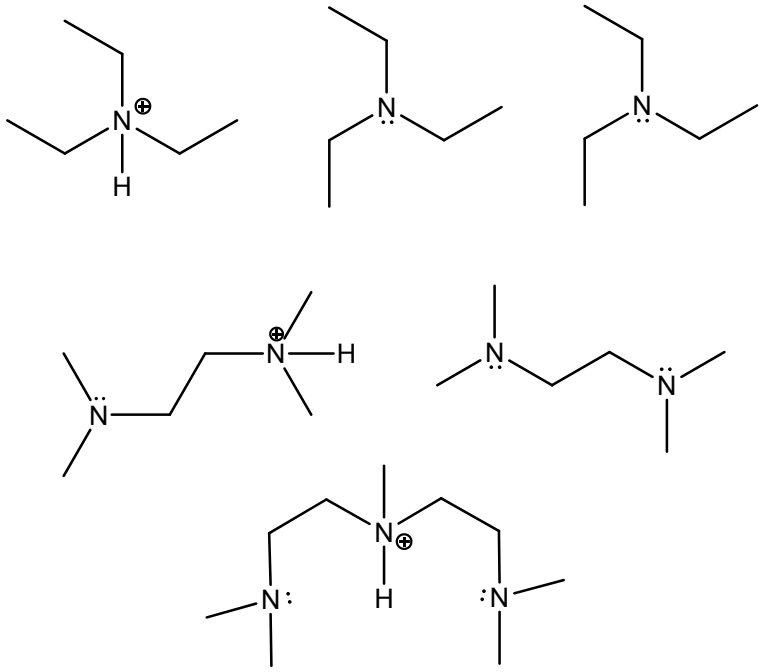

**Figure 2.14:** Deactivating effects of a single protonation for monoamines, diamines, and triamines

In Figure 2.15, which shows only on PMDTA and HMTTA, it is evident that at some of the lower and intermediate pH values, HMTTA undergoes more oxidation than PMDTA. This would seem to contradict the hypothesis that more nitrogens leads to less oxidation. However, this difference only becomes obvious after pH 3, indicating that under very acidic condtions, neither amine is oxidized significantly. The lower onset of oxidation for HMTTA can be rationalized by looking at distribution of protonated states for each molecule as shown in Figures 2.16 and 2.17.

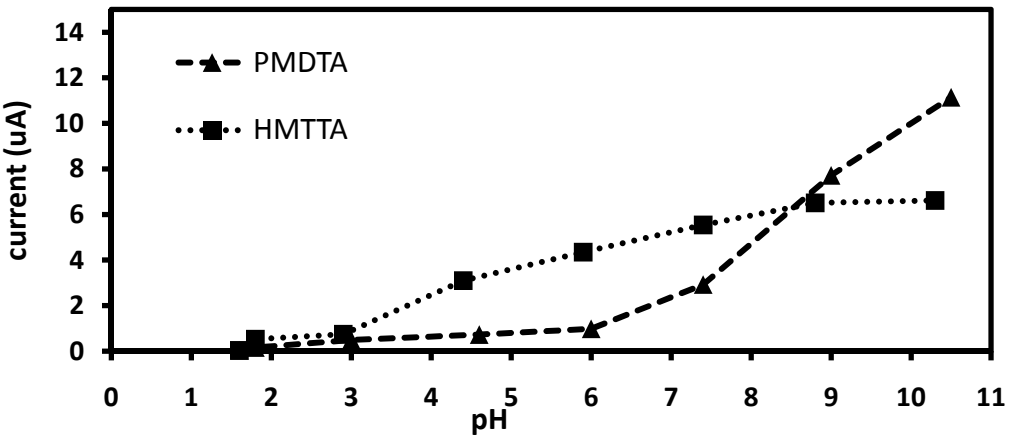


**Figure 2.15:** pH vs. current plots for PMDTA and HMTTA

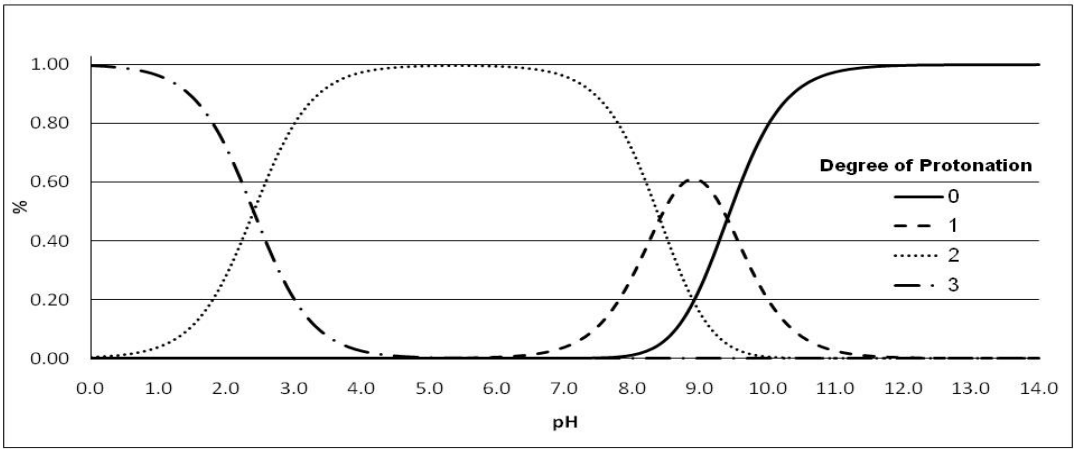


**Figure 2.16:** Protonation distribution for PMDTA

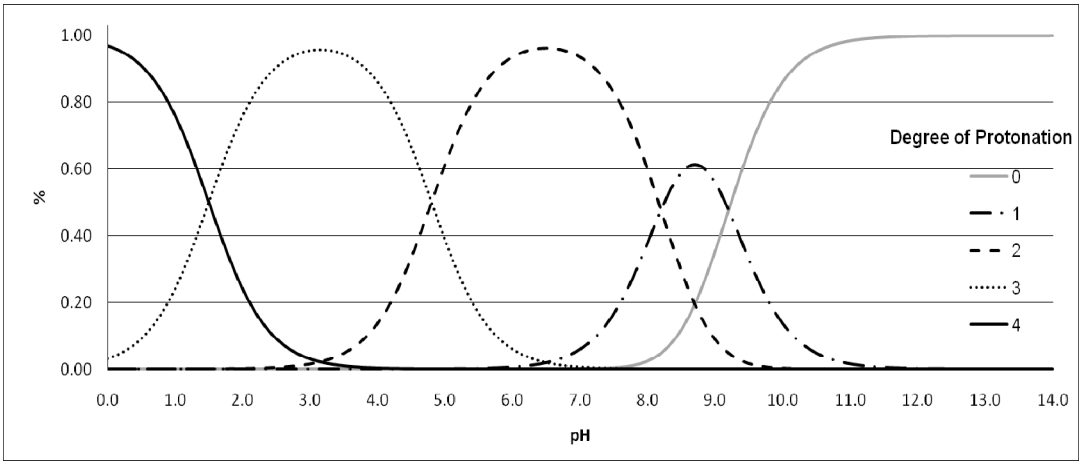


**Figure 2.17:** Protonation distribution for HMTTA

As seen in the above figures, PMDTA and HMTTA have similar protonation distributions at pH values greater than 8.0, but they differ at lower pH values due to the extra nitrogen on HMTTA. According to the prediction, PMDTA maintains a fully protonated or di-protonated state from pH 0 through about 7. This behavior is most likey responsible for the fact that the oxidative current for PMDTA does not increase significantly until around pH 7. The addition of a third positive charge onto an already di-protonated molecule is simply energetically unfavorable at this potential. On the other hand, due to its two acidic protons, two of the four nitrogens on HMTTA become slightly oxidizable beginning at pH 3.0. This behavior is mostl likely responsible for the low oxdiation onset potential on this plot. At a pH of ~ 8.5 on the pH vs. current plot, the currents for each amine are similar. This can also be rationalized by the protonation distribution as each amine solution contains about 50% monoprotonated amine and 50% diprotonated amine. Once the solutions reach a pH of 10.5, the free amine dominates the protonation distribution and the phenomenon occurs similar to the diamine/monoamine comparison in which a higher concentration of free HMTTA (1.6 times higher) actually yields a lower current relative to PMDTA. These two examples of "oligo-amines" show how model compounds provide a good estimation of what the larger polymer could behave like, but also show that model compound results might not be completely consistent with what is expected with the polymer. The somewhat backwards behavior of HMTTA between pH 3 and 8.5 could just be an exception in the progression from monoamines to polyamines where adding a nitrogen actually makes the molecule easier to oxidize under certain conditions.

Overall, the progression from a monoamine to tetramine shows that as more nitrogens are added to the molecule, two consequences arise dealing with the oxidation of the molecules: On one hand, adding nitrogens to the molecule seems to lower the pH at which oxidation starts, which is due to the lower $pK_a$'s of polyprotonated polyamines. However, once the oxidative current begins to appear, each added nitrogen inhibits the oxidation more and more at intermediate and high pH values.

*Constant Potential Amperometry of Polyamines*

Figure 2.18 shows the pH vs. current plots for PMDTA, HMTTA, and polymethyl(ethylenimine) (PMEI). A remarkable change occurs in the behavior of PMEI vs. the behavior of PMDTA and HMTTA. Instead of reaching a certain pH and showing an increase in current, the oxidation of PMEI never seems to increase when compared to the other two amines. This shows that extending the molecule from small to polymeric results in a significant change in the ease of oxidation at intermediate and high pH values, most likely due to a large neighboring ion effect.

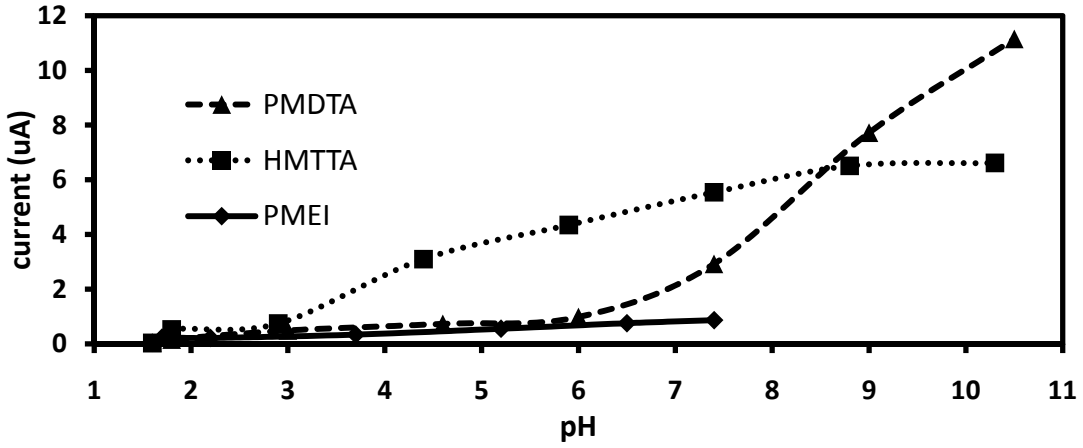


**Figure 2.18:** pH vs. current plots for PMDTA, HMTTA, and PMEI at 1.0 V vs. SCE, 0.1M triflic acid, with stirring

As was discussed in the introduction, at low pH values, polyamines have been speculated to have a significant amount of free nitrogens due to the saturation of positive charges on the molecule. However, the result of this experiment shows that all of the amines including PMEI are difficult to oxidize under acidic conditions, which further verifies that the neighboring ion effect can prevent oxidation of free nitrogens on polyamines. Using the simple model in Figure 2.14, it would seem that in order for PMEI to retain this behavior across the whole pH range, it must remain approximately 33% protonated - even at more neutral pH values. This amount of protonation would result in each nitrogen being protonated or next to a protonated nitrogen, thereby deactiviating it from being oxidized. However, a closer look reveals that PMEI may not be quite as stable as it appears.

Figure 2.19 shows the pH vs. current plots for PMEI and LPEI. This enlargement of the PMEI plot reveals a slight increase in oxidative current with increasing pH, although the maximum current reached is a mere 1 uA.

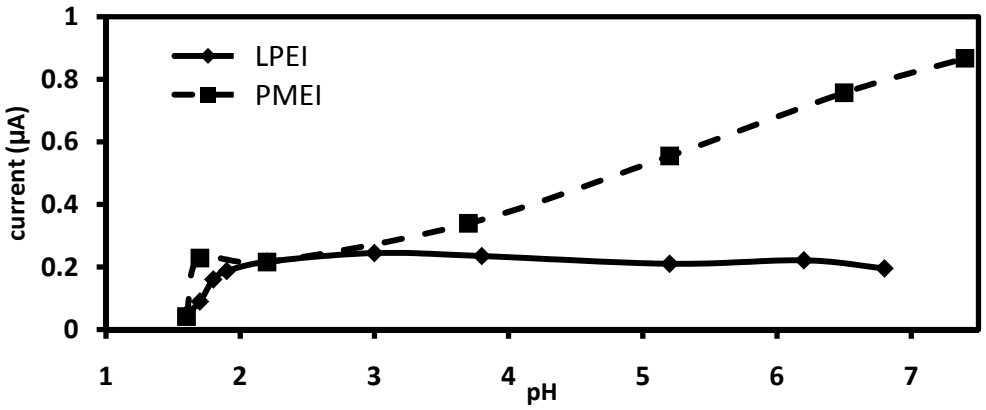


**Figure 2.19:** pH vs. current plots for the polymeric amines LPEI and PMEI

On the other hand, after a small initial increase in current, the oxidative current for LPEI stays constant across a wide range of pH values and only reaches ~0.2 uA at pH

6.8 (pH values higher than this were not accessible with LPEI due to precipitation of the polymer). These slightly different behaviors mimic the differences in the pH vs. current plots for N,N'-DMEDA and TMEDA. The oxidative current of the secondary amine forms a plateau, while the tertiary amine current continues to increase with increasing pH.

LPEI is a secondary polyamine, which means that it should be more difficult to oxidize than PMEI, a tertiary polyamine. This hypothesis is confirmed both at low pH and high pH. When analyzing the very acidic region below pH 2, the initial rise in oxidative current which appears for each polymer is surprising considering the expected amount of protonation. It can be hypothesized that a few nitrogens on each polymer which may not be affected by protonation or neighboring ions could contribute to this initial rise in current at low pH. This initial rise is slower for LPEI than for PMEI, showing the enhanced stability of the secondary amine groups. After pH 2.0, the current for PMEI continues to rise, showing that a small increase in "free" nitrogens from increasing the pH results in a small rise in oxidative current. However, the current for LPEI after pH 2.0 stays constant, indicating that the number of nitrogens which remain protonated is enough to prevent any further oxidation of neighboring nitrogens. It is estimated that at pH 4.1, LPEI is ~70% protonated,[26] which would provide more than enough neighboring ion effects to prevent significant oxidation. As the pH increases, it is expected that LPEI becomes less protonated, but from the results of this experiment, it can be estimated that even at values as high as pH 6.8, ~33% of the nitrogens remain protonated. This would indicate a fairly low $pK_a$ for LPEI.

It is impossible to directly test this hypothesis by simply adding LPEI to water and taking a pH measurement, as LPEI is only soluble in water above 80$^{o}$ C. However, low molecular weight LPEI ($M_n$ = 423) is soluble in water at room temperature and could be used for an estimate of the pKa of LPEI. When a 0.1 solution of LMW LPEI was made in neutral water, the pH rose to 10.0. Using fundamental acid-base calculations, this means that LMW LPEI has a $pK_b$ of 7.0. Accordingly, the $pK_a$ of protonated LMW LPEI can be calculated to be 7.0 (pKa + pKb = 14.0). This is much more acidic than normal amines, but that is to be expected due to the aforementioned neighboring ion effects. If we assume that this $pK_a$ stays the same under all conditions (most certainly not true, but some assumptions must be made), it can be calculated that up to pH 7.3, one third of all nitrogens are protonated, which is enough to prevent significant electrochemical oxidation. A similar experiment using a 0.1 M solution of PMEI yields a pH of 9.7. From this, it can be calculated that the $pK_a$ of protonated PMEI is 6.4, which is lower than that of protonated LPEI. This lower $pK_a$ in combination with the more easily oxidized tertiary nitrogens most likely leads to the behaviour of PMEI in Figure 2.18 which shows a slight increase in current as the pH increases.

*Aqueous Electrochemistry of Imidazole Relative to PMEI and LPEI*

In order to apply these findings to the real-world problem of oxidative instability, the obvious quesiton to ask is how this relates to more established proton conducting materials that are used in fuel cells. Imidazole is an amine with lone pairs of electrons that could be oxidized electrochemically. Polymers with tethered

imidazoles have been studied as materials for PEMFCs due to the favorable proton-conducting properties of imidazole.[36-39] Imidazole is known to undergo electrochemical oxidation and can undergo electropolymerization reactions similar to pyrrole and thiophene.[40] It is oxidized in organic solvents at potentials in the same range as aliphatic amines,[40] so it is a bit surprising that none of the fuel cell research using imidazole mentions concerns about stability or side reactions. Figure 2.20 shows the pH vs. current plot for PMEI, LPEI, and imidazole. The results of these experiments show that imidazole is very electrochemically stable at 1.0 V vs. SCE across a wide range of pH values. This stability probably arises from one nitrogen lone pair being deocalized into the aromatic pi system, and the other lone pair being on a nitrogen which is protonated under acidic conditions, making it unlikely to oxidize. Imidazole has a pKa of 7.0, and therefore neutral imidazole is not present in significant amounts until the pH rises above 6.0 (according to a protonation distribution plot, not shown).

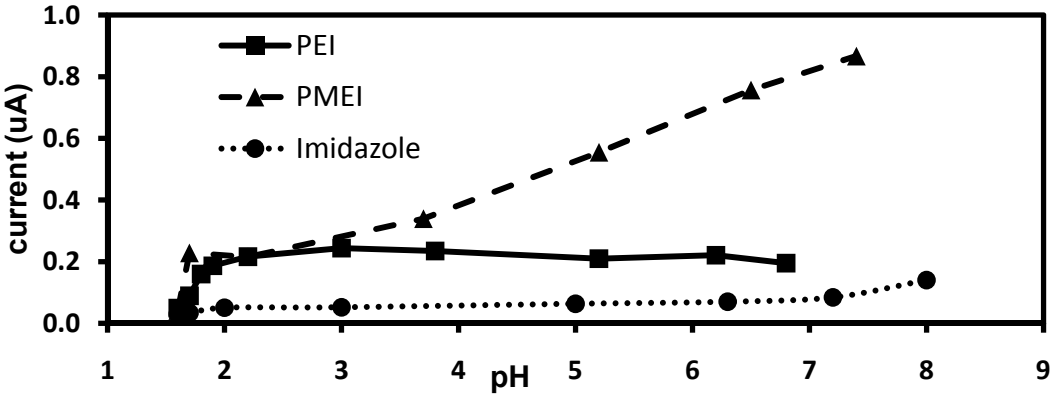


**Figure 2.20:** pH vs. current plots for LPEI, PMEI, and imidazole at 1.0 V vs. SCE, 0.1M triflic acid, stirring

Furthermore, even after significant amounts of neutral imidazole are present at neutral and slightly basic conditions, the available lone pair is located on an $sp^2$-hybridized carbon, which lowers the stability of any positive charge that might be formed there.

When comparing the results for imidazole to the plot for PMEI, it is evident that imidazole is slightly more stable than PMEI at more acidic pH values and significantly more stable than PMEI as the pH increases. For LPEI and imidazole, the trends are similar to each other. An initial rise (appears very small for imidazole) in the current for each species is followed by a plateau which contintues out to neutral pH's. The plateau for imidazole occurs at roughly four times lower current, which indicates that it is slightly more stable that LPEI to oxidation. However, one must remember that the primary application for this study is the use of these materials as membranes in fuel cells, which operate under acidic conditions. Therefore the acidic region of the graph is the most useful for this applications.

Figure 2.21 shows the lower pH region of the plot in figure 2.19. From these plots, it is evident that PMEI is not as stable as imidazole and LPEI at low pH as illustrated by the 230 nA jump in current after the first addition of the polymer. However, the initial increase in current for PEI is much less significant. The error in this experiment would most likely be larger than the error obtained in the experiments using simple monoamines. Polymer systems are much more complex than simple amines and therefore experimental results could vary from one trial to another. Therefore, it can be concluded that the initial increase in current from the addition of PEI to triflic acid is insignificant with respect to the background current. The stabilities

of LPEI and imidazole under acidic conditions are similar and neither compound undergoes any siginificant oxidation.

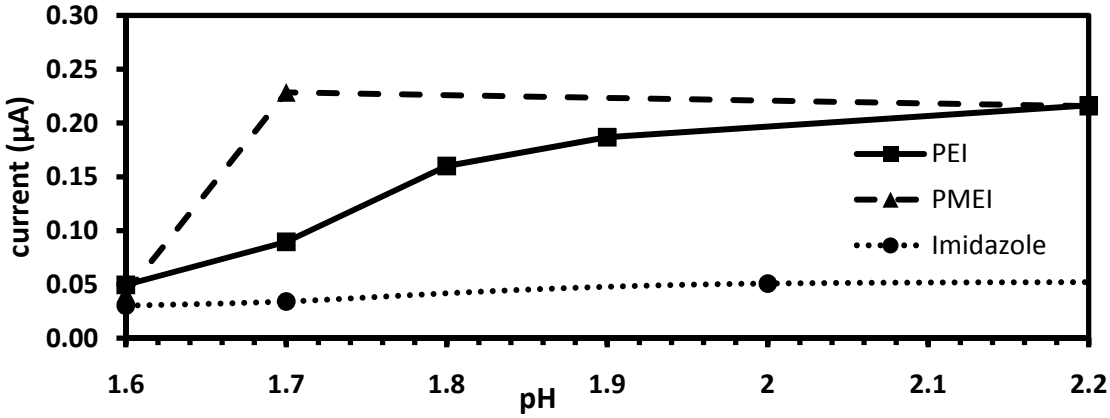


**Figure 2.21:** Low pH region of Figure 2.19 showing pH vs. current plots for LPEI, PMEI, and imidazole at 1.0 V vs. SCE, 0.1M triflic acid, stirring

*Conclusions*

Using qualitative electrochemical analysis, a progression of mono, di-, tri-, and tetra- amines have been examined as model compounds for the polyamines LPEI and PMEI. At pH values less than 3, every amine studied is fully protonated and therefore not significantly oxidized. At higher pH values, partially and fully free amine species became more prominent in solution and could be oxidized. As the series of amines progresses from 1 nitrogen to 2, 3, and 4 nitrogens, the pH where this electrochemical oxidaiton begins becomes lower due to the increased acidity of polyprotonated amines. This result was initially discouraging. However, this neighboring ion effect lowers the maximum amount of oxidation that is possible on a given amine, and each successive addition of a nitrogen actually inhibits electrochemical oxidation at intermediate and high pH values.

Unfortunately, the cyclic voltammetry of diamines did not yield distinct redox potentials of the mono-protonated and free amine species. That is, a clear shift to a higher potential $E_{pa}$ was not seen in the transition from free amine to mono-protonated amine, meaning that no exact change in potential can be assgined to the neighboring ion effect. What was clear was that the onset of oxidation for the free amine is much lower than for the mono-protonated amine, indicating an increase in the ease of oxidation.

This series of small molecule amines culminated with the polymers, which showed dramatic increases in stability (at intermediate pH values) relative to their model compounds. It has been shown that in aqueous media, LPEI and PMEI behave much differently than normal aliphatic amines under electro-oxidative conditions. For PMEI, a slow but steady rise in electro-oxidative current occurss corresponding to an increase in pH. This indicates that tertiary amines should only be used under acidic conditions when potentials of 1.0 V (vs. SCE) are applied. Conversely, LPEI does not undergo a significant amount of oxidation at sufficiently low pH values and at higher pH values it retains a constant level of electrochemical stability comparable to that of imidazole, which is considered an accecptable material for use in PEMFC's. Because of this, LPEI should be considered an acceptable substrate for PEM fuel cells which operate under acidic conditions. This study also revealed that LPEI is fairly oxidatively stable at intermediate pH values when subjected to a potential of 1.0 V vs. SCE. This shows that LPEI is an acceptable substrate for glucose biosensors and biofuel cells as they normally operate in the potential range of -0.1 V to 0.8 V vs. SCE, where oxidation of the amine groups would be even less significant.

## References


1. Kundu, S.; Simon, L. C.; Fowler, M.; Grot, S., *Polymer* **2005,** *46* (25), 11707-11715.

2. Rama, P.; Chen, R.; Andrews, J., *Proceedings of the Institution of Mechanical Engineers Part a-Journal of Power and Energy* **2008,** *222* (A5), 421-441.

3. Alentiev, A.; Kostina, J.; Bondarenko, G., *Desalination* **2006,** *200* (1-3), 32-33.

4. Casciola, M.; Alberti, G.; Sganappa, M.; Narducci, R., *J. Power Sources* **2006,** *162* (1), 141-145.

5. Zawodzinski, T., *J. Electrochem. Soc.* **1993,** *140* (4), 1041-1047.

6. Yoshitake, M.; A.Watakabe, Perfluorinated Ionic Polymers for PEFCs (Including Supported PFSA). In *Adv. Polym. Sci.*, Springer: 2008; Vol. 215, pp 127-155.

7. Liu, Y. H.; Yi, B. L.; Shao, Z. G.; Xing, D. M.; Zhang, H. M., *Electrochem. Solid St.* **2006,** *9* (7), A356-A359.

8. Maier, G.; Meier-Haack, J., Sulfonated Aromatic Polymers for Fuel Cell Membranes. In *Adv. Polym. Sci.*, Springer: 2008; Vol. 216, pp 1-62.

9. Lund, H.; Hammerich, O., *Organic Electrochemistry*. 4 ed.; Marcel Dekker: 2001.

10. Mann, C. K., *Anal. Chem.* **1964,** *36* (13), 2424-&.

11. Barnes, K. K.; Mann, C. K., *J. Org. Chem.* **1967,** *32* (5), 1474-&.

12. Masui, M.; Sayo, H.; Tsuda, Y., J. Chem. Soc. *B* **1968,** (9), 973-&.

13. Adenier, A.; Chehimi, M. M.; Gallardo, I.; Pinson, J.; Vila, N., *Langmuir* **2004,** *20* (19), 8243-8253.

14. Portis, L. C.; Bhat, V. V.; Mann, C. K., *J. Org. Chem.* **1970,** *35* (7), 2175-&.

15. Chiba, T.; Takata, Y., *J. Org. Chem.* **1977,** *42* (18), 2973-2977.

16. Smith, P. J.; Mann, C. K., *J. Org. Chem.* **1969,** *34* (6), 1821-&.

17. Ue, M.; Takeda, M.; Takehara, M.; Mori, S., *J. Electrochem. Soc.* **1997,** *144* (8), 2684-2688.

18. Dubois, J. E.; Monvernay, A. D.; Lacaze, P. C., *Electrohcimica Acta* **1970,** *15*, 315-323.

19. Sanders, R. A.; Snow, A. G.; Frech, R.; Glatzhofer, D. T., *Electrochemica Acta* **2003,** *48*, 2247-2253.

20. Snow, A. G.; Sanders, R. A.; Frech, R.; Glatzhofer, D. T., *Electrochemica Acta* **2003,** *48*, 2065-2069.

21. Glatzhofer, D. T.; Erickson, M. J.; Frech, R.; Yepez, F.; Furneaux, J. E., *Solid State Ionics* **2005,** *176*, 2861-2865.

22. Giffin, G. A.; Castillo, F. Y.; Frech, R.; Glatzhofer, D. T.; Burba, C. M., *Polymer* **2009,** *50*, 171-176.

23. Merchant, S.; Glatzhofer, D. T.; Schmidtke, D. W., *Langmuir* **2007,** *23*, 11295.

24. Merchant, S.; Tran, T. O.; Meredith, M. T.; Cline, T. C.; Glatzhofer, D. T.; Schmidtke, D. W., *Langmuir* **2009,** *25* (13), 7736-7742.

25. Merchant, S.; Meredith, M. T.; Tran, T. O.; Brunski, D.; Johnson, M. B.; Glatzhofer, D. T.; Schmidtke, D. W., *J. Phys. Chem. C, ASAP* **2010**.

26. Kobayashi, S.; Hiroishi, K.; Tokunoh, M.; Saegusai, T., *Macromolecules* **1987,** *20*, 1496-1500.

27. Smits, R. G.; Koper, G. J. M.; Mandel, M., *J. Phys. Chem.* **1993,** *97*, 5745-5751.

28. Bianchi, A. B. A.; Garcia-Espana, E.; Micheloni, M.; Ramirez, J. A., *Coord. Chem. Rev.* **1999**, 97-156.

29. York, S.; Frech, R.; Snow, A.; Glatzhofer, D., *Electrochim. Acta* **2001,** *46*, 1533-1537.

30. Tanaka, R.; Ueoka, I.; Takaki, Y.; Kataoka, K.; Saito, S., *Macromolecules* **1983,** *16*, 849-853.

31. Lide, D. R., *CRC Handbook of Chemistry and Physics*. 87 ed.; Taylor and Francis: Boca Raton, FL, 2007.

32. Bjerrum, J., J. *Chem. Soc., London* **1958**.

33. Herlem, G.; Reybier, K.; Trokourey, A.; Fahys, B., *J. Electrochem. Soc.* **2000,** *147* (2), 597-601.

34. Herlem, G.; Goux, C.; Fahys, B.; Dominati, F.; Goncalves, A. M.; Mathieu, C.; Sutter, E.; Trokourey, A.; Penneau, J. F., *J. Electroanal. Chem.* **1997,** *435* (1-2), 259-265.

35. Rometsch, R.; Marxer, A.; Miescher, K., *Helv. Chim. Acta* **1951,** *34* (5), 1611-1618.

36. Frutsaert, G., *J Polym Sci A1* **2009**, 223-231.

37. Munch, W.; Kreuer, K. D.; Silvestri, W.; Maier, J.; Seifert, G., *Solid State Ionics* **2001,** *145* (1-4), 437-443.

38. Schuster, M. F. H.; Meyer, W. H.; Schuster, M.; Kreuer, K. D., *Chem. Mater.* **2004,** *16* (2), 329-337.

39. Scharfenberger, G.; Meyer, W. H.; Wegner, G.; Schuster, M.; Kreuer, K. D.; Maier, J., *Fuel Cells* **2006,** *6* (3-4), 237-250.

40. Wang, H. L.; Omalley, R. M.; Fernandez, J. E., *Macromolecules* **1994,** *27* (4), 893-901.

# CHAPTER 3: EFFECT OF SUBSTITUTION PERCENTAGE ON THE ELECTROCHEMICAL PROPERTIES OF FERROCENE-MODIFIED LINEAR POLY(ETHYLENIMINE)

## Introduction

The treatment and management of diabetes is a growing concern as 23.6 million Americans were officially diagnosed with the disease as of 2007.[1] In addition to this group of people, another 57 million are "pre-diabetic," meaning that they are predisposed to the condition.[1] As such, there is a large demand for the development of better materials for use in the monitoring of blood-glucose levels, both *in vitro* and *in vivo*. Most currently used glucose sensing devices come in the form of testing strips. They use mediated electron transfer between an enzyme (glucose oxidase) and an electrode to determine the amount of glucose present in a sample of blood. The mediator and enzyme are normally immobilized in some type of polymer or gel on top of an electrode, and this effectively "wires" the enzyme to the electrode. Devices using this technology have been shown to exhibit reproducible results, high current response, and high sensitivity.[2-5] A more ideal system for glucose monitoring would be a fully implantable sensor which can give glucose concentrations in real time and be replaced as needed (ideally after multiple weeks of use). This technology requires a system that has all of the properties listed above as well as low cost, high stability, low operating potential, and biocompatibility. Very few of the systems currently used for diabetes management exhibit all of these properties, and many improvements in biosensor development must be made in order to realize the goal of a cheap, reliable implantable sensor.

One way that mediated electron transfer between enzyme and electrode can be achieved is through the use of redox polymers. A redox polymer consists of a polymer backbone with redox centers covalently attached to it. Normally, the redox polymer also has reactive sites which can be used to cross-link the polymer. When the polymer, enzyme, and a cross-linker are all mixed together and allowed to react, a cross-linked, semi-permeable hydrogel forms which allows for the flow of ions, water, and other small molecules (i.e. glucose) in and out of the film. Heller's group has demonstrated that osmium-based redox polymers can effectively wire glucose oxidase to an electrode[6-8] and this technology has even been used industrially for diabetes management.[9] Current densities as high as 1 mA/cm$^2$ (at 37$^o$ C)[2] have been achieved using these redox polymers and they are considered to be the benchmark for mediated electron transfer with glucose oxidase. Drawbacks to using osmium-based redox polymers are the price of osmium reagents and the fact that osmium (in its free form) is extremely toxic, which could be a deterrent for *in vivo* applications. Because of these drawbacks, there is a need for cheap, safe, mediated electron transfer systems which can be used in glucose biosensors.

Recently, our group synthesized a new redox polymer based on the attachment of ferrocene to linear poly(ethylenimine) (LPEI) (Figure 3.01). In addition to having interesting fundamental redox characteristics,[10] Fc-$C_1$-LPEI can effectively enhance the

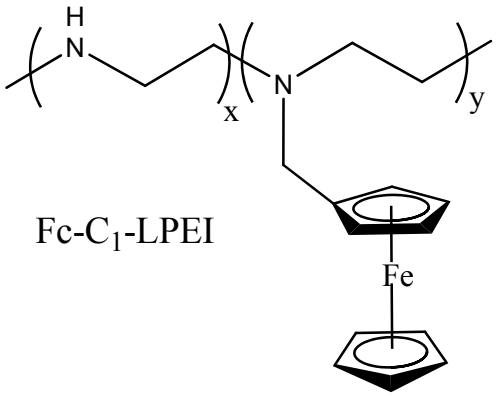


**Figure 3.01**: Structure of Fc-$C_1$-LPEI(x%)

communication between glucose oxidase and an electrode surface by "wiring" the enzyme through the ferrocene groups.[5, 10] Glucose sensors fabricated with this polymer were sensitive to small changes in glucose concentration (73 nA/cm$^2$·μM ) and had limiting current densities of 1.2 mA/cm$^2$ at room temperature. These high current densities, which were among the highest values obtained using ferrocene-based redox polymers, did not seem to be due to high electron diffusion coefficients ($cDe^{1/2}$), which were three orders of magnitude lower than those reported for osmium-based redox polymers with similar current densities.[2, 10] This led us to believe that some factor other than electron diffusion was responsible for the high current densities obtained with sensors made with Fc-$C_1$-LPEI.

As with any new material, optimization of all of the variables involved in the fabrication and operation processes was important. The different variables which were previously optimized were crosslinker percent, enzyme percent, buffer, and pH.[5, 10] One aspect of sensor performance which was not optimized was the amount of ferrocene substitution on the nitrogens. Optimization of this parameter was slightly more difficult as it required considerable synthetic work and the development of a new synthetic method for making the polymers. However, studying the effect of ferrocene substitution on the polymer backbone could lead to a better understanding of the behavior of biosensors made with Fc-$C_1$-LPEI and why they exhibit such high current responses to glucose while having only moderate electron diffusion coefficients ($D_{app}$). This study will cover the optimization of ferrocene substitution percentage on LPEI through the use of a new method for synthesizing the polymer. Also, the fundamental solution electrochemistry of this series of redox polymers will be investigated in order

to learn more about the general electrochemical properties of the polymers and gain more insight into their behavior as cross-linked hydrogels.

## Results and Discussion

*Development of the Synthetic Method*

The original synthesis for Fc-$C_1$-LPEI (Figure 3.02) involved the reductive amination of ferrocene carboxaldehyde with LPEI. This method was fairly simple and could be carried out in a short amount of time. However, the inherent mechanism of the method prevented the synthesis of higher amounts of ferrocene substitution: When more than 0.15 equivalents of ferrocene carboxaldehyde were added, the LPEI backbone became saturated with positive charges from iminium ion formation, and the polymer precipitated out of the methanolic solution. Once this happened, the mixture was no longer homogeneous and the reaction could not yield an evenly substituted product.

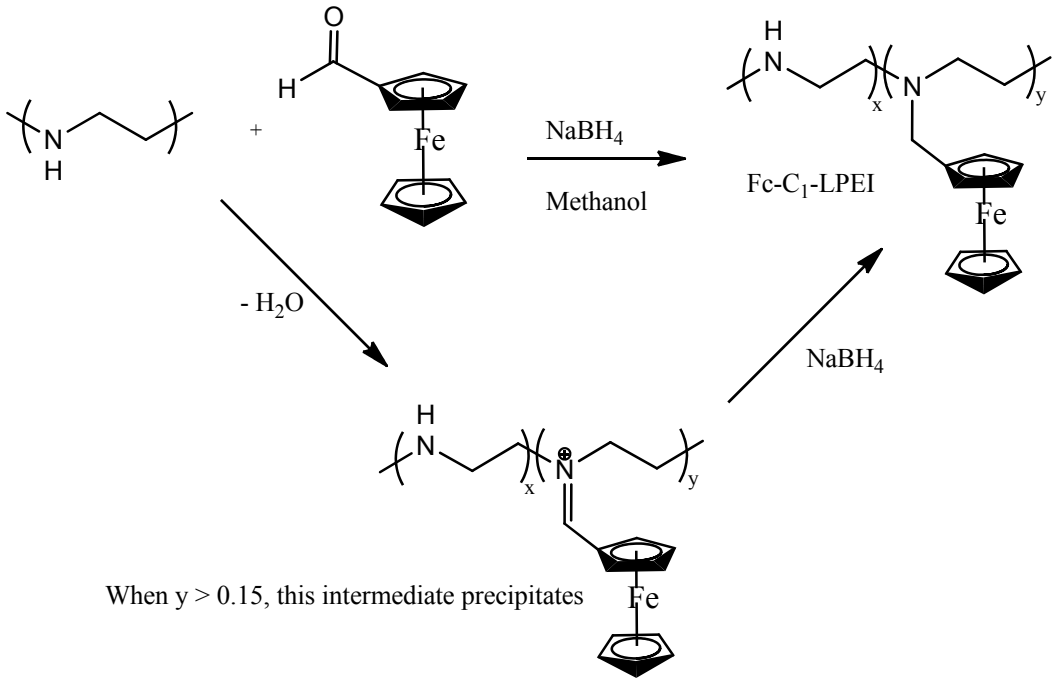


**Figure 3.02:** Original synthesis of Fc-$C_1$-LPEI including iminium intermediate

A method was sought out which would avoid this problem and allow for the synthesis of homogenous polymers which were substituted anywhere from 1% to 100%.

Ferrocene is a well-studied compound and has been shown to undergo electrophilic aromatic substitution reactions under fairly mild conditions compared to benzene or other "normal" aromatics. The aminomethylation of ferrocene was one of the first electrophilic aromatic substitution reactions carried out using ferrocene.[11, 12] This reaction proved extremely useful because of the synthetic utility of the fully N-methylated salt (FcMTMAI) which was easily produced in one step from (dimethylaminomethyl)ferrocene (DMAMFc) (Figure 3.03). This compound can be converted into any number of ferrocene derivatives through simple nucleophilic addition reactions.[12, 13] Based on this reactivity, we postulated that the nitrogens on LPEI would be nucleophilic enough to add to the FcMTAMI and eliminate trimethylamine gas. If this type of reaction was carried out under basic conditions, the still-protonated substituted LPEI backbone could be neutralized *in situ* and this would prevent a saturation of positive charges on the polymer. As was hypothesized, the reaction was successful and yielded Fc-$C_1$-LPEI polymers with substitution percentages corresponding to the amount of FcMTMAI added to the reaction mixture (Figure 3.03).

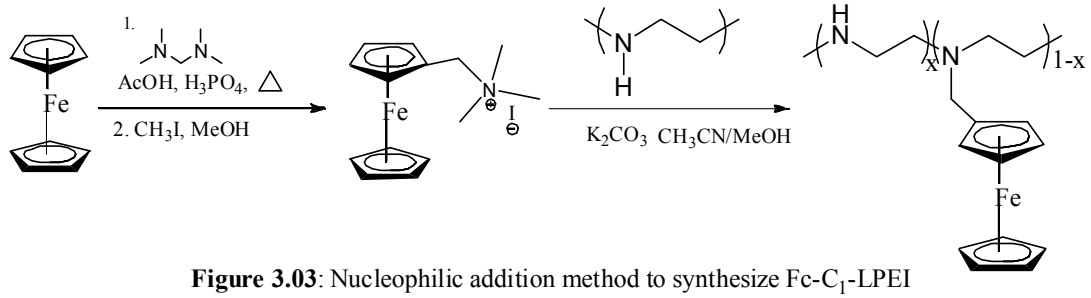


**Figure 3.03**: Nucleophilic addition method to synthesize Fc-$C_1$-LPEI

*NMR Characterization of Fc-$C_1$-LPEI(x%)*

The characterization of these polymers by NMR is worth a small discussion as it gives some insight into the general nature of the polymers and shows that NMR is a reliable method for calculating the ferrocene substitution percentage. In Figure 3.04, the spectra of six of the polymers are shown in an overlapped fashion in order to compare them effectively. The ferrocene ring protons (δ ~4.2) are split into two broad singlets, which represent the Cp ring which is tethered to the backbone and the Cp ring which is not attached to anything. The ratio of these protons to the backbone protons (δ ~2.75) increases as the substitution percentage increases. The backbone protons appear as a large, broad singlet with a small hump slightly upfield. This small hump increases in size with increasing substitution, indicating that it represents backbone protons which

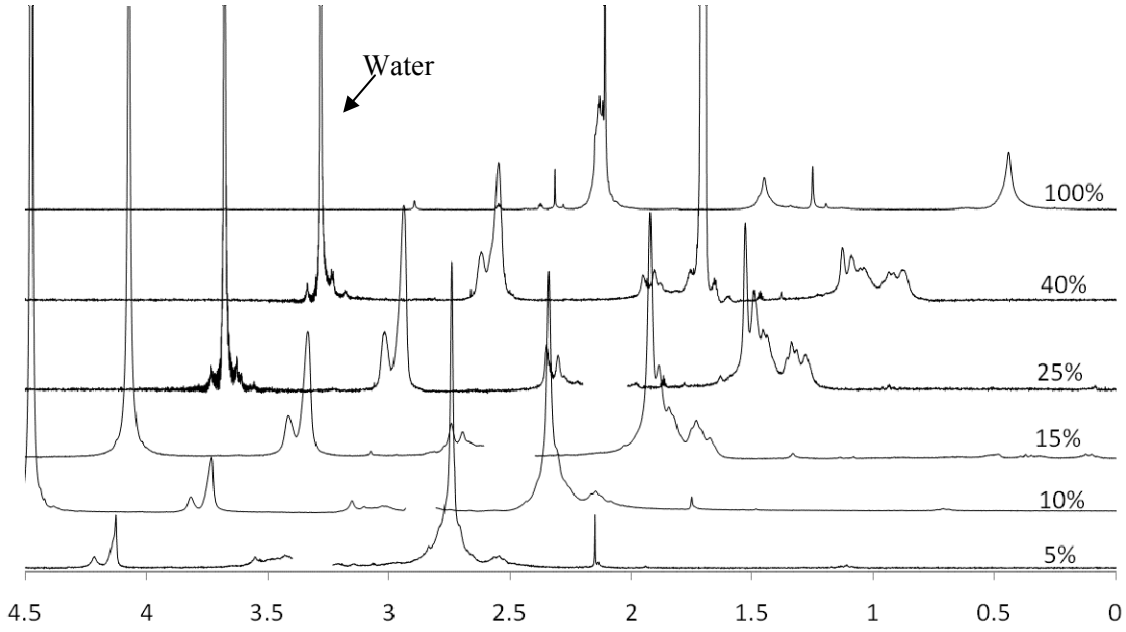


**Figure 3.04:** NMR spectra of Fc-$C_1$-LPEI(5%-100%) in $CD_3OD$ (except 100%, which was in $CDCl_3$). Spectra are offset for graphical purposes. The residual peaks from $CD_3OD$ at ca. δ 3.2 - 3.3 are removed for clarity.

are affected by the ferrocene tether. Also, as the amount of substitution increases, the amount of "disorder" in the backbone region increases due to the many possible local structures which could exist on the polymer. From 5% to 25%, the backbone region changes from a singlet with a small upfield hump to a complex multiplet. However, at 40%, the backbone region begins to become more symmetrical due to a decrease in disorder and the presence of a more regular structure (on average, almost every other nitrogen is substituted). At 100%, the whole spectrum appears roughly as it would for a model compound of the polymer due to every polymeric repeat unit being identical. These trends suggest that the ferrocene is truly being added onto the polymer backbone in a random fashion, which is desirable for attaining an even distribution of redox centers

*Solution Electrochemistry of Fc-$C_1$-LPEI and its Model Compound*

The polymers designated Fc-$C_1$-LPEI(x%) were completely new polymers and as such an investigation into their fundamental properties was important. Also, cross-linked gels of this polymer displayed interesting multi-wave redox behavior which was not easily explained,[10] so observing the electrochemical properties of these polymers under less complex conditions could reveal more about their nature when used as biosensor materials. To get an idea of what is "normal" for polymer behavior, it can be useful to examine small molecules known as model compounds. These compounds exhibit similar molecular structure to the polymer repeat units of interest and can be

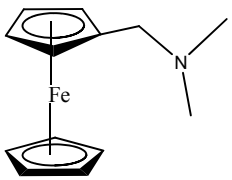


**Figure 3.05:** Structure of dimethylaminomethylferrocene, a model compound for Fc-$C_1$-LPEI

studied under similar conditions to gain insight into how the polymer of interest might behave. For Fc-$C_1$-LPEI, an appropriate model compound is (dimethylaminomethyl)ferrocene (DMAMFc), seen in Figure 3.05. DMAMFc is similar to Fc-$C_1$-LPEI in that it has a tertiary amine group two atoms away from the ferrocene. As such, its aqueous electrochemistry under different pH conditions should be a good model for what could happen with the polymer (Figure 3.06).

When the nitrogen on DMAMFc becomes protonated, the $E_{pa}$ of the molecule shifts from 220 mV to 370 mV due to the proximity of the two positive charges which are formed. There is likely to be a large electrostatic repulsion between the two positive charges, making the ferrocenium ion more unstable in the protonated species. The decrease in peak current for the neutral species was expected as it has a lower solubility in water because of the deprotonated nitrogen.

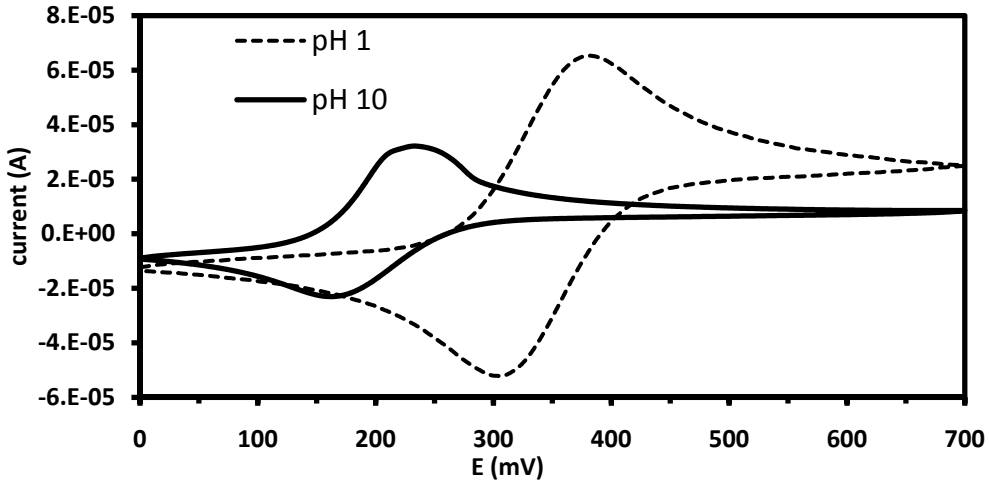


**Figure 3.06:** Cyclic voltammograms of 0.01 M DMAMFc in water with added HCl or NaOH. Scan rate = 100 mV/s

From these results, it was expected that the solution electrochemistry of Fc-$C_1$-LPEI would be similar and show pH-dependent behavior. However, the nature of un-substituted LPEI under acidic conditions raised questions as to how the ferrocene-

modified LPEI would behave electrochemically. The protonation behavior of LPEI has been studied extensively and is still not well-understood.[14-19] It is known, however, that LPEI is not 100% protonated under highly acidic conditions due to large neighboring ion effects, as discussed in the previous chapter. Because of this, it was expected that at low pH, Fc-$C_1$-LPEI might contain ferrocene groups which have two distinct oxidation potentials, corresponding to their attachment to protonated or deprotonated nitrogens.

Figure 3.07 shows the solution electrochemistry of Fc-$C_1$-LPEI(25%) under acidic and basic conditions. The first observation to note is the disappearance of the multi-wave behavior at high pH. This most likely corresponds to the complete deprotonation of the polymer backbone, leading to only one possible redox potential of the ferrocene. The anodic (oxidative) voltage at peak current ($E_{pa}$) for this oxidation occurs at 224 mV, which is identical to the $E_{pa}$ for DMAMFc at pH 10, suggesting that this peak corresponds to the fully deprotonated polymer.

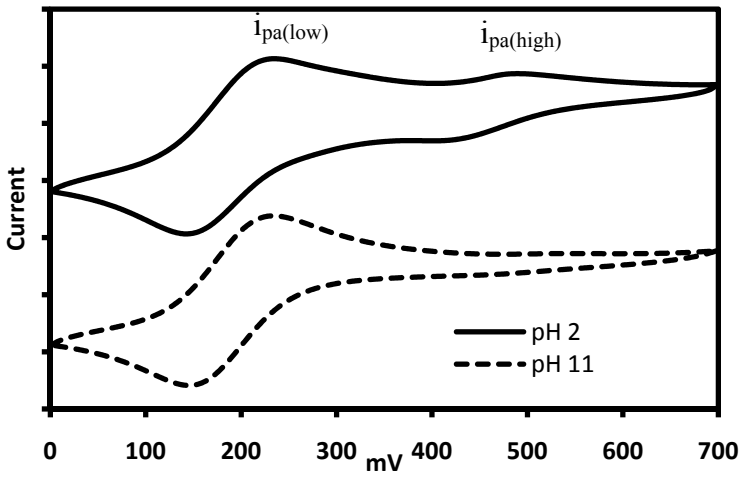


**Figure 3.07:** Cyclic voltammetry of 2 mg/mL Fc-$C_1$-LPEI(25%) under acidic and basic conditions with HCl and/or NaOH. Scan rate = 100 mV/s

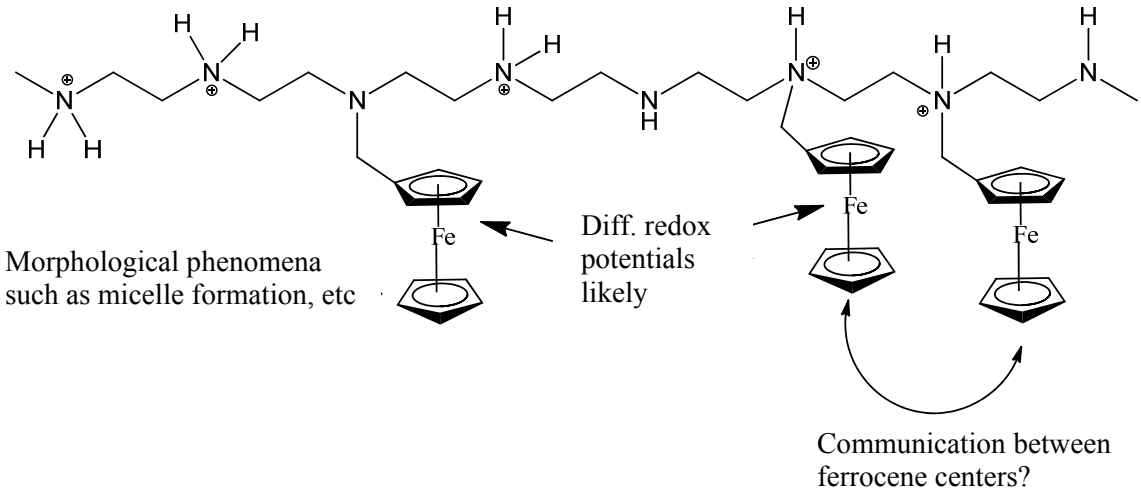


**Figure 3.08**: Snapshot of poly-protonated Fc-$C_1$-LPEI showing various phenomena that could affect the solution electrochemistry of the polymer

As expected, under acidic conditions, the plot shows that two distinct populations of ferrocene are present in solution. As outlined in Figure 3.08, the polymer system under these pH conditions is actually quite complex and these two peaks could be due to a number of different phenomena, including changes in the morphology of the polymer and communication between neighboring ferrocenes. For a similar model system investigated by Alvarez et al., communication between ferrocene centers has been shown to be hindered by the presence of positive charges,[20, 21] which suggests that the presence of the high $E_{pa}$ peak is unlikely to be due to a change in the redox potential of a neighboring ferrocene. Also, it is likely that morphological changes that could affect the electrochemistry, such as micelle formation, are minimal under acidic conditions, as LPEI has been shown to exist in an extended chain form when protonated.[15] The assumption that neither of these effects occur in the polymer means that the double-wave behavior should be primarily due to protonation effects. One further assumption which should be made when observing the cyclic voltammetry of Fc-$C_1$-LPEI is that

electron transfer to the electrode surface is much faster than proton transfer. This means that the CV is essentially a "snapshot" of the polymer, showing which substituted nitrogens are protonated at a given moment in time.

The relative amounts of each type of ferrocene (attached to a neutral or protonated nitrogen), can be estimated using the $i_{pa}$'s of the cyclic voltammogram, and the ratio of the two $i_{pa}$'s can be used to calculate the amount of protonated aminomethylferrocenyl groups on the polymer, e.g. the relative amount of protonated tertiary amines. For 25% substitution, it was calculated that 10.6% of the nitrogens substituted with ferrocene moieties were protonated at pH 2. This number seems quite small for such acidic conditions. One possible explanation for the low amount of protonation could be that a difference in pKa's between the substituted and non-substituted nitrogens caused the protons to "choose" the secondary, non-substituted amino groups over the tertiary, substituted ones. A possible way to investigate this

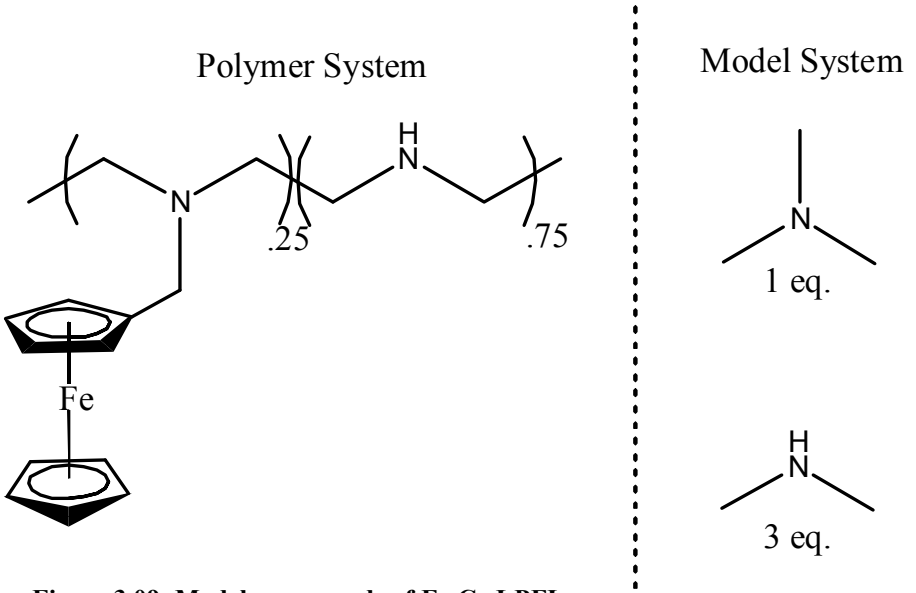


**Figure 3.09: Model compounds of Fc-$C_1$-LPEI**

hypothesis would be to examine the degree of protonation of model compounds with known pKa values. It is known that, in general, secondary amines are more basic than tertiary amines, with the difference in pKa's ranging from ~ 1 pKa unit to 0.2 pKa units, depending on which amines are being compared.[22] As shown in Figure 3.09, the closest model compounds for the two different repeat units in Fc-$C_1$-LPEI are trimethylamine (TMA) and dimethylamine (DMA). Ideally, DMAMFc should be used as the model compound for the substituted polymer unit, but its pKa is unknown. DMA and TMA have a pKa difference of 0.93,[22] which translates to DMA being almost 10 times more basic than TMA.

Using the model compounds, a theoretical experiment was simulated using the known pKa values of the amines (10.73 for DMA, 9.80 for TMA)[22] and a composition which mimics that of the Fc-$C_1$-LPEI (25% tertiary amines). Using this model system, it was calculated that a 40.2% degree of total protonation would be required to protonate 10.6% of the tertiary nitrogens in the system. The calculations also predicted that protonated tertiary amines accounted for only 6.6% out of the total 40.2%, illustrating how a small difference in pKa's can lead to a large difference in the distribution of protonated amines. Unfortunately, the 40.2% degree of total protonation could not be verified experimentally using the cyclic voltammograms of Fc-$C_1$-LPEI(25%) because the secondary, non-substituted nitrogens were not electrochemically active.

In order to investigate this phenomenon further and examine the prediction that ~40% of the nitrogens in Fc-$C_1$-LPEI were protonated, cyclic voltammetry was carried out on polymers ranging from 5% substitution to 100% substitution under acidic

conditions. Figure 3.10 shows the results of these experiments. As seen in the figure and accompanying graph (Figure 3.11), the relative amount of $i_{pa(high)}$ (as estimated by the formula $\%[i_{pa(high)}] = i_{pa(high)}/(i_{pa(high)}+i_{pa(low)})$) seems to increase linearly with increasing substitution percentage.

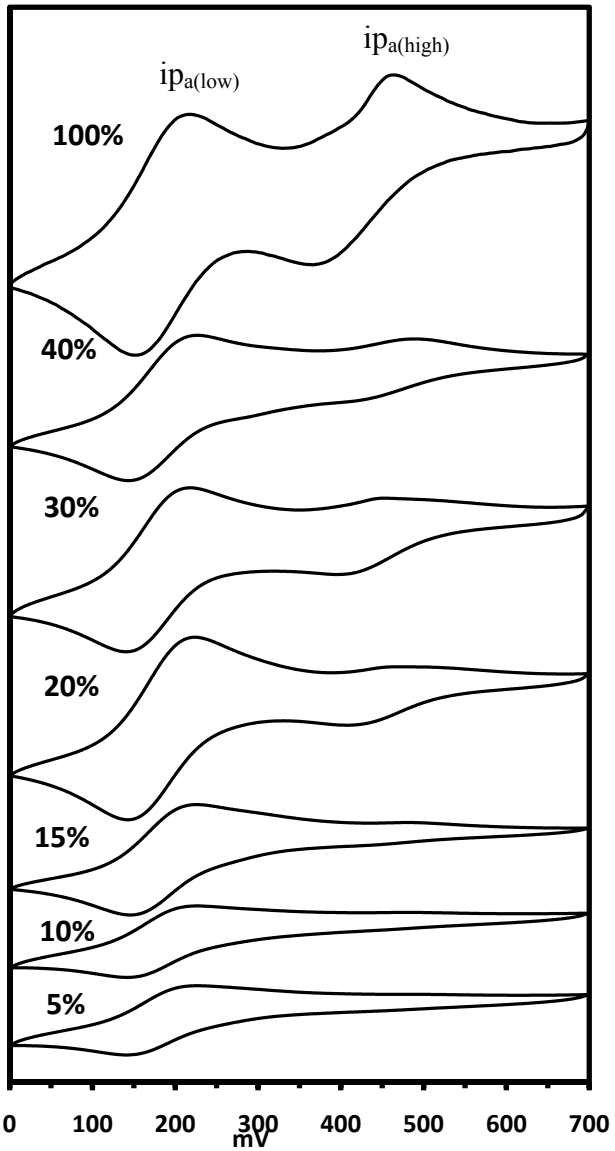


**Figure 3.10:** Cyclic voltammetry of 2 mg/mL Fc-$C_1$-LPEI(x%) at pH 2. Scan rate 100 mV/s

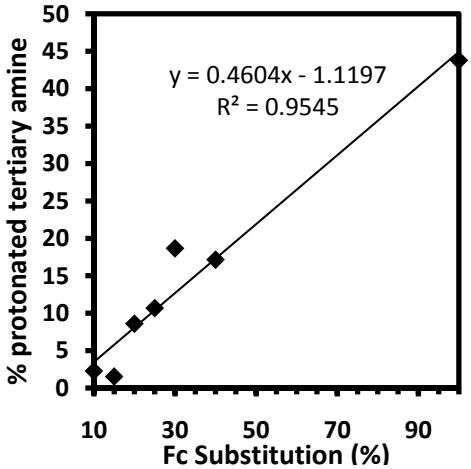


**Figure 3.11:** % tertiary amine protonation as calculated from the ratio of $ip_{a(high)}$ to $ip_{a(low)}$ from the cyclic voltammograms in Figure 3.10

At 5% substitution, there is no evidence of the higher oxidation potential species, suggesting that it either is not present at this substitution amounts or that it is too small to appear above the background current. It is possible that the pKa differences discussed above caused the tertiary amines in Fc-$C_1$-LPEI(5%) to be selectively deprotonated, which would result in the disappearance of the $i_{pa(high)}$ peak. As the substitution increased, the relative amount $i_{pa(high)}$ increased, reaching a maximum of 44% for the fully substituted polymer.

Fc-$C_1$-LPEI(100%) is a unique polymer in that every nitrogen has a ferrocene attached. This means that if protonation was the only factor affecting the aqueous electrochemistry of Fc-$C_1$-LPEI(100%), the $i_{pa(high)}/i_{pa(low)}$ ratio should be a direct measurement of protonation and could be used to calculate a pKa for the polymer with the Henderson-Hasselbalch equation. This calculation results in a pKa of 1.9, which correlates quite well with the slightly higher pKa of fully protonated LPEI (2.7, as calculated from the pH change from the addition of LPEI-HCl to neutral water), and agrees with assumption that secondary amines are more basic than tertiary amines. This also correlates well with the results in the previous chapter, which showed that neutral LPEI was more basic than neutral poly(N-methylethylenimine) (PMEI) by 0.6 pKa units.

To determine whether the difference in tertiary and secondary amine pKa's of could account for the electrochemical behavior of the series of polymers shown in Figures 3.10 and 3.11, the TMA/DMA model and calculations discussed earlier were expanded to include different amounts of each amine. Concentrations of TMA and DMA were used which mimicked the amounts of tertiary and secondary amines on the

various polymers, and plots relating the percent of protonated tertiary amines were then generated and compared to the experimental data (Figure 3.12).

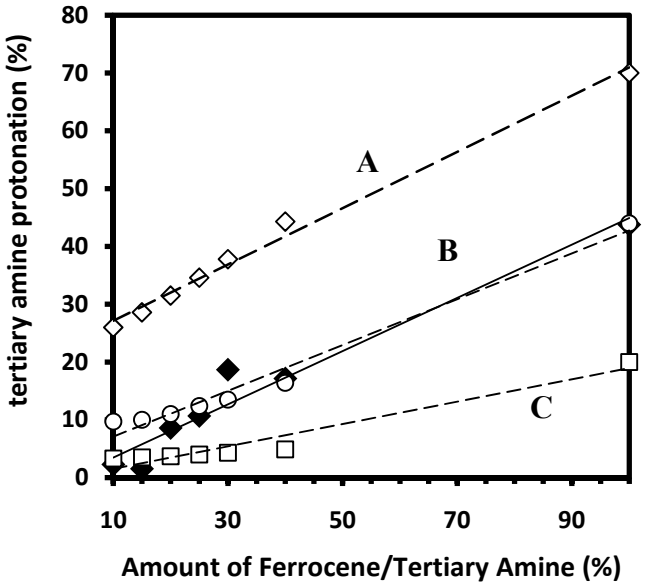


**Figure 3.12:** Percent tertiary amine protonation, as estimated from cyclic voltammetry (closed squares) and DMA/TMA model system calculations. **A** assumes 70% total amine protonation, and **B** assumes 44% total amine protonation, and **C** assumes 20% total amine protonation.

Since the protonation of the polymers was not known, simulations were carried out with three different assumed protonation states. Simulation A assumes that 70% of the amines are protonated, simulation B assumes that the total protonation of the amines is 44%, as suggested by the cyclic voltammetry of Fc-$C_1$-LPEI(100%), and simulation **C** assumes 20% total protonation. It should be noted that the pKa (and thus the degree of protonation) of the series of polymers likely changes with different amounts of ferrocene (i.e. tertiary amine) substitution. This factor was not considered in the simulations.

The slope of simulation **A** is almost the same as the experimental plot, but it lies on a line about 30 percentage units above the experimental plot. This suggests that the

overall change in the amount of tertiary amine protonation as observed in the cyclic voltammograms was due to a pKa difference between tertiary and secondary amines, as was hypothesized. However, it does not come close to producing the actual values that were obtained experimentally. Simulation **C** had a slight correlation with the experimental data at low substitution, but overall did not match up with the intermediate and high amounts of substitution. When the data from simulation **B** was plotted with the experimental data, the slope of the data *and* the values were similar to the experimental data. These simulations, while somewhat rudimentary in nature, suggest that the polymers have a degree of protonation around 45%.

*Cyclic Voltammetry of Cross-linked films of Fc-$C_1$-LPEI(x%)*

Cyclic voltammetry of cross-linked films of Fc-$C_1$-LPEI(x%) could reveal important, fundamental differences in the polymers which occur when the amount of ferrocene substation is changed. These differences could include, but are not limited to, stability, redox potential, anion interaction, and electron diffusion.

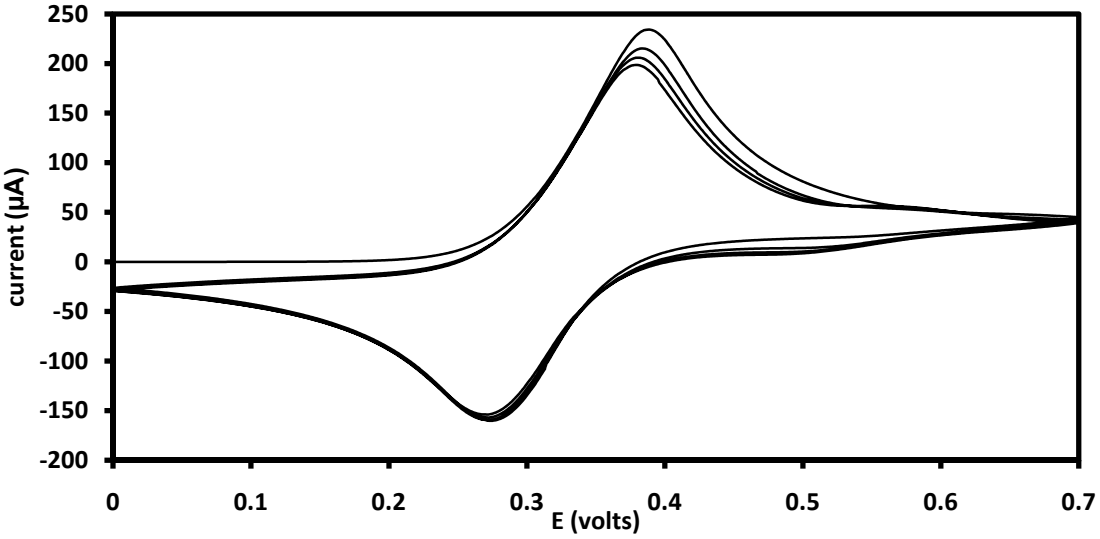


**Figure 3.13:** Cyclic voltammetry of Fc-$C_1$-LPEI(30%) cross-linked with EGDGE on a 3 mm GC electrode in PBS buffer. Scan rate = 50 mV/s, pH = 7.4 First 8 scans shown.

Figure 3.13 shows the first 10 scans of a typical cyclic voltammogram for a cross-linked film of Fc-$C_1$-LPEI (30%). The film shows reversible electrochemical behavior with two oxidation peaks at ~370 mV and ~600 mV. At first glance, this appears to mimic the solution electrochemistry. However, this multi-wave behavior has been observed in these polymers previously, and cannot be correlated with the degree of polymer protonation.[10] When cyclic voltammograms of the series are plotted together, a number of interesting trends are revealed (Figure 3.14).

Only the oxidation direction of these CVs was shown for convenience and all voltammograms displayed reversible behavior in the reductive direction. The third of 10 scans is shown, and as expected, the $i_{pa}$ decreased with each successive scan for all polymers (not shown). The first observation regarding this series is that the $i_{pa}$ increases for each polymer up to 20%. This was expected as the concentration of ferrocene groups near the electrode increases with each increasing substitution amount. Also, increasing the substitution most likely facilitates better electron diffusion due to a

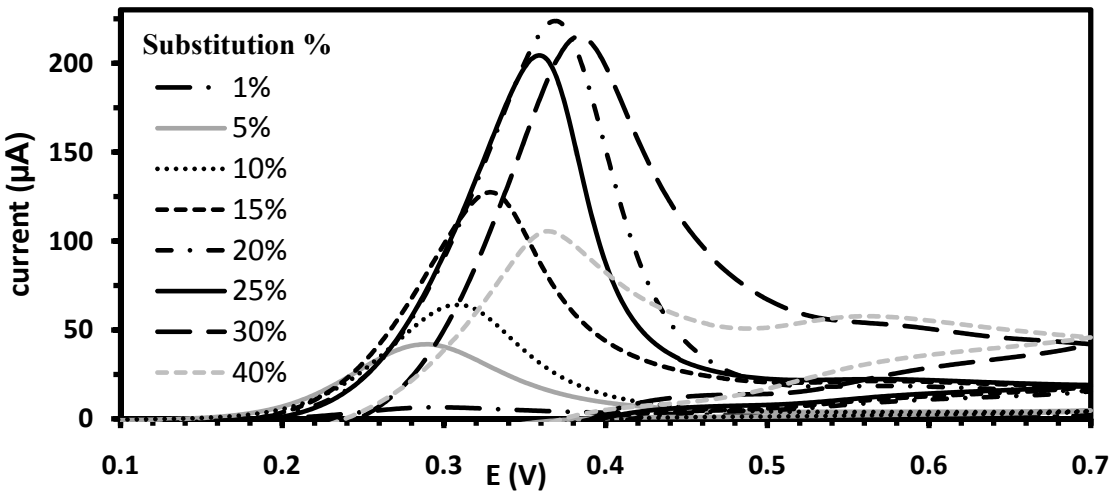


**Figure 3.14:** Cyclic voltammetry of Fc-$C_1$-LPEI(x%) cross-linked with EGDGE on a 3 mm GC electrode in PBS buffer. Scan rate = 50 mV/s, pH = 7.4. Only the oxidative direction is shown.

decrease in distance between ferrocenes in the film. The $i_{pa}$'s for films made with Fc-$C_1$-LPEI(20%-30%) remained relatively constant even though the concentration of ferrocene moieties in the films increased, which suggests that a maximum was reached as far as electron transfer is concerned. This hypothesis would need to be verified with an electron diffusion study. Surprisingly, the $i_{pa}$ for the polymer with 40% substitution drops dramatically. Also, the second, higher potential oxidation peak for Fc-$C_1$-LPEI(40%) was much larger (relative to the low E peak) than in any of the other polymers. The drop in current and the increase in size of the second peak could be due to a number of factors including incomplete cross-linking, swelling changes due to the increasing hydrophobic nature of the polymer, or delamination of the film (which could be due to incomplete cross-linking).

Another noticeable change which occurs within this series of polymers is the shift in anodic potential at peak current, or $E_{pa}$. While each CV shows an onset of oxidative current at the same potential, the $E_{pa}$ shifts anodically as the substitution

percentage increases. The $E_{pa}$ for Fc-$C_1$-LPEI(1%) is 280 mV, and this value increases gradually until Fc-$C_1$-LPEI(20%), which has an $E_{pa}$ of 358 mV. At values higher than 20% substitution, the $E_{pa}$ seems to fluctuate randomly. Both of these $E_{pa}$ values are significantly higher than the $E_{pa}$ for the neutral model compound, indicating that many of the nitrogens on the polymer backbone were protonated. This was expected, as LPEI has been estimated to be around 50% protonated under physiological conditions.[17] The gradual increase of $E_{pa}$ is an interesting phenomenon and could be related to the protonation behavior seen in the solution electrochemistry of the polymers. At low substitution amounts, most of the substituted (tertiary) nitrogens were likely deprotonated due to the lower basicity of those sites. As the amount of ferrocene substitution increased, more tertiary nitrogens likely became protonated, which could cause the shift of the $E_{pa}$ seen in the graph. One problem with this argument is that the solution electrochemistry of the polymers showed two distinct peaks corresponding to protonated or deprotonated nitrogens, while the cross-linked films only showed an 80 mV shift in $E_{pa.}$ However, the conditions of each experiment were quite different (dissolved polymer vs. cross-linked polymer, pH 2 vs. pH 7 with PBS buffer), and as such, differences in electrochemical behavior would be expected.

*Effect of Ferrocene Substitution Percentage on Enzymatic Biosensor Performance*

The primary purpose of the synthesis of the Fc-$C_1$-LPEI(x%) polymers was to investigate their electrochemical properties when cross-linked in the presence of glucose oxidase and used as sensors for glucose. Sensors were fabricated and constant potential amperometry was carried out on the films in the presence of increasing

amounts of glucose to obtain calibration curves. An example of a calibration curve is depicted in Figure 3.15.

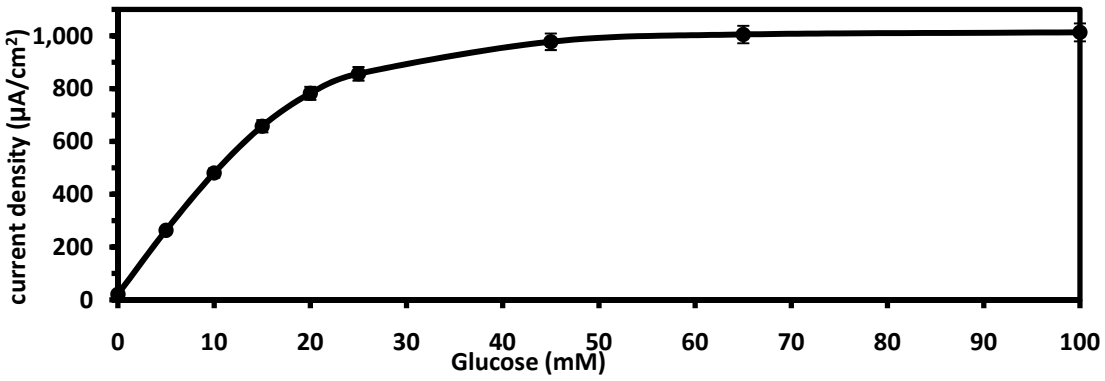


**Figure 3.15:** Calibration curve for Fc-$C_1$-LPEI(20%). PBS, pH 7.4, 25° C, stirring, E = 0.4 V vs. SCE

In order to evaluate the effect of ferrocene substitution percentage on biosensor performance, calibration curves were taken for each polymer in the series and their maximum current densities ($j_{max}$) were plotted vs. the amount of substitution (Figure 3.16). It was expected that the amount of ferrocene substitution could greatly influence the sensor performance at low amounts, and a few hypotheses were drawn: Limiting currents ($j_{max}$) of glucose biosensors made from redox polymers are known to depend on electron diffusion through the polymer films, which depends significantly on the mobility of the redox centers and the frequency of their collisions.[6, 7, 23, 24] It was therefore hypothesized that attaching only small amounts of ferrocene onto LPEI should greatly reduce those collisions due to large distances between ferrocene moieties. This effect has been observed in some osmium polymers where lowering the osmium substitution ratio from 20% to 10% significantly lowered $D_e$.[25] For the intermediate region of ferrocene substitution, one previous study by Heller's group showed that varying the substitution percentage of the mediator between 16% and 33% showed little

difference in electron diffusion,[24] therefore it was expected that after a certain amount of substitution (speculated to be somewhere around 15%), $j_{max}$ in our system would remain fairly constant. At higher amounts of ferrocene loading, it seemed logical that the polymer would become too hydrophobic to have an efficient interaction with glucose oxidase, which would lead to lower current densities even if electron diffusion remained high.

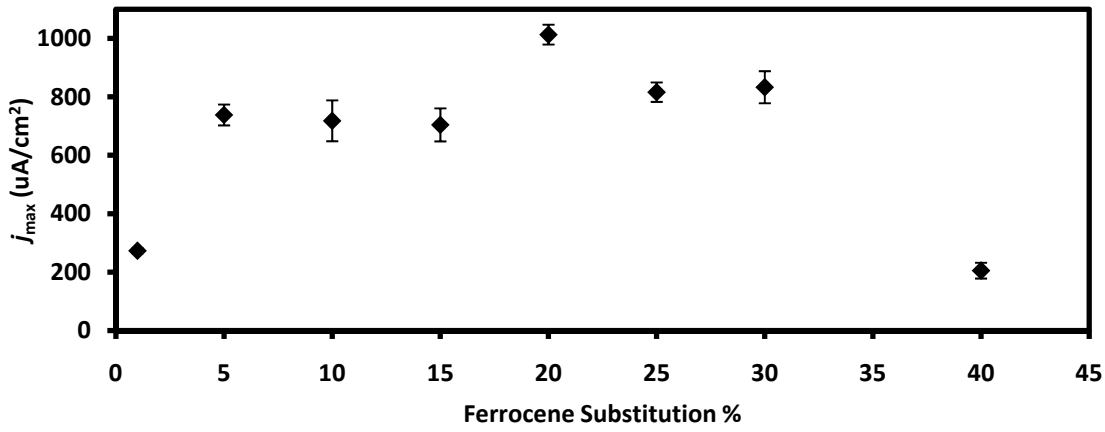


**Figure 3.16:** Plot of $j_{max}$ vs. substitution percentage for Fc-$C_1$-LPEI(x%) in PBS buffer, pH 7.4, 25° C, stirring

Based on the above discussion, it was expected that the $j_{max}$ vs. subst. percentage plot would resemble a bell-shaped curve. On the contrary, this plot shows that between the substitution percentages of 5% and 30%, the biggest difference in $j_{max}$ between any two points is only ~300 μA/cm$^2$. This lack of correlation and the fact that increasing the substitution from 5% to 15% makes no significant difference in the performance of the sensor suggests that electron diffusion through the film is not the primary factor responsible for the high current densities observed. This hypothesis agrees with the relatively low apparent electron diffusion coefficient discussed previously and indicates that other factors such as an enhanced interaction with the enzyme could be responsible

for the exceptional performance of these sensors. Another fact which would enforce this hypothesis is the performance of the sensors with 1% ferrocene substitution. At this extremely low percentage, one would expect almost no catalytic response from the addition of glucose due to large distances between mediators, but a steady-state current density above 250 μA/cm$^2$ is obtained, showing a substantial "wiring" of the enzymes to the electrode. The plot also shows that the optimum substitution percentage for the these high current density sensors was likely 20%. This is around the amount that was expected and is within the realm of what is commonly used for redox polymer biosensors.[2, 26, 27] However, in order to determine if the $j_{max}$ of sensors made with Fc-$C_1$-LPEI was significantly different than that of the other substitution amounts around it (e.g. 15% and 25%), a more extensive statistical analysis should be carried out.

Sensors constructed with Fc-$C_1$-LPEI(40%) yielded the lowest current densities, indicating that high concentrations of mediator produce unfavorable sensor performance. This decrease in current was most likely due to a combination of the enhanced hydrophobicity of the polymer (which might lower the enzyme/polymer interaction) and the possibility of incomplete cross-linking/rapid film degradation as evidenced from the unstable cyclic voltammogram of cross-linked Fc-$C_1$-LPEI(40%).

**Conclusions**

Overall, the series of polymers designated Fc-$C_1$-LPEI(x%) are fundamentally interesting and useful as redox polymers for glucose biosensors. The solution electrochemistry of this series of polymers indicates that when the polymer is deprotonated, all of the ferrocene groups on the polymer have one redox potential.

However, when the polymer is significantly protonated, two different types of ferrocene arise with significantly different redox potentials. These different redox potentials are most likely linked to the protonation (or lack thereof) of the tethered nitrogen, but the currents of these polymers from cyclic voltammetry experiments do not line up with the expected amount of protonation. While it seems like this protonation phenomenon could be a linked to the dual peak behavior seen in the cross-linked films of Fc-$C_1$-LPEI, it is unlikely due to the fact that the higher $E_{pa}$ peak in the cross-linked films actually grows under basic conditions rather than disappearing.[10]

The cyclic voltammetry of Fc-$C_1$-LPEI(x%) films cross-linked with EGDGE in the presence of glucose oxidase gave results which were expected, with a correlation between $i_{pa}$ and substitution percentage. More ferrocene in the films led to higher $i_{pa}$ values due to increased concentrations of ferrocene and shorter ferrocene-to-ferrocene distances. At 40% substitution, the $i_{pa}$ dropped and the cyclic voltammograms were very unstable, indicating rapid degradation of the films or incomplete cross-linking.

The current densities of sensors fabricated with these polymers suggest that the performance of these materials is only loosely tied to amount of ferrocene in the films. The highest current densities were obtained using 20% substituted polymer, but only small differences in biosensor performance were observed between 5% and 30% substitution. This strengthens the hypothesis that the exceptional sensor performance with Fc-$C_1$-LPEI is linked strongly to other factors besides electron diffusion. A detailed study to determine the true concentration of ferrocene in these films along with the electron diffusion coefficients (rather than $D_{app}$) could provide even more evidence

for this hypothesis and give some insight into whether or not mediator-to-mediator electron transfer is the limiting step in the wiring of the enzyme to the electrode.

## Experimental

*Chemicals and Solutions*

Glucose Oxidase, Ferrocene, methyl iodide, *N,N,N',N'*-tetramethyldiaminomethane, ferrocene carboxaldehyde, sodium borohydride, and all solvents and salts were purchased from Aldrich and used as received. Ethylene glycol diglycidyl ether (EGDGE) was purchased from Polysciences.

*Synthesis of Fc-$C_1$-LPEI(x%)*

LPEI (avg. MW ca. 86,000) was obtained by acidic hydrolysis of poly(2-ethyl-2-oxazoline) (avg. MW 200,000), followed by neutralization with sodium hydroxide.[28, 29] (Dimethylaminomethyl)ferrocene (DMAMFc) and (Ferrocenylmethyl) trimethylammonium iodide (FcMTMAI) were synthesized according to previously published literature procedures[11, 30] and the analytical data from these products matched what was reported previously.[12, 31] For the polymer synthesis, 0.2 g of LPEI was dissolved in a heated mixture of 10 mL acetonitrile and 1.5 mL methanol in a round-bottom flask. Once it was completely dissolved, the required amount of FcMTMAI (dissolved in 3 mL acetonitrile) was added dropwise. Potassium carbonate (1 eq.) was added and the mixture was stirred and heated to reflux solvent for 16 hrs. For substitution amounts higher than 20%, ~1 mL of benzene was added to the mixture to reduce polymer precipitation and maintain homogeneity. After this, the mixture was

cooled down and the solvents were evaporated under reduced pressure. Following this, there were two different workup procedures, depending on the substitution amount:

For substitution amounts less than 20%, the polymer and residual salts were dissolved into 10 mL water, heated to 80$^{o}$ C, and 1 g sodium hydroxide was added. The mixture was then cooled to 10$^{o}$ C, causing the polymer to precipitate. The polymer was filtered and washed with copious amounts of cold water to remove any residual salts. The polymer was then allowed to dry on the filter overnight, and after that it was dissolved into methanol and placed in a flask. The methanol was removed under reduced pressure to yield the final product.

For substitution amounts of 20% or greater, benzene was added to the crude polymer/salt mixture to dissolve the polymer. The benzene solution was then dried over magnesium sulfate to remove any water, and filtered to remove residual salts and unreacted starting materials. Benzene was removed under reduced pressure to yield the final product. Yields for these polymers ranged from 70%-90%.

*$^{1}$H-NMR Characterization of the Polymers*

To measure the amount of ferrocene substitution for each polymer, the integral of the area under the peaks for the ferrocene ring hydrogens at ca. δ 4.0-4.3 was set as nine, and the remaining peaks were integrated relatively. In a normal repeat unit (-$CH_2CH_2NH$-), the polymer backbone has four non-exchanging hydrogens. For Fc-$C_1$-LPEI, this means that four divided by the integral of the backbone hydrogens (δ 2.4-2.9) gives the substitution percentage as seen in equation 3.01. Table 3.01 gives the substitution percentages calculated for each polymer using this equation and the

chemical shifts of each spectrum. Calculated substitution percentages were within ~3% of the expected values.

**Equation 3.01:** Fc-$C_1$-LPEI ferrocene substitution percentage = $\frac{4}{backbone\ hydrogen\ integration}\ x\ 100$

| % Fc | δ -CH2-N- | δ Fc-$CH_2$-N- | δ Fc ring |
|---|---|---|---|
| 1.54 | br s, 2.60-2.90 | br, 3.48-3.58 | br, 4.12-4.24 |
| 6.52 | br, 2.52-2.90 | br, 3.52-3.60 | br, 4.12-4.26 |
| 9.9 | br, 2.40-2.85 | br, 3.52-3.58 | br, 4.12-4.27 |
| 17.3 | br, 2.44-2.88 | br, 3.46-3.58 | br, 4.10-4.26 |
| 21.1 | br, 2.45-2.86 | br, 3.48-3.56 | br, 4.12-4.24 |
| 25.8 | br, 2.44-2.78 | br, 3.48-3.58 | br, 4.12-4.26 |
| 31.2 | br, 2.44-2.80 | br, 3.48-3.58 | br, 4.10-4.26 |
| 40.05 | br, 2.42-2.82 | br, 3.48-3.58 | br, 4.10-4,28 |
| 103.3 | br s, 2.36-2.52 | br s, 3.40-3.50 | br, 4.08-4.20 |

**Table 3.01**: Chemical shifts and calculated ferrocene substitution amounts (using equation 1) for each polymer

*Methods*

Solution-based experiments were carried out on solutions of Fc-$C_1$-LPEI(x%) (2.0 mg/mL) in deionized water. To dissolve the polymer, HCl was added slowly and the solution was stirred until it was completely dissolved. The pH of these solutions was adjusted with concentrated NaOH.

For sensor fabrication, the Fc-LPEI polymer was dissolved in water by the addition of a 0.1M HCl solution until the final concentration of the polymer solution was 10 mg/mL and the pH was 5.0 ± 0.2. Glucose sensors were prepared by cross-linking glucose oxidase to Fc-LPEI to form enzymatic redox hydrogels: 14 μL of polymer solution (10 mg/mL), 6 μL of glucose oxidase solution (10mg/mL), and 0.75 μL of EGDGE solution (10%v/v) were mixed; 3 μL

aliquots were placed onto the glassy carbon electrode surface; and the mixture was allowed to cure for 18-24 h.

*Electrochemical Measurements*

Solution-based cyclic voltammetry experiments were carried out with a CV-50W Voltammetric Analyzer from BAS. Experiments were carried out using a typical three electrode cell configuration with a 1 mm Pt disc working electrode, a Pt wire counter electrode, and a saturated calomel reference electrode (SCE). Prior to each experiment, the Pt electrode was polished and rinsed thoroughly with deionized water.

Cyclic voltammetry and constant potential experiments with the hydrogels were carried out with a bipotentionstat (model 832) and 3mm glassy carbon electrodes purchased from CH instruments (Austin, TX). These experiments were also conducted using a typical three electrode cell configuration with a saturated calomel reference electrode and a platinum wire counter electrode. Prior to use, all electrodes were polished successively on three grades of alumina (5, 1, and 0.3 *u*m) and washed thoroughly with Nanopure water after each polishing step. An Accumet AR25 pH meter (Fisher Scientific) was used to determine the pH of the solutions.

## References


1. National Diabetes Fact Sheet, 2007. Prevention, C. f. D. C. a., Ed. Atlanta, GA, 2008.

2. Mao, F.; Mano, N.; Heller, A., *J. Am. Chem. Soc.* **2003,** *125* (16), 4951-4957.

3. Mano, N.; Heller, A., *Anal. Chem.* **2005,** *77* (2), 729-732.

4. Heller, A.; Feldman, B., *Chem. Rev. (Washington, DC, U. S.)* **2008,** *108* (7), 2482-2505.

5. Merchant, S.; Tran, T. O.; Meredith, M. T.; Cline, T. C.; Glatzhofer, D. T.; Schmidtke, D. W., *Langmuir* **2009,** *25* (13), 7736-7742.

6. Heller, A., *Curr. Opin. Chem. Biol.* **2006,** *10* (6), 664-672.

7. Heller, A., *J. Am. Chem. Soc.* **2003,** *125*.

8. Forster, R. J.; Walsh, D. A.; Mano, N.; Mao, F.; Heller, A., *Langmuir* **2004,** *20* (3), 862-868.

9. Heller, A., *AIChE J.* **2005,** *51* (4), 1054-1066.

10. Merchant, S.; Glatzhofer, D. T.; Schmidtke, D. W., *Langmuir* **2007,** *23*, 11295.

11. Osgerby, J. M.; Pauson, P. L., *J. Chem. Soc.* **1958,** (Feb), 656-660.

12. Lindsay, J. K.; Hauser, C. R., *J. Org. Chem.* **1957,** *22* (4), 355-358.

13. Nesmeyanov, A. N.; Perevalova, E. G., *Ann. N.Y. Acad. Sci*.

14. Smits, R. G.; Koper, G. J. M.; Mandel, M., *J. Phys. Chem.* **1993,** *97*, 5745-5751.

15. Kobayashi, S.; Hiroishi, K.; Tokunoh, M.; Saegusai, T., *Macromolecules* **1987,** *20*, 1496-1500.

16. Ger J.M, K.; Duijvenbode, R. C. v.; Stam, D. D. P. W.; Steuerle, U.; Borkovec, M., *Macromolecules* **2003,** *36*, 2500-2507.

17. Ziebarth, J. D.; Wang, Y., *Biomacromolecules* **2010,** *11*, 29-38.

18. Kokufuta, E.; Suzuki, H.; Yoshida, R.; Yamada, K.; Hirata, M.; Kaneko, F., *Langmuir* **1998,** *14* (4), 788-795.

19. Weyts, K. F.; Goethals, E. J., *Makromol. Chem., Rapid Commun.* **1989,** *10* (6), 299-302.

20. Alvarez, J.; Ren, T.; Kaifer, A. E., *Organometallics* **2001,** *20* (16), 3543-3549.

21. Alvarez, J.; Ni, Y.; Ren, T.; Kaifer, A., *J. Supramol. Chem.* **2001,** *1*, 7-16.

22. Lide, D. R., *CRC Handbook of Chemistry and Physics*. 87 ed.; Taylor and Francis: Boca Raton, FL, 2007.

23. Aoki, A.; Heller, A., *J. Phys. Chem.* **1993,** *97*, 11014-11019.

24. Aoki, A.; Rajagopalan, R.; Heller, A., *J. Phys. Chem.* **1995,** *99*, 5102-5110.

25. Ohara, T. J.; Rajagopalan, R.; Heller, A., *Anal. Chem.* **1993,** *65* (23), 3512-3517.

26. Chuang, C. L.; Wang, Y. J.; Lan, H. L., *Anal. Chim. Acta* **1997,** *353* (1), 37-44.

27. Heller, A., *J. Phys. Chem.* **1992,** *96*.

28. York, S.; Frech, R.; Snow, A.; Glatzhofer, D., *Electrochem. Acta* **2001,** *46*, 1533-1537.

29. Tanaka, R.; Ueoka, I.; Takaki, Y.; Kataoka, K.; Saito, S., *Macromolecules* **1983,** *16*, 849-853.

30. Lednicer, D; Hauser, C., *Org. Synth.* **1960,** *40*, 31.

31. Lousada, C. M.; Pinto, S. S.; Lopes, J. N. C.; da Piedade, M. F. M.; Diogo, H. P.; da Piedade, M. E. M., *J. Phys. Chem. A* **2008,** *112* (13), 2977-2987.

# CHAPTER 4: EFFECT OF MEDIATOR SPACING ON ELECTROCHEMICAL AND ENZYMATIC RESPONSE OF FERROCENE REDOX POLYMERS

Significant portions of this chapter are taken from Merchant et al., *J. Phys. Chem. C* **2010,** *114*, 11627-11634

## Introduction

Redox polymers are a class of conducting macromolecules that contain spatially and electronically localized redox sites.[1] They occupy a unique place in the field of conducting polymers as they can be permeable, hydrophilic, and relatively "disordered" yet still conduct electrons efficiently. The redox sites can be incorporated directly into the polymer backbone,[2] covalently attached as pendant groups,[3, 4] or electrostatically bound.[5, 6] The electrochemical properties (e.g. redox potential, electron transport) of a redox polymer can depend upon a number of variables: the type of polymer backbone,[7-9] the type of redox mediator,[10, 11] the concentration of redox mediator,[12, 13] and the polymer charge.[14] Understanding the effects of these different variables is critical in modifying the properties of a redox polymer for the specific application (e.g. electrocatalysis,[15, 16] biosensing,[17-20] biofuel cells[21-24]) it will be used in.

In redox polymers where the redox site is attached as a pendant group, the distance between the pendant group and the polymer backbone, and the flexibility of the spacer that attaches the pendant group can have significant impact on the electrochemical properties. One of the fundament electrochemical properties which can be affected by these variables is the apparent electron diffusion coefficient ($D_{app}$). For example, Mao et al. reported[25] an order of magnitude increase in the apparent electron diffusion coefficient when osmium redox centers were extended from the polymer

backbone by a 13-atom-long flexible tether. Likewise, Suzuki et al. reported[26] that intra-polymer electron transfer between cobalt(II) schiff-base complexes and quaternized imidazolium residues increased 2-3 fold as the tether was increased from 2 to 6 carbons. It has been suggested that because electron transfer in redox films is primarily due to collisions between reduced and oxidized redox centers, a longer tether increases electron transfer by allowing the redox center to sweep out a larger volume element [27]thereby increasing the number of successful electron-transferring collisions.[25]

An additional benefit of increasing the length of tethers that link redox centers to the polymer backbone is that several studies have reported that this enhances the rate at which electrons are transferred between an enzyme's redox center and the polymer's redox sites. For example, Hale et al.[4] reported a 2-fold increase in the electrocatalytic response of ferrocene redox centers and the FAD centers of Glucose Oxidase (GOX) by increasing the tether length from 2 to 9 carbons, whereas Mao reported that a 13-atom tether increased the response with GOX 10-fold.[25] Similar increases with tether length have been observed by Willner et al.[27] with the enzyme Glutathione Reductase (GR, 8-fold increase) and Guschin et al.[9] with Horseradish peroxidase (HRP, 2-fold increase). For the interaction with enzymes, it has been proposed that a longer tether enables the polymer redox centers to penetrate the protein backbone and reduce the electron transfer distance, thereby increasing electrical communication with the enzyme's redox center which is often buried and inaccessible.

Recently we have reported the synthesis of a novel redox polymer based on attaching ferrocene to a linear poly(ethylenimine) (LPEI) backbone.[28, 29] We have demonstrated that this polymer (Fc-$C_1$-LPEI) was able to efficiently communicate with

the redox centers of two enzymes: glucose oxidase and horseradish peroxidase,[29] producing current densities of 1 mA/cm$^2$ or greater. A potential limitation of this redox polymer is that in the presence of phosphate this redox polymer exhibits multiwave redox behavior that degrades the film.[28] This instability and multiwave behavior was somewhat surprising given the fact that this behavior had not been reported for redox polymers based on attaching ferrocene to polyacrylamide,[30, 31] polyallylamine,[32, 33] or polysiloxane.[4] It should be noted that Ikeda et al.[34] reported a decrease in the electrochemical response of a ferrocene-polysiloxane redox polymer in phosphate, and that multiwave behavior has been reported for ferrocene dendrimers[35] and (ferrocenylmethyl)trialkylammonium cations[36] in the presence of phosphate.

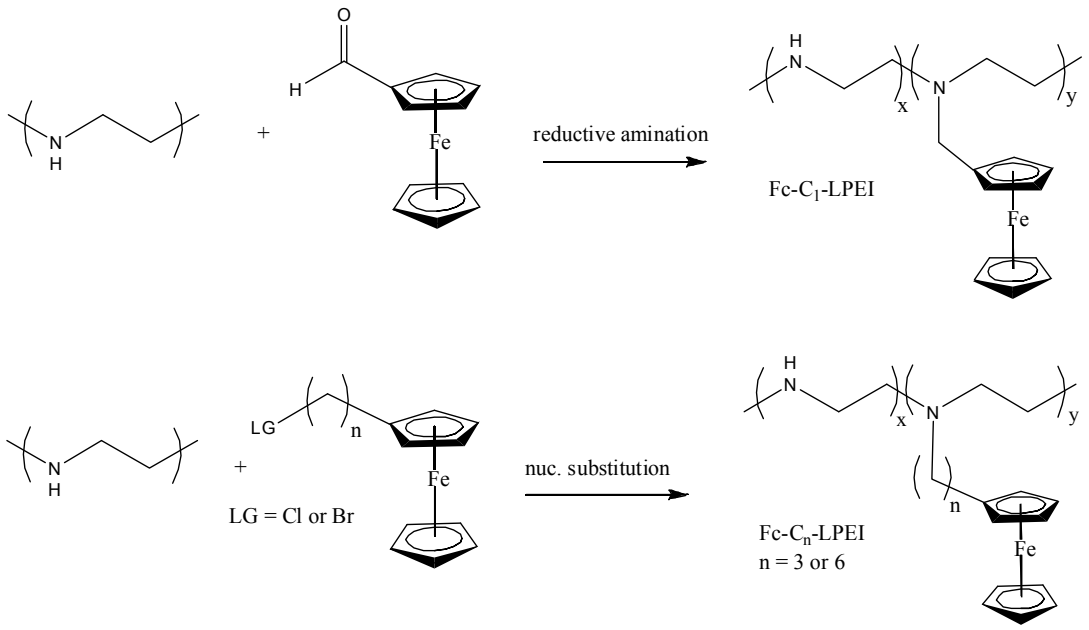


**Figure 4.01:** Summary of synthetic routes and structures of Fc-$C_1$-LPEI, Fc-$C_3$-LPEI, and Fc-$C_6$-LPEI redox polymers.

With the objective to gain further understanding of the structure-property relationships of tether length in ferrocene redox polymers, two new redox polymers based on a LPEI backbone have been synthesized (Figure 4.01). Specifically we synthesized polymers where the ferrocene redox centers were extended away from the LPEI backbone by three carbon atoms (Fc-$C_3$-LPEI) and six carbon atoms (Fc-$C_6$-LPEI). We observed that crosslinked films of both polymers exhibit stable responses both at high pH and in the presence of dibasic phosphate. In addition, we report the effect of tether length on electron transport and the enzymatic response of films containing the enzyme glucose oxidase.

**Results and Discussion**

*Electrochemistry of Crosslinked films in PBS*

To determine whether increasing the distance between the attached ferrocene redox couple and the PEI backbone would influence the electrochemistry of these films in solutions containing phosphate, we performed cyclic voltammetry on crosslinked Fc-$C_1$-LPEI, Fc-$C_3$-LPEI and Fc-$C_6$-LPEI in phosphate buffered saline (PBS). Figure 4.02A shows cyclic voltammograms of crosslinked Fc-$C_1$-LPEI films in PBS at pH 3, 7, and 11. As reported previously,[28] the electrochemical response of crosslinked Fc-$C_1$-LPEI films exhibit a single oxidation peak (350 mV) and reduction peak (250 mV) that are relatively stable in solutions containing phosphate at pH < 7 (Fig. 4.02A).

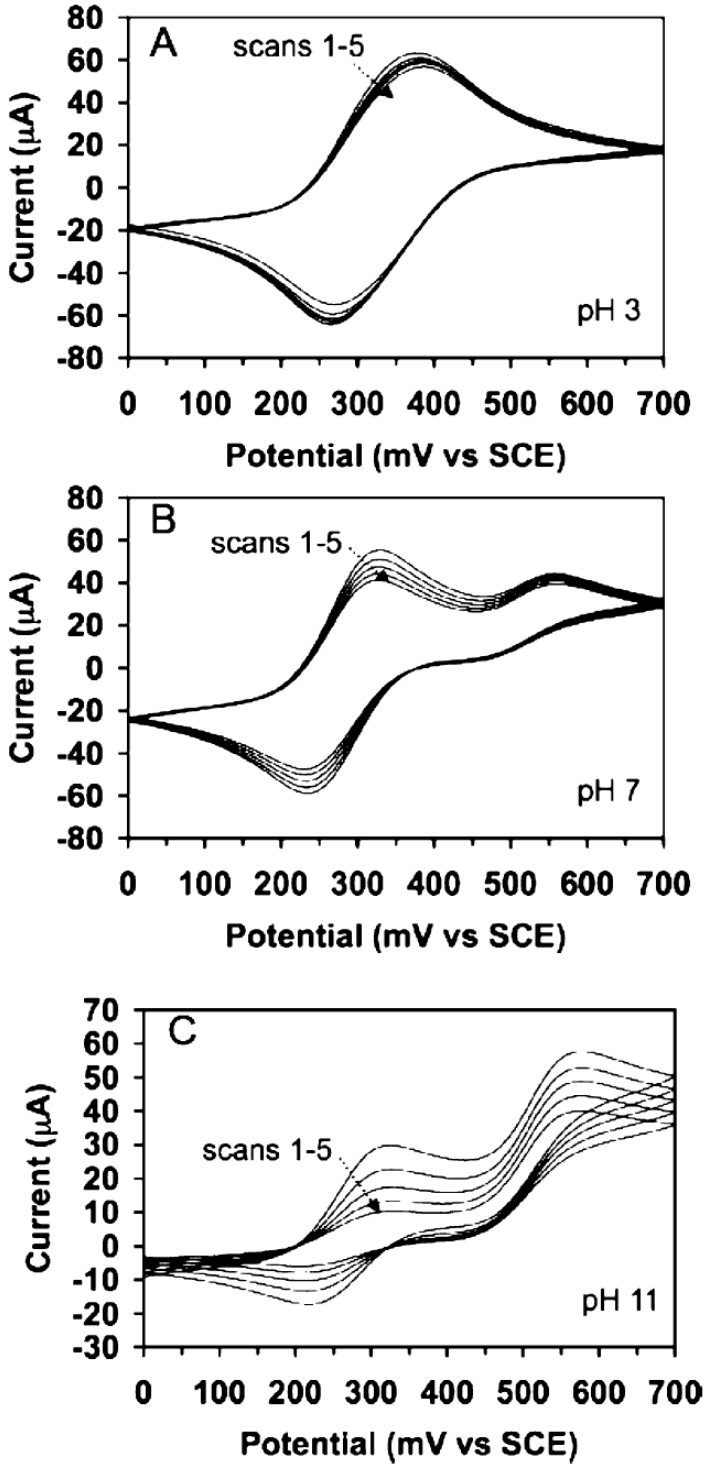


**Figure 4.02:** Cyclic voltammograms of crosslinked Fc-C1-LPEI films in PBS at (A) pH 3, (B) pH 7, and (C) pH 11. Potential scans 1-5, scan rate = 50 mV/s, T= 25° C.

However, these films exhibit multiple redox wave behavior and instability in phosphate containing solutions when the pH ≥ 7. The instability refers to the degradation of the anodic peak current at 335 mV with each subsequent potential cycle. At pH 7 (Figure 4.02B) there is a ~ 30% loss of in the peak current from scan 1 to 5, while at pH 11 (Figure 4.02C) this phenomena is increased to a ~70% loss. In addition, as the pH is increased the second oxidation peak at 550 mV becomes more prominent.

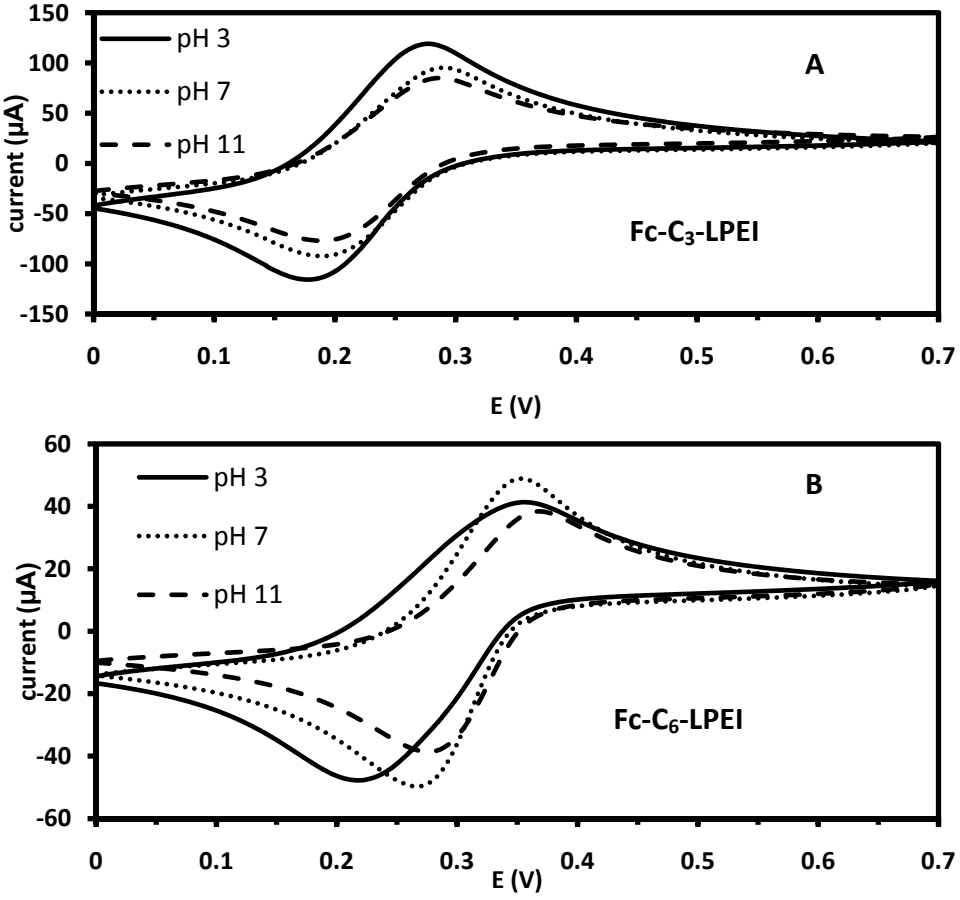


**Figure 4.03:** Cyclic voltammograms of crosslinked films of Fc-$C_3$-LPEI (A) and Fc-$C_6$-LPEI (B) in PBS as a function of pH. scan rate = 50 mV/s, T = 25°C.

In contrast to the results obtained with Fc-$C_1$-LPEI films, the cyclic voltammograms of crosslinked Fc-$C_3$-LPEI (Figure 4.03A) and Fc-$C_6$-LPEI films

(Figure 4.03B) were extremely stable over the entire pH range and exhibited a single oxidation and reduction peak. The oxidation peak potentials for Fc-$C_3$-LPEI and Fc-$C_6$-LPEI films were relatively constant at 265-285 mV and 355-368 mV vs. SCE respectively. Similarly the reduction peak for the Fc-$C_3$-LPEI was relative constant (173 – 185 mV), while the reduction peak for Fc-$C_6$-LPEI did shift to lower potentials (277 to 218 mV) as the pH was lowered. This data demonstrates that extension of the ferrocene groups further away from the LPEI backbone eliminated the detrimental effects of phosphate on these films. The electrochemical stability of the Fc-$C_3$-LPEI and Fc-$C_6$-LPEI films at pH 7 in the presence of phosphate is particularly important, since redox polymer based biosensors are routinely operated at physiological pH and in phosphate containing solutions.

The overall lower redox potential of Fc-$C_3$LPEI compared to Fc-$C_1$-LPEI and Fc-$C_6$-LPEI is a curious phenomenon. It was expected that the polymers with longer tethers would have a slightly lower redox potential due to the increased distance of the ferrocene from the positively charged nitrogen backbone. While the polymer with the three-carbon spacer clearly shows this result, extending the tether further to six carbons resulted in a redox potential close to that of the one-carbon tethered polymer. This phenomenon is not easily explained an further experiments are needed to determine the cause of this phenomenon.

At this time the exact cause for the instability of Fc-$C_1$-LPEI in the presence of phosphate is unknown and under investigation in our lab. At pH 7 or greater the $HPO_4^{2-}$ dianion can simultaneously function as a hydrogen-bond acceptor (through its negatively charged oxides) and a hydrogen-bond donor (through its acidic OH group).[37]

Therefore we hypothesize that a complex is formed in which the phosphate dianion interacts simultaneously with the ferrocenium ions and the secondary amines on the polymer backbone via electrostatic interactions and/or hydrogen bonding and causes the oxidation of neighboring ferrocenes to be more difficult. In contrast, when the ferrocene is more distant from the polymer backbone (e.g. Fc-$C_3$-LPEI and Fc-$C_6$-LPEI) this simultaneous binding and complex formation to the ferrocene and the backbone amines does not occur. In support of this argument are the observations that water-soluble poly(azaferrocene) macrocycles[38] are able to electrochemically recognize phosphate anions such as $HPO_4^{2-}$ or adenosine-5'-triphosphate ($ATP^{2-}$). Similarly (Ferrocenylmethyl)trimethylammonium cations[36] have been reported to bind dihydrogen phosphate and $ATP^{2-}$ in organic solvents. Finally, Bunte et al. reported the irreversible uptake of phosphate into ferrocene modified poly(dimethylacrylamide) polymers upon oxidation.[39] This irreversible uptake was highlighted as a possible reason for ferrocenium degradation and occurred when the ferrocene was one atom away from a nitrogen atom. Also, in another study by Bunte et al., the stability of the ferrocene modified poly(dimethylacrylamide) polymers was greatly improved when the amino group adjacent to the ferrocene was substituted with a group that was not positively charged under aqueous conditions.[40] These studies support our theory that moving the ferrocene away from the amines in the LPEI backbone should increase the stability of the ferrocenes by removing any possibility of di-basic phosphate coordination with the ferrocenium ions and the charged amines in the backbone.

To verify that phosphate was taken up by the Fc-C1-LPEI films during the cycling process, we measured XPS spectra of electrodes modified with polymer that

had been subjected to either electrochemical cycling or soaking alone in PBS buffer at pH 7.4.

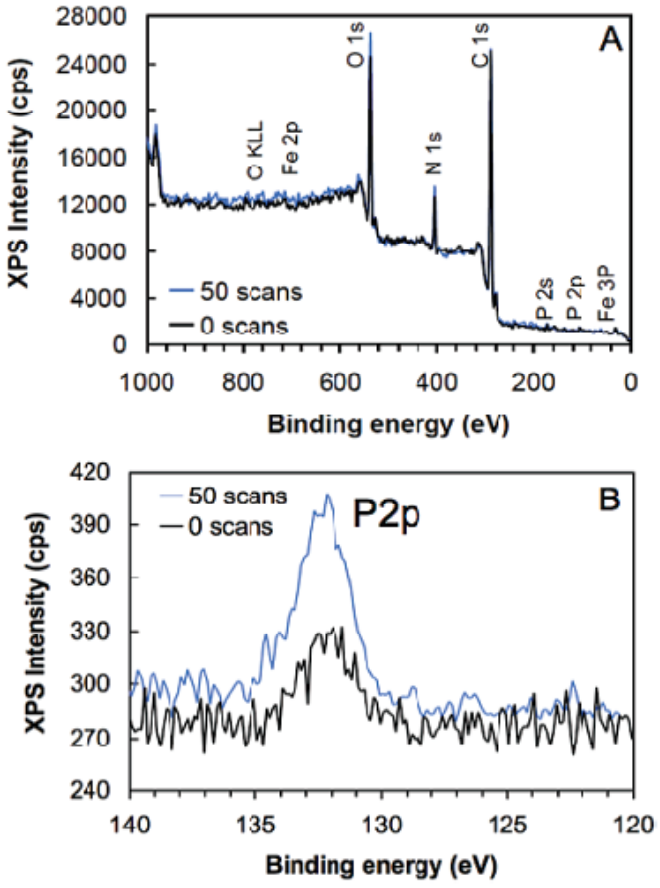


**Figure 4.04.** Effect of electrochemical cycling on phosphate incorporation. (A) X-ray photoelectron survey and (B) detailed spectra of cross-linked Fc-$C_1$-LPEI/GOX films soaked in PBS for 3 h without electrochemical cycling and films that were subjected to 50 electrochemical scans between 0 and 700 mV (vs. SCE) in PBS.

As can be seen from Figure 4.04, exposing the films to electrochemical cycling in PBS resulted in an increase in the P2p peak. These results are similar to those reported by Bunte et al.[39] and support the hypothesis that there is irreversible uptake of phosphate during electrochemical cycling of the Fc-$C_1$-LPEI films.

*Electrochemical Stability CV experiments*

To quantitatively determine how tether length effects the electrochemical stability of cross-linked Fc-LPEI films, we cycled the potential of electrodes coated with these films between 0.0 and 0.7 V vs. SCE or between 0.0 and 0.5 V vs. SCE measured the integrated area (i.e. charge) of the oxidation wave as a function of time for the three different polymer films.

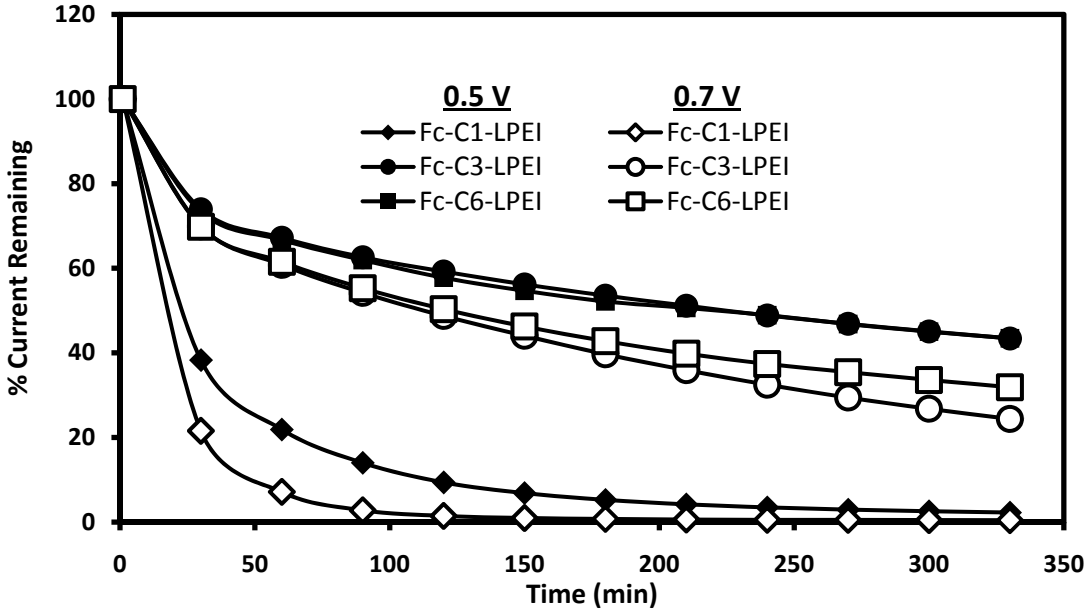


**Figure 4.05:** Plot of the changes in the area of integrated voltammetric waves for cross-linked films of Fc-$C_1$-LPEI, Fc-$C_3$-LPEI, Fc-$C_6$-LPEI, during cycling the applied potential between 0.0 and 0.5 or 0.7 V vs. SCE in PBS (pH 7.4, T = 25°C)

Figure 4.05 shows that when the films were cycled between 0.0 to 0.7 V, the Fc-$C_1$-LPEI films lost 50% of their response in 0.3 hrs, while a 50% decrease occurred for the Fc-$C_3$-LPEI and Fc-$C_6$-LPEI films at ~ 2 hrs. As discussed previously, we believe that the increased degradation rate in the Fc-$C_1$-LPEI films was primarily due to phosphate binding to the ferrocenium ion and the neighboring amines at oxidizing potentials. For

the Fc-$C_3$-LPEI and Fc-$C_6$-LPEI films we believe that the observed decreases were related to the well-known inherent instability of the ferrocenium ion in aqueous solutions.[41] To test this hypothesis, we decreased the amount of time that the ferrocenium ion was present by repeating the experiment but cycling only to 0.5 V. Reducing the amount of time that the unstable ferrocenium ion was present increased the half-life of the Fc-$C_1$-LPEI films to 0.4 hrs and the Fc-$C_3$-LPEI & Fc-$C_6$-LPEI films to 3.5 hours. These results quantitatively demonstrate that the both the Fc-$C_3$-LPEI and Fc-$C_6$-LPEI were electrochemically more stable then the Fc-$C_1$-LPEI and suggest that (a) increasing the distance between the ferrocene and the polymer backbone decreases the degrading effects of phosphate binding, and (b) the instability of these films is related to the formation of the ferrocenium ion.

*Film Swelling*

The effect of polymer structure on macroscopic film hydration/swelling was investigated by profilometry and optical imaging. Dry thicknesses of cross-linked films of the three different polymers were measured by a profilometric method similar to that reported by Gallaway et al.[11] As shown in Figure 4.06, the dry films were not uniform in thickness but exhibited a "coffee ring" pattern. This pattern is caused by evaporation-driven flow of solvent toward the solid/liquid/air interface at the droplet edge.

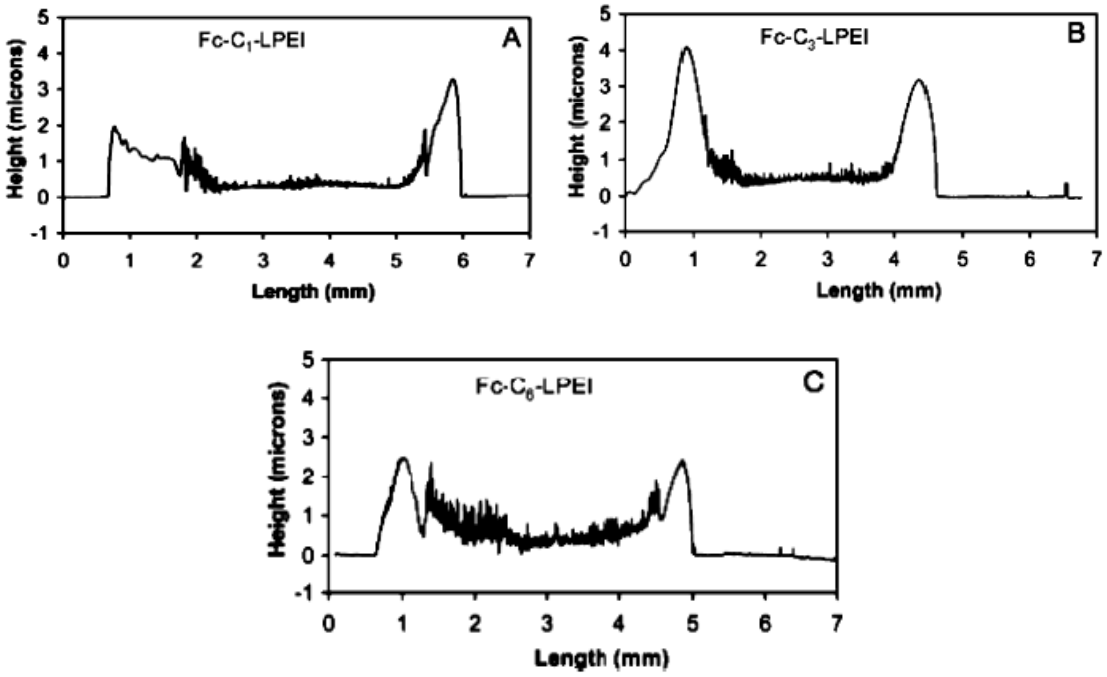


**Figure 4.06:** Dry film thickness profiles. Profilometry traces for cross-linked films of Fc-$C_1$-LPEI, Fc-$C_3$-LPEI, and Fc-$C_6$-LPEI formed on glass slides.

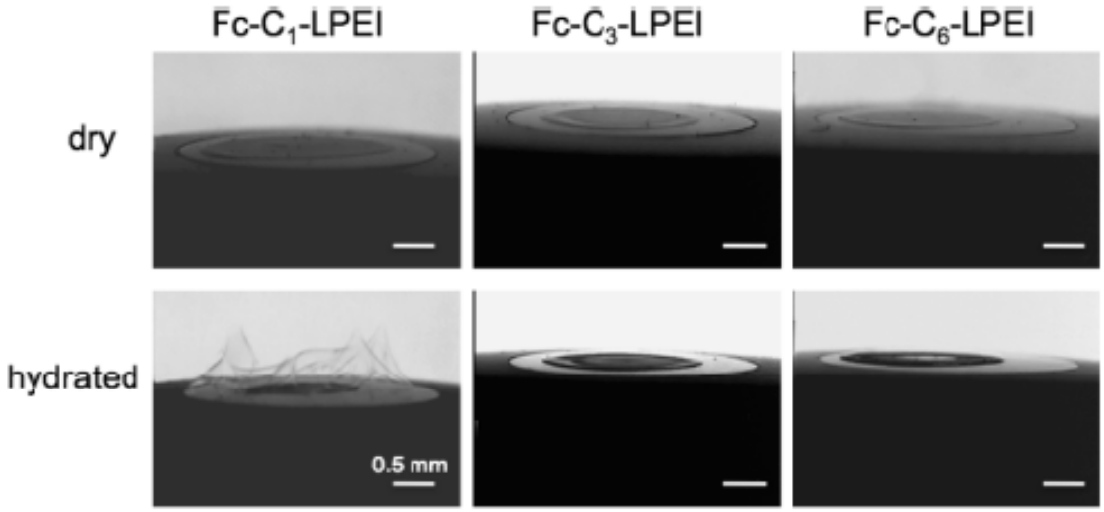


**Figure 4.07:** Effect of polymer type on film swelling. Optical images of 3 mm glassy carbon electrodes coated with cross-linked films of Fc-$C_1$-LPEI, Fc-$C_3$-LPEI, and Fc-$C_6$-LPEI before (i.e., dry) and following exposure (i.e., hydrated) to water solutions at pH 3 and T = 25$^o$ C.

As the solvent flows outward, it carries polymer with it, and a ring of polymer is deposited as the solvent evaporates. The coffee ring pattern was similar for all three polymers, with the thickness of the outer edge ranging from 2 to 4 $\mu$m and the inner portion of the film $\leq$ 0.5 $\mu$m. We investigated the effect of macroscopic polymer swelling by optically imaging the change in film structure upon exposure to water solutions of pH 3 (Figure 4.07). In contrast with the dry film thickness, there were significant differences in the behavior of the films upon exposure to aqueous solutions. The outer edge of the cross-linked films of Fc-$C_1$-LPEI swelled considerably, whereas the swelling of the center of the film was less pronounced. In contrast, there was only minimal swelling of the outer edge of either the Fc-$C_3$-LPEI or Fc-$C_6$-LPEI films. The discrepancy between the different swelling behaviors could be due to differences in film properties such as degree of cross-linking, hydrogen bonding, and/or hydrophobicity. This experiment highlights the fact that the use of dry film thicknesses to predict swollen film thicknesses is not very reliable. The impact of these different swelling behaviors on the electrochemical properties is currently being investigated in our lab.

*Wired GOx Glucose Sensors*

Previously we demonstrated that despite the multi-wave electrochemical behavior, Fc-$C_1$-LPEI redox polymers efficiently communicated with the redox centers of enzymes reaching saturating current densities of 1.2 mA/cm$^2$ for glucose oxidase (GOX) and 0.9 mA/cm$^2$ for horseradish peroxidase (HRP).[29] To determine whether extending the ferrocene redox center from the polymer backbone would affect the

electrical communication with enzymes, we immobilized GOX in crosslinked films of Fc-$C_3$-LPEI and Fc-$C_6$-LPEI and performed cyclic voltammetry in the presence and

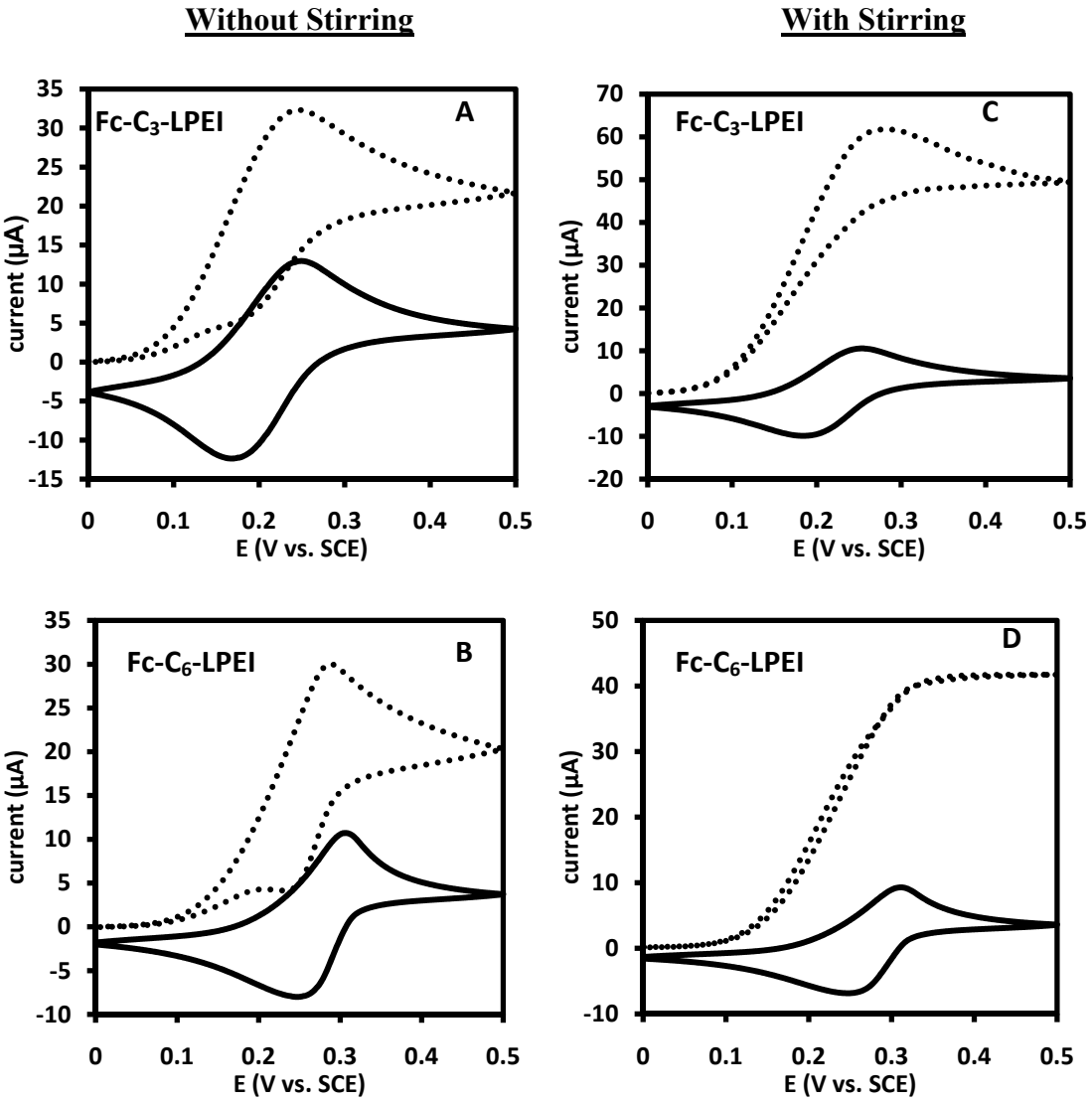


**Figure 4.08: Biocatalytic Response of Redox Polymer-Enzyme Modified Electrodes to Glucose.** Cyclic voltammograms of crosslinked films of A) Fc-$C_3$-LPEI and B) Fc-$C_6$-LPEI with glucose oxidase in the presence and absence of glucose and no stirring. (C) and (D) with stirring. Phosphate buffered saline (pH = 7.4), Scan rate = 5 mV/s, T = 25°C.

absence of glucose. Addition of 100 mM glucose to the solution caused an increase in the oxidation peak and a decrease in the reduction peak (Figures 4.08A & 4.08B). This

behavior is characteristic of glucose transferring two electrons to GOX (Rxn 1), the reduced GOX transferring electrons to ferrocenium redox centers (Rxn 2), electrons exchanged between neighboring ferrocene and ferrocenium redox centers (Rxn 3), and electrons being transferred to the electrode surface (Rxn 4).[42]

$$GOx(FAD) + Glucose \rightarrow GOx(FADH_2) + gluconolactone \quad \text{(Rxn 1)}$$

$$GOx(FADH_2) + 2Fc^{+}\text{-LPEI} \rightarrow GOx(FAD) + 2Fc\text{-LPEI} + 2H^{+} \quad \text{(Rxn 2)}$$

$$2Fc\text{-LPEI} + 2Fc^{+}\text{-LPEI} \rightarrow 2Fc+\text{-LPEI} + 2Fc\text{-LPEI} \quad \text{(Rxn 3)}$$

$$2Fc\text{-LPEI} \rightarrow 2Fc^{+}\text{-LPEI} + 2e- \quad \text{(Rxn 4)}$$

It should be noted that in neither case was the reduction peak completely eliminated. The presence of the reduction peak suggested that the number of electrons generated by the glucose/glucose oxidase reaction was insufficient to reduce all of the ferrocenium ions in the film to ferrocene. However, if the flux of glucose to the film was increased by stirring (Figures 4.08C & 4.08D), the reduction peaks were eliminated.

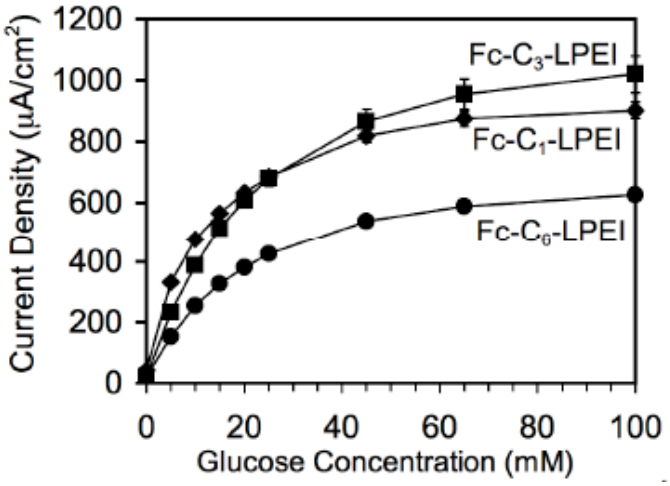


**Figure 4.09:** Glucose calibration curves of electrodes modified with crosslinked films of Fc-$C_1$-LPEI, Fc-$C_3$-LPEI and Fc-$C_6$-LPEI containing glucose oxidase. Phosphate Buffer Saline, pH 7.4, T = 25° C, 0.4V vs. SCE.

**Table 4.01: Effects of Redox Polymer Type on Biosensor Response**

| Redox Polymer | Sensitivity ($\mu A/cm^2 \cdot mM$) | $J_{Max}$ ($\mu A/cm^2$) | $K_M$ (mM) |
|---|---|---|---|
| Fc-$C_1$-LPEI | 67 ± 1 | 902 ± 28 | 9.8 ± 1.1 |
| Fc-$C_3$-LPEI | 47 ± 2 | 1020 ± 61 | 20.7 ± 2.3 |
| Fc-$C_6$-LPEI | 30 ± 1 | 625 ± 6 | 21.3 ± 2.0 |

$J_{Max}$ is the maximum current obtained experimentally at saturating glucose concentrations. $K_M$ was determined graphically from a Lineweaver-Burke plot. Sensitivity was determined from the experimental current response at 5 mM glucose concentration. Values are expressed as mean ± standard error of the mean

Glucose response curves of crosslinked films of Fc-$C_1$-LPEI, Fc-$C_3$-LPEI, Fc-$C_6$-LPEI were measured at 0.4V vs. SCE in a well-stirred solution of PBS. As shown in Figure 4.09 and Table 4.01, increasing the tether length from one carbon to three carbons decreased the sensitivity at 5 mM glucose, however the maximum current density increased slightly and the $K_M$ doubled. An increase in $K_M$ and enzymatic response was expected, and the $K_M$ of 20.7 is near the value of 33 mM previously reported for glucose oxidase in solution.[43] Previously it has been reported that as the space between a redox center and the polymer backbone is lengthened there is an increase in the volume that can be swept out by the redox center and hence an increase in the number of electron transfer collisions[25] and an increased enzymatic response. In contrast, further increasing the tether length to six carbons reduced both the maximum current and sensitivity, while the $K_M$ was similar to the three carbon results. The significant decrease in maximum current and sensitivity were unexpected based on our results with the three-carbon tether and the "tether-length" theory previously discussed. The decrease in the sensitivity and $K_M$ values of the Fc-$C_6$-LPEI films could be tied to unique physical properties of each polymer such as swelling and/or film permeability.

For example, if the films made with Fc-$C_6$-LPEI swelled considerably less than those made with the other polymers, a significant drop in sensitivity and $j_{max}$ might be expected due to a lower rate of glucose permeation throughout the film.

*Electron Transport in Crosslinked Films of Fc-$C_3$-LPEI and Fc-$C_6$-LPEI*

To determine whether the differences in the sensitivities to glucose of the Fc-$C_3$-LPEI and Fc-$C_6$-LPEI films were due to differences in the rate of electron transport through the films, we measured $cD_e^{1/2}$ ($D_e$ = apparent electron diffusion coefficient, and $c$ = the electroactive redox site concentration) by Electrochemical Impedance Spectroscopy (EIS).[28] Figure 4.10 shows no correlation between electron transport and tether length.

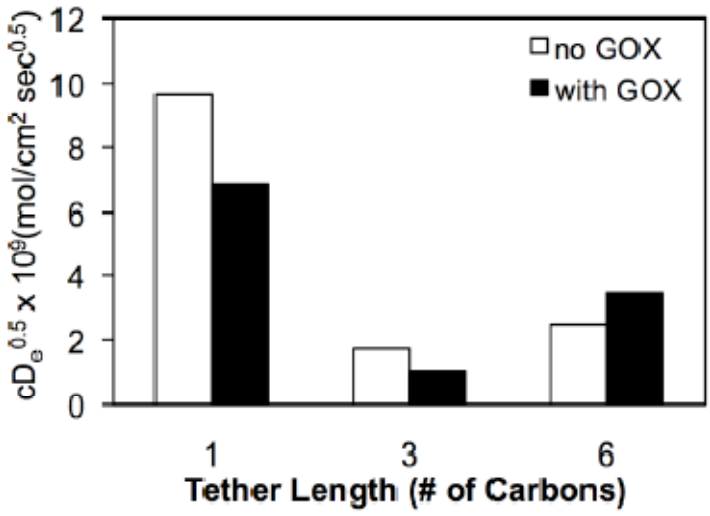


**Figure 4.10: Effect of tether length on electron transport.** Electrodes were modified with crosslinked films of Fc-$C_1$-LPEI, Fc-$C_3$-LPEI and Fc-$C_6$-LPEI both with and without GOX and the electron transport was measured by EIS. PBS (pH 7.4), T = 25°C.

This is somewhat surprising given the reports of others (see Introduction) that electron transport should increase with tether length. It is worth noting that the film (Fc-$C_3$-

LPEI) with the lowest electron transport produced the highest maximum current (Figure 4.09, Table 4.01). This would suggest that other factors such as film permeability, degree of complexation between the redox polymer and enzyme, are involved in producing these high current responses. Experiments are underway to determine the importance of these other interactions.

Another factor which could lead to this unexpected behavior deals with the flexibility and charge density of the polymer backbone. Some of the polymers which have been used to show that electron diffusion increases with increasing tether length are based on a poly(vinylpyridine) (PVP) backbone.[13, 25] These polymers swell and their backbones become more mobile when the pyridine groups are quaternized or protonated due to positive charge repulsion between the polymer chains. The fact that redox centers attached to long tethers greatly increase the $D_{app}$ and $J_{max}$ for these films shows that the polymer backbone is quite rigid. The long tethers allow the redox centers to remain mobile even though the polymer backbones do not have a high mobility. In the case of the Fc-$C_x$-LPEI polymers, the LPEI backbone should be highly protonated at physiological pH and consists only of $sp^3$ carbon-carbon or carbon-nitrogen bonds, which could make it very flexible (assuming the rigidity resulting from the elongation of the backbone is not too high). In addition, the protonation of LPEI should have a more significant "mobility effect" than the protonation/quaternization of PVP. The proximity of charges in LPEI should lead to inter- *and* intra-chain charge repulsion and a high amount of polymer backbone flexibility. Therefore, attaching longer tethers to LPEI may not have a measurable effect on electron transport because the mobility of the ferrocene groups in Fc-$C_1$-LPEI is already at a maximum due to the

highly protonated, flexible polymer backbone. An experiment to verify this hypothesis might be to purposely attach the ferrocene groups to more rigid tethers and observe how $D_{app}$ changes.

*Long Term Stability of Wired GOx Sensors*

Enzymatic stability tests were performed to determine whether the electrochemical stability observed in the cyclic voltammetric response of the Fc-$C_3$-LPEI and Fc-$C_6$-LPEI hydrogels would translate to stability of glucose sensors based on these polymers. Figure 4.11 shows continuous operation stability tests for sensors made with the different polymers. The half-life of the Fc-$C_1$-LPEI based sensor was ~3 hours while the half lives of Fc-$C_3$-LPEI and Fc-$C_6$-LPEI based sensors were ~38 and ~32

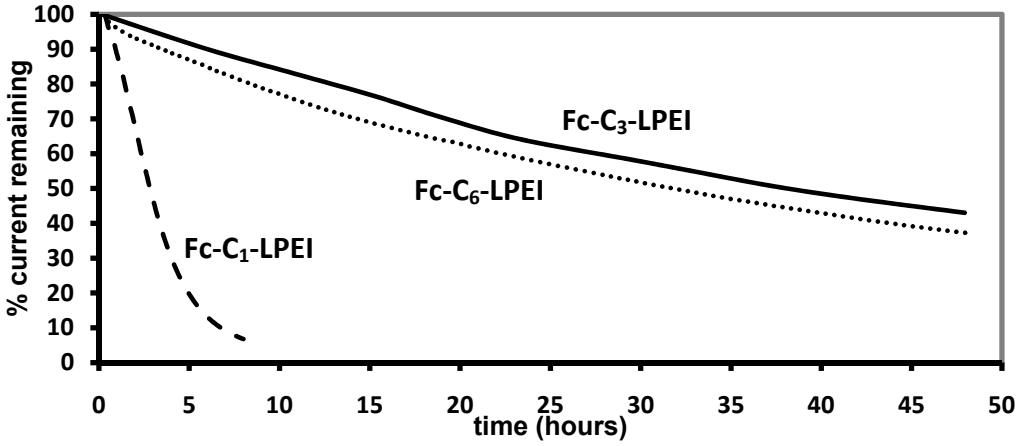


**Figure 4.11**: Effect of tether length on the operational enzymatic stability of glucose biosensors. Cross-linked films of GOx and Fc-$C_1$-LPEI, Fc-$C_3$-LPEI, and Fc-$C_6$-LPEI were operated continuously in PBS at pH 7.4 and 10 mM glucose. E = 0.4 V, T = 25$^o$ C.

hours respectively. These increases in half-life relative to the electrochemical stability experiments are likely due to the smaller amount of time that the ferrocenes are kept in an oxidized state. In this experiment, once a ferrocene was oxidized, it was quickly

reduced by an enzyme or by another ferrocene (connected to an enzyme). In the cycling experiment, once the redox potential of the ferrocenes in the films was exceeded, they remained oxidized until the potential was cycled back to a reducing value, which allowed more time for phosphate binding or nucleophilic attack on the ferrocenium ion. These results clearly indicate that in addition to the electrochemical stability, extension of the ferrocene group away from the LPEI backbone with a longer tether also results in a more stable enzymatic response as well.

**Summary and Conclusions**

In this chapter we report the synthesis of two new poly(ethylenimine)-based redox polymers: Fc-$C_3$-LPEI and Fc-$C_6$-LPEI. We demonstrate that the extension of the ferrocene groups away from the LPEI backbone eliminates the multi-wave redox behavior and the oxidative degradation observed in crosslinked films of Fc-$C_1$-LPEI in the presence of dibasic phosphate, and at high pH. We hypothesize that this is due to the mitigation of simultaneous binding of the phosphate to the polymer backbone amines and the ferrocenium. In addition, we also show that both Fc-$C_3$-LPEI and Fc-$C_6$-LPEI are able to exchange electrons with the FAD centers in GOX and produced current densities at saturation of ~600-1000 μA/$cm_2$. Finally, we demonstrate that the stability observed in the electrochemical response of the crosslinked Fc-$C_3$-LPEI and Fc-$C_6$-LPEI films translates to an enhanced stability in the sensor response under continuous operation in comparison to the Fc-$C_1$-LPEI. The elimination of the degrading phosphate effects and the increased stability are important steps in developing these redox polymers for biosensing and biofuel cell applications. The sum of these results

indicate that for redox polymers based on LPEI and ferrocene, a three-carbon spacer between the redox centers and the polymer backbone gives optimal performance in the areas of current response and stability.

## Experimental

*Chemicals and Solutions*

Glucose oxidase (GOX) from Aspergillus niger (EC 1.1.3.4, Type X-S, 246 units/mg of solid, 75% protein), ferrocenecarboxaldehyde, poly(2-ethyl-2-oxazoline), (6-bromohexyl)ferrocene, and all salts and acids were purchased from Sigma-Aldrich and used as received. Ethylene glycol diglycidyl ether (EGDGE) was purchased from Polysciences Inc., Warrington, PA. Stock solutions of 2 M glucose were allowed to mutarotate for 24 hr before use and subsequently kept refrigerated at 4°C.

Ferrocene was acylated[37] using aluminum chloride and 3-chloropropionyl chloride to give 3-chloropropionylferrocene,[38] which was reduced with trifluoroacetic acid/sodium borohydride[39] to give (3-chloropropyl)ferrocene. Spectral characterization of (3-chloropropyl)ferrocene showed it to be identical to the known compound.[40]

*Redox Polymer Syntheses*

Linear poly(ethylenimine) (LPEI) and the redox polymer designated as Fc-$C_1$-LPEI was synthesized by coupling ferrocenecarboxaldehyde to linear poly(ethylenimine) (LPEI) according to our previously published protocol.[29] Hexylferrocenyl-LPEI [Fc-$C_6$-LPEI] was synthesized as the partial hydrobromide salt

by adding 300 mg (7.00 mmol repeat units) of LPEI to 10 mL of acetonitrile in a flask fitted with a reflux condenser. The mixture was heated to reflux solvent for 10 minutes. Methanol (2 mL) was added and the solution changed from cloudy to clear. (6-Bromohexyl)ferrocene (380 mg, 1.09 mmol) was added slowly to the polymer solution using a pipette. The solution was heated to reflux solvent overnight and the solvent was removed under reduced pressure. The residue was rinsed with diethyl ether to remove residual ferrocenyl impurities and dried under vacuum to yield ~ 600 mg of Fc-C6 LPEI.

(Ferrocenylpropyl)-LPEI (Fc-$C_3$-LPEI) was synthesized by adding 100 mg (2.3 mmol repeat units) of LPEI to 10 mL of a 10:1 mixture of acetonitrile and methanol in a flask fitted with a reflux condenser. (3-Chloropropyl)ferrocene (100 mg, 0.38 mmol) was added along with 1 eq. of $K_2CO_3$ and the mixture was heated to reflux solvent for 3 days. The solvent was removed under reduced pressure and diethylether was added to remove residual ferrocenyl impurities. The polymer was dissolved in benzene and the mixture was filtered to remove any salts. The solvent was removed under reduced pressure to yield ca. 170 mg Fc-$C_3$-LPEI.

*$^1$H-NMR Characterization of the Polymers*

To measure the amount of ferrocene substitution for each polymer, the integral of the area under the peaks for the ferrocene ring hydrogens at ca. δ 4.0-4.3 was set as nine, and the remaining peaks were integrated relatively. In a normal repeat unit (-$CH_2CH_2NH$-), the polymer backbone has four non-exchanging hydrogens. For Fc-$C_1$-

LPEI, this means that four divided by the integral of the backbone hydrogens (δ 2.4-2.9) gives the substitution percentage as seen in equation 1.

**Fc-$C_1$-LPEI**

$^1$H NMR ($CD_3OD$): ca. δ 2.4-2.9 (br, -$CH_2$N-) 3.4-3.6 (br, -N-$CH_2$-Fc), 4.1-4.3 (br, Fc ring H)

**Equation 1:** Fc-$C_1$-LPEI percent substitution = $\frac{4}{backbone\ hydrogen\ integration}\ x\ 100$

For Fc-$C_3$-LPEI and Fc-$C_6$-LPEI the equation is slightly different: The hydrogens in the first methylene group that is attached to the ferrocene tether have a similar chemical shift relative to the backbone hydrogens. Therefore, we must alter the formula by subtracting the first two tether hydrogens from the backbone integration before the division step (equation 2). Using these equations, it was calculated that all three of the polymers were between 15% and 17% substituted.

**Fc-$C_3$-LPEI**

$^1$H NMR ($CD_3OD$): ca. δ 1.6-1.8 (br, -$CH_2$-), 2.3-2.4 (br t,-$CH_2$Fc), 2.5-3.0 (br, -$CH_2$N-), 4.0-4.2 (br, Fc ring H)

**Fc-$C_6$-LPEI**

$^1$H NMR ($CD_3OD$): ca. δ 1.25-1.45 (br, -$CH_2$-), 1.45-1.6 (br, -$CH_2$-), 2.3-2.4 (br t, -$CH_2$Fc), 2.5-3.0 (br, -$CH_2$N-), 4.0-4.1 (br, Fc ring H)

**Equation 2**: Fc-$C_3$-LPEI and Fc-$C_6$-LPEI percent substitution = $\frac{4}{backbone\ hydrogen\ integration - 2}\ x\ 100$

*Enzyme Sensor Construction*

Glassy carbon electrodes (3 mm diameter) were cleaned before use by polishing them successively on three grades of alumina (5, 1, 0.3 μm) and washing thoroughly with Nanopure water after each polishing step. Solutions of the three different redox polymers (Fc-$C_1$-LPEI, Fc-$C_3$-LPEI, Fc-$C_6$-LPEI) were all prepared in the same way by dissolving them in water by addition of a 0.1 M HCl solution until the final concentration of the polymer solution was 10 mg/ml and a pH of 5.0 ±0.2. Glucose sensors were prepared by crosslinking glucose oxidase to the redox polymers to form enzymatic redox hydrogels: 14 ml of polymer solution (10 mg/ml), 6 ml of glucose oxidase solution (10 mg/ml), and 0.75 ml of EGDGE solution (10% v/v) were mixed together and 3 ml aliquots were placed onto the glassy carbon electrode surface. The mixture was allowed to dry for 18-24 hours.

*Electrochemical Measurements*

Constant potential experiments and cyclic voltammetry were performed with a CH Instruments Model 832 bipotentiostat, while electrochemical impedance measurements were performed with a Solartron SI 1260 impedance/gain-phase analyzer in conjunction with a SI 1287 potentiostat. Unless otherwise noted, experiments were conducted in a three-electrode cell configuration with a saturated calomel reference electrode (SCE), and a platinum wire counter electrode with phosphate buffered saline (PBS), pH 7.4, as the background electrolyte. Constant temperature (25±1°C) was maintained during the

experiments by using a water-jacketed electrochemical cell connected to a circulating water bath.

*XPS Measurements*

X-ray photoelectron spectroscopy (XPS) was performed on cross-linked films of Fc-$C_1$-LPEI and GOX that were either (a) soaked in PBS (pH 7.4) for 3 h, washed with distilled water, and dried or (b) subjected to electrochemically cycling (scan rate ) 50 mV/s) in PBS (pH 7.4) between 0 and 0.7 V (vs. SCE), washed with distilled water, and dried. To test these films in the XPS instrument, we prepared the Fc-$C_1$-LPEI/GOX films on 2 mm flat gold electrodes on glass slides. XPS measurements were recorded with a Physical Electronics PHI 5800 ESCA system with monochromatic Al KR X-rays (photon energy of 1486.6 eV). The system was operated at 350 W and 15 kV with a background pressure of $2 \times 10^{-9}$ Torr.

*Swelling and Film Thickness Measurements*

Thickness profiles of cross-linked redox polymer films were measured by profilometry. Cross-linked polymer films were formed by depositing 3.3 $\mu$L drops of the appropriate redox polymer-crosslinker solution on clean glass slides and curing them overnight. The thickness of the cross-linked films was then measured with a Ambios XP2 Profilometer at a scan speed of 0.05 mm/s and a scan force of 0.05 mg. Optical images of the swelling of cross-linked redox polymer films were acquired in real time (30 frames per second) with a Zeiss Stemi DV4 microscope equipped with a cooled CCD camera (DAGE-MTI CCD-300) and recorded on a VHS recorder. Individual images were captured and analyzed with MetaMorph Imaging Software. To image the swelling process, 3 mm glassy carbon electrodes were coated with the appropriate cross-linked

polymer film and horizontally assembled into an imaging cell. Prior to filling the cell with aqueous solution, the microscope was focused to image the dry polymer film on the electrode surface and the video recording was started. With the electrode surface in focus, the cell was then quickly filled with water (pH 3, T = 25 °C) and continually imaged for at least 5 min.

*Calculations and Statistics*

Values are presented as mean ± standard error of the mean (SEM) unless otherwise specified.

**Acknowledgements**

We would like to thank Dr. Min Shen for help in performing the XPS measurements and Dr. Joel C. Keay for his help in performing the film thickness measurements.

## References


1. Inzelt, G., Mechanism of Charge Transport in Polymer-Modified Electrodes. In *Electroanal. Chem.*, Bard, A. J., Ed. Marcel Dekker: New York, 1994; Vol. 18.

2. Wang, X. J.; Wang, L.; Wang, J. J.; Chen, T., *J. Phys. Chem. B* **2004,** *108* (18), 5627-5633.

3. Forster, R. J.; Vos, J. G., *Macromolecules* **1990,** *23* (20), 4372-4377.

4. Hale, P. D.; Boguslavsky, L. I.; Inagaki, T.; Karan, H. I.; Lee, H. S.; Skotheim, T. A.; Okamoto, Y., *Anal. Chem.* **1991,** *63* (7), 677-682.

5. Martin, C. R.; Rubinstein, I.; Bard, A. J., *J. Am. Chem. Soc.* **1982,** *104* (18), 4817-4824.

6. Oyama, N.; Anson, F. C., *J. Electrochem. Soc.* **1980,** *127* (1), 247-248.

7. Inzelt, G., *Electrochim. Acta* **1989,** *34* (2), 83-91.

8. Leech, D.; Forster, R. J.; Smyth, M. R.; Vos, J. G., *J. Mater. Chem.* **1991,** *1* (4), 629-635.

9. Guschin, D. A.; Sultanov, Y. M.; Sharif-Zade, N. F.; Aliyev, E. H.; Efendiev, A. A.; Schuhmann, W., *Electrochim. Acta* **2006,** *51* (24), 5137-5142.

10. Taylor, C.; Kenausis, G.; Katakis, I.; Heller, A., *J. Electroanal. Chem.* **1995,** *396* (1-2), 511-515.

11. Galloway, J. W.; Barton, S. C., *J. Am. Chem. Soc.* **2008,** *130*, 8527.

12. Ohara, T. J.; Rajagopalan, R.; Heller, A., *Anal. Chem.* **1993,** *65* (23), 3512-3517.

13. Aoki, A.; Rajagopalan, R.; Heller, A., *J. Phys. Chem.* **1995,** *99*, 5102-5110.

14. Rajagopalan, R.; Aoki, A.; Heller, A., *J. Phys. Chem.* **1996,** *100*, 3719-3727.

15. Gulce, H.; Celebi, S. S.; Ozyoruk, H.; Yildiz, A., *Pure Appl. Chem.* **1997,** *69* (1), 173-177.

16. Heller, A.; Calabrese Barton, S., *J. Phys. Chem. B* **2001,** *105*, 11917-11921.

17. Kulagina, N. V.; Michael, A. C., *Anal. Chem.* **2003,** *75* (18), 4875-4881.

18. Smutok, O.; Ngounou, B.; Pavlishko, H.; Gayda, G.; Gonchar, M.; Schuhmann, W., *Sensors and Actuators B: Chemical* **2006,** *113* (2), 598.

19. Timur, S.; Yigzaw, Y.; Gorton, L., *Sensors and Actuators B: Chemical* **2006**, 684-691.

20. Wagner, J. G.; Schmidtke, D. W.; Quinn, C. P.; Fleming, T. F.; Bernacky, B.; Heller, A., *Proc. Natl. Acad. Sci. U. S. A.* **1998,** *95* (11), 6379-6382.

21. Heller, A., *Phys. Chem. Chem. Phys.* **2004,** *6* (2), 209-216.

22. Tasca, F.; Gorton, L.; Harreither, W.; Haltrich, D.; Ludwig, R.; Noll, G., *J. Phys. Chem. C* **2008,** *112* (35), 13668-13673.

23. Kavanagh, P.; Boland, S.; Jenkins, P.; Leech, D., *Fuel Cells* **2009,** *9* (1), 79-84.

24. Chen, T.; Barton, S. C.; Binyamin, G.; Gao, Z. Q.; Zhang, Y. C.; Kim, H. H.; Heller, A., *J. Am. Chem. Soc.* **2001,** *123*, 8630-8631.

25. Mao, F.; Mano, N.; Heller, A., *J. Am. Chem. Soc.* **2003,** *125* (16), 4951-4957.

26. Suzuki, M.; Kobayashi, S.; Kimura, M.; Hanabusa, K.; Shirai, H.; Kurimura, Y., *J. Chem. Soc., Faraday Trans.* **1996,** *92* (22), 4511-4513.

27. Willner, I.; Lapidot, N.; Riklin, A.; Kasher, R.; Zahavy, E.; Katz, E., *J. Am. Chem. Soc.* **1994,** *116* (4), 1428-1441.

28. Merchant, S.; Glatzhofer, D. T.; Schmidtke, D. W., *Langmuir* **2007,** *23*, 11295.

29. Merchant, S.; Tran, T. O.; Meredith, M. T.; Cline, T. C.; Glatzhofer, D. T.; Schmidtke, D. W., *Langmuir* **2009,** *25* (13), 7736-7742.

30. Calvo, E. J.; Danilowicz, C.; Diaz, L., *J. Chem. Soc., Faraday Trans.* **1993,** *89* (2), 377-384.

31. Bu, H. Z.; Mikkelsen, S. R.; English, A. M., *Anal. Chem.* **1995,** *67* (22), 4071-4076.

32. Calvo, E. J.; Danilowicz, C.; Diaz, L., *J. Electroanal. Chem.* **1994,** *369* (1-2), 279-282.

33. Calvo, E. J.; Etchenique, R.; Danilowicz, C.; Diaz, L., *Anal. Chem.* **1996,** *68* (23), 4186-4193.

34. Ikeda, S.; Oyama, N., *Anal. Chem.* **1993,** *65* (14), 1910-1915.

35. Ruiz, J.; Medel, M. J. R.; Daniel, M. C.; Blais, J. C.; Astruc, D., *Chem. Commun. (Cambridge, U. K.)* **2003,** (4), 464-465.

36. Reynes, O.; Moutet, J. C.; Royal, G.; Saint-Aman, E., *Electrochim. Acta* **2004,** *49* (22-23), 3727-3735.

37. Alonso, E.; Labande, A.; Raehm, L.; Kern, J. M.; Astruc, D., *C. R. Acad. Sci. Paris, serie IIc* **1999,** *2*, 209-213.

38. Beer, P. D.; Chen, Z.; Drew, M. G. B.; Johnson, A. O. M.; Smith, D. K.; Spencer, P., *Inorg. Chim. Acta* **1996,** *246* (1-2), 143-150.

39. Bunte, C.; Prucker, O.; Konig, T.; Ruhe, J., *Langmuir* **2010,** *26* (8), 6019-6027.

40. Bunte, C.; Ruhe, J., *Macromoecular Rapid Communications* **2009,** *30*, 1817-1822.

41. Prins, R.; Korswagen, A. R.; Kortbeek, A. G. T. G., *J. Organomet. Chem.* **1972**, 335-344.

42. Gregg, B. A.; Heller, A., *Anal. Chem.* **1990,** *62* (3), 258-263.

43. Swoboda, E. P. B.; Massey, V., J. Biol. Chem. **1965,** *240* (5), 2209-2215

# CHAPTER 5: HIGH CURRENT DENSITY FERROCENE-MODIFIED LINEAR POLY(ETHYLENIMINE) BIOANODES AND THEIR USE IN BIOFUEL CELLS

Major portions of this chapter are taken from Meredith, M. T.; Glatzhofer, D.; Kao, D.-Y.; Schmidtke, D. W.; Hickey, D., *J. Electrochem. Soc.* **2010,** *Submitted*.

## Introduction

The development of fuel cells that can operate using biological catalysts and renewable fuels has gained recent attention.[1-4] Biofuel cells resemble traditional fuel cells in their fundamental operating principles (oxidation of a fuel to produce protons/reduction of oxygen to water) but differ greatly in other ways. Biofuel cells use renewable catalysts (microbes or enzymes) and are operated under mild conditions (usually 25 or 37$^{o}$ C, pH 5-7) relative to traditional fuel cells. The enzymes used in biofuel cells are extremely selective for their respective substrates, allowing for the removal of separator membranes and the operation of many biofuel cells in compartment-less containers. These properties make biofuel cells attractive as alternative energy sources for implantable electronic devices and other portable electronics.

However, because biofuel cells use enzymes as catalysts, the stabilities of bioanodes and biocathodes can be fairly low and the highest power densities produced using single-enzyme electrodes in compartment-less biofuel cells to date are in the 100's of $\mu W/cm^2$, where the limiting electrodes are anodic.[5, 6] In order to improve these power densities, some groups are working on complex enzyme cascades[7-9] to allow for complete oxidation of biofuels to $CO_2$, and others are working with hybrid

enzymatic/direct methanol fuel cells in order to increase the low power densities typically obtained from biofuel cells.[10, 11] Still others are using innovative nanomaterials to enhance the connection between enzymes and electrode surfaces.[12-16]

Because these systems are complex, expensive, and/or use precious metal catalysts, there is a need for simple, low-cost, single enzyme bioelectrodes, especially bioanodes, which generate high current and power densities when used in compartment-less biofuel cells. One common method for creating this type of biofuel cell uses a dual enzyme system with an oxidase/dehydrogenase enzyme immobilized on the anode and an oxygen-reducing enzyme (usually bilirubin oxidase (BOD) or laccase) at the cathode (e.g. Scheme 5.01).[17-20] In these examples, the enzymes are entrapped in cross-linked, semi-permeable polymer hydrogels and electrons are "wired" from the active sites to the electrode surfaces by utilizing covalently attached organic or organometallic mediators. This method allows many enzymes to be immobilized near the electrode surface without the need to orient the active sites within direct electron transfer distance of the electrodes.

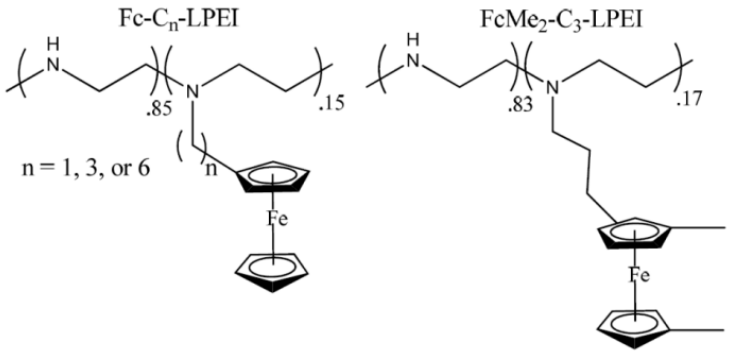


**Figure 5.01: Structures of Polymers Discussed or Used in this Study**

Recently, our group synthesized several new redox polymers (Figure 5.01, Fc-$C_n$-LPEI) based on linear poly(ethylenimine) (LPEI) and ferrocene[21-23] which allowed for the efficient shuttling of electrons between the FAD cofactor in GOx and an electrode surface. Anodic sensors constructed with Fc-$C_1$-LPEI gave current densities of up to 1.2 mA/cm$^2$ at room temperature under saturating glucose conditions.[21] However, this polymer was unstable at higher pH values and in the presence of dibasic phosphate.[23] To address this issue, we carried out studies to optimize the spacer length between LPEI and the ferrocene moiety, as previous studies had shown that extending the redox center away from the polymer backbone could improve the performance of sensors by increasing electron diffusion rates.[24-26] This study showed that a 6-carbon spacer (Fc-$C_6$-LPEI) improved the stability while reducing the maximum current density ($j_{max}$) of the sensors, while a polymer with a 3-carbon spacer (Fc-$C_3$-LPEI) both improved the stability and produced a $j_{max}$ of approx. 1 mA/cm$^2$.[23]

The high current densities obtained with these polymers led us to investigate the possibility of using them as materials for biofuel cell anodes. It is known that one primary factor which influences the operating voltage of a mediated enzymatic biofuel cell is the difference in redox potentials of the anodic and cathodic mediators, as they are primarily responsible for electron transfer at each electrode.[4] This voltage, in combination with the current that is generated, determines the power output of the biofuel cell. Sensors constructed with the polymers previously developed in our group were capable of generating high anodic current densities in the presence of glucose. However, we sought to lower the redox potential of the ferrocene-modified LPEI polymers in order to create an increased potential difference between the cathodic and

anodic mediators to more effectively drive the current from anode to cathode and increase the power densities.

Ferrocenes substituted with alkyl substituents are known to exhibit lower redox potentials than unsubstituted ferrocenes.[27-29] This is due to the electron donating nature of each attached alkyl group, with each group lowering the redox potential of the ferrocenes by ~ 50 mV. Another consequence of methylation is that the stability of a methylated ferrocenium cation is higher than that of a non-methylated ferrocenium cation.[30, 31] Therefore, we hypothesized that using 1,1'-dimethylferrocene as the redox mediator tethered to LPEI would lower the redox potential of the polymer by ~ 100 mV and increase the electrochemical stability of films made with this polymer.

In this study, we characterize and compare the electrochemical properties of 1,1'-dimethylferrocene-modified LPEI (Figure 5.01, $FcMe_2$-$C_3$-LPEI) and Fc-$C_3$-LPEI. The use of these two polymers as anodic mediators in compartment-less, glucose/$O_2$ biofuel cells, which utilize an oxygen-reducing cathode comprised of laccase and cross-linked poly[(vinylpyridine)Os(bipyridyl)$_2$Cl$^{2+/3+}$] (PVP-Os) as a mediator,[32, 33] is discussed.

**Results and Discussion**

*Effect of Ferrocenyl Moiety Methylation on Redox Potential and Electrochemical Stability*

In order to evaluate the effect of ferrocenyl moiety methylation on the electrochemical properties of Fc-$C_3$-LPEI, cyclic voltammetry and stability tests were

performed on cross-linked films of Fc-$C_3$-LPEI and $FcMe_2$-$C_3$-LPEI in phosphate buffered saline (PBS).

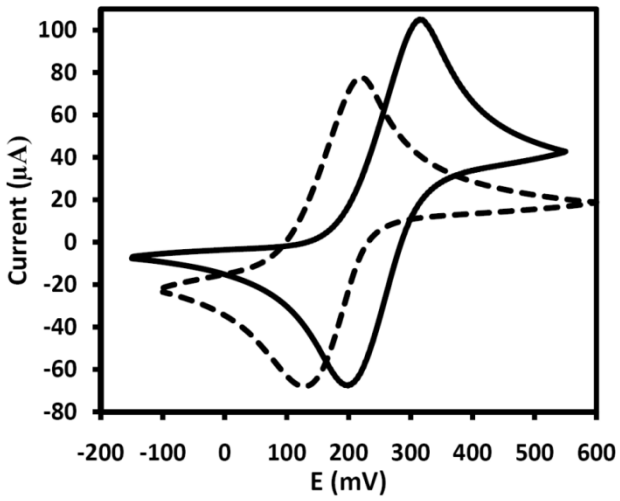


**Figure 5.02: Electrochemistry of Anodic Redox Polymers.** Cyclic voltammogram of cross-linked films of Fc-$C_3$-LPEI (solid line) and $FcMe_2$-$C_3$-LPEI (dashed line). PBS, pH 7.4, scan rate = 50 mV/s, T = 25$^o$ C

Figure 5.02 shows the cyclic voltammograms of these cross-linked polymer films at pH 7.4 in PBS. The redox potential, ($E_{1/2}$, estimated by ($E_{pa}$+$E_{pc}$)/2) of $FcMe_2$-$C_3$-LPEI was 0.17 V, which is lower by 0.09 V from the redox potential of the Fc-$C_3$-LPEI (Table 5.01). This agrees with the earlier prediction that each methyl group should lower the redox potential of the ferrocene by ~50 mV.

To evaluate the effect of methyl groups on the electrochemical stability of these polymers, we cycled the potential of electrodes coated with cross-linked films of Fc-$C_3$-LPEI (0 → 0.5 or 0.7 V) and $FcMe_2$-$C_3$-LPEI (-0.1 → 0.5 or 0.7 V) and plotted the change in area beneath the oxidation wave (charge) as a function of time. Figure 5.03 shows the results of these experiments.

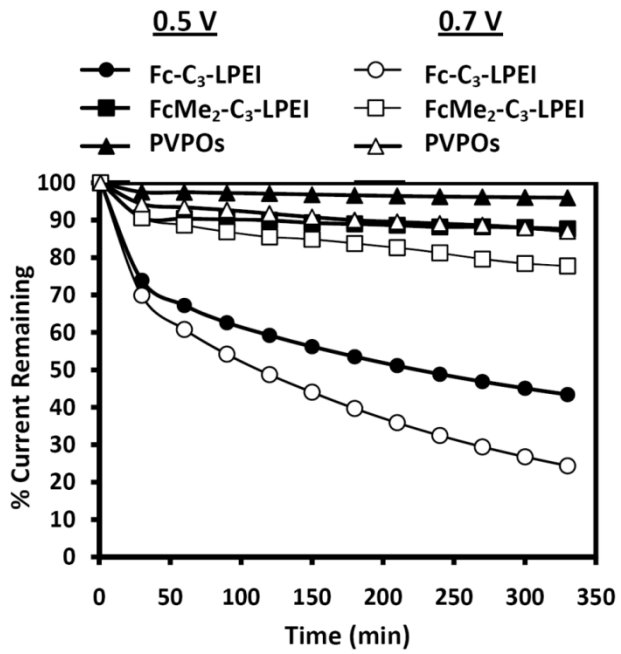


**Figure 5.03: Electrochemical Stability of Cathodic and Anodic Films.** Plot of the changes in area of integrated voltammetric waves for cross-linked films of $FcMe_2$-$C_3$-LPEI, Fc-$C_3$-LPEI*, and PVPOs cycled to either 0.7 V or 0.5 V at 50 mV/s in PBS buffer, pH 7.4, T = 25° C. *Data from reference 23.

After 330 minutes of cycling between 0 and 700 mV, the Fc-$C_3$-LPEI films lost 75% of their original current, with the first 30% of that loss occurring in the first 30 minutes of cycling. When the scan was shortened in the oxidative direction to 0.5 V, the Fc-$C_3$-LPEI films lost 57% of their original current, with 26% of that loss occurring within the first 30 minutes. For the methylated version of the polymer, the electrochemical stability was greatly improved. After 330 minutes of cycling between -0.1 V and 0.7 V, the $FcMe_2$-$C_3$-LPEI films lost 23% of their original current, with the first 10% of that loss occurring in the first 30 minutes of cycling. When the scan was shortened to -0.1V - 0.5 V, the $FcMe_3$-$C_3$-LPEI films lost only 13% of their original current, again with 10% of that loss occurring within the first 30 minutes. The initial loss in current (~30% for Fc-$C_3$-LPEI and 10% for $FcMe_2$-$C_3$-LPEI), which occurred regardless of the maximum cycling potential for each polymer, was somewhat unexpected and suggests

that there was an initial break-in period which occurred regardless of the maximum cycling potential. This extended break-in phenomenon could be due to a gradual collapse of the films due to phosphate binding to the LPEI backbone,[34, 35] which could lower the number of electrochemically accessible ferrocenes. This mechanism has been suggested in the past as a possible reason for the instability in our polymer films at pH 7 or greater.[22, 23] Once this initial break-in period was complete, the stability of the films was dependent on the amount of time that they were in an oxidized state, suggesting that the primary mechanism for electrochemical degradation in this region was probably related to the known degradation mechanisms seen with ferrocenium species when nucleophiles, protons, and/or $O_2$ molecules are present in the solution.[36, 37]

In order to compare the stability of these films with a more well-known redox polymer (also the redox polymer used in our biocathode), we cycled films of cross-linked PVP-Os from 0 → 0.5 V or 0.7 V, as seen in Figure 5.03. After cycling to 0.7 V for 330 minutes, the PVPOs film lost 13% of its original current, which is 10% less than the current loss for $FcMe_2$-$C_3$-LPEI over the same period of time. Cycling out to 0.5 V greatly improved the stability of the PVPOs film and it only lost 4% of its original charge, whereas cycling in this range for $FcMe_2$-$C_3$-LPEI yielded a charge loss of 13% - again, a roughly 10% difference between the two polymers.

Overall, the electrochemical cycling experiment showed that a large improvement was made over previously reported aqueous electrochemical stabilities of polymers containing non-methylated ferrocenes.[23, 38, 39] The 1,1'-dimethylated polymer retained twice as much current as the non-methylated polymer when cycling out to 0.7 V, and retained three times as much current when cycling to 0.5 V. This stability

increase occurs in spite of the fact that the 1,1'-dimethylferrocenium moiety was present in these experiments for even longer than the ferrocenium moiety due to the 90 mV difference in redox potentials between the two polymers. Because this substantial improvement was accomplished with only two methyl groups, we hypothesize that further methylation of the ferrocene moiety should increase stability even further and could yield redox polymers with electrochemical stabilities equal to or greater than those of redox polymers such as the osmium-based PVP polymers developed by Heller's group.[40] Experiments to investigate this hypothesis are currently underway in our lab.

*Effect of Ferrocenyl Moiety Methylation on Electron Transport*

As seen in Figure 5.02, the $i_{pa}$ for $FcMe_2$-$C_3$-LPEI (75 μA) was slightly lower than for that of Fc-$C_3$-LPEI (100 μA). This could be due to slower electron diffusion through the $FcMe_2$-$C_3$-LPEI film, and electrochemical impedance spectroscopy (EIS) was used to determine the $cDe^{1/2}$ for each polymer film (*De* = apparent electron diffusion coefficient and c = the electroactive redox site concentration). The impedance spectroscopy measurements were carried out at a DC potential of E = 0.25 V (for $FcMe_2$-$C_3$-LPEI) or 0.35 V (for Fc-$C_3$-LPEI) (vs. SCE) and an AC perturbation of 10 mV as previously described.[22] In the low frequency range, the impedance response was analyzed using the Randles circuit by plotting the imaginary impedance, Im(Z), versus the inverse square root of frequency, $w^{-1/2}$, with a slope equal to the Warburg coefficient, $s_w$:

$$Im(Z) = s_w w^{1/2}$$

The value of $cDe^{1/2}$ was determined directly from $s_w$:

$$s_w = RT/n^2F^2cDe^{1/2}$$

The $cDe^{1/2}$ values for cross-linked films of $FcMe_2$-$C_3$-LPEI with enzyme and without enzyme (Table 5.01) were in the same order of magnitude as what we have observed for other polymers based on linear PEI and ferrocene[23] and are actually slightly higher than the $cDe^{1/2}$ values for Fc-$C_3$-LPEI (Table 5.01), indicating that the addition of two methyl groups to the ferrocene does not significantly alter the rate of electron diffusion through cross-linked films of the polymer.

*Anodic Response to Glucose*

In order to evaluate how these polymers would perform in a biosensor or biofuel cell, we measured their steady-state response to glucose and determined their maximum current densities ($j_{max}$) and operational stabilities. Figure 5.04 shows steady-state glucose response curves for Fc-$C_3$-LPEI and $FcMe_2$-$C_3$-LPEI between 0 and 100 mM glucose at 25° C and 37° C. The sensitivities and $K_M$ values for each polymer were almost identical (Table 5.01), suggesting that methylation of the ferrocene moiety does not significantly alter the enzyme/polymer interaction or affect the way the polymers shuttle electrons from GOx to the electrode surface.

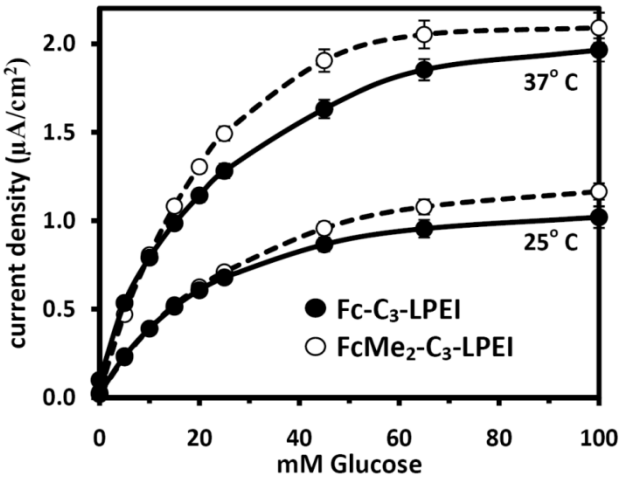


**Figure 5.04: Steady-State Enzymatic Response to Glucose.** Glucose calibration curves of electrodes modified with cross-linked films of each polymer at 25° C and 37°C. Phosphate-buffered saline, pH 7.4, E = 0.4 V (Fc-$C_3$-LPEI) or 0.3 V ($FcMe_2$-$C_3$-LPEI) vs. SCE

The $j_{max}$ at room temperature for both polymers was ca. 1 mA/cm$^2$. Increasing the temperature to 37° C led to an increase in current density, with a $j_{max}$ for each polymer of ca. 2 mA/cm$^2$. These values are among the highest reported current densities to date for planar, low surface area, single enzyme, mediated bioelectrodes. This data suggests that bioanodes constructed using Fc-$C_3$-LPEI and $FcMe_2$-$C_3$-LPEI could be capable of producing very high currents and power densities in a biofuel cell if the biocathode is of sufficiently high voltage and efficiency. In addition, these high current densities could be useful for the application of these redox polymers in mediated glucose biosensors.

We hypothesized that the increased electrochemical stability gained from adding the two methyl groups onto the ferrocene would translate to operational biocatalytic stability as well. Figure 5.05 shows continuous operation stability tests for Fc-$C_3$-LPEI and $FcMe_2$-$C_3$-LPEI.

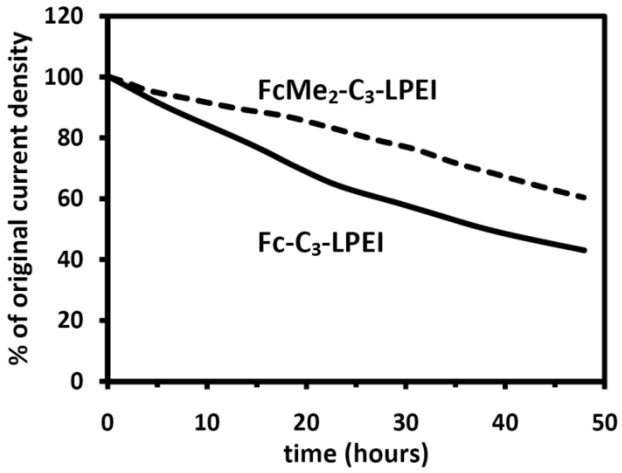


**Figure 5.05: Effect of Methylation on Stability of Steady-State Response to Glucose.** Cross-linked films of GOx and Fc-$C_3$-LPEI* or $FcMe_2$-$C_3$-LPEI, operated continuously in PBS at pH 7.4, E = 0.4 V vs. SCE for Fc-$C_3$-LPEI and E = 0.3 V for $FcMe_2$-$C_3$-LPEI. *Data from reference 23.

After 48 hours of operation, glucose sensors constructed with Fc-$C_3$-LPEI retained 40% of their original current density, while sensors made with $FcMe_2$-$C_3$-LPEI retained 60% of their original current density. This data clearly shows that the addition of the two methyl groups results in a more stable enzymatic response to glucose.

**Table 5.01: Effect of Redox Polymer Type on Electrochemical and Biocatalytic Properties**

| Redox Polymer | $E_{1/2}$ vs. SCE | $cDe^{1/2} \times 10^9$ (mol/cm$^2$ sec$^{1/2}$) With Enzyme (**Without Enzyme**) | Glucose Sensitivity ($\mu A/cm^2 \cdot mM$) | $J_{max}$ 25° C (**37° C**) (mA/cm$^2$) | $K_M$ (mM) |
|---|---|---|---|---|---|
| Fc-$C_3$-LPEI | 0.26 V | 1.06 ± 1.0 (**1.72 ± 0.64**) | 47 ± 2.0* | 1.01 ± 0.06* (**1.96 ± 0.07**) | 20.7 ± 2.3* |
| $FcMe_2$-$C_3$-LPEI | 0.17 V | 3.91 ± 0.44 (**5.42 ± 0.60**) | 45 ± 1.6 | 1.16 ± 0.05 (**2.09 ± 0.09**) | 21.7 ± 1.9 |

$E_{1/2}$ was calculated with the formula $(E_{pa} + E_{pc})/2$. Sensitivity was determined from the experimental current response at 5 mM glucose concentration. $J_{Max}$ is the maximum current obtained experimentally at saturating glucose concentrations. $K_M$ values were determined graphically from a Lineweaver-Burke plot. Values are expressed as mean ± standard error of the mean. *Values from reference 23.

*Cathode Development*

In order to construct a biofuel cell with the anodic polymers, a suitable cathode had to be developed in order to draw as much current out of the anode as possible at the highest possible voltage. As a first attempt, we tried using platinum as the cathode in the form of an E-TEK gas diffusion electrode (GDE) which is normally used in a polymer electrolyte membrane fuel cell. However, GDE's have also been used as biofuel cell cathodes,[8, 9] often with favorable results.

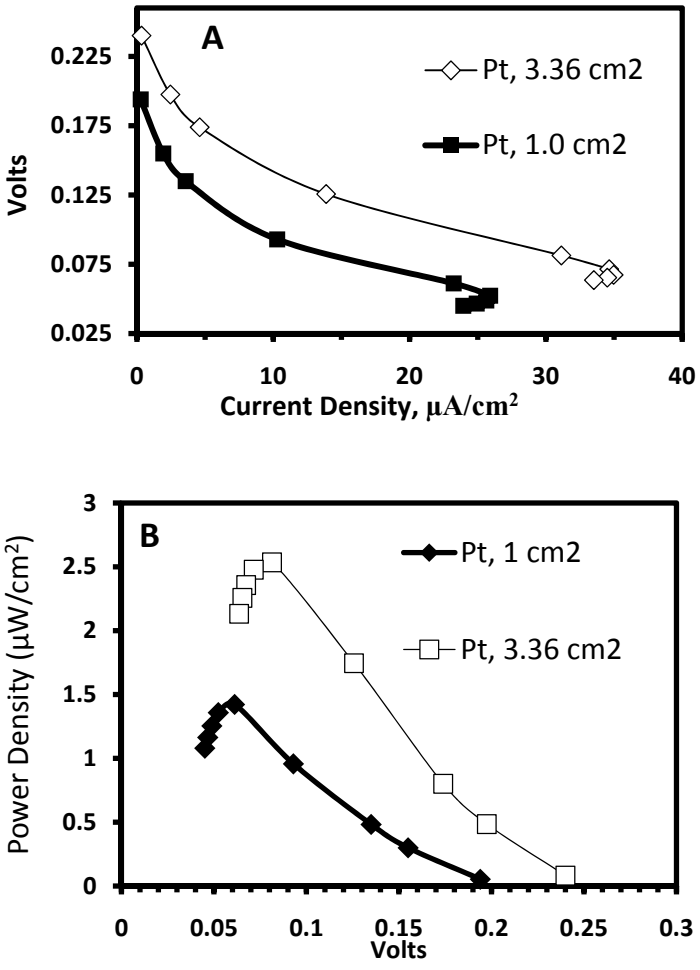


**Figure 5.06:** Polarization (A) and Power Density (B) curves for biofuel cell constructed with $FcMe_2$-$C_3$-LPEI and an E-TEK GDE. 60 mM glucose, PBS buffer, pH 7.4, air saturating conditions

Most of the GDE's used in the literature are coated with a proton exchange membrane such as Nafion,™ but as a first attempt, a GDE (1 $cm^2$) was submerged in PBS buffer along with a $FcMe_2$-$C_3$-LPEI/GOx anode. The performance of this biofuel cell is shown in Figure 5.06. An open circuit voltage (OCV) of 0.21 V was obtained with a maximum power density of 2.5 $\mu W/cm^2$ at 0.081 V. These values were lower than expected based on the reduction potential of $O_2$ at a platinum electrode (0.82 V vs. NHE at pH 7) and the redox potential of the anode (0.41 V vs. NHE). With a difference of 0.41 V, it was hoped that an open circuit voltage of at least 0.4 V would be produced. Also, in the polarization curve of the cell (Figure 5.06A), the current density reached a maximum and then decreased, which suggests that at lower resistances where current should be flowing freely through the circuit, mass transport of one of the substrates (most likely $O_2$) prevented the current from staying constant. To determine which electrode was limiting, a larger cathode was used (~ 3X larger in area) and this resulted in an increase the maximum power density by 78% (Figure 5.06B), suggesting that the cathode was the limiting electrode.

The poor performance of the cathode could have been due to many things, including mass transport of protons, $O_2$ and/or overpotential losses. Overall, the fact that a maximum current density of only 35 $\mu A/cm^2$ could be obtained from the cell indicated that the simple use of a platinum GDE as the cathode was inefficient. Current densities of up to 1 $mA/cm^2$ at room temperature could be obtained from the anodes using a potentiostat, and a large GDE could only produce 3.5% of that possible current.

In order to try to optimize the cell further and realize the potential of the anodes to produce high currents, we decided to develop enzymatic biocathodes. Two enzymes,

laccase and bilirubin oxidase (BOD), have been used by others to construct enzymatic biocathodes with much success. These enzymes are known as multi-copper oxidases based on their four copper atoms which are used to catalyze the reduction of $O_2$ to water. They can be utilized in either a direct electron transfer mode,[41-44] or a (more commonly) mediated electron transfer mode,[5, 18, 33] in which osmium-based polymers have been shown to effectively mediate electron transfer from laccase or BOD to an electrode surface. Our group has used PVPOs for previous studies involving other mediated enzymatic electrodes,[22, 45] and as such, it seemed that PVPOs was a good mediator to employ as the mediator between BOD or laccase and an electrode in order to try and produce more current out of the anode and increase the power of the biofuel cell.

The first enzyme which was selected for the biocathode was BOD. BOD can function at a high activity under physiological conditions, which favors its use in a compartment-less biofuel cell with GOx. On the other hand, BOD is known to have a lower redox potential than laccase[46] which could make the electron transfer to the osmium slower and lower the operating potential of the biofuel cell. In spite of this, we hypothesized that BOD would be the optimal enzyme for a biocathode due to the fact that it can operate under physiological conditions which mirror the optimal conditions of GOx (pH 7, $Cl^-$ present).

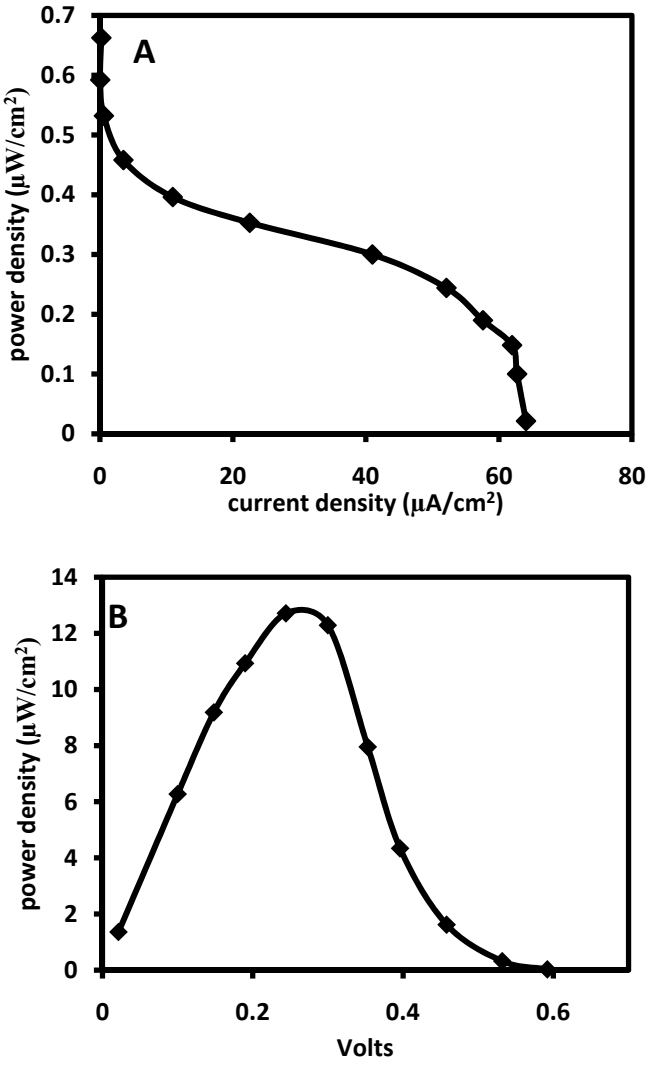


**Figure 5.07: Biofuel Cell With PVPOs/BOD Cathode.** Polarization (A) and Power Density (B) curves for a $FcMe_2$-$C_3$-LPEI/GOx anode coupled with a PVPOs/BOD cathode, operated in air-saturated PBS buffer at pH 7 with 60 mM glucose

Figure 5.07 shows a polarization and power curve for a biofuel cell using $FcMe_2$-$C_3$-LPEI/GOx as the anode and PVPOs/BOD as the cathode. The cell had an open circuit voltage of 0.530 V and a maximum power density of 13 $\mu W/cm^2$ at 0.244 V. As evidenced by the operating voltage, the use of the enzyme electrode provided a substantial increase from the operating potential (at max. power) obtained with the GDE cathode. However, the maximum current density of the cell was only 64 $\mu A/cm^2$,

which was lower than expected for this system and only double what was produced using the GDE cathode. The reason for this low current was due to the performance of the cathode, which only produced ca. 85 $\mu A/cm^2$ of current density when operated as an oxygen sensor with a potentiostat (not shown). This low performance could be due to multiple factors, including low enzyme activity (only ~ 8 units/mg, as reported on the bottle), low oxygen flux to the electrode, or the lack of any enhancers such as large surface-area electrodes or carbon nanotubes.

Because the biofuel cell performance with BOD as the cathodic enzyme was lower than what we expected, laccase was investigated for use as the cathodic enzyme. Laccase is a cheaper enzyme than BOD with a higher activity in its crude fungal extract (ca. 20 units/mg from Aldrich). Also, it has a higher redox potential than BOD by ca. 0.1 V.[47] The drawback to using laccase is that it has virtually no activity at pH 7 and can be inhibited with chloride ions, which are present in any physiological solution. Nevertheless, we took a systematic approach to the development of laccase cathodes, again using PVPOs as an electron transfer mediator.

The amount of enzyme incorporated into redox hydrogels is an important parameter to optimize, as it can have a large effect on the electrode performance. This parameter can vary widely depending on the redox polymer, enzyme, and purity of enzyme used. Lower amounts of enzyme typically do not produce high currents because there are not enough enzymes present to catalyze a high number of reactions at the electrode surface. Higher amounts of enzyme typically produce an insulating effect and prevent the diffusion of electrons through the film. Figure 5.08 shows the result of the laccase loading study. At low enzyme loadings, the current densities produced were

lower, and gradually increased with more enzyme with a maximum at 60% loading. As expected, electrodes with very high enzyme loading (>60%) produced low amounts of current due to the insulating nature of the enzymes.

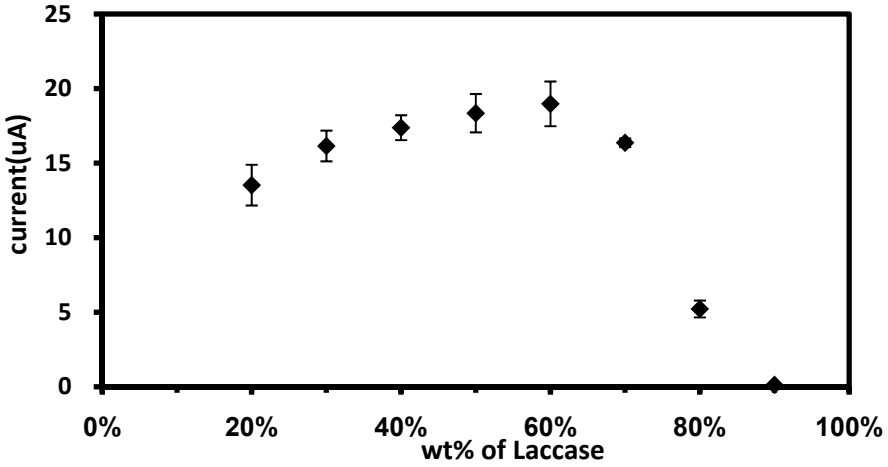


**Figure 5.08**: **Effect of laccase weight percent on biocathode current output.** PVPOs/laccase biocathodes were constructed with differing amounts of laccase and poised at 0.15 V vs. SCE in a pH 5.0 citrate solution. The maximum current produced for each wt. % was measured and plotted.

The PVPOs/laccase biocathodes gave the highest current densities of any of the cathodes, so we decided to use them to evaluate the anodic polymers Fc-$C_3$-LPEI and $FcMe_2$-$C_3$-LPEI in working biofuel cells.

*Glucose/$O_2$ Biofuel Cell*

To test the performance of these bioelectrodes in a biofuel cell, we constructed compartment-less biofuel cells using the mediated laccase biocathodes and bioanodes made with Fc-$C_3$-LPEI/GOx or $FcMe_2$-$C_3$-LPEI/GOx. A diagram of a biofuel cell utilizing Fc-$C_3$-LPEI as the anodic redox polymer is shown in Scheme 5.01. The electrons from the oxidation of glucose are passed from the GOx to the oxidized ferrocenium ions which are tethered to the LPEI. These electrons are transported

through the Fc-$C_3$-LPEI film until they reach the surface of the electrode, where they pass through the circuit and reach oxidized osmium species which are immobilized on the cathode.

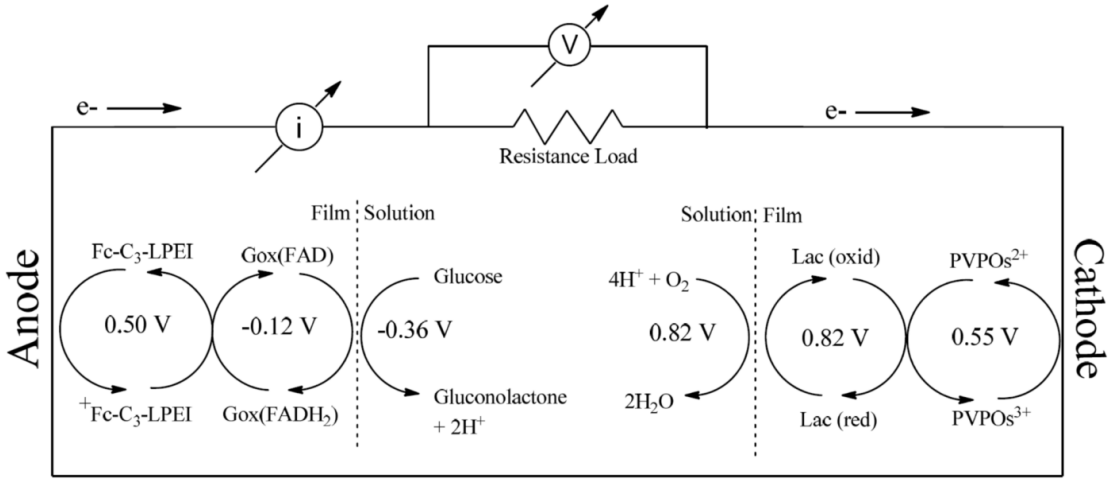


**Scheme 5.01: Biofuel Cell Schematic.** Flow of electrons from the oxidation of glucose to the reduction of oxygen showing the potentials of the involved redox reactions.[33, 48-50] All potentials are vs. SHE. GOx = glucose oxidase, FAD = flavin adenine dinucleotide, Lac = laccase.

The electrons then pass through the hydrogel until they reach the T1 site of laccase, where they travel to the T2/T3 trinuclear cluster and are utilized for the reduction of molecular oxygen to water.[51] The biggest source of loss in this biofuel cell is obviously due to the difference in potentials between the mediators and the enzymes, in particular on the anode side with a ΔE of 0.62 V. When combined with the ΔE of the cathodic mediator/enzyme couple (0.24 V), the total voltage loss due to enzyme/mediator overpotentials is 0.86 V. This large loss of theoretical cell voltage re-emphasizes the need to lower the redox potential of the anodic mediator and place it as close to the GOx redox potential as possible. The use of 3-(1,1-dimethylferrocenyl)propyl groups satisfies this need, and if Fc-$Me_2$-$C_3$-LPEI is used in the schematic, the loss in theoretical cell potential drops to 0.77 V.

Before testing the biofuel cell, the optimal pH conditions for each electrode were evaluated. Laccase is known to operate optimally in solution at slightly acidic pH values ranging from 3-5,[52] but glucose oxidase optimally catalyzes the reduction of glucose at fairly neutral pH values. Therefore, it was expected that the pH should be optimized to be as close to 7 as possible without affecting the cathode in order to maximize the current output from each electrode.

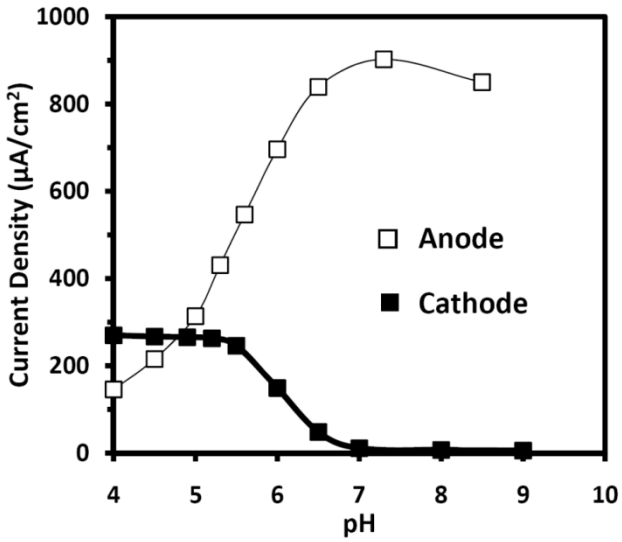


**Figure 5.09: pH Analysis of Anode and Cathode.** Steady-state measurements of current density for a $FcMe_2$-$C_3$-LPEI/GOx anode and PVPOs/laccase cathode at different pH values. Stirred solution under air-saturating conditions, 25° C, 0.05 M citrate, 60 mM glucose, E = 0.15 V vs. SCE (cathode) or 0.30 V vs. SCE (anode).

Figure 5.09 shows the plots of the pH profiles for the PVPOs/laccase biocathode and a $FcMe_2$-$C_3$-LPEI/GOx bioanode. As can be seen from the graph, the cathodic current density did not drop significantly until the pH was raised above pH 5.5. The anode behaved as expected, with the current density increasing significantly with each rise in pH up to 7.3. Therefore it was concluded that a pH of 5.5 should be the optimal pH for

the biofuel cells as the current density at the anode was maximized without significantly affecting the cathode performance.

Figure 5.10 shows polarization curves for the biofuel cell anodes and cathode at pH 5.5 and 25$^{o}$ C. The onset for the catalytic electro-oxidation current of glucose appeared at ca. 0.15 V for Fc-$C_3$-LPEI and reached a maximum at ca. 0.35 V. As expected, these values were shifted negatively for $FcMe_2$-$C_3$-LPEI, but only by ca. 0.05 V and not the 0.09 V that was expected by comparing the redox potentials of each polymer.

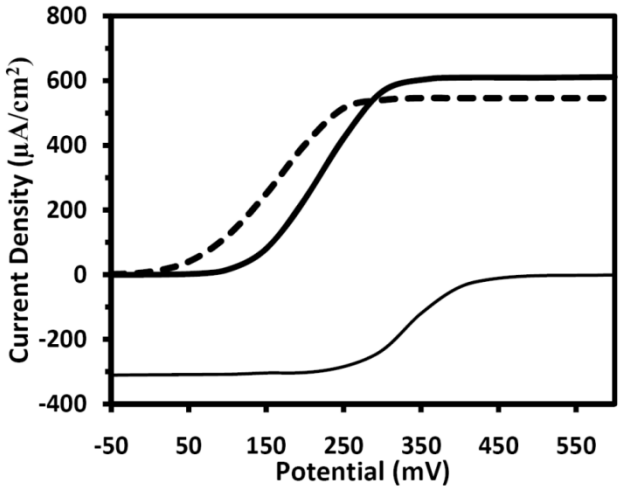


**Figure 5.10: Polarization Curves of the Electrodes.** Polarization of the Fc-$C_3$-LPEI anode (solid, thick line), $FcMe_2$-$C_3$-LPEI anode (dotted, thick line), and PVPOs/laccase cathode (thin line). Stirred solution under air-saturating conditions, 0.05 M citrate, pH 5.5, 60 mM glucose, scan rate = 1 mV/s.

The onset for the catalytic electro-reduction current of oxygen at the cathode occurred at ca. 0.25 V and reached a maximum at ca. 0.4 V. Comparing the midpoints of each anodic polarization curve to the midpoint of the cathodic curve, we calculated that biofuel cells constructed with these polymers should have cell voltages of ca. 0.15 V or 0.20 V at maximum power, depending on which anodic polymer is used. These

estimations of operating voltage were higher than what was predicted based on the redox potentials of the mediators at each electrode and show that the redox potentials of each enzyme play a role in determining biofuel cell operating voltages. The current densities at the anodes were 610 μA/cm$^2$ and 550 μA/cm$^2$ for Fc-$C_3$-LPEI and $FcMe_2$-$C_3$-LPEI, respectively, and the current density at the cathode was 320 uA/cm$^2$. Therefore, in a biofuel cell with stationary electrodes of equivalent surface areas, the cathode limits the maximum possible power output. Typically, the bioanode is the limiting electrode. The high current density of the bioanodes was exceptional, given that the glucose electrode was operating significantly far from the optimum pH for GOx (pH 7), and emphasizes the high efficiency with which these polymers mediate electron transfer between GOx and electrode surfaces. The limiting performance of the biocathode is most likely a consequence of using crude laccase and a smooth, stationary, low surface area electrode, as various reports suggest that wired laccase cathodes using osmium-based redox polymers should yield much higher current densities when purified laccase and rotating disc electrodes are used to increase the mass transport of $O_2$ to the cathode.[33 53]

Figures 11A and 11C show the polarization of stationary, compartment-less biofuel cells using each anodic polymer vs. the PVPOs/laccase cathode. The dependence of the cell power densities on voltage is also shown (Figures 11B and 11D), and a summary of the data from these fuel cells is provided in Table 5.02. As seen in the table, the difference in open circuit voltages (OCV) for each of the polymers was 0.05 V regardless of temperature. This likely reflects the 0.05 V difference seen in the polarization curves of each anode (Figure 5.10). The methylation of the ferrocene

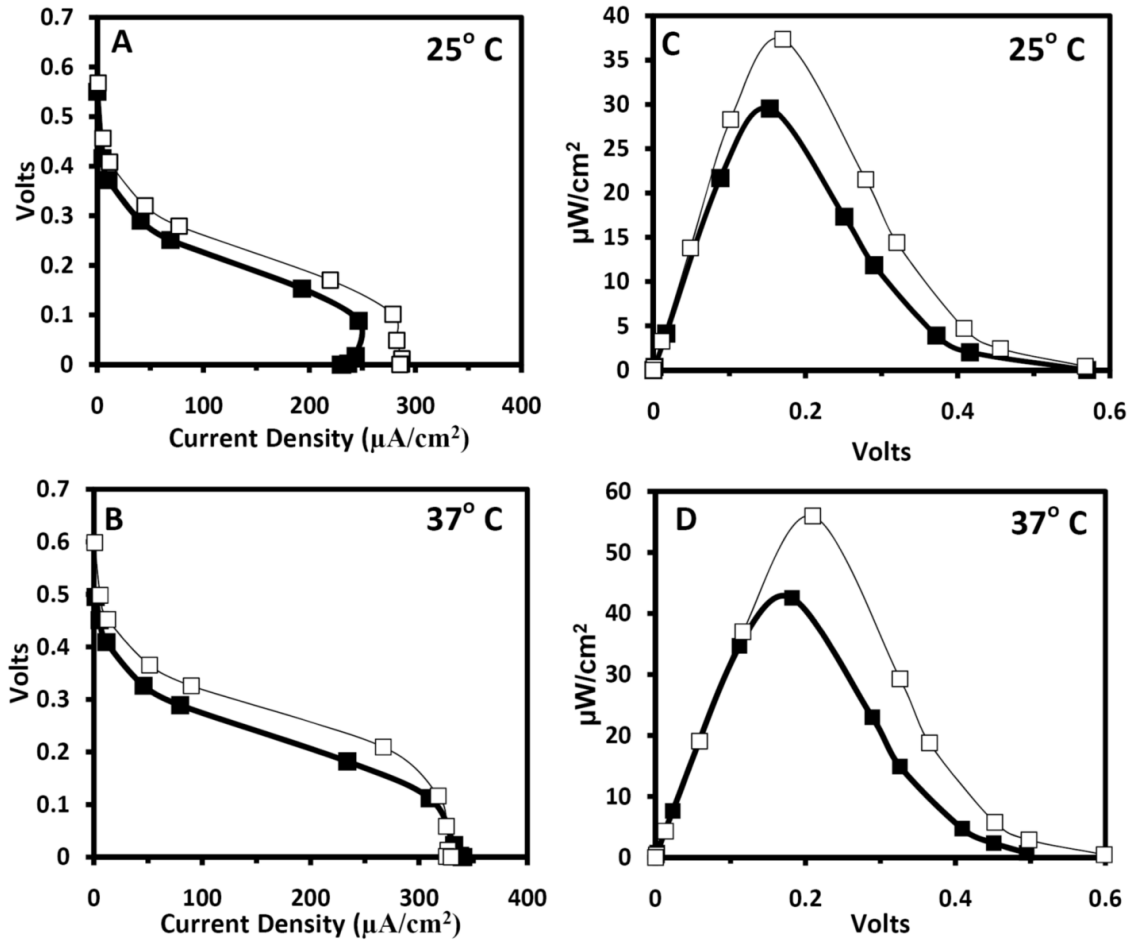


**Figure 5.11: Effect of Temperature and Polymer Type on Biofuel Cell Performance.** Polarization of the biofuel cells at 25° C (A) and 37° C (B) and dependence of the biofuel cell power density on cell voltage at 25° C (C) and 37° C (D) using Fc-$C_3$-LPEI (solid squares) and $FcMe_2$-$C_3$-LPEI (open squares). Cathode was PVPOs/laccase on a 3mm GC electrode. Stirred solution under air-saturating conditions, 0.05 M citrate, pH 5.5, 60 mM glucose.

moiety produced a less significant change in the operating potentials (at maximum current density), with a 0.02 V difference occurring at 25° C and a 0.03 V difference occurring at 37° C. Even though this difference was smaller than the ΔE for the OCV's, it produced a significant increase in power density at 25° C (27% increase), and at 37° C (33% increase).

In order to increase the power of the biofuel cells further, we sought a method to improve the current output of the cathode (since it was limiting). Multiple studies have

shown that mediated enzymatic biocathodes are limited by the mass-transport of $O_2$ to the electrode surface and that rotation of the biocathode can increase the rate of oxygen transport to the electrode surface and cause a dramatic increase in catalytic current.[33, 48, 54-56] As such, we fabricated PVPOs/laccase cathodes using rotating disc electrodes and used them in biofuel cells with the stationary anodes described above.

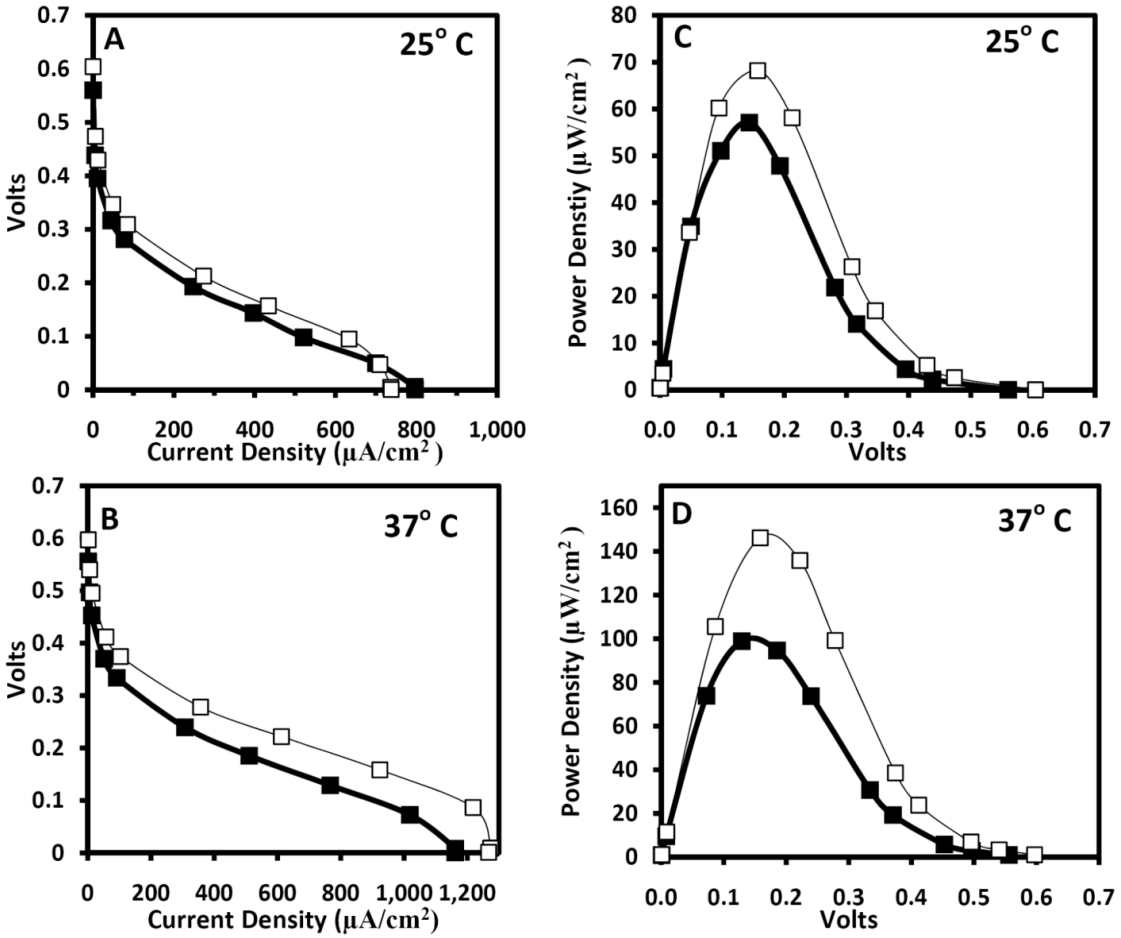


**Figure 5.12: Biofuel Cell Performance with RDE cathodes.** Polarization of the biofuel cells at 25° C (A) and 37° C (B) and dependence of the biofuel cell power density on cell voltage at 25° C (C) and 37° C (D) using Fc-$C_3$-LPEI (solid squares) and $FcMe_2$-$C_3$-LPEI (open squares). PVPOs/laccase cathode was cast on a 5 mm glassy carbon RDE and rotated at 2000 rpm. Stirred solution under air-saturating conditions, 0.05 M citrate, pH 5.5, 60 mM glucose. Current and power densities were calculated using the 3mm electrode area.

Figure 5.12 shows the polarization of these cells and the dependence of the cell power densities on voltage at 25° C and 37° C. A summary of the data from these fuel cells is also provided in Table 5.02. As expected, the use of the rotating biocathode resulted in a large increase in the power densities of the biofuel cells, indicating that mass transport of $O_2$ to the cathode was indeed limiting the cell's performance.

**Table 5.02: Summary of Biofuel cells with Stationary or Rotating Biocathodes at 25° and 37° C**

| Anodic Redox Polymer | Open Circuit Voltage (V) | Max. Power Density ($\mu W/cm^2$) | Max. Current Density ($\mu A/cm^2$) | Temp (°C) | Type of Biocathode |
|---|---|---|---|---|---|
| Fc-$C_3$-LPEI | 0.56 | 30 at 0.15 V | 240 | 25 | Stationary |
| | 0.59 | 42 at 0.18 V | 330 | 37 | |
| | 0.56 | 57 at 0.14 V | 797 | 25 | RDE |
| | 0.61 | 99 at 0.13 V | 1,160 | 37 | |
| $FcMe_2$-$C_3$-LPEI | 0.61 | 38 at 0.17 V | 280 | 25 | Stationary |
| | 0.64 | 56 at 0.21 V | 330 | 37 | |
| | 0.61 | 68 at 0.16 V | 738 | 25 | RDE |
| | 0.65 | 146 at 0.16 V | 1,267 | 37 | |

Conditions for these biofuel cells are detailed in Figures 11 and 12. The cells were operated in a stirred solution under air saturating conditions, 0.05 M citrate buffer, pH 5.5, 60 mM glucose. Biocathodes were either stationary or rotated at 2000 rpm.

It should be noted that rotation of the bioanodes did not increase power or current, indicating that mass transport of glucose was not a limiting factor. The OCV's for these biofuel cells were similar to the stationary cells, and the cell voltages at maximum power were roughly the same as well (Table 5.02). The large increase in power densities was due to the significant increase in current for each biofuel cell. Use of the RDE's resulted in a very significant 2-3 fold increase in the maximum current densities for the biofuel cells, with current densities greater than 1 $mA/cm^2$ being produced for

each polymer at 37° C. Similar to the stationary biofuel cells, the methylation of the ferrocene moiety resulted in a significant increase in power density at 25° C (16%) and at 37° C (47%). The large increase in power density at 37° C is promising and shows that the effects of ferrocene moiety methylation are most significant when the biofuel cells are operating at the optimal temperature for enzymatic activity.

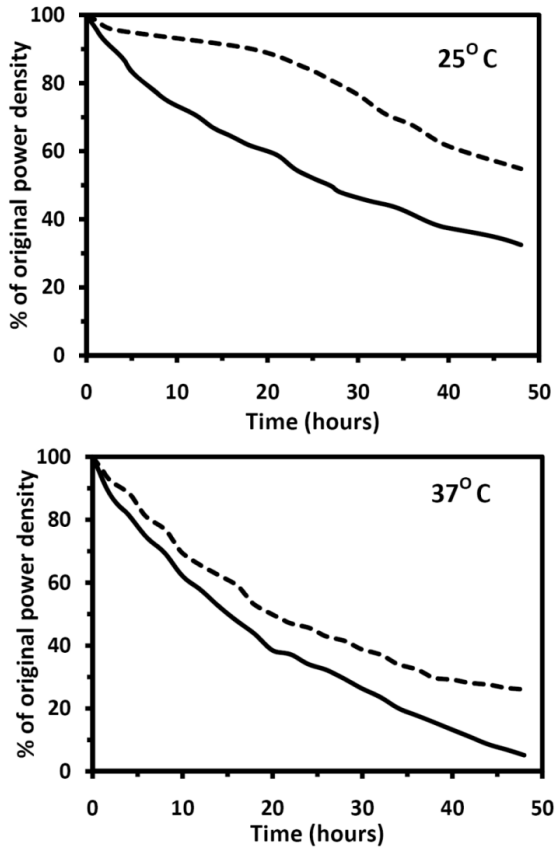


**Figure 5.13: Biofuel Cell Stability.** Biofuel cells with Fc-$C_3$-LPEI/GOx (solid line) or $FcMe_2$-$C_3$-LPEI/GOx (dotted line) anodes and a PVPOs/laccase cathode were continuously operated at maximum power for 48 hours at 25° C or 37° C. Citrate buffer (0.05 M), pH 5.5, 60 mM glucose, air saturating conditions, stirring.

Figure 5.13 shows the stability the biofuel cells at 25° C and 37° C. After two days of continuous operation at maximum power, the cell with the Fc-$C_3$-LPEI anode

retained 35% of its original power density at 25° C and the cell using $FcMe_2$-$C_3$-LPEI retained 55% of its original power density under the same conditions. At 37° C, the Fc-$C_3$-LPEI cell lost almost all of its original power density, with only 5% retained after 48 hours. The cell with the $FcMe_2$-$C_3$-LPEI anode was significantly better, retaining 27% of its original power density. The increase in biofuel cell operational stability obtained by using the dimethylferrocene moiety mirrored that of the increase in stability of the biosensors in Figure 5, with an approximate 20% gain in residual power density at both temperatures. Previous enzymatic biofuel cells employing osmium mediators at both electrodes have been reported to lose only ~10% of their original power density per day operating at 37° C.[57, 58] Therefore, we hypothesize that the limiting electrode for biofuel cell stability is the anode and that the majority of the instability is a result of the degradation of the anodic ferrocene mediators. We also suggest that further methylation of the ferrocene moieties should lead an additional increase in anodic stability and therefore more stable biofuel cells.

**Conclusions**

We have shown that the redox polymers Fc-$C_3$-LPEI and $FcMe_2$-$C_3$-LPEI are extremely efficient mediators of electrons between glucose oxidase and an electrode surface. Bioanodes made with these polymers, when operated under physiological conditions, produced exceptional current densities of ca. 1 mA/cm$^2$ and 2 mA/cm$^2$ at 25° C and 37° C, respectively. The use of 1,1'-dimethylferrocenyl moieties in place of ferrocenyl moieties lowered the redox potential of the polymer and increased its electrochemical and operational stability while maintaining its biocatalytic activity.

To utilize the high current densities produced by these bioanodes, compartment-less glucose/$O_2$ biofuel cells were constructed with a laccase cathode using PVPOs as a redox mediator. The polymer designated as $FcMe_2$-$C_3$-LPEI was shown to be a superior bioanode material due to its lower redox potential, larger operating potentials, and higher stability. Even though there was up to 0.77 V of loss built in to the biofuel cell due to mediator/enzyme overpotentials, a static power density as high as 56 $\mu W/cm^2$ was obtained. This power density was obtained using stationary, planar, low surface area electrodes, and the biofuel cell performance was not enhanced with any nanomaterials (ex: nanowires, carbon nanotubes, high surface area electrode materials). It is among the highest power densities obtained using these types of electrodes in a compartment-less biofuel cell[18, 59] and experiments to enhance its performance with some of the nanomaterials described above are underway.

The $\Delta E$ at maximum power density for the two biofuel cells was 0.02 V or 0.03 V, depending on the operating temperature. This showed that the lowering of the anodic redox potential had the desired effect of increasing the cell voltage and power density. However, these $\Delta E$ values were smaller than expected based on the $\Delta E$ of the redox potentials of each polymer (0.09 V). It should be mentioned that because a continuous polarization curve of the biofuel cells was not generated (obtaining points at every 1 mV), it is possible that the true maxima for each biofuel cell were not reached and that the $\Delta E$ between the cells could be greater than the 0.02 V/0.03 V reported here. If the values are accurate as reported within this chapter, it shows that the lowering of a mediator's redox potential does not necessarily translate to an equivalent increase in operating voltage in a biofuel cell. The effect of ferrocenyl moiety methylation on

operating voltage and power density was the most significant at 37$^{o}$ C, which suggests that operation of the biofuel cells at the optimal temperature for enzymatic catalysis enhances the effect of a lower potential mediator.

Ideally, a biofuel should be able to produce large amounts of current when the electrodes are both stationary to maximize the total amount of energy produced. However, to show that the bioanodes in this study could produce high amounts of current in a biofuel cell, rotating biocathodes were used, which increased the mass transport of $O_2$ to the hydrogels and allowed for higher currents to be produced. When these rotating electrodes were used, a large increase in current density and power density was observed for each biofuel cell; the $FcMe_2$-$C_3$-LPEI polymer again proving to be a better anodic material due to its lower redox potential. A maximum power density of 146 $\mu W/cm^2$ was obtained, and the effect of ferrocenyl moiety methylation was enhanced at the higher temperatures, similar to the effect seen with the stationary cells.

Improvements to the biocathode could increase the power densities of these biofuel cells further, especially in the case of the stationary electrodes. These improvements include purification of the laccase, the use of higher potential mediators, the use of nanomaterials, and utilizing high surface area electrodes. Further methylation of the ferrocenyl moieties of the anodic redox polymers should lead to more stable, lower redox potential mediators which could lower the enzyme/mediator over-potential and increase cell voltage and power density. Research to investigate these possibilities is on-going.

## Experimental

*Chemicals and Solutions*

Glucose oxidase (GOX) from Aspergillus niger (EC 1.1.3.4, Type X-S, 246 units/mg of solid, 75% protein), laccase from *Trametes Versicolor,* ferrocene, 1,1'-dimethylferrocene, poly(2-ethyl-2-oxazoline), 3-chloropropionyl chloride, aluminum chloride, and all salts and acids were purchased from Sigma-Aldrich and used as received. Ethylene glycol diglycidyl ether (EGDGE) and poly(ethylene glycol diglycidyl ether) (PEGDGE) were purchased from Polysciences Inc., Warrington, PA. Stock solutions of 2 M glucose were allowed to mutarotate for 24 hr before use and subsequently kept refrigerated at 4°C. The PVP-Os was synthesized by partially complexing the pyridine nitrogens of poly(4-vinylpyridine) with $Os(bpy)_2Cl^{+/2+}$ and then partially quaternizing the resulting polymer with 2-bromoethylamine according to a previously published protocol.[32, 45]

*Notes on Synthesis and NMR Characterization*

As expected, the reaction described below involving the acylation of 1,1'-dimethylferrocene yielded a product that was a mixture of two isomers.[60, 61] We expected that carrying these isomers throughout the synthesis would have little effect on the electrochemical properties of the final polymer, and therefore we did not make an effort to separate them. Because the compounds described below are mixtures of isomers, the NMR assignments of these compounds are not as straightforward as those of pure compounds, as one would expect (See supporting information for full NMR spectra). In instances where the presence of the two isomers was clear, the NMR peaks

were labeled as such (i.e. "overlapping triplets," "multiple peaks," etc.). In cases where there was no observable effect on the chemical shifts of similar protons of different isomers, the peaks were assigned as though only a single isomer was present (for example, there are technically 4 different methyl groups in the acylation products, but all of the methyl groups appear as two singlets, and are labeled as such).

The amount of 3-(1,1'-dimethylferrocenyl)propyl substitution on the polymer was determined by NMR in a fashion analogous to that described previously.[23] The integral of the area under the peaks for the 1,1'-dimethylferrocenyl ring hydrogens at ca. δ 3.72-3.94 was set as seven, and the remaining peaks were integrated relatively. In a normal repeat unit, (-$CH_2CH_2$-NH-), the polymer backbone has four non-exchanging hydrogens which appear at 2.30 – 2.82 ppm. This means that four divided by the backbone hydrogen integration should give the substitution percentage. However, the two hydrogens in the tether which are part of the methylene group that is adjacent to the nitrogen have a similar chemical shift to the backbone hydrogens and must be subtracted out of the backbone integration. Therefore, Equation 1 can be used to evaluate the substitution percentage.

**Equation 1**: $FcMe_2$-$C_3$-LPEI percent substitution = [*4/(backbone hydrogen integration – 2)] x 100*

*Acylation of 1,1'-Dimethylferrocene with 3-Chloropropionyl Chloride*

1,1'-Dimethylferrocene was acylated according to a known procedure for ferrocene[62] using aluminum chloride and 3-chloropropionyl chloride as follows: 2.0 g (15 mmol) of $AlCl_3$ was added to 30mL of $CH_2Cl_2$ and 1.78 g (14 mmol) of 3-chloropropionyl

chloride was added dropwise over 10 minutes at room temperature. This mixture was stirred for 2 hours and then cooled to $0^o$ C. This mixture was added to 3.0 g (14 mmol) of 1,1'-dimethylferrocene in 30 mL of $CH_2Cl_2$ at $0^o$ C over 5 minutes, and the mixture was allowed to warm to room temperature while stirring overnight. The solution was poured over ice, and the organic layer was separated and washed 2x with saturated $Na_2CO_3$, once with $H_2O$, and dried over $Na_2SO_4$. After evaporating the solvent to a minimal level, the crude product was purified on an acidic alumina column ($CH_2Cl_2$ eluent), yielding 2.8 g (65% yield) of a mixture of 1-(3-chloropropionyl)-2,1'-dimethylferrocene and 1-(3-chloropropionyl)-3,1'-dimethylferrocene as a purple oil (this mixture of isomers was not separated). $^1$H NMR ($CDCl_3$): δ 1.5 (s, 3H Fc-$CH_3$,) 2.05 (s, 3H Fc-$CH_3$), 3.15 (t, 2H -$CH_2$-Cl), 3.90 (t, 2H -CO-$CH_2$-), 4.0-4.72 (multiple peaks, 7H, Fc ring H).

*Reductive Deoxygenation of 1-(3-chloropropionyl)-(2 and 3),1'-dimethylferrocenes*

The mixture of (3-chloropropionyl)dimethylferrocenes was reduced with trifluoroacetic acid (TFA)/sodium borohydride according to the method Battacharyya et. al. used for various acylferrocenes.[63] The mixture of (3-chloropropionyl)dimethylferrocenes (2.8 g) was dissolved in 30 mL of a 1:1 mixture of dry $CH_2Cl_2$ and TFA. Sodium borohydride (4 eq.) was added carefully over 10 minutes and the reaction mixture was stirred at r.t. for 1.5 hrs. The reaction was diluted with 30 mL of $CH_2Cl_2$ and concentrated NaOH was added slowly until the pH was basic. The organic layer was separated, dried over $Na_2SO_4$, and removed under reduced pressure. This crude mixture was purified on flash silica gel using 10:1 hexanes:ether as the eluent to yield 1.3 g of a mixture of 1-(3-

chloropropyl)-2,1'-dimethylferrocene and 1-(3-chloropropyl)-3,1'-dimethylferrocene (49% yield). $^1$H NMR ($CDCl_3$): δ 1.86-2.0 (multiple peaks, 8H, 2[Fc-$CH_3$], and -$CH_2$-) 2.4-2.55 (overlapping triplet/doublet of triplets, 2H, Fc-$CH_2$-), 3.5-3.6 (overlapping triplets, 2H, -$CH_2$-Cl), 3.84-4.0 (mult. peaks, 7H, Fc ring H)

*Halide Exchange Reaction of 1-(3-chloropropyl)-(2 and 3),1'-dimethylferrocenes*

A Finkelstein reaction was carried out to convert the mixture of (3-chloropropyl)dimethylferrocenes to (3-iodopropyl)dimethylferrocenes according to the method of Kanato et al.[64] The mixture of (3-chloropropyl)dimethylferrocenes (1.0 g) was added dropwise to a solution of NaI in 2-butanone, and the mixture was heated to reflux solvent overnight. Water was added and the solution was extracted with hexanes, dried, and the solvent was removed under reduced pressure. The crude product was purified by passing it through a column of alumina to yield 1.2 g of 1-(3-iodopropyl)-2,1'-dimethylferrocene and 1-(3-iodopropyl)-3,1'-dimethylferrocene (92% yield). $^1$H NMR ($CDCl_3$): δ 1.86-2.0 (mult. peaks, 8H 2[Fc-$CH_3$], and -$CH_2$-) 2.36-2.55 (mult. peaks, 2H Fc-$CH_2$-), 3.15-3.25 (overlapping triplets, 2H -$CH_2$-I), 3.84-4.0 (m, 7H, Fc ring H)

*Redox Polymer Synthesis*

Linear PEI was synthesized from poly(2-ethyl-2-oxazoline) according to a previously reported protocol,[65, 66] and the redox polymer designated as Fc-$C_3$-LPEI (ca. 15% substituted) was synthesized by coupling (3-chloropropyl)ferrocene to LPEI as previously reported.[23] 3-(1,1-Dimethylferrocenyl)propyl-modified LPEI ($FcMe_2$-$C_3$-

LPEI) was synthesized by dissolving 100 mg (2.3 mmol repeat units) of LPEI into 10 mL of a heated 10:1 mixture of acetonitrile and methanol in a flask fitted with a reflux condenser. The mixture of (3-iodoopropyl)dimethylferrocenes (100 mg, 0.38 mmol) was added along with 1 eq. of $K_2CO_3$ and the mixture was heated to reflux solvent for 16 hours. The solvent was removed under reduced pressure and diethyl ether was added to remove residual ferrocenyl impurities. The polymer was dissolved in benzene and the mixture was filtered to remove any salts. The solvent was removed under reduced pressure to yield ca. 170 mg $FcMe_2$-$C_3$-LPEI. $^1$H NMR ($CD_3OD$): δ 1.48-1.72 (br, -$CH_2$-), δ 1.80-1.94 (br, 2[Fc-$CH_3$]), δ 2.15-2.25 (br t, Fc-$CH_2$-), 2.30-2.82 (br, -$CH_2$N-), 3.72-3.94 (br, Fc ring H). Using Equation 1, it was calculated that the $FcMe_2$-$C_3$-LPEI was ~ 17% substituted with 3-(1,1'-dimethylferrocenyl)propyl groups.

*Enzyme Electrode Construction*

Glassy carbon (3 mm diameter or 5 mm rotating disc) electrodes were cleaned before use by polishing them successively on three grades of alumina (5, 1, 0.3 μm) and washing thoroughly with Nanopure water after each polishing step. For the anodic enzyme electrodes, solutions of $FcMe_2$-$C_3$-LPEI and Fc-$C_3$-LPEI were prepared by dissolving the polymer in water by addition of a 0.1 M HCl solution until the final concentration of the polymer solution was 10 mg/ml and the pH was 5.0 ± 0.2. Glucose sensors were prepared by cross-linking the redox polymers in the presence of GOx to form enzymatic redox hydrogels: 14 μL of polymer solution (10 mg/ml), 6 μL of glucose oxidase solution (10 mg/ml in DI water), and 0.75 μL of EGDGE solution (10% v/v) were mixed together and 3 μL aliquots were placed onto the glassy carbon

electrode surface. The mixture was allowed to dry for 18-24 hours under ambient conditions. Cathodic enzyme electrodes were prepared by cross-linking laccase in the presence of the PVPOs: 14 μL of polymer solution (10 mg/mL), 6 μL of laccase solution (35 mg/mL in DI water), and 1 μL of PEGDGE (2.5 mg/mL) were mixed together and 3 μL aliquots were placed onto the glassy carbon electrode surface. For the rotating disc electrodes, 5 μL aliquots were used. The mixture was allowed to dry for 18-24 hours under ambient conditions.

*Electrochemical Measurements*

Constant potential experiments and cyclic voltammetry were performed with a CH Instruments Model 832 bipotentiostat, while electrochemical impedance measurements were performed with a Solartron SI 1260 impedance/gain-phase analyzer in conjunction with a SI 1287 potentiostat. Rotating disk electrode experiments were performed with a Pine Instruments AFMSRX rotator. Unless otherwise noted, experiments utilizing the potentiostat were conducted in a three-electrode cell configuration with a saturated calomel reference electrode (SCE), and a platinum wire counter electrode with phosphate buffered saline (PBS, pH 7.4) or sodium citrate (0.05 M) as the background electrolyte. Constant temperature (25 ± 1°C or 37 ± 1$^{o}$C) was maintained during the experiments by using a water-jacketed electrochemical cell connected to a circulating water bath.

The compartment-less biofuel cell was assembled by placing one anodic enzyme electrode and one cathodic enzyme electrode into a one-compartment electrochemical cell filled with buffer (0.05 M citrate) and glucose (60 mM). The current and voltage

produced by the biofuel cell were measured while varying an external resistor (as depicted in Scheme 5.01). A Keithley 485 picoammeter and a Keithley 175 autoranging multimeter were used to measure the current and voltage, respectively.

*Calculations and Statistics*

Values are presented as mean ± standard error of the mean (SEM) unless otherwise specified.

**Acknowledgements**

I would like to thank Der-You Kao for her help in characterizing the PVPOs/laccase biocathodes and David Hickey for his help in carrying out the RDE biofuel cell experiments.

## References


1. Willner, I.; Yan, Y. M.; Willner, B.; Tel-Vered, R., *Fuel Cells* **2009,** *9* (1), 7-24.

2. Cracknell, J. A.; Vincent, K. A.; Armstrong, F. A., *Chem. Rev.* **2008,** *108* (7), 2439-2461.

3. Higson, P. J.; Davis, F., *Biosens. Bioelectron.* **2007,** *22*, 1224-1235.

4. Barton, S. C.; Gallaway, J.; Atanassov, P., *Chem. Rev. (Washington, DC, U. S.)* **2004,** *104* (10), 4867-4886.

5. Soukharev, V.; Mano, N.; Heller, A., *J. Am. Chem. Soc.* **2004,** *126*, 8368-8369.

6. Heller, A.; Mano, N.; Mao, F., *ChemBioChem* **2004,** *5*, 1703-1705.

7. Sokic-Lazic, D.; Minteer, S. D., *Electrochem. Solid St.* **2009,** *12* (9), F26-F28.

8. Sokic-Lazic, D.; Minteer, S. D., *Biosens. Bioelectron.* **2008,** *24* (4), 939-944.

9. Akers, N. L.; Moore, C. M.; Minteer, S. D., *Electrochim. Acta* **2005,** *50*, 2521-2525.

10. Hudak, N. S.; Gallaway, J. W.; Barton, S. C., *J. Electrochem. Soc.* **2009,** *156* (1), B9-B15.

11. Barton, S. C., *J. Electrochem. Soc.* **2005,** *152* (5), A876-A881.

12. Ivnitski, D.; Artyushkova, K.; Rincon, R. A.; Atanassov, P.; Luckarift, H. R.; Johnson, G. R., *Small* **2008,** *4* (3), 357-364.

13. Ivnitski, D.; Branch, B.; Atanassov, P.; Apblett, C., *Electrochem. Commun.* **2006,** *8* (8), 1204-1210.

14. Tan, Y. M.; Deng, W. F.; Li, Y. Y.; Huang, Z.; Meng, Y.; Xie, Q. J.; Ma, M.; Yao, S. Z., *J. Phys. Chem. B* **2010,** *114* (15), 5016-5024.

15. Murata, K.; Kajiya, K.; Nakamura, N.; Ohno, H., *Energy Environ. Sci.* **2009,** *2* (12), 1280-1285.

16. Kamitaka, Y.; Tsujimura, S.; Setoyama, N.; Kajino, T.; Kano, K., *Phys. Chem. Chem. Phys.* **2007,** *9* (15), 1793-1801.

17. Stoica, L.; Dimcheva, N.; Ackermann, Y.; Karnicka, K.; Guschin, D. A.; Kulesza, P. J.; Rogalski, J.; Haltrich, D.; Ludwig, R.; Gorton, L.; Schuhmann, W., *Fuel Cells* **2009,** *9* (1), 53-62.

18. Leech, D., *Electrochim. Acta* **2006,** *51*, 5187-5192.

19. Heller, A., *Phys. Chem. Chem. Phys.* **2004,** *6* (2), 209-216.

20. Kim, H. H.; Mano, N.; Zhang, X. C.; Heller, A., *J. Electrochem. Soc.* **2003,** *150* (2), A209-A213.

21. Merchant, S.; Tran, T. O.; Meredith, M. T.; Cline, T. C.; Glatzhofer, D. T.; Schmidtke, D. W., *Langmuir* **2009,** *25* (13), 7736-7742.

22. Merchant, S.; Glatzhofer, D. T.; Schmidtke, D. W., *Langmuir* **2007,** *23*, 11295.

23. Merchant, S.; Meredith, M. T.; Tran, T. O.; Brunski, D.; Johnson, M. B.; Glatzhofer, D. T.; Schmidtke, D. W., *J. Phys. Chem. C, ASAP* **2010**.

24. Mao, F.; Mano, N.; Heller, A., *J. Am. Chem. Soc.* **2003,** *125* (16), 4951-4957.

25. Heller, A., *J. Am. Chem. Soc.* **2004,** *126*.

26. Suzuki, M.; Kobayashi, S.; Kimura, M.; Hanabusa, K.; Shirai, H.; Kurimura, Y., *J. Chem. Soc., Faraday Trans.* **1996,** *92* (22), 4511-4513.

27. Hoh, G. L.; Kleinberg, J.; Mcewen, W. E., *J. Am. Chem. Soc.* **1961,** *83* (19), 3949

28. Kuwana, T.; Bublitz, D. E.; Hoh, G., *J. Am. Chem. Soc.* **1960,** *82* (22), 5811-5817.

29. Reynolds, L. T.; Wilkinson, G., *J. Inorg. Nucl. Chem.* **1959,** *9* (1), 86-92.

30. Hradsky, A.; Bildstein, B.; Schuler, N.; Schottenberger, H.; Jaitner, P.; Ongania, K. H.; Wurst, K.; Launay, J. P., *Organometallics* **1997,** *16* (3), 392-402.

31. Bashkin, J. K.; Kinlen, P. J., *Inorg. Chem.* **1990,** *29* (22), 4507-4509.

32. Gregg, B. A.; Heller, A., *Anal. Chem.* **1990,** *62* (3), 258-263.

33. Galloway, J. W.; Barton, S. C., *J. Am. Chem. Soc.* **2008,** *130*, 8527.

34. Glatzhofer, D. T.; Erickson, M. J.; Frech, R.; Yepez, F.; Furneaux, J. E., *Solid State Ionics* **2005,** *176*, 2861-2865.

35. Birnbaum, E. R.; Rau, K. C.; Sauer, N. N., *Sep. Sci. Technol.* **2003,** *38* (2), 389-404.

36. Prins, R.; Korswagen, A. R.; Kortbeek, A. G. T. G., *J. Organomet. Chem.* **1972**, 335-344.

37. Fomin, V. M.; Markin, A. V., *J. Therm. Anal. Calorim.* **2008,** *92*, 985-987.

38. Ikeda, S.; Oyama, N., *Anal. Chem.* **1993,** *65* (14), 1910-1915.

39. Bunte, C.; Prucker, O.; Konig, T.; Ruhe, J., *Langmuir* **2010,** *26* (8), 6019-6027.

40. Heller, A., *J. Am. Chem. Soc.* **2003,** *125*.

41. Gellett, W.; Schumacher, J.; Kesmez, M.; Le, D.; Minteer, S. D., *J. Electrochem. Soc.* **2010,** *157* (4), B557-B562.

42. Coman, V.; Vaz-Dominguez, C.; Ludwig, R.; Herreither, W.; Haltrich, D.; De Lacey, A. L.; Ruzgas, T.; Gorton, L.; Shleev, S., *Phys. Chem. Chem. Phys.* **2008,** *10* (40), 6093-6096.

43. Ivnitski, D.; Atanassov, P., *Electroanalysis* **2007,** *19* (22), 2307-2313.

44. Blanford, C. F.; Heath, R. S.; Armstrong, F. A., *Chem. Commun. (Cambridge, U. K.)* **2007,** (17), 1710-1712.

45. Joshi, P. P.; Merchant, S. A.; Wang, Y.; Schmidtke, D. W., *Anal. Chem.* **2005,** *77*, 3183-3188.

46. Christenson, A.; Shleev, S.; Mano, N.; Heller, A.; Gorton, L., *Biochim. Biophys. Acta* **2006,** *1757*, 1634-1641.

47. Xu, F.; Shin, W.; Brown, S. H.; Wahleithner, J. A.; Sundaram, U. M.; Solomon, E. I., *Biochim. Biophys. Acta* **1996,** *1292*, 303-311.

48. Barton, S. C.; Kim, H.-H.; Binyamin, G.; Zhang, Y.; Heller, A., *J. Phys. Chem. B* **2001,** *105*, 11917-11921.

49. Stankovich, M. T.; Schopfer, L. M.; Massey, V., *J. Biol. Chem.* **1978,** *253* (14), 4971-4979.

50. Alberty, R. A., *Biochem. Educ.* **2000,** *28*, 12-17.

51. Solomon, E. I.; Sundaram, U. M.; Machonkin, T. E., *Chem. Rev. (Washington, DC, U. S.)* **1996,** *96*, 2563-2605.

52. Baldrian, P., *FEMS Microbiol. Rev.* **2006,** *30* (2), 215-242.

53. Gallaway, J. W.; Barton, S. A. C., *J. Electroanal. Chem.* **2009,** *626* (1-2), 149-155.

54. Barton, S. C.; Kim, H.-H.; Binyamin, G.; Zhang, Y.; Heller, A., *J. Am. Chem. Soc.* **2001,** *123*, 5802-5803.

55. Mano, N.; Kim, H.-H.; Heller, A., *J. Phys. Chem. B* **2002,** *106*, 8842-8848.

56. Mano, N.; Kim, H.-H.; Zhang, Y.; Heller, A., *J. Am. Chem. Soc.* **2002,** *124*, 6480-6486.

57. Chen, T.; Barton, S. C.; Binyamin, G.; Gao, Z. Q.; Zhang, Y. C.; Kim, H. H.; Heller, A., *J. Am. Chem. Soc.* **2001,** *123*, 8630-8631.

58. Mano, N.; Mao, F.; Shin, W.; Chena, T.; Heller, A., *Chem. Commun. (Cambridge, U. K.)* **2003**, 518-519.

59. Tsujimura, S.; Kano, K.; Ikeda, T., *Electrochemistry* **2002,** *70*, 940.

60. Knox, G. R.; Morrison, G.; Sandhu, P. L. P. M. A.; Watts, W. E., *J. Chem. Soc. C* **1967**, 1853-1856.

61. Rinehart, K. L.; Motz, K. L.; Moon, S., *J. Am. Chem. Soc.* **1957,** *79* (11), 2749-2754.

62. Fort, Y.; Caubere, P.; Gautier, J. C.; Mondet, J. C., *J. Organomet. Chem.* **1993,** *452*, 111-113.

63. Bhattacharyya, S., *J. Chem. Soc., Perk. Trans. 1* **1996**, 1381-1382.

64. Kanato, H.; Takimiya, K.; Otsubo, T.; Aso, Y.; Nakamura, T.; Araki, Y.; Ito, O., *J. Org. Chem.* **2004,** *69* (21), 7183-7189.

65. York, S.; Frech, R.; Snow, A.; Glatzhofer, D., *Electrochim. Acta* **2001,** *46*, 1533-1537.

66. Tanaka, R.; Ueoka, I.; Takaki, Y.; Kataoka, K.; Saito, S., *Macromolecules* **1983,** *16*, 849-853.

# CHAPTER 6: SYNTHESIS OF TETRAMETHYLFERROCENE-MODIFIED LINEAR POLY(ETHYLENIMINE) AND ITS USE AS AN ANODIC REDOX POLYMER IN BIOSENSORS AND BIOFUEL CELLS

## Introduction

Since its discovery as the one of the first organometallic molecules, the fundamental chemistry of ferrocene has been extensively studied and many derivatives of it have been synthesized.[1, 2] Besides its interesting reactivity and redox behavior, many applications for ferrocene have evolved over the years, including its use in the areas of fuel additives,[3] pharmaceutical compounds,[4, 5] ligand scaffolds,[6] charge transfer complexes,[7, 8] macromolecules,[9, 10] and redox sensors.[11-13] Ferrocene is an attractive molecule to study because it is cheap, can be easily modified, and is non-toxic. In particular, the use of ferrocene and some of its derivatives as redox mediators between enzymes and electrodes have been of recent interest to our group. Ferrocene derivatives have been studied as mediators for glucose oxidase since the 1980's[14] and more recently, ferrocene has been studied for use in "redox polymers" for amperometric glucose biosensors.[11, 15-17]

The development of novel redox polymers which effectively shuttle electrons between enzymes and electrode surfaces continues to be an important area of research in the field of bioelectronics. Redox polymers are favorable substrates for enzyme "wiring" because they provide a permeable matrix in which to immobilize the enzyme as well as the individual redox centers which connect the enzyme active sites to the electrode surface. They have been used in various applications, most notably biosensors and biofuel cells.[18-22] The specific type of biosensor or biofuel cell for which redox polymers are developed plays a major role in their targeted structure and

properties, and it is desirable to develop redox polymer systems which can be modified to fit the needs of the specific application. The desired/favorable properties of redox polymers for biosensor/biofuel cell applications actually overlap in many aspects and, as such, many properties which make a redox polymer effective at biosensing can make it an efficient anode/cathode in a biofuel cell. Some of these properties which overlap are biocompatibility, stability, high electron diffusion rates, optimized redox potential, high sensitivity to a particular analyte/fuel, and the ability to be cross-linked into a hydrogel.

Our group has synthesized a series of redox polymers based on linear poly(ethylenimine) (LPEI) and ferrocene for use in glucose biosensors[23-25] and biofuel cells.[26] When these polymers were cross-linked in the presence of glucose oxidase, hydrogels were formed which effectively "wired" the FAD redox centers of GOx to the electrode. These bioelectrodes, when poised at an oxidizing potential (relative to ferrocene), were sensitive to the presence of glucose and produced extremely high catalytic current densities (up to 2 $mA/cm^2$). Two of these polymers, Fc-$C_3$-LPEI and $FcMe_2$-$C_3$-LPEI (*vide supra*), were evaluated as anodes for use in a compartment-less glucose/$O_2$ biofuel cell. The use of dimethylferrocene moieties in $FcMe_2$-$C_3$-LPEI lowered the redox potential of the polymer by 0.09 V (relative to Fc-$C_3$-LPEI, which used ferrocene moieties) and resulted in more stable glucose biosensors and biofuel cells. When $FcMe_2$-$C_3$-LPEI was used as the anode in a biofuel cell, power densities of up to 146 $\mu W/cm^2$ were produced when it was coupled with a wired laccase cathode. This power density was produced at a potential of 0.16 V, which is quite low for a biofuel cell. The low voltage was mainly a result of the large overpotential between the

anodic mediator (dimethylferrocene) and glucose oxidase, which was 0.55 V. To increase the power density of this biofuel cell further, it was necessary to lower this overpotential, which should result in higher operating voltages and therefore higher power densities. To do this, we sought to synthesize a ferrocene derivative with a redox potential lower than that of $FcMe_2$-$C_3$-LPEI.

Another drawback to the use of ferrocene-based redox polymers is that ferrocene derivatives are known to be somewhat unstable under aqueous conditions.[27-29] This phenomenon was observed, and the operational stabilities of biosensors and biofuel cells fabricated with ferrocene-modified LPEI were lower than the stabilities of some osmium-based redox polymers.[23, 30-32]

Adding methyl groups to ferrocene is a proven method for lowering the redox potential in a predictable manner[33-35] and also provides more stability[28, 36] for the ferrocenium cation due to in part to increased steric hindrance around the iron atom. In our previous study, we used commercially available dimethylferrocene to show that methyl groups could increase the stability of ferrocene/LPEI redox polymers. However, we still desired to increase the stability of these redox polymers further, and speculated that this could be done with additional methyl groups. When deciding how many methyl groups to add onto the ferrocene, we surveyed the literature and found one report suggesting that large amounts of ferrocene methylation can actually hinder the interaction of the ferrocenium ion with glucose oxidase[37] and that the use of octa- or nonamethylferrocene could drastically lower the currents produced with these polymers. Also, we felt it necessary to approach this problem in a systematic fashion rather than an all-or-nothing approach with octa- or nonamethylferrocene, so tetramethylferrocene

(**1**) was chosen as the target for synthesis. We hypothesized that adding only two more methyl groups should not affect the enzyme/polymer interaction significantly, while adding stability and increasing the biofuel cell operating voltage, thereby giving a significant increase in power (assuming similar high currents are produced from the anode).

In addition, the predicted properties of a tetramethylferrocene-modified LPEI polymer could lead to favorable glucose biosensor performance. The additional methyl groups should provide a higher level of electrochemical and operational stability for a glucose biosensor. The lower redox potential of $FcMe_4$-$C_3$-LPEI could allow the electrode to be poised at a low enough potential to remove the unwanted detection of interfering species such as ascorbate (vitamin C), which is a large obstacle which arises when using redox polymers for in-situ biosensing applications. We hypothesize that the use of tetramethylferrocene-modified LPEI ($FcMe_4$-$C_3$-LPEI) in a glucose biosensor should lower the operating potential, increase the stability, and remove or reduce interference from ascorbate while maintaining a high limiting current density ($j_{max}$) and sensitivity to glucose.

## Results and Discussion

*Synthesis of Tetramethylferrocene*

When deciding how to approach this synthetic goal, two synthetic methods to synthesize tetramethylferrocene became apparent: The addition of two methyl groups to dimethylferrocene by an electrophilic aromatic substitution (EAS)/reduction method or the synthesis of dimethylcyclopentadiene and subsequent reaction with $FeCl_2$ to form

the tetramethylferrocene directly. The second method has been reported sparingly in the literature and requires many reactions which use highly reactive alkyl lithium reagents and air-sensitive conditions.[38] The benefit, however, of using this method is that isomerically pure tetramethylferrocene can be obtained, while the first method would yield a mixture of tetramethylferrocene isomers. However, because our ultimate goal in adding the methyl groups was to lower the redox potential of the ferrocene, it was not important to us control where the methyl groups were added, so the first method was chosen as it used techniques that were more facile to carry out.

Ideally, we desired an EAS method which could substitute each Cp ring of the ferrocene once in the same reaction and yield two new moieties which could be reduced to methyl groups. Two reactions seemed plausible for this step, as outlined in Figure 6.01: A di-formylation, or a di-aminomethylation. However, the Villsmeier-Haack formylation has been shown to only formylate one Cp ring per reaction (even on the highly nucleophilic octamethylferrocene).[39, 40] On the other hand, a report by Pauson et. al. indicated that methyl and dimethylferrocene could be mono- or di-aminomethylated.[41] Their studies were focused on obtaining the mono-aminomethylated species and separating the isomers, but it seemed plausible that a slight alteration of reaction conditions could lead to a

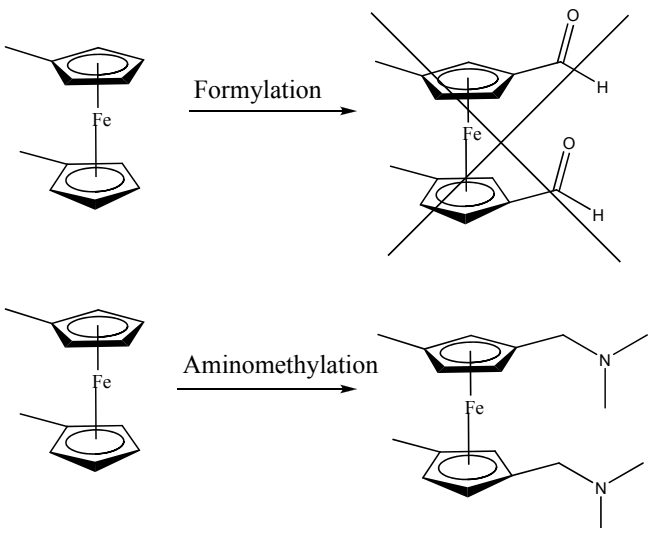


**Figure 6.01:** Outline of possible synthetic routes to di-substituted dimethylferrocene products

significant yield of the di-substituted product. Beginning with this reaction, the synthesis of tetramethylferrocene is outlined in Figure 6.02A.

We found that when the aminomethylation reaction was carried out with excess amine (3 eq.) and a longer heating time, a significant amount of the di-aminomethylated products (**3**) were obtained (27% yield). These isomers were reacted with 2 eq. of iodomethane to give the di-methiodides (**4**). The reaction of **4** with excess $NaBH_4$ in refluxing acetonitrile completely removed the trimethylamine groups and led to a mixture of tetramethylferrocenes (**1).**

Since the major product of the aminomethylation reaction were mono-substituted species (**2**, 46% yield), we sought a reaction pathway (Figure 6.02B) which could convert those products to **1** as well. First, **2** was methylated to give methiodides **5**. The methiodides (**5**) were reduced with $NaBH_4$ to give a mixture of 1,2,1'-trimethylferrocene and 1,3,1'-trimethylferrocene (**6**). The mixture of trimethylferrocenes **6** was then formylated with $POCl_3$ and DMF to form a mixture of trimethylferrocenecarboxaldehyde isomers (**7**). Finally, **7** was reduced with borane-dimethylsulfide to give **1** in good yield. As mentioned earlier, the only drawback to this method is the number of isomers of tetramethylferrocene which are obtained (5 possible). However, the presence of many isomers was not believed to have any significant effect on the electrochemistry or reactivity of the tetramethylferrocenes.

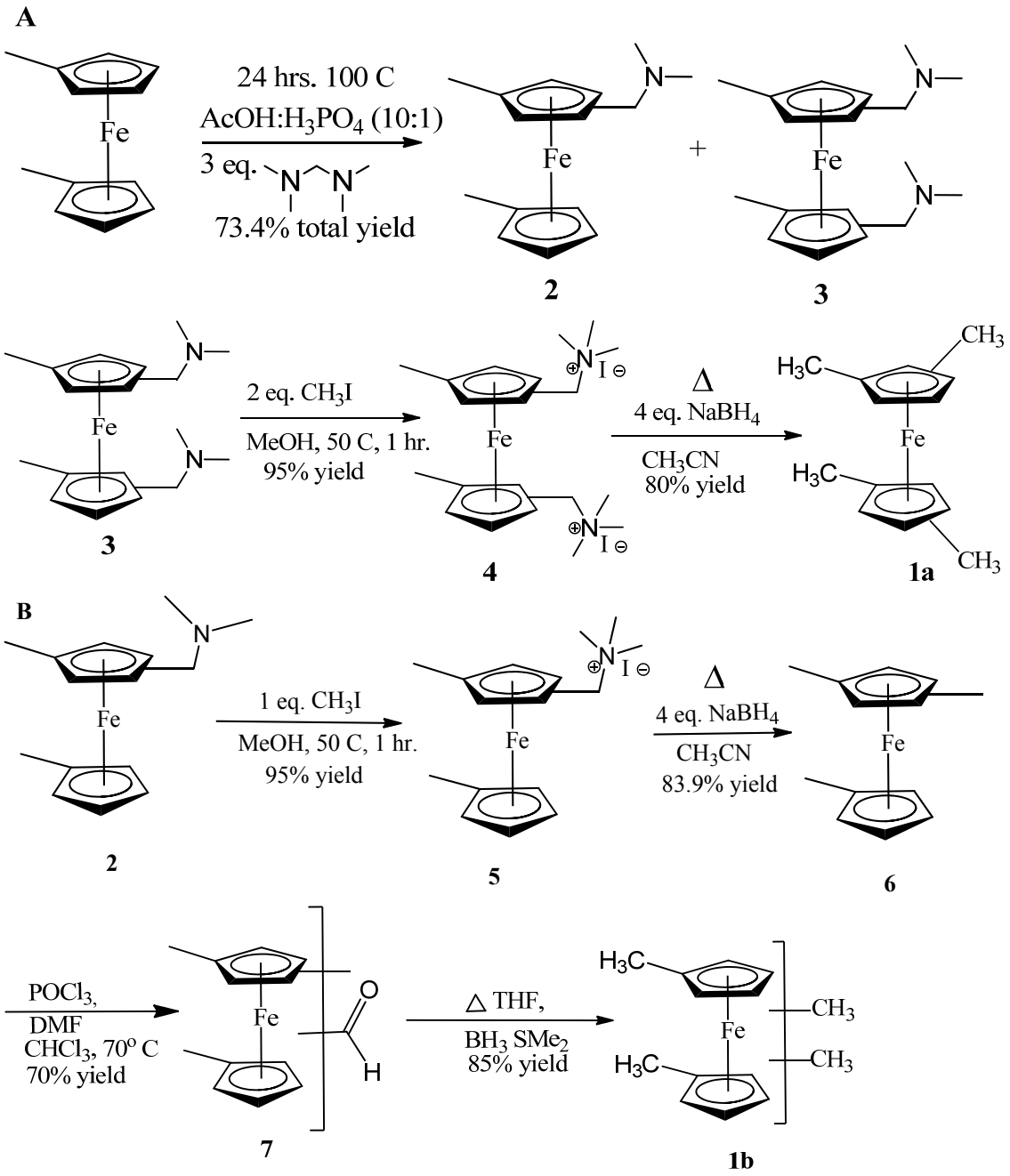


**Figure 6.02: Reaction Sequences to Synthesize Tetramethylferrocene.** Reaction products which were isomers are indicated either by drawing the bond directly to the side of the ring or by using brackets.

*Modification of Tetramethylferrocenes (**1**) with a Three-Carbon Tether*

Because our eventual goal was to attach tetramethylferrocene to LPEI, a tether with a leaving group had to be attached to **1**. Three carbons was selected as the desired

tether length based upon previous studies which have shown that a three-carbon tether gives the optimal blend of electrochemical stability and current density with the Fc-LPEI polymers.[23] The method which seemed obvious was the acylation/reduction method which was used previously for the attachment of three-carbon tethers to ferrocene[23] and dimethylferrocene[26] (Figure 6.03)

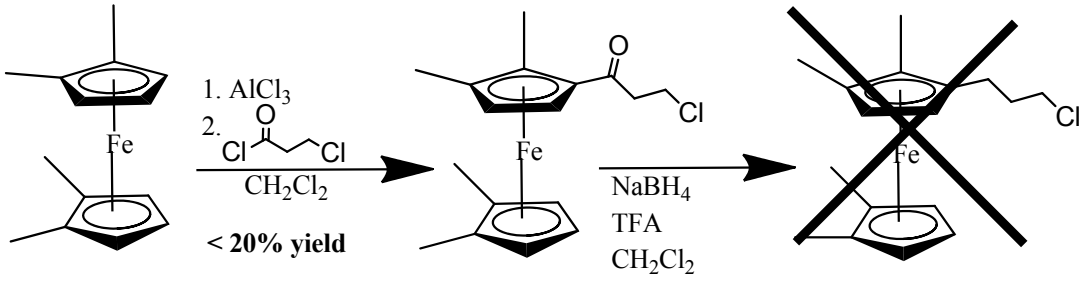


**Figure 6.03: Reaction Scheme for Failed Acylation/Reductive Deoxygenation of 1**. Compounds are drawn as one isomer, while in fact, many isomers were present in the actual reactions

However, this synthesis was riddled with problems and none of the desired product was obtained. The problems in this synthetic scheme lay in the fact both reactions involved oxidizing conditions, and **1** is more easily oxidized than dimethylferrocene or ferrocene. Much of **1** was immediately oxidized in the acylation reaction, rendering it un-reactive towards EAS. This was not surprising as octamethylferrocene is virtually impossible to acylate using the Friedel-Crafts method due to its low oxidation potential.[40] The small amount of **1** which was acylated was carried on to the next reaction, where a reductive deoxygenation with trifluroracetic acid and $NaBH_4$ was attempted. This reaction works quite well for ferrocenoyl compounds[42] and we showed that it could give acceptable yields with a dimethylferrocenoyl moiety as well.[26] However, in this case, none of the desired product was obtained from the reaction. Alternative reductive deoxygenations were attempted in addition to the TFA/$NaBH_4$ reaction ($BF_3$/$BH_3$,

TFA/poly(methylsiloxane), $AlCl_3/LiAlH_4$, $BH_3 \cdot SMe_2$) and none gave the desired product. Because of these problems, another synthetic route was sought which could attach a three-carbon tether under milder, less oxidizing conditions and did not involve a reductive deoxygenation step.

The Wittig reaction is a useful carbon-carbon bond forming reaction for converting aldehydes into alkenes. Because ferrocenecarboxaldehydes can be formed in good yields using the Villsmeier-Haack reaction as discussed above, we investigated the Wittig reaction as a possible method for attaching a three-carbon unit to tetramethylferrocene. A quick review of the literature revealed that multiple research groups have in fact used this method to modify ferrocenecarboxaldehyde with a three-carbon unsaturated ester moiety and have performed various transformations using the ester to synthesize saturated ferrocenylpropyl alcohols, bromides, and carboxylic acids.[43-45]

The first step of the Wittig reaction involves the reaction of a phosphine (normally triphenylphosphine) with an alkyl halide. A base is added to deprotonate the resulting phosphonium salt and a phosphonium ylide is formed. Witting reactions are normally carried out in organic solvents, and, depending on the ylide being formed, need strong bases due to the high $pK_a$ of the carbon-hydrogen bond. Also, the ylide is normally formed in a separate step, isolated, and then reacted with the aldehyde.[43-45] However, one recent variation of the Wittig reaction investigated by El-Batta et. al. uses α-bromoesters, which, when reacted with triphenylphosphine, can be deprotonated with bicarbonate.[46] This facile deprotonation allows for the reaction to be carried out in one pot and in aqueous media, making it an attractive and easy alternative to the normal

multi-step Wittig reactions. We decided to use this as the pivotal carbon-carbon bond forming reaction with tetramethylferrocene in order to avoid the oxidizing conditions involved with Friedel-Crafts acylation. In addition, the oxygen of the tetramethylferrocenecarboxaldehyde is removed in the Wittig reaction, which avoids the need for a reductive deoxygenation reaction. To carry out the Wittig reaction, **1** had to be formylated, and beginning with a Villsmeier-Haack formylation, the synthesis of **1** modified with a three-carbon tether is outlined in Figure 6.04.

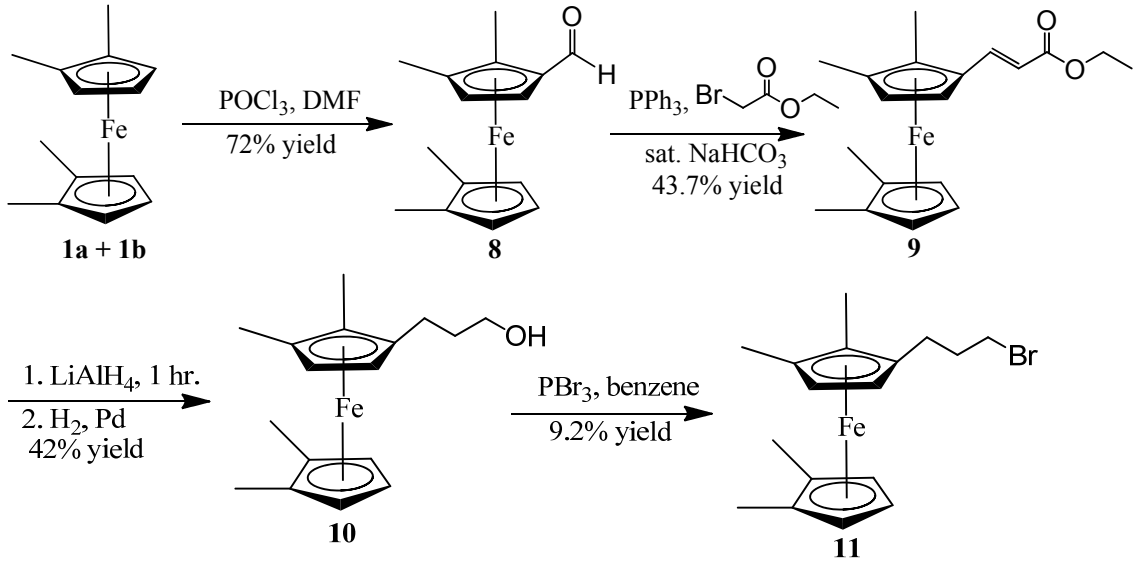


**Figure 6.04: Synthetic Route for Attachment of Three-carbon Tether to 1.** Structures are shown as pure compounds, when, in fact, each was a mixture of isomers.

The mixture of tetramethylferrocene isomers was formylated using the same modified Villsmeier-Haack reaction as described above to yield a mixture of tetramethylferrocenecarboxaldehydes (**8**). Compound **8** was used in the Wittig reaction with triphenylphosphine and ethyl bromoacetate in saturated sodium bicarbonate to yield a mixture of ethyl 3-tetramethylferrocenylpropenoates (**9**), which was separated from unreacted starting material by column chromatography. The unsaturated esters (**9**)

were then reduced in two separate reactions: First, **9** was reduced with LAH in order to reduce the ester group to an alcohol. We had hoped that this reduction might reduce the double bond first, as indicated with other aromatic esters.[47] However, the LAH reduction yielded a mixture of unsaturated and saturated alcohols. As such, a hydrogenation was carried out on the mixture of alcohols to reduce any double bonds to give a mixture of saturated 1-(3-hydroxypropyl)tetramethylferrocenes (**10**), which were easily purified by column chromatography. Finally, a reaction was necessary to convert the –OH group in **10** to a good leaving group. Many reactions are possible to convert primary alkyl alcohols to halides - especially chlorides and bromides. However, many of these reactions use harsh reagents such as thionyl chloride or hydrobromic acid, which could promote the oxidation of the tetramethylferrocene. As such, we wanted a reaction which had been carried out on a ferrocenyl alcohol with proven results. Lapic et. al. successfully carried out the conversion of (3-hydroxypropyl)ferrocene to (3-bromopropyl)ferrocene using phosphorus tribromide ($PBr_3$).[48] We were concerned that the by-product of this reaction, phosphorus acid, would cause the oxidatively sensitive tetramethylferrocene to become oxidized. But, after trying many other reactions, we found $PBr_3$ as the best reagent for converting **10** to the bromide (**11**). A significant amount of starting material was oxidized and un-recoverable, and as such yields for this reaction were quite low (~10%).

*Characteristics of Enzyme Electrodes Made with $FcMe_4$-$C_3$-LPEI*

With the (3-bromopropyl)tetramethylferrocenes in hand, they were easily added onto the LPEI backbone in a nucleophilic addition reaction to give a small amount (23 mg)

of tetramethylferrocene-modified LPEI ($FcMe_4$-$C_3$-LPEI) with which to work. When carrying out our standard procedure for the cross-linking of ferrocene-modified LPEI polymers in the presence of glucose oxidase, a few important observations were made about $FcMe_4$-$C_3$-LPEI. Normally, the polymers are mixed with water and HCl is added to lower the pH to ca. 5.0 in order to make sure the polymer backbone is highly protonated and will interact favorably with the negatively charged GOx. However, when the pH of an aqueous $FcMe_4$-$C_3$-LPEI solution was lowered to 5.0, the solution turned bright green, indicating a large amount of tetramethylferrocene moiety oxidation. In theory, this should not harm the enzyme-polymer interaction and could actually improve it by giving the GOx more positive charges to interact with on the polymer. However, when the $FcMe_4$-$C_3$-LPEI was mixed with GOx, a yellow/white precipitate formed, which indicated the formation of some type of complex between the polymer and the enzyme, or that the polymer and/or enzyme was precipitating out of solution. However, the polymer/enzyme mixtures did still cross-link, and the cyclic voltammetry of these films is shown in Figure 6.05. As seen in the cyclic voltammetry, the lower oxidation potential of the mediator did in fact occur, with an $E_{1/2}$ of ca. 0.08 V vs. SCE. This confirmed our hypothesis that a tetramthylated ferrocene should lower the redox potential of the polymers approximately 100 mV from that of $FcMe_2$-$C_3$-LPEI. A large break-in phenomenon occurred during the first 10 scans of the cross-linked $FcMe_4$-$C_3$-LPEI (Figure 6.05 A), causing the cyclic voltammograms to decay rapidly, with the initial $i_{pa}$ of 40 μA shrinking down to ca. 26 μA. This decay in the CV could be due to incomplete cross-linking, delamination of the film, or general film instability.

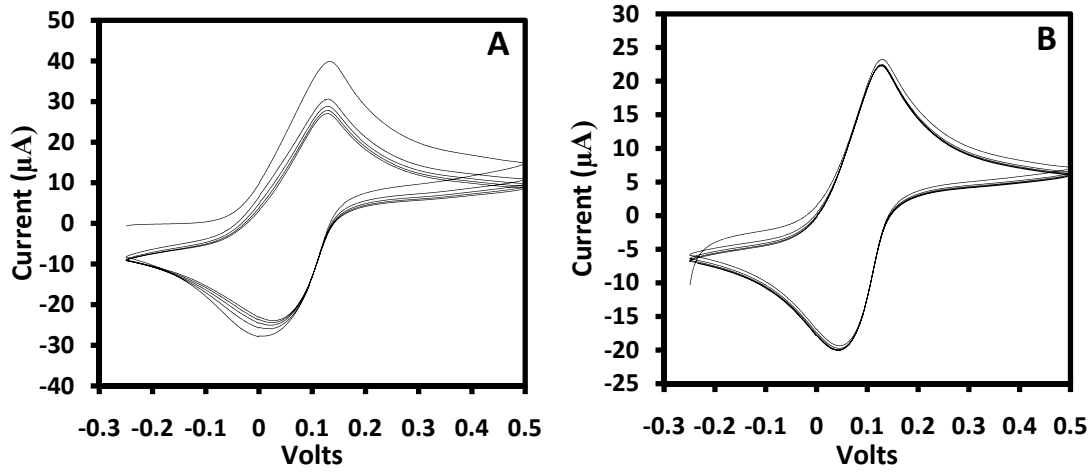


**Figure 6.05: Cyclic Voltammetry of $FcMe_4$-$C_3$-LPEI/GOx Films.** pH of the polymer solution was 5.0 ± 0.2. PBS buffer, pH 7.4, scan rate = 50 mV/s. A = First 10 scans. B = Next 10 scans

After the first 10 scans, the cyclic voltammograms stabilized considerably with an $i_{pa}$ of ca. 22 µA (Figure 6.05 B). This $i_{pa}$ was fairly low compared to cyclic voltammograms of other Fc-LPEI polymers studied in the past, again indicating that either much of the film was degraded or delaminated. Another possibility could be that the electron diffusion in the film was much slower than in our previous polymers. In an attempt to improve the electrochemical properties of the polymer, the $FcMe_4$-$C_3$-LPEI was cross-linked in the presence of GOx at a more basic pH of 6.8, which is the pH of the polymer when it is dissolved into pure water. This appeared to result in less of the tetramethylferrocene moieties being oxidized when the bioelectrodes were being mixed and cured. Figures 6.06 A and B show the cyclic voltammograms from these bioelectrodes, which showed a significant improvement over the previous CV's.

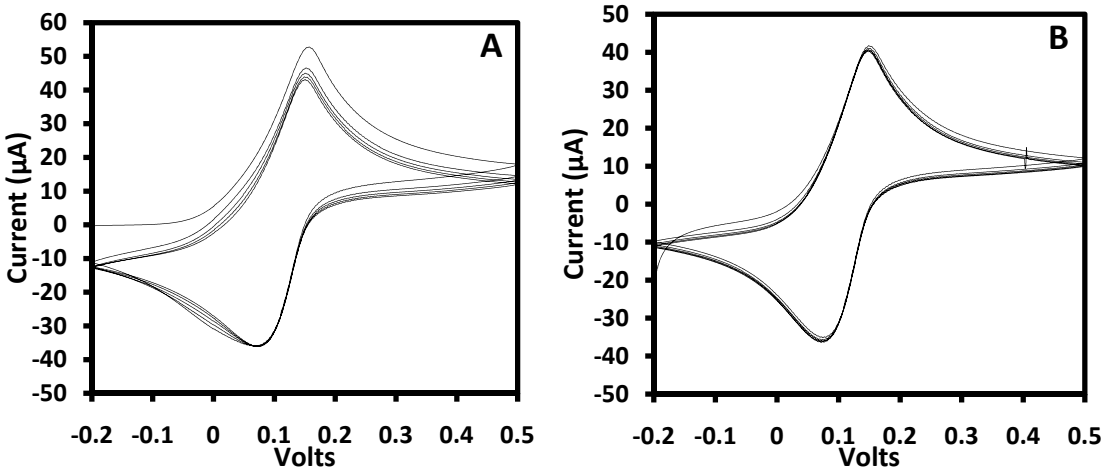


**Figure 6.06: Cyclic Voltammetry of $FcMe_4$-$C_3$-LPEI/GOx Films.** pH of the polymer solution was 6.8 ± 0.2. PBS buffer, pH 7.4, scan rate = 50 mV/s. A = First 10 scans, B = next 10 scans.

The $i_{pa}$ of the first scan was ca. 55 μA, and while the $i_{pa}$ decreased with each scan (Figure 6.06A), the drop was less significant than in Figure 6.05A, and the $i_{pa}$ actually stabilized at a higher current of ~40 μA (Figure 6.06B). While these results were better, the yellow/white precipitate was still observed when mixing the polymer with the enzyme at pH 6.8. The reasons for this precipitate are unknown at this point and studies to determine its origin and effect on the bioelectrodes are ongoing.

To determine the effect on electron transport in the films, electrochemical impedance spectroscopy was carried out to determine $cDe^{1/2}$(the apparent electron diffusion coefficient).

*Electron Diffusion in $FcMe_4$-$C_3$-LPEI Films*

The rate of electron diffusion through redox polymers films can be useful in characterizing their performance as bioelectrodes. Using the electrochemical impedance spectroscopy (EIS) method previously described,[25] it was found that the

$cDe^{1/2}$ for cross-linked films of $FcMe_4$-$C_3$-LPEI (with GOx present) was an order of magnitude less than for the other polymers (Table 6.01, *vide infra*). This could be an explanation for the lower $i_{pa}$ seen in the CVs of $FcMe_4$-$C_3$-LPEI and the lower limiting current densities obtained with $FcMe_4$-$C_3$-LPEI/GOx films. The reason for the lower $cDe^{1/2}$ is unknown, but could have to do with the precipitate which was observed when the polymer and enzyme were mixed. If a complex formed between the oxidized tetramethylferrocenes and the enzyme, the segmental motion of some of the redox centers could be lowered and thereby reduce the $cDe^{1/2}$.

Regardless of the effect on electron diffusion, it was expected that adding two additional methyl groups to the ferrocene would increase the electrochemical stability of films made with $FcMe_4$-$C_3$-LPEI relative to the previously characterized $FcMe_2$-$C_3$-LPEI.

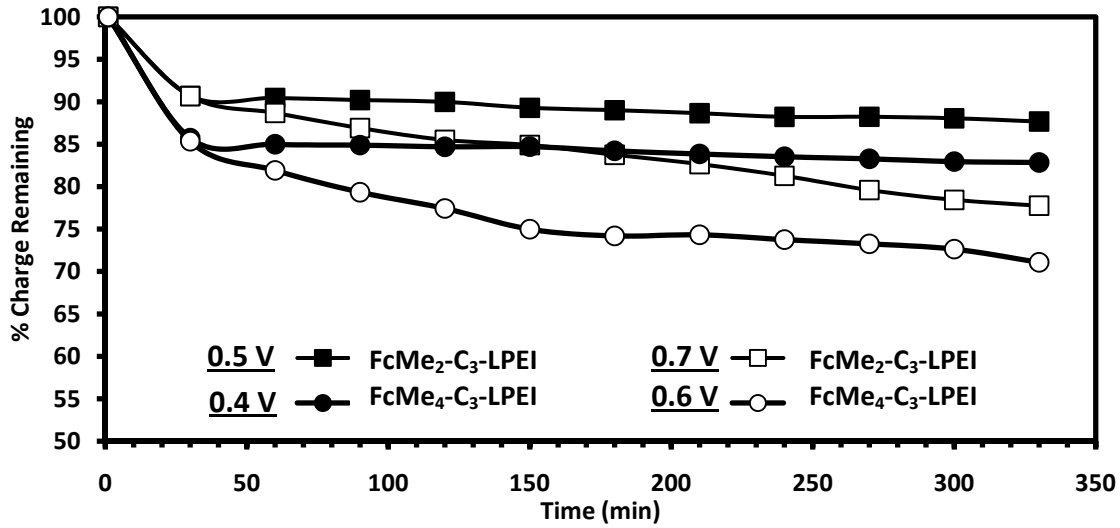


**Figure 6.07: Electrochemical Stability of Anodic Films.** Plot of the changes in area of integrated voltammetric waves for cross-linked films (with GOx) of $FcMe_2$-$C_3$-LPEI* (cycled to 0.5 or 0.7 V), and $FcMe_4$-$C_3$-LPEI (cycled to 0.4 or 0.6 V) at 50 mV/s in PBS buffer, pH 7.4, T = 25° C *Data taken from reference 26.

Figure 6.07 shows a comparison of the electrochemical stabilities of films made with $FcMe_2$-$C_3$-LPEI and $FcMe_4$-$C_3$-LPEI. The scan "windows" in which the films were cycled caused the ferrocenium moieties to be present for the same amount of time in each film, allowing for a direct comparison of electrochemical stability. As seen in the graph, films made with $FcMe_4$-$C_3$-LPEI were actually less stable in terms of the percent of charge remaining at the end of the cycling experiment, which was unexpected. However, a close examination of the data revealed that after the initial "break in" period was over for each cycling experiment, the electrochemical stability for $FcMe_4$-$C_3$-LPEI was virtually identical to that of $FcMe_2$-$C_3$-LPEI. The films made with $FcMe_4$-$C_3$-LPEI lost 15% of their original charge after the first 30 minutes of cycling, while the films made with $FcMe_2$-$C_3$-LPEI only lost 10% of their original charge in the first 30 minutes. After this initial loss, the films which were held at an oxidizing potential for a shorter amount of time lost only 3% of their charge in the remaining 300 minutes of cycling. The films which were cycled out to the higher potentials lost 14% of their charge after the initial break-in period. Therefore, it is likely that the electrochemical stability of the actual tetramethylferrocenium moieties in the $FcMe_4$-$C_3$-LPEI films are at least as stable as the dimethylferrocenium moieties in the $FcMe_2$-$C_3$-LPEI films, as evidenced by the similar behavior after the initial break-in period. The initial break-in period has been observed for every LPEI-based polymer studied in this work and could be due to factors other than ferrocenium stability such as film collapse or the formation of a ferrocenium/phosphate complex. In this specific set of experiments, the films made with $FcMe_4$-$C_3$-LPEI were not as homogeneous (due to the precipitate) as those made with $FcMe_2$-$C_3$-LPEI, and effect of this behavior on

electrochemical stability cannot be predicted. As such, it cannot be confirmed that the use of tetramethylferrocene increases or decreases the electrochemical stability of the films. Further investigation of the enzyme/polymer precipitate and the initial break-in period should be carried out to determine the amount of stability gained by adding the two additional methyl groups onto the ferrocene.

*Glucose Biosensors with $FcMe_4$-$C_3$-LPEI*

To evaluate the bioelectrocatalytic ability of $FcMe_4$-$C_3$-LPEI to shuttle electrons from GOx to an electrode surface, glucose calibrations were carried out while poising the bioelectrodes at an oxidizing potential (0.2 V). Sensors were cured at the different pH's (5.0 and 6.8) in order to determine if the seemingly improved electrochemical behavior using a curing pH of 6.8 translated to an improved biocatalytic response to glucose. Figure 6.08 shows these results, and clearly the sensors constructed using polymer solutions at pH 6.8 performed better, with an average saturating current density ($j_{max}$) of 600 μA/cm$^2$, compared to ca. 400 μA/cm$^2$ for the sensors constructed using polymer solutions at pH 5.

**Table 6.01: Effect of Redox Polymer Type on Electrochemical and Biocatalytic Properties**

| Redox Polymer | $E_{1/2}$ (vs. SCE) | $cDe^{1/2}$ x $10^9$ with enzyme (**without enzyme**) ($mol/cm^2 \cdot sec^{1/2}$) | Glucose Sensitivity ($\mu A/cm^2 \cdot mM$) | $J_{max}$ 25° C (**37° C**) ($mA/cm^2$) | $K_M$ (mM) |
|---|---|---|---|---|---|
| Fc-$C_3$-LPEI | 260 mV | 1.72 ± 1.0 (**1.06 ± 0.5**) | 47 ± 2 | 1.01 ± 0.06 (**1.96 ± 0.07**) | 20.7 ± 2.3 |
| $FcMe_2$-$C_3$-LPEI | 170 mV | 3.91 ± 0.44 (**5.42 ± 0.6**) | 45 ± 1.6 | 1.16 ± 0.05 (**2.09 ± 0.09** ) | 21.65 ± 1.9 |
| $FcMe_4$-$C_3$-LPEI | 80 mV | 0.294 ± 0.074 | 41 ± 3.2 | 0.606 ± 0.04 (**0.983 ± 0.05)** | 10.4 ± 3.4 |

$E_{1/2}$ was determined by the formula $(E_{pa} + E_{pc})/2$. Sensitivity was determined from the experimental current response at 5 mM glucose concentration. $J_{Max}$ is the maximum current obtained experimentally at saturating glucose concentrations. $K_M$ values were determined graphically from a Lineweaver-Burke plot. Values are expressed as mean ± standard error of the mean. Values for Fc-$C_3$-LPEI and $FcMe_2$-$C_3$-LPEI were reported previously.[23, 26]

This could indicate that increasing the amount of oxidized ferrocenes on the polymer backbone creates an undesired interaction with the enzyme which leads to a lower efficiency of bioelectrocatalysis. Glucose biosensors made with $FcMe_4$-$C_3$-LPEI were also tested at 37° C in order to determine if the increase in temperature would lead to a large increase in current density, as seen with previous systems. As seen in Figure 6.08 and Table 6.01, increasing the temperature resulted in a 62% increase in the limiting current density. This increase was smaller than that observed for sensors made using Fc-$C_3$-LPEI and $FcMe_2$-$C_3$-LPEI, which displayed a 100% increase in current density at 37° C (Table 6.01 and previous chapter).

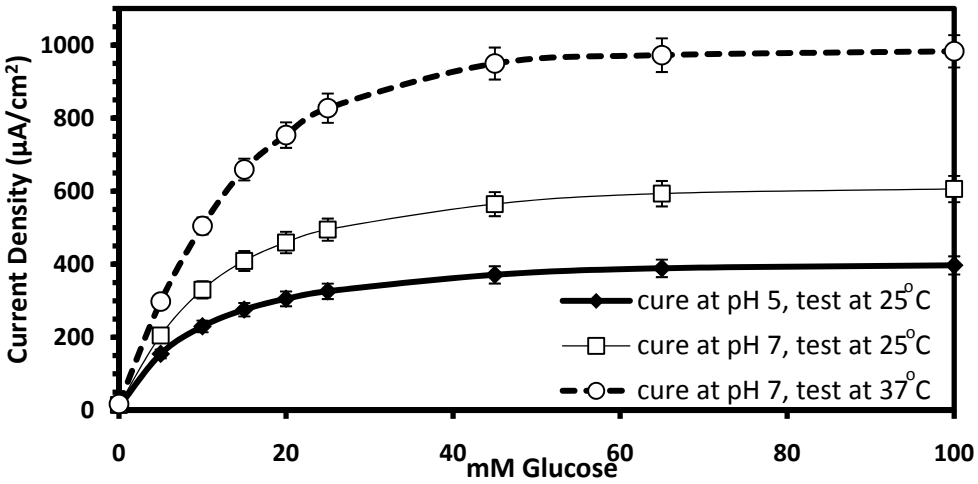


**Figure 6.08: Calibration curves for $FcMe_4$-$C_3$-LPEI under different curing pH conditions and at 37° C**. PBS, pH 7.4, 25° C, stirring, E = 0.2 V vs. SCE

The smaller increase could again be due to a less efficient communication between the enzyme and electrode due to the complex formed when the polymer and enzyme were mixed. Even though the performance of $FcMe_4$-$C_3$-LPEI was not as exceptional as that of the other $C_3$ polymers, this experiment did show that current densities of almost 1 mA/cm$^2$ could be obtained with $FcMe_4$-$C_3$-LPEI/GOx sensors and that these films could likely be utilized as biofuel cell anodes.

*Ascorbate Interference*

While the performance of the glucose biosensors made with $FcMe_4$-$C_3$-LPEI was not as high as we hoped, they were operated at 0.2 V vs. SCE, which is quite low for a ferrocene-based redox polymer.[11, 49, 50] This low potential allowed for the testing of the sensors' sensitivity to ascorbate, which is a common interferant in amperometric glucose biosensors. We wanted to compare the ascorbate sensitivity of $FcMe_4$-$C_3$-LPEI to the other $C_3$ polymers discussed in previous chapters to see if any improvement was

made by lowering the operating potential to 0.2 V, so they were evaluated as well. To investigate how the presence of physiological concentrations of ascorbate affected sensor performance, the steady-state currents of sensors made with Fc-$C_3$-LPEI, $FcMe_2$-$C_3$-LPEI, and $FcMe_4$-$C_3$-LPEI were measured at 5 mM glucose and then 0.1 mM ascorbate was added to the solution and the changes in current were measured. The results of these experiments are summarized in Table 2.

**Table 6.02: Effect of Ascorbate on Catalytic Current Density**

| Redox Polymer | Catalytic Current Density at 5 mM Glucose ($\mu A/cm^2$) | Change in Current Density with 0.1 mM ascorbate (%) |
|---|---|---|
| Fc-$C_3$-LPEI | 281 | 5.9 ± 0.12 |
| $FcMe_2$-$C_3$-LPEI | 181 | 6.2 ± 0.88 |
| $FcMe_4$-$C_3$-LPEI | 188 | 6.5 ± 1.0 |

Sensors poised at 0.4 V (Fc-$C_3$-LPEI), 0.3 V ($FcMe_2$-$C_3$-LPEI), or 0.2 V ($FcMe_4$-$C_3$-LPEI) in PBS buffer. Ascorbate was added (0.1 mM) after the current at 5 mM glucose had stabilized. Values represent the average of 6 measurements for each polymer.

As seen in the table, the change in current density from the addition of 0.1 mM ascorbate was ~6%, regardless of the redox polymer used. It was hoped that the sensors which were being poised at higher operating potentials would show a greater increase in current density with the addition of ascorbate and indicate that $FcMe_4$-$C_3$-LPEI was less sensitive to ascorbate interference. However, this was not the case and there was no significant change in the "error" caused by ascorbate in the glucose readings for each polymer. In one study, ascorbate was shown to have an oxidation onset as low as 0.14 V (vs. SCE) at a glassy carbon electrode surfaces, and a steady-state current maximum occurred around 0.25 V vs. SCE.[51] Therefore, the reason for the similar ascorbate

errors in this study could be that the ascorbate oxidation is already close to a maximum at 0.2 V. If this was the case, additional increases in voltage would not produce increases in current from ascorbate oxidation, similar to what is shown in the table. Another factor which could complicate this interference test is that the ascorbate oxidation likely occurred at the surface of the electrode *and* at individual ferrocenium sites in the polymer. The electrocatalytic oxidation of ascorbate by ferrocenium moieties in the LPEI hydrogels would not be unprecedented, as ferrocene derivatives have been shown to be effective electrocatalysts for ascorbate oxidation.[52, 53] Regardless of how the ascorbate was oxidized, it appears that a mediator with a redox potential lower that of $FcMe_4$-$C_3$-LPEI could be necessary to completely eliminate ascorbate interferences. Further studies are necessary to determine if the ascorbate is being oxidized by the ferrocenium moieties or at the electrode surface.

*Performance of $FcMe_4$-$C_3$-LPEI Anodes in a Biofuel Cell*

While there was a decrease in the $j_{max}$ of glucose sensors fabricated with $FcMe_4$-$C_3$-LPEI, the desired decrease in redox potential was obtained, and we wanted to exploit this decrease in order to show that the voltage of the biofuel cell could be increased with this mediator. For comparison's sake, the $FcMe_4$-$C_3$-LPEI/GOx anodes will be compared to $FcMe_2$-$C_3$-LPEI/GOx anodes, which were previously determined to give the highest power output in our biofuel cells.

Figure 6.09 shows the polarization curves for the anodes made with $FcMe_2$-$C_3$-LPEI and $FcMe_4$-$C_3$-LPEI and for the cathode in this study (PVPOs/laccase)

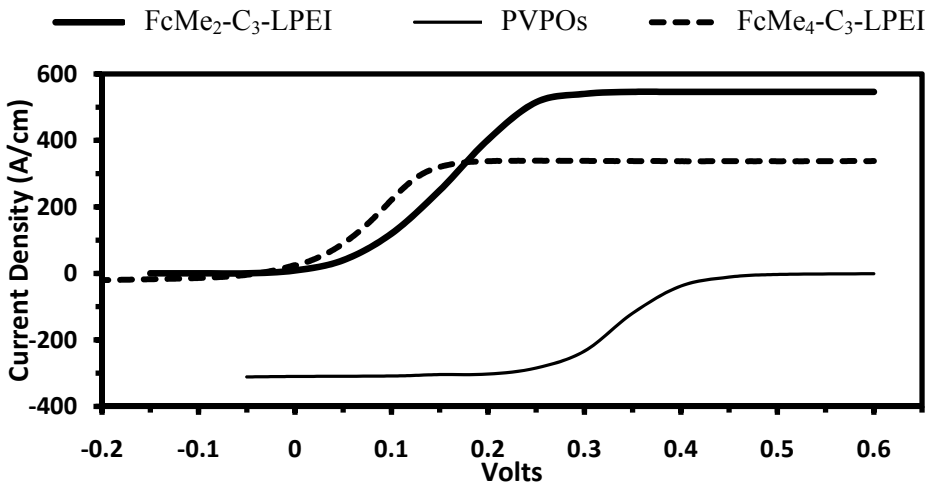


**Figure 6.09: Polarization Curves of the Electrodes.** Polarization of the bioanodes and biocathode. Stirred solution under air-saturating conditions, 0.05 M citrate, pH 5.5, 60 mM glucose, scan rate = 1 mV/s.

As expected, the maximum current density for the polarization of the $FcMe_4$-$C_3$-LPEI anode was significantly lower than for the $FcMe_2$-$C_3$-LPEI anode. The onset of glucose oxidation for the $FcMe_4$-$C_3$-LPEI anode occurred at ~ 0.0 V, which is 0.05 V less than the oxidation onset for $FcMe_2$-$C_3$-LPEI. There was also a ~0.05 V difference in the midpoints of the polarization curves of anodes made with $FcMe_2$-$C_3$-LPEI and $FcMe_4$-$C_3$-LPEI. This 0.05 V difference is similar to the difference previously reported for the polarization curve midpoints of Fc-$C_3$-LPEI and $FcMe_2$-$C_3$-LPEI.

To determine if the $FcMe_4$-$C_3$-LPEI/GOx anode would provide improved voltages and powers in a biofuel cell, it was coupled with a PVPOs/laccase cathode to construct a compartment-less, stationary biofuel cell. The performance of this biofuel cell was compared to a biofuel cell using $FcMe_2$-$C_3$-LPEI as the anodic polymer, and the results are shown in Figure 6.10. The use of $FcMe_4$-$C_3$-LPEI resulted in a small increase in the power density at 25$^o$ C (Figure 6.10B and Table 6.03) and a rather

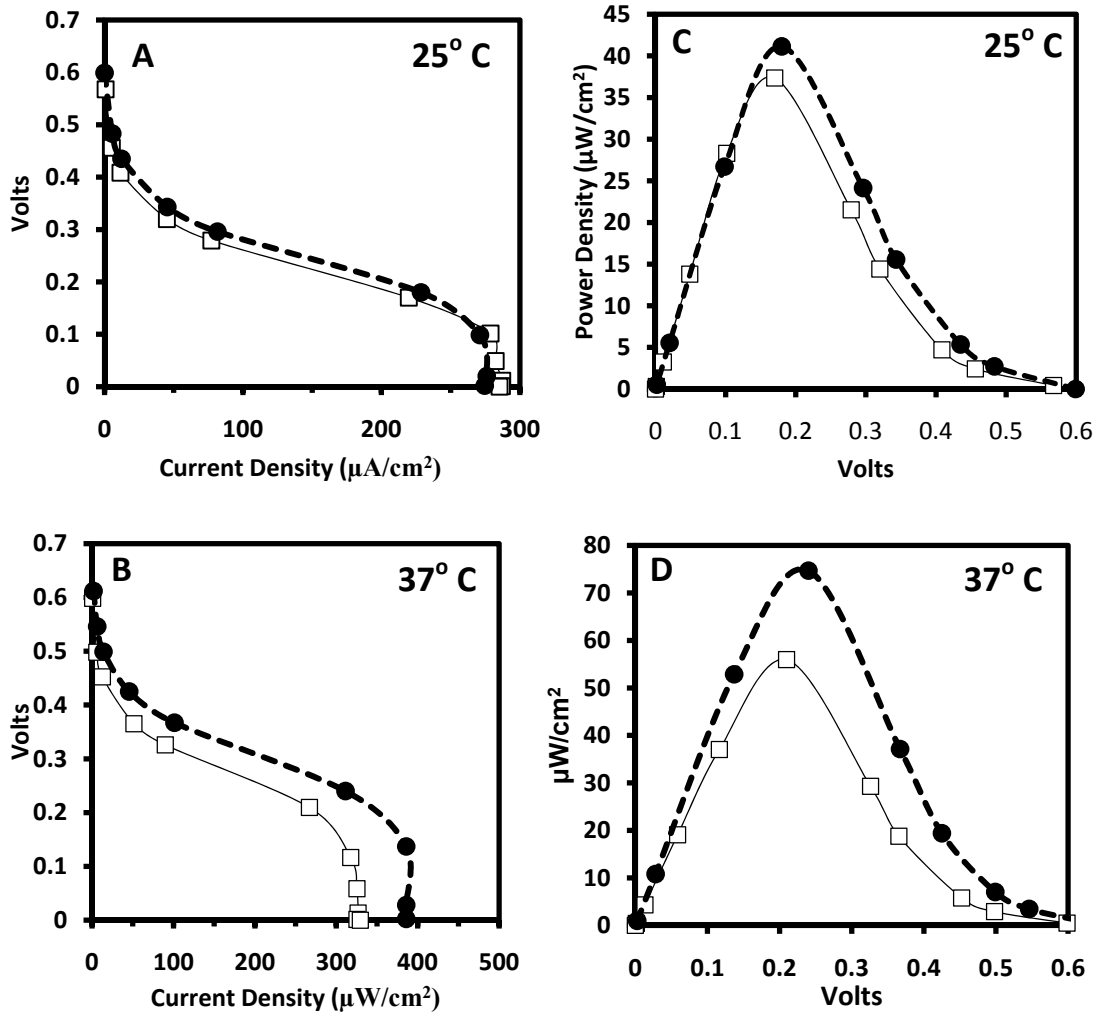


**Figure 6.10: Effect of Temperature and Polymer Type on Biofuel Cell Performance.** Polarization of the biofuel cells at 25° C (A) and 37° C (B) and dependence of the biofuel cell power density on cell voltage at 25° C (C) and 37° C (D) using $FcMe_2$-$C_3$-LPEI* (open squares), and $FcMe_4$-$C_3$-LPEI (filled circles) Cathode was PVPOs/laccase on a 3mm GC electrode. Stirred solution under air-saturating conditions, 0.05 M citrate, pH 5.5, 60 mM glucose. *Data from reference 26

significant improvement occurred in the power density at 37° C (Figure 6.10D and Table 6.03). The polarization of the 25° C biofuel cells shows that the voltages and current densities for the $FcMe_4$-$C_3$-LPEI anode were almost identical to the $FcMe_2$-$C_3$-LPEI anode, with a slight increase in the voltage at maximum power (0.01 V), resulting in a 10% increase in power density. However, when the temperature was raised, the voltages and current densities of the biofuel cell using $FcMe_4$-$C_3$-LPEI were

significantly higher than those using the $FcMe_2$-$C_3$-LPEI anode. At 37° C, the difference in voltage at maximum power for the two cells increased to 0.03 V, (Table 6.03) which resulted in a 33% increase the power density at 37° C. This "amplification" of the ferrocenyl methylation effect at higher temperatures has also been observed with the biofuel cells discussed in the previous chapter. Because the biocathode current was limiting relative to both polymers, the lower $j_{max}$ of the $FcMe_4$-$C_3$-LPEI anode did not translate to a lower biofuel cell current density, as seen in the polarizations of each biofuel cell (Figure 6.10A and 6.10C). In fact, a significant power increase was seen in the biofuel cells using $FcMe_4$-$C_3$-LPEI because of the lower redox potential of the tetramethylferrocene moieties (relative to the dimethylferrocene moieties).

**Table 6.03: Summary of Biofuel Cells with Stationary or Rotating Biocathodes at 25 and 37° C**

| Anodic Redox Polymer | Open Circuit Voltage (V) | Maximum Power Density ($\mu W/cm^2$) | Max. Current Density ($\mu A/cm^2$) | Temp (° C) | Type of Biocathode |
|---|---|---|---|---|---|
| $FcMe_2$-$C_3$-LPEI | 0.61 V | 38 at 0.17 V | 280 | 25 | Stationary |
| | 0.64 V | 56 at 0.21 V | 330 | 37 | |
| | 0.61 V | 68 at 0.16 V | 738 | 25 | RDE |
| | 0.65 V | 146 at 0.16 V | 1,267 | 37 | |
| $FcMe_2$-$C_4$-LPEI | 0.66 V | 41 at 0.18 V | 275 | 25 | Stationary |
| | 0.70 V | 75 at 0.24 V | 385 | 37 | |
| | 0.67 V | 67 at 0.22 V | 380 | 25 | RDE |
| | 0.71 V | 135 at 0.22 V | 850 | 37 | |

*Biofuel cell with $FcMe_4$-$C_3$-LPEI/GOx Anode and Rotating PVPOs/laccase Cathode*

As was discussed in the previous chapter, the use of a rotating biocathode has been shown to significantly increase the amount of current that can be produced from

the reduction of oxygen by laccase or bilirubin oxidase.[21, 54, 55] As such, we coupled the stationary $FcMe_4$-$C_3$-LPEI/GOx anodes with rotating PVPOs/laccase biocathodes, and

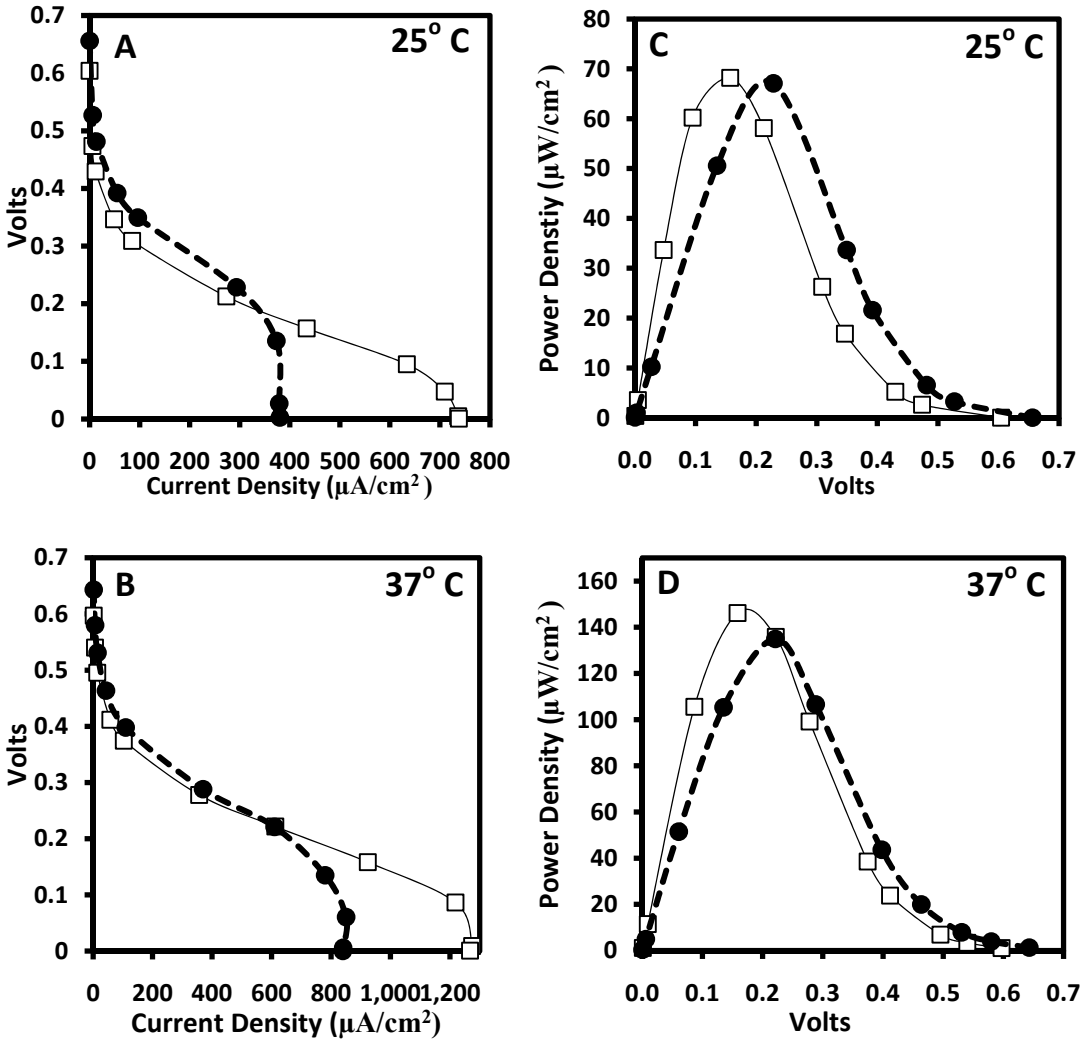


**Figure 6.11: Biofuel Cell Performance with RDE cathodes.** Polarization of the biofuel cells at 25° C (A) and 37° C (B) and dependence of the biofuel cell power density on cell voltage at 25° C (C) and 37° C (D) using $FcMe_2$-$C_3$-LPEI* (open squares), and $FcMe_4$-$C_3$-LPEI (filled circles). PVPOs/laccase cathode was cast on a 5 mm glassy carbon RDE and rotated at 2000 rpm. Stirred solution under air-saturating conditions, 0.05 M citrate, pH 5.5, 60 mM glucose. Current and power densities were calculated using the 3mm electrode area. *Data from reference 26

the results from these experiments are shown in Figure 6.11. The polarization of the biofuel cells at 25° C (Figure 6.11 A) shows that the $FcMe_4$-$C_3$-LPEI anodes have a

much lower maximum current density than the $FcMe_2$-$C_3$-LPEI anodes. This was expected based on the glucose calibrations in PBS and the polarization curves of the individual electrodes. However, when the maximum power densities were examined, the biofuel cell with the $FcMe_4$-$C_3$-LPEI anode produced an equal maximum power density to that of $FcMe_2$-$C_3$-LPEI due to its lower oxidation potential. When the temperature was raised to 37$^o$ C, the polarizations of the biofuel cells displayed similar trends, with the $FcMe_4$-$C_3$-LPEI anodes producing a lower maximum current density. However, the maximum power density of the biofuel cell using the $FcMe_4$-$C_3$-LPEI was lower than the max. power density of the $FcMe_2$-$C_3$-LPEI fuel cell, even though the $FcMe_4$-$C_3$-LPEI biofuel cell had a higher voltage at that power density. This indicates that when the biofuel cells were operating close to their maximum efficiency (rotating cathode and 37$^o$ C), the cell using the $FcMe_2$-$C_3$-LPEI anode produced a high enough current density to overcome its lower operating voltage and produce slightly more power than the cell using $FcMe_4$-$C_3$-LPEI.

The biofuel cells which used rotating cathodes also produced a large enhancement in the "methylation effect" in that the ΔE at max. power between the two biofuel cells was 0.06 V (at both temperatures). This is a much larger ΔE than was seen for the stationary biofuel cells (0.01 and 0.03 V) and comes close to the true ΔE of the redox potentials for the two polymers (0.09 V).

*Levich Analysis of the Biofuel Cells*

When rotating electrodes are used to obtain electrochemical measurements, the effect of rotation rate on current density can provide information about the properties of

the electrochemical reactions occurring on the electrode. The Levich equation states that if the reaction occurring at the rotating electrode is limited by mass transport of the analyte to the electrode, the current will increase linearly vs. the square root of the rotation rate:[54, 56, 57] (Equation 6.01)

$$i_L = (0.620)nFAD^{\frac{2}{3}}w^{\frac{1}{2}}v^{\frac{-1}{6}}C$$

**Equation 6.01: Levich Equation.** $i_L$ is the limiting current, $n$ is the number of electrons transferred in the half reaction, $F$ is the Faraday constant, $A$ is the electrode area, $D$ is the diffusion coefficient, $\omega$ is the angular rotation rate of the electrode, $v$ is the kinematic viscosity, and $C$ is the analyte concentration

If the reaction is limited by something else (for instance the kinetics of the reaction occurring on the electrode surface), the plot will deviate from linearity and flatten out. This analysis is normally applied to single electrodes which are controlled by a potentiostat, so this Levich analysis of a biofuel cell is somewhat unconventional, but provides some useful information about the biofuel cells.

Figure 6.12A shows the polarization of a biofuel cell using a stationary $FcMe_2$-$C_3$-LPEI anode and a rotating PVPOs/laccase biocathode at different cathodic rotation rates. As illustrated in the figure, the polarization curves changed with respect to rotation rate, but only when biofuel cell was operating at medium and low resistances. This behavior is graphed in a Levich plot in Figure 6.12B. At the lowest resistance, the current density increased linearly with the square root of the rotation rate, indicating that mass transport of $O_2$ was likely limiting the current density and the cathode was still the limiting electrode up to 3000 rpm. However, at a higher resistance, the current density only increased significantly between 0 and 500 rpm, and faster rotation did not affect the current density. This indicates that when operating the biofuel cell at

maximum power, rotation of the biocathode is advantageous and improves performance, but the cathodic rotation rate has no effect above 500 rpm. One possible explanation for this phenomenon is that the resistor in the circuit is actually what limited the current output of the cell (rather than one of the electrodes).

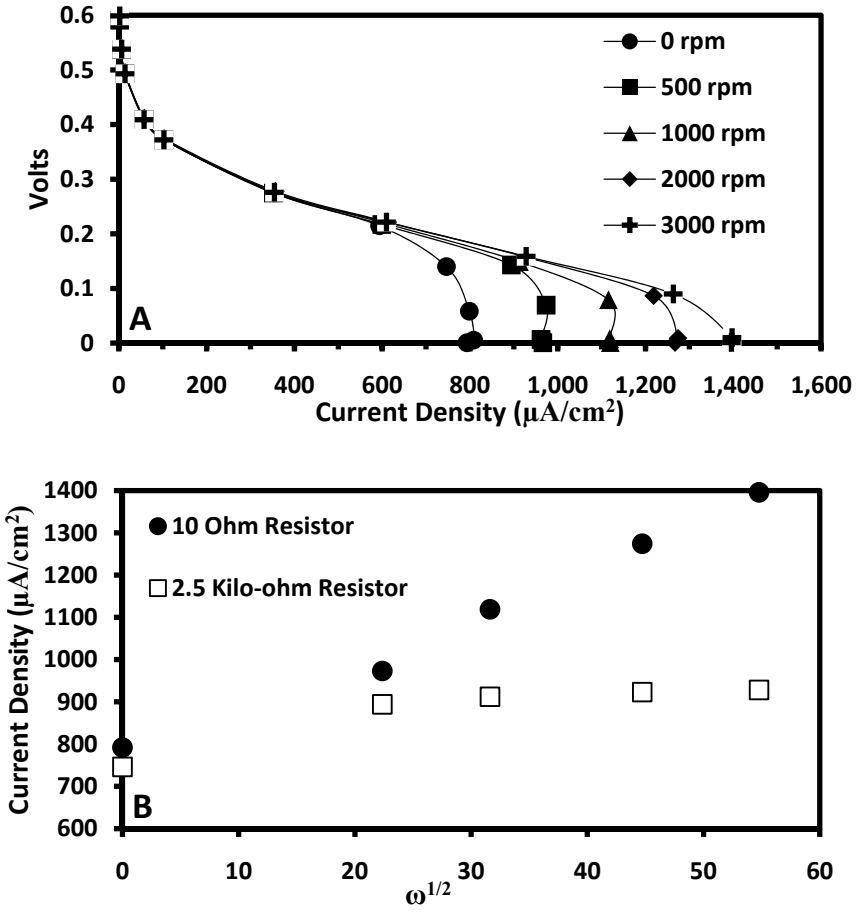


**Figure 6.12: Effect of Cathode Rotation Rate on $FcMe_2$-$C_3$-LPEI Biofuel Cell Performance.** Effect of rotation rate on the polarization of a biofuel cell using $FcMe_2$-$C_3$-LPEI as the anode (A) and a Levich plot showing the effect of rotation rate on current density at two resistances. Compartment-less cell, 0.05 M citrate, pH 5.5, 37° C, 60 mM glucose.

Because the resistor impeded the current flow, the electrons produced by the bioanode reached the biocathode at a slower rate than the rate of mass transport of $O_2$, and

therefore rotation of the biocathode would not produce an increase in current, as mass transport would not be limiting in this scenario.

Regarding the other anodic polymer, Figures 6.13A and B show that the rotation of the cathode had little effect on the performance of the $FcMe_4$-$C_3$-LPEI biofuel cell.

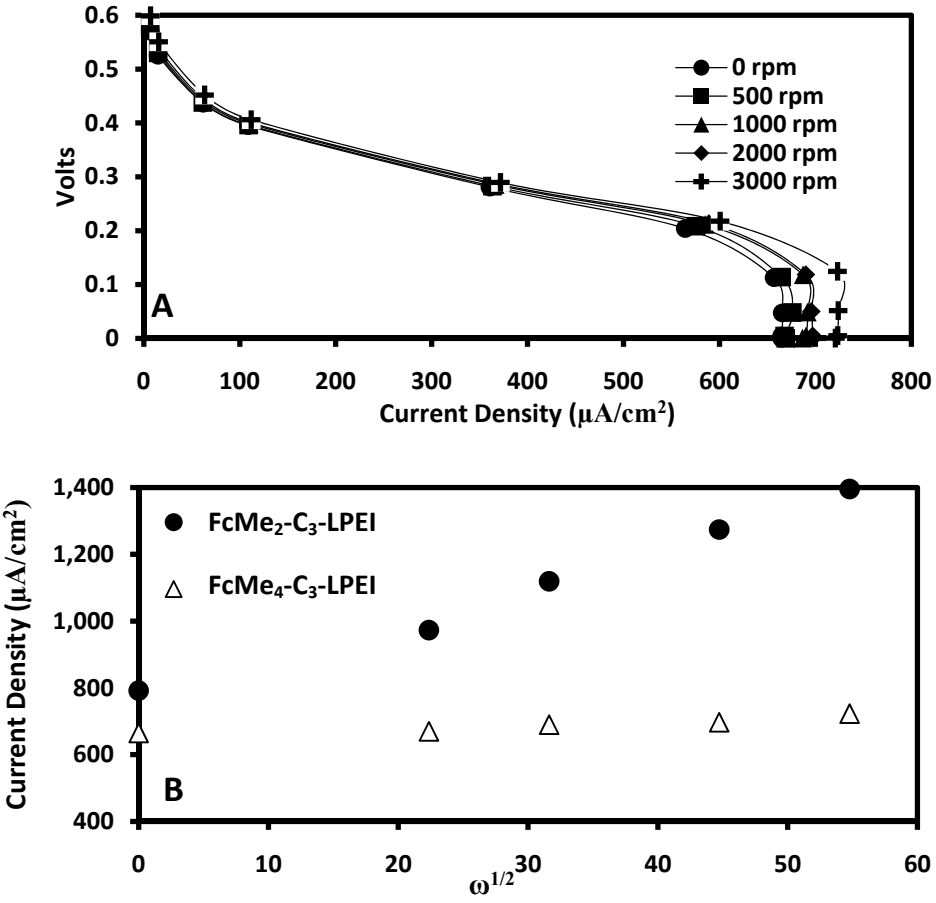


**Figure 6.13: Effect of Cathode Rotation Rate on $FcMe_4$-$C_3$-LPEI Biofuel Cell Performance.** Effect of rotation rate on the polarization of a biofuel cell using $FcMe_4$-$C_3$-LPEI as the anode (**A**) and a Levich plot showing the effect of rotation rate on current density in a $FcMe_4$-$C_3$-LPEI biofuel cell (with the plot from the $FcMe_2$-$C_3$-LPEI biofuel cell for comparison) (**B**) Compartment-less cell, 0.05 M citrate, pH 5.5, 37° C, 60 mM glucose. Levich plot uses 10 Ω resistors for both biofuel cells.

A very small increase in maximum current density occurred with increasing rotation rate, but this increase was insignificant, as shown in the Levich plot vs. the $FcMe_2$-$C_3$-LPEI biofuel cell (Figure 6.13B). This behavior is likely a result of the lower efficiency

of bioanodes made with $FcMe_4$-$C_3$-LPEI, as seen in the glucose calibrations and anode polarization curves. Because the anode was limiting, no enhancement of biofuel cell performance at any voltage was seen with increasing cathode rotation rate.

Overall, the results of this Levich study showed that rotation of the biocathode can significantly increase the performance of biofuel cells using $FcMe_2$-$C_3$-LPEI as the anodic polymer. In addition, it can be assumed that if the performance of anodes utilizing $FcMe_4$-$C_3$-LPEI as the mediator can be improved, rotation of an accompanying biocathode will produce similar increases in performance.

**Conclusions**

The synthesis of tetramethylferrocene was accomplished in moderate yields from commercially available dimethylferrocene. When the tetramethylferrocene was modified for attachment to LPEI by means of a 3-carbon tether, a redox polymer was produced which had the predicted effect of a lower redox potential (0.09 V lower than $FcMe_2$-$C_3$-LPEI). However, the redox polymer designated as $FcMe_4$-$C_3$-LPEI formed an unknown precipitate when it was mixed with glucose oxidase, which may have hindered its performance as a bioelectrode compared to previous $C_3$-LPEI polymers (Table 6.01). Even though this unknown precipitate was formed, sensors constructed with $FcMe_4$-$C_3$-LPEI and GOx were able to produce current densities of almost 1 $mA/cm^2$. Because this sensor could be operated at a relatively low potential of 0.2 V vs. SCE, the influence of physiological levels of ascorbate on the biosensor performance was tested and compared to ascorbate interferences of two previously discussed, higher redox potential polymers. Ascorbate was shown to induce a ~6% error in the measurement of 5 mM glucose for all of the polymers which were

evaluated, which was indicated that the ascorbate oxidation current was already at a maximum at 0.2 V vs. SCE. Also, the electrocatalytic oxidation of ascorbate by the ferrocenium moieties in the films likely played a role in producing the ascorbate interferences.

When $FcMe_4$-$C_3$-LPEI/GOx anodes were utilized in stationary, compartment-less biofuel cells, the cells operated at higher voltages than the $FcMe_2$-$C_3$-LPEI cells and produced power densities of up to 70 $\mu W/cm^2$, which is among the highest power densities for this type of cell[58, 59] and exceeded our previous high power density of 56 $\mu W/cm^2$ which was obtained using $FcMe_2$-$C_3$-LPEI as the anodic polymer.[26] When the $FcMe_4$-$C_3$-LPEI anodes were used in biofuel cells with rotating biocathodes, the power densities increased significantly, but the lower limiting current density of the $FcMe_4$-$C_3$-LPEI anodes prevented the power densities from exceeding those obtained when using the $FcMe_2$-$C_3$-LPEI anodes with the rotating cathodes. The biofuel cells using the RDE cathodes did, however, have voltages at max. power which were ca. 0.06 V higher than the max. power voltages of the $FcMe_2$-$C_3$-LPEI biofuel cells, indicating that the use of tetramethylferrocene-modified LPEI could produce much higher power densities with the use of rotating cathodes if the $j_{max}$ can be increased to the same level as the other $C_3$ polymers. The large increase in operating potential (0.06 V at max. power) induced by the use of tetramethylferrocene suggests that further methylation of the ferrocene could produce similar increases in voltage, and this should be explored as a possible method for increasing biofuel cell power density with these polymers. Again, it should be mentioned that because continuous polarization curves of the biofuel cells were not generated (obtaining points at every 1 mV), it is possible that the true maxima for each

biofuel cell were not reached and that the ΔE between the cells could be greater than the values reported in this chapter.

Further studies involving $FcMe_4$-$C_3$-LPEI should first entail an attempt to find a better synthetic transformation of the (3-hydroxypropyl)tetramethylferrocene into the bromide, as the yields for that reaction are poor. As for the polymer itself, an investigation into why it forms a precipitate when it is mixed with GOx and how this could be avoided would be advantageous, as well as further electrochemical and operational stability studies. Also, some preliminary results (not discussed here) have shown that the performance of biosensors and biofuel cells utilizing $FcMe_4$-$C_3$-LPEI can be significantly enhanced with carbon nanotubes. This enhancement should be fully investigated as a way to increase current and power densities of the biosensors and biofuel cells.

## Experimental

*Chemicals and Solutions*

All chemicals and enzymes were purchased from Sigma-Aldrich unless otherwise noted and used as received. Ethylene glycol diglycidyl ether (EGDGE) and poly(ethylene glycol diglycidyl ether) (PEGDGE) were purchased from Polysciences Inc., Warrington, PA. Stock solutions of 2 M glucose were allowed to mutarotate for 24 hr before use and subsequently kept refrigerated at 4°C. The redox polymer, designated as PVP-Os, was synthesized by partially complexing the pyridine nitrogens of poly(4-vinylpyridine) with $Os(bpy)_2Cl^{+/2+}$ and then partially quaternizing the resulting polymer with 2-bromoethylamine according to a previously published protocol.[60, 61] The redox

polymers designated as Fc-$C_3$-LPEI and $FcMe_2$-$C_3$-LPEI (ca. 15-17% ferrocenyl moiety substitution) were synthesized as previously reported.[23]

*Aminomethylation of Dimethylferrocene*

1,1'-Dimethylferrocene was di-aminomethylated with a procedure similar to that of Pauson et. al.[41] For our procedure, we increased the amount of amine and lengthened the reaction time as follows: N,N,N',N'-tetramethyldiaminomethane (14.7 g, 0.144 mol) was added drop-wise over 15 minutes to an ice-cooled mixture of 100 mL of glacial acetic acid and 10 mL of 85% phosphoric acid. Dimethylferrocene (10.3 g, 0.048 mol) was added and the mixture was heated slowly until it reached a temperature of 100$^o$ C, where it was held for 24 hours. The reaction mixture was cooled to room temperature, 400 mL of water was added, and the acidic solution was neutralized by slowly adding NaOH pellets until a pH > 11 was reached. This mixture was extracted 5 times with diethyl ether. The ether extracts were combined, dried over $Mg_2SO_4$, and the solvent was removed under reduced pressure to yield a mixture of mono- and di-aminomethylated dimethylferrocene. This mixture was loaded onto a basic alumina column and eluted with a 10:1 mixture of ether and hexanes to separate the mono- and di-substituted isomers. Removal of the solvents under reduced pressure yielded 6.03 g of a mixture of 1-Dimethylaminomethyl-2,1'-dimethylferrocene and 1-Dimethylaminomethyl-3,1'-dimethylferrocene (**2**) (46.3% yield) and 4.50 g of a mixture of 1,1'-*Bis*-Dimethylaminomethyl-3,3'-dimethylferrocene, 1,1'-*Bis*-Dimethylaminomethyl-2,2'-dimethylferrocene, and 1,1'-*Bis*-Dimethylaminomethyl-2,3'-dimethylferrocene (**3**) (27.1% yield).

Compounds **2** eluted off of the column first and was obtained as an orange, viscous liquid. $^{1}$H NMR ($CDCl_3$): δ 1.90-1.98 (multiple peaks (m.p.), 6H, 2Fc-$CH_3$), 2.18-2.20 (overlapping singlets, 6H, -N-$(CH_3)_2$), 3.16-3.36 (m.p., 2H, -N-$CH_2$-Fc), 3.84-4.04 (m.p., 7H, Fc ring H).

Compounds **3** eluted off of the column second and was obtained as an orange liquid. $^{1}$H NMR ($CDCl_3$): δ 1.88-1.98 (m.p., 6H, 2[Fc-$CH_3$]), 2.12-2.20 (br s, 12H, 2[-N-$(CH_3)_2$]), 3.10-3.32 (m.p., 4H, 2[-N-$CH_2$-Fc]), 3.78-4.16 (m.p., 6H, Fc ring H).

*Methylation of **3***

Iodomethane (3.90 g, 0.027 mol) was added dropwise to a stirred solution of **3** (4.50 g, 0.014 mol) in methanol. The flask was fitted with a reflux condenser and the mixture was heated to 50$^{o}$ C for 1 hr. The methanolic solution was cooled to room temperature and added dropwise to a rapidly stirring solution of ether to precipitate the product as a yellow powder, a mixture of 1,l'-bis-(NN-dimethylaminomethyl)-2,2'-dimethylferrocene dimethiodide, 1,l'-bis-(NN-dimethylaminomethyl)-2,3'-dimethylferrocene dimethiodide, and 1,l'-bis-(NN-dimethylaminomethyl)-3,2'-dimethylferrocene dimethiodide (**4**) was isolated by filtration of the precipitate (8.0 g, 95.3% yield). $^{1}$H NMR ($CD_3OD$): δ 1.95-2.18 (m.p., 6H, 2[Fc-$CH_3$]), 3.0-3.15 (m.p., br, 18H, 2[-N-$(CH_3)_3$]), 4.25-4.85 (m.p., 10H, 2[-N-$CH_2$-Fc] and Fc ring H)

*Reduction of Compound **4** with $NaBH_4$*

Compound **4** (8.0 g, 0.013 mol) was dissolved in 200 mL of acetonitrile and 4 eq. of $NaBH_4$ was added over 5 minutes (light bubbling at first). The reaction mixture was heated to reflux solvent for 24 hours. The solvent was evaporated under reduced pressure and the dry mixture was triturated with hexanes. The hexane solution was concentrated and passed through a plug of alumina, and then the solvent was removed under reduced pressure to yield a mixture of 1,2,1',2'-tetramethylferrocene, 1,3,1'-2'-tetramethylferrocene, and 1,3,1',3'-tetramethylferrocene (**1a**) (2.5 g, 80% yield) $^1$H NMR ($CDCl_3$): δ 1.88-1.94 (m.p.,, 12H, 4[Fc-$CH_3$]), 3.72-3.84 (m.p., 6H, Fc ring H)

*Methylation of **2***

Iodomethane (3.15 g, 0.022 mol) was added dropwise to a stirred solution of **2** (6.0 g, 0.022 mol) in methanol. The flask was fitted with a reflux condenser and the mixture was heated to 50$^o$ C for 1 hr. The methanolic solution was cooled to room temperature and added dropwise to a rapidly stirring solution of ether to precipitate the product as a yellow powder. A mixture of (2,1'-dimethyl-1-ferrocenylmethyl)trimethylammonium iodide and (3,1'-dimethyl-1-ferrocenylmethyl)trimethylammonium iodide (DADmFc methiodide) was isolated by filtration of the precipitate (8.7 g, 95% yield). $^1$H NMR ($D_2O$): δ 1.80-1.95 (m.p., 6H, 2[Fc-$CH_3$]), 2.82 (overlapping singlets, 9H, -N-$(CH_3)_3$), 3.95-4.35 (m.p., 9H, -N-$CH_2$-Fc and Fc ring H)

*Reduction of Compounds **5** with $NaBH_4$*

Compounds **5** (8.7 g, 0.021 mol) was dissolved into 200 mL of acetonitrile and 4 eq. of $NaBH_4$ was added over 5 minutes (light bubbling). The reaction mixture was heated to reflux solvent for 24 hours. The solvent was evaporated under reduced pressure and the dry mixture was triturated with hexanes. The hexane solution was concentrated, passed through a plug of alumina, and the solvent was removed under reduced pressure to yield a mixture of 1,2,1'-trimethylferrocene and 1,3,1'-trimethylferrocene, (**6**) (4.03 g, 83.9% yield) $^1$H NMR ($CDCl_3$): δ 1.82-1.90 (m, 9H, 3[Fc-$CH_3$]), 3.76-3.86 (m, 7H, Fc ring H)

**NOTE: From this point on in the experimental, the number of possible reactant and product isomers is extremely numerous, and therefore each compound will be referred to as simply as possible without any reference to specific isomers.**

*Villsmeier-Haack Formylation of **6***

Compound **6** was formylated according to the ferrocene formylation method of Sato et. al. in a modified Villsmeier-Haack reaction.[62] Trimethylferrocene (4.0 g, 0.018 mol) and 2.6 g (2 eq.) of dimethylformamide (DMF) were dissolved into 50 mL of dry chloroform and 5.37 g (2 eq.) of $POCl_3$ was added dropwise over 15 minutes under nitrogen. The reaction was slowly heated to 60$^o$ C and was stirred for 15 hours. At the end of the reaction, most of the chloroform was removed under reduced pressure (water bath set to 40$^o$ C) and the residue was dissolved in 200 mL $H_2O$. The aqueous mixture was carefully neutralized with sodium carbonate (vigorous bubbling occurs) and stirred for 3 hours. The aqueous solution was extracted repeatedly with diethylether until all of

the product was removed from the aqueous layer. The organic layers were combined, dried over $Mg_2SO_4$ and removed under reduced pressure. The crude product was purified on basic alumina using hexanes to elute unreacted trimethylferrocene and ether to elute compound **7**, trimethylferrocenecarboxaldehyde (8 possible isomers) (3.14 g, 70% yield). $^1$H NMR ($CDCl_3$): δ 1.85-2.22 (m, 9H, 3[Fc-$CH_3$]), 3.90-4.60 (m, 6H, Fc ring H), 9.80-10.0 (m, 1H, -CHO)

*Reductive Deoxygenation of **7** with $BH_3 \cdot SMe_2$*

Compound **7** was reduced using $BH_3 \cdot SMe_2$ according to the method of Routaboul et. al. for ferrocenecarboxaldehyde:[63] Borane-dimethylsulfide complex (1.5 mL of a 10 M solution) was added dropwise to a stirring solution of 3.14 g (0.012 mol) of **7** in THF at room temperature. The reaction mixture was heated to reflux solvent and stirred for 30 min. The mixture was then cooled in an ice bath and water was added slowly (exothermic!!) until the excess borane was reacted. Excess water was added, and the THF was removed under reduced pressure. The resulting aqueous mixture was extracted with hexanes, and the organic layer was dried over $Mg_2SO_4$ and removed under reduced pressure to yield a mixture of tetramethylferrocene isomers (**1b**) (2.52 g, 85% yield). $^1$H NMR ($CDCl_3$): δ 1.86-1.94 (m, 12H, 4[Fc-$CH_3$]), 3.72-3.84 (m, 6H, Fc ring H)

*Villsmeier-Haack Formylation of **1***

Tetramethylferrocene mixtures **1a** and **1b** were mixed and formylated according to the ferrocene formylation method of Sato et. al. in a modified Villsmeier-Haack reaction.[62]

Compounds **1a/1b** (4.0 g, 0.017 mol) and 2 eq. of DMF were dissolved into 50 mL of dry chloroform and 5.37 g (2 eq.) of $POCl_3$ was added dropwise over 15 minutes under nitrogen. The reaction was slowly heated to 60° C and was stirred for 6 hours. At the end of the reaction, most of the chloroform was removed under reduced pressure (water bath set to 40° C) and the residue was dissolved in 200 mL $H_2O$. The aqueous mixture was carefully neutralized with sodium carbonate (vigorous bubbling occurs) and stirred for 3 hours. The aqueous solution was extracted repeatedly with diethylether until all of the product was removed from the aqueous layer. The organic layers were combined, dried over $MgSO_4$ and removed under reduced pressure. The crude product was purified on basic alumina using hexanes to elute unreacted **1** and diethylether to elute compound **8,** tetramethylferrocenecarboxaldehyde (3.21 g, 72% yield). $^1$H NMR ($CDCl_3$): δ 1.80-2.20 (m, 12H, 4[Fc-$CH_3$]), 3.80-4.50 (m, 5H, Fc ring H), 9.80-9.95 (m, 1H, -CHO)

*Wittig Reaction of **8** with Ethyl Bromoacetate*

According to the method of El-Batta et. al. for aqueous Wittig reactions,[46] tetramethylferrocenecarboxaldehyde (2.0 g, 0.0074 mol) was added to a rapidly stirring solution of triphenylphosphine (2.9 g, 1.5 eq.) and ethyl bromoacetate (2.10 g, 1.7 eq.) in saturated $NaHCO_3$. This solution was stirred rapidly with a rotary stirrer for six hours. Dilute (1 M) $H_2SO_4$ was added dropwise to this mixture until the pH reached ~ 5.0, and $CH_2Cl_2$ was added to extract the products. The organic layer was separated, dried over $Mg_2SO_4$ and the solvent was removed under reduced pressure. To remove most of the unreacted $PPh_3$ and triphenylphosphine oxide, the crude reaction product

mixture was dissolved into a minimal amount of ethyl acetate and added dropwise to 300 mL of hexanes while stirring. This caused most of the phosphine compounds to precipitate out of solution where they were filtered. The solvents were again removed under reduced pressure. The crude products were separated on a basic alumina column using ethyl acetate/cyclohexane (1:20) as the eluent, yielding 1.1 g of compound **9,** ethyl 3-tetramethylferrocenylpropenoate (43.7% yield). $^1$H NMR ($CDCl_3$): δ 1.25 (m, 3H, -$CH_3$), 1.80-2.20 (m, 12H, 4[Fc-$CH_3$]), 3.70-4.30 (m, 7H, Fc ring H and –COO-$CH_2$-), 5.88-6.0 (m, 1H, CH), 7.30-7.40 (m, 1H, CH). NOTE: While the yield was not great for this reaction, most of the unreacted aldehyde is easily recovered from the column chromatography step.

*Two-step LAH/$H_2$ Reduction of **9***

Ethyl 3-tetramethylferrocenylpropenoate (**9**) was reduced to (3-hydroxypropyl)tetramethylferrocene (**10**) in two steps, beginning with a lithium aluminum hydride (LAH) reduction. Ethyl 3-tetramethylferrocenylpropenoate (1.1g, 0.0032 mol) was dissolved into dry ether and 0.15 g LAH was added. The reaction was stirred at room temperature for 1 hr. and water was carefully added to quench any unreacted LAH. The organic layer was separated, dried over $MgSO_4$ and the solvent was removed under reduced pressure. This product was dissolved into ethanol (100%) and 30 weight percent of 10% Pd on activated carbon was added to the mixture. The flask was purged with $H_2$ once and then stirred overnight under $H_2$ atmosphere (using a balloon). The Pd on carbon was filtered off and the ethanol was removed under reduced pressure to yield the crude product. The product was dissolved in ether and loaded onto

a basic alumina column. Any over-reduced alkylferrocene eluted with the ether, and the alcohol was eluted with methanol. The methanol was removed under reduced pressure to yield (3-hydroxypropyl)tetramethylferrocene (**10**) (0.41 g, 42% yield). $^1$H NMR ($CDCl_3$): δ 1.72 (m, 2H, -$CH_2$-), 1.85-1.92 (m.p., 12H, 4[Fc-$CH_3$]), 2.35 (m.p., 2H, Fc-$CH_2$-), 3.55-3.72 (m.p., 7H, Fc ring H and –$CH_2$-OH)

*Bromination of **10** with $PBr_3$*

This synthesis was carried out according to the method of Lapic et al. for the bromination of (3-hydroxypropyl)ferrocene:[48] Compound **10** (127 mg) was dissolved into 10 mL of dry benzene under $N_2$. Phosphorus tribromide ($PBr_3$, 38 mg) was added and the mixture was stirred under $N_2$ at room temperature for 5 hours. Aqueous $NaHCO_3$ (5 mL) was added and the organic layer was separated and dried over $MgSO_4$. The benzene was evaporated under reduced pressure and the crude product was dissolved in hexanes and passed through a basic alumina column. The hexanes were evaporated to yield 14 mg of (3-bromopropyl)tetramethylferrocene (**11**) (9.2% yield). $^1$H NMR ($CDCl_3$): δ 1.76-1.82 (m.p., 12H, 4[Fc-$CH_3$]), 1.90 (m, 2H, -$CH_2$-), 2.40 (m, Fc-$CH_2$-), 3.34 (overlapping triplets, 2H, -$CH_2$-Br), 3.50-3.68 (m.p., 5H, Fc ring H)

*Synthesis of $FcMe_4$-$C_3$-LPEI*

Linear Poly(ethylenimine) (11 mg), was dissolved in 3 mL of a 10:1 of acetonitrile and methanol in a small flask. The mixture was heated to reflux to dissolve the LPEI, and 14 mg of (3-bromopropyl)tetramethylferrocene was added. The mixture was refluxed overnight, and then the solvent was removed under reduced pressure. Diethylether was

added to the product in order to remove any ferrocenyl impurities, and then any residual ether was removed under reduced pressure to yield 23 mg of $FcMe_4$-$C_3$-LPEI (92% yield). $^1$H NMR ($CD_3OD$): δ 1.48-1.95 (br, 4[Fc-$CH_3$]), 2.05-2.40 (br, Fc-$CH_2$-), br, 2.50-3.12 (br, -HN-$CH_2$-), 3.35-4.15 (br, Fc ring H and –$H_2N^+$-$CH_2$)

*Notes on Synthesis and NMR Characterization*

As expected, the reaction involving the aminomethylation of dimethylferrocene yielded a product that was a mixture of isomers.[41] We expected that carrying these isomers throughout the synthesis would have little effect on the electrochemical properties of the final polymer, and therefore we made no efforts to separate them. In addition, the references cited for the reactions involving the attachment of the three-carbon tether provided us with $H^1$ NMR spectra of the non-methylated ferrocene derivatives and allowed us to be confident in our NMR characterizations. Because the compounds listed above are mixtures of isomers, the NMR assignments of these compounds are not as straightforward as those of pure compounds, as one would expect. In incidences where the presence of the two isomers was clear, the NMR peaks were labeled as such (i.e. “overlapping triplets,” “multiple peaks,” etc.). In cases where there was no observable effect on the chemical shifts of similar protons of different isomers, the peaks were assigned as though only a single isomer was present (for example, there are technically 3 different aminomethyl groups in the diaminomethylation products, but all of the methyl groups show up as a singlet, and are labeled as such).

The amount of dimethylferrocene substitution on the polymer was determined by NMR in a similar method as described previously:[23] The integral of the area under

the peaks for the dimethylferrocene methyl hydrogens at ca. δ 1.5 – 2.0 was set as 12, and the remaining peaks were integrated relatively. In a normal repeat unit, (-$CH_2CH_2$-NH-), the polymer backbone has four non-exchanging hydrogens, and the hydrogens in the first methylene group that is attached to the dimethylferrocene tether have a similar chemical shift to the backbone hydrogens. Therefore, Equation 6.01 can be used to evaluate the substitution percentage.

**Equation 6.01**: $FcMe_2$-$C_4$-LPEI percent substitution = $\frac{4}{backbone\ hydrogen\ integration-2}\ x\ 100$

## References


1. Arimoto, F. S.; Jr., A. C. H., *J. Am. Chem. Soc.* **1955,** *77*, 6295.

2. Britton, W. E.; Kashyap, R.; El-Hashash, M.; El-Kady, M., *Organometallics* **1986,** *5*, 1029-1031.

3. Kasper, M.; Sattler, K.; Siegmann, K.; Matter, U.; Siegmann, H. C., *J. Aerosol Sci.* **1999,** *30*, 217-225.

4. Schechter, B.; Caldwell, G.; Neuse, E. W., *J. Inorg. Organomet. Polym.* **2000,** *10* (4), 177.

5. Fujimoto, K.; Kawai, H.; Amano, M.; Inouye, M., *J. Org. Chem.* **2008,** *73* (13), 5123-5126.

6. Atkinson, R. C. J.; Long, N. J., Monodentate Ferrocene Donor Ligands. In *Ferrocenes: Ligands, Materials and Biomolecules*, Stepnicka, P., Ed. John Wiley and Sons, Ltd.: 2008.

7. Adman, E.; Rosenblum, M.; Sullivan, S.; Margulis, T. N., *J. Am. Chem. Soc.* **1967**, 4540.

8. Tatistcheff, H. B.; Hancock, L. F.; Wrighton, M. S., *J. Phys. Chem.* **1995,** *99*, 7689-7693.

9. Byrne, P. D.; Mller, P.; Swager, T. M., *Langmuir* **2006,** *22* (25), 10596-10604.

10. Gallei, M.; Schmidt, B. V. K. J.; Klein, R.; Rehahn, M., *Macromol. Rapid Commun.* **2009,** *30*, 1463-1469.

11. Sulak, M. T.; Gokdogan, O.; Gulce, A.; Gulce, H., *Biosens. Bioelectron.* **2006,** *21* (9), 1719-1726.

12. Gulce, A.; Gulce, H., *J. Biochem. Biophys. Methods* **2005,** *62* (1), 81-92.

13. Chuang, C. L.; Wang, Y. J.; Lan, H. L., *Anal. Chim. Acta* **1997,** *353* (1), 37-44.

14. Giampietro, O., *Clinical Chemistry* **1982,** *28* (12), 2405-2407.

15. Bunte, C.; Ruhe, J., *Macromol. Rapid Commun.* **2009,** *30*, 1817-1822.

16. Losada, J.; Zamora, M.; Armada, P. G.; Cuadrado, I.; Alonso, B.; Casado, C. M., *Anal. Bioanal. Chem.* **2006,** *385* (7), 1209-1217.

17. Patel, H.; Li, X.; Karan, H. I., *Biosens. Bioelectron.* **2003,** *18* (8), 1073-1076.

18. Heller, A.; Feldman, B., *Chem. Rev. (Washington, DC, U. S.)* **2008,** *108* (7), 2482-2505.

19. Heller, A., *Curr. Opin. Chem. Biol.* **2006,** *10* (6), 664-672.

20. Willner, I.; Yan, Y. M.; Willner, B.; Tel-Vered, R., *Fuel Cells* **2009,** *9* (1), 7-24.

21. Galloway, J. W.; Barton, S. C., *J. Am. Chem. Soc.* **2008,** *130*, 8527.

22. Higson, P. J.; Davis, F., *Biosens. Bioelectron.* **2007,** *22*, 1224-1235.

23. Merchant, S.; Meredith, M. T.; Tran, T. O.; Brunski, D.; Johnson, M. B.; Glatzhofer, D. T.; Schmidtke, D. W., *J. Phys. Chem. C,* **2010,** *114,* 11627-11634.

24. Merchant, S.; Tran, T. O.; Meredith, M. T.; Cline, T. C.; Glatzhofer, D. T.; Schmidtke, D. W., *Langmuir* **2009,** *25* (13), 7736-7742.

25. Merchant, S.; Glatzhofer, D. T.; Schmidtke, D. W., *Langmuir* **2007,** *23*, 11295.

26. Meredith, M. T.; Glatzhofer, D.; Kao, D.-Y.; Schmidtke, D. W.; Hickey, D., *J. Electrochem. Soc.* **2010,** *Submitted*.

27. Fomin, V. M.; Markin, A. V., *J. Therm. Anal. Calorim.* **2008,** *92*, 985-987.

28. Bashkin, J. K.; Kinlen, P. J., *Inorg. Chem.* **1990,** *29* (22), 4507-4509.

29. Prins, R.; Korswagen, A. R.; Kortbeek, A. G. T. G., *J. Organomet. Chem.* **1972**, 335-344.

30. Mao, F.; Mano, N.; Heller, A., *J. Am. Chem. Soc.* **2003,** *125* (16), 4951-4957.

31. Mano, N.; Mao, F.; Heller, A., *ChemBioChem* **2004,** *5*, 1703-1705.

32. Mano, N.; Mao, F.; Shin, W.; Chena, T.; Heller, A., *Chem. Commun. (Cambridge, U. K.)* **2003**, 518-519.

33. Reynolds, L. T.; Wilkinson, G., *J. Inorg. Nucl. Chem.* **1959,** *9* (1), 86-92.

34. Hoh, G. L.; Kleinberg, J.; Mcewen, W. E., *J. Am. Chem. Soc.* **1961,** *83* (19), 3949

35. Kuwana, T.; Bublitz, D. E.; Hoh, G., *J. Am. Chem. Soc.* **1960,** *82* (22), 5811-5817.

36. Hradsky, A.; Bildstein, B.; Schuler, N.; Schottenberger, H.; Jaitner, P.; Ongania, K. H.; Wurst, K.; Launay, J. P., *Organometallics* **1997,** *16* (3), 392-402.

37. Ryabov, A. D.; Amon, A.; Gorbatova, R. K.; Ryabova, E. S.; Gnedenko, B. B., *J. Phys. Chem.* **1995,** *99* (38), 14072-14077.

38. Miller, L. L.; Valentine, J. R., *J. Am. Chem. Soc.* **1988**, 3982.

39. Hobi, M.; Ruppert, O.; Gramlich, V.; Togni, A., *Organometallics* **1997,** *16*, 1384-1391.

40. Zou, C.; Wrighton, M. S., *J. Am. Chem. Soc.* **1990,** *112*, 7578-7584.

41. Pauson, P. L.; Sandhu, M. A.; Watts, W. E.; Haley, R. C.; Knox, G. R., *J. Chem. Soc. C* **1967,** (19), 1851

42. Bhattacharyya, S., *J. Chem. Soc., Perk. Trans. 1* **1996**, 1381-1382.

43. Navarro, A.-E.; Spinelli, N.; Moustrou, C.; Chaix, C.; Mandrand, B.; Brisset, H., *Nucleic Acids Res.* **2004,** *32* (17), 5310.

44. Gnoatto, S. C. B.; Dassonville-Klimpt, A.; Nascimento, S. D.; Galera, P.; Boumediene, K.; Gosmann, G.; Sonnet, P.; Moslemi, S., *Eur. J. Med. Chem.* **2008,** *43*, 1865.

45. Debroy, P.; Naskar, D.; Roy, S., *Inorganica Chemica Acta* **2006,** *359*, 1215-1221.

46. El-Batta, A.; Jiang, C.; Zhao, W.; Anness, R.; Cooksy, A. L.; Bergdahl, M., *J. Org. Chem.* **2007,** *72*, 5244-5259.

47. Fukuzawa, S.; Fujinami, T.; Yamauchi, S.; Sakai, S., *J. Chem Soc. Perkin Trans. 1* **1986**, 1929-1932.

48. Lapic, J.; Rapic, V., *Croat. Chem. Acta* **2000,** *73* (3), 755-771.

49. Bunte, C.; Prucker, O.; Konig, T.; Ruhe, J., *Langmuir* **2010,** *26* (8), 6019-6027.

50. Andrieux, C. P.; Audebert, P.; Bacchi, P.; Divisiablohorn, B., *J. Electroanal. Chem.* **1995,** *394* (1-2), 141-148.

51. Araminaite, R.; Garjonyte, R.; Malinauskas, A., *Central European Journal of Chemistry* **2009,** *7* (4), 739-744.

52. Raoof, J. B.; Ojani, R.; Kiani, A., *J. Electroanal. Chem.* **2001,** *515* (1-2), 45-51.

53. Liu, A. H.; Anzai, J., *Anal. Bioanal. Chem.* **2004,** *380* (1), 98-103.

54. Barton, S. C.; Kim, H.-H.; Binyamin, G.; Zhang, Y.; Heller, A., *J. Phys. Chem. B* **2001,** *105*, 11917-11921.

55. Barton, S. C.; Kim, H.-H.; Binyamin, G.; Zhang, Y.; Heller, A., *J. Am. Chem. Soc.* **2001,** *123*, 5802-5803.

56. Bard, A. J., *Electrochemical Methods: Fundamentals and Applications*. 2nd ed.; Wiley: 2000.

57. Mano, N.; Kim, H.-H.; Heller, A., *J. Phys. Chem. B* **2002,** *106*, 8842-8848.

58. Leech, D., *Electrochim. Acta* **2006,** *51*, 5187-5192.

59. Tsujimura, S.; Kano, K.; Ikeda, T., *Electrochemistry* **2002,** *70*, 940.

60. Gregg, B. A.; Heller, A., *Anal. Chem.* **1990,** *62* (3), 258-263.

61. Joshi, P. P.; Merchant, S. A.; Wang, Y.; Schmidtke, D. W., *Anal. Chem.* **2005,** *77*, 3183-3188.

62. Sato, M.; Kono, H.; Shiga, M.; Motoyama, I.; Hata, K., *Bull. Chem. Soc. of Jpn.* **1967,** *41* (1), 252.

63. Routaboul, L.; Chiffre, J.; Balavoine, G. G. A.; Jean-Claude Daran; Manoury, E., *J. Organomet. Chem.* **2001,** *637-639*, 364.

# CHAPTER 7: CONCLUSIONS AND RECCOMENDATIONS FOR FUTURE WORK

## *Conclusions*

The contents of this work describe the synthesis of a series of redox polymers based on linear poly(ethylenimine) (LPEI) and ferrocene, and their application as mediators in amperometric glucose biosensors and biofuel cells. Glucose biosensors constructed with these polymers produced current densities higher than any other known sensor made with glucose oxidase (GOx) and ferrocene (or any other mediator), suggesting that LPEI could have properties which make it an ideal polymer for enzyme immobilization (especially with GOx). These studies have shown that the structures of the ferrocene-modified LPEI polymers play an important role in their (bio)electrochemical behavior, and that methylation of the ferrocene moieties which are attached to the LPEI backbone can lower the redox potential of the polymers in a predictable manner.

An alternate synthesis of the first polymer described in this work, Fc-$C_1$-LPEI, was developed which allowed for exact tuning of the substitution of ferrocene on the polymer. A series of Fc-$C_1$-LPEI polymers with ferrocene substitution percentages between 1% and 100% was synthesized and it was determined that the 20% substituted polymer gave the highest limiting current densities for glucose sensors made with Fc-$C_1$-LPEI. In addition, the novel solution electrochemistry of these polymers was investigated and could have promise as an indicator of poly-amine protonation behavior.

Next, a tether optimization study was carried out. It was shown that the distance between the ferrocene moieties and the polymer backbone is an important variable which can have a large effect on the properties of the polymers. A six-carbon tether proved to increase the stability of the redox polymers significantly, while lowering the enzymatic response to glucose. A three-carbon tether increased the stability of the films similar to the six-carbon tether and glucose biosensors made with Fc-$C_3$-LPEI produced high current densities in the range of 1 mA/cm$^2$, indicating that three carbons is the optimal spacer length. The polymers made with three different spacers (1, 3, and 6 carbons) had surprisingly similar electron diffusion coefficients, suggesting that electron diffusion rates do not necessarily correlate with high biosensor current densities. The films with the longer spacers did not swell as much as the 1-carbon spacer films, suggesting that the tether length can have a significant effect on the physical properties of the films as well.

The use of dimethylferrocene in place of ferrocene ($FcMe_2$-$C_3$-LPEI) was shown to lower the redox potential of the polymers by ~ 90 mV (as predicted) and also increased the electrochemical and operational stabilities of cross-linked films of the polymers. A compartment-less biofuel cell was constructed using $FcMe_2$-$C_3$-LPEI as the anodic redox polymer and the cathode was a mediated laccase bioelectrode. When the performance of this biofuel cell was compared to one using Fc-$C_3$-LPEI as the anodic polymer, the $FcMe_2$-$C_3$-LPEI was shown to be a superior anodic mediator due to its lower redox potential and higher stability. Coupling of the anodes to rotating biocathodes showed that the main factor which limited the biofuel cell performance was the mass transport of $O_2$ to the biocathode surface.

To increase the biofuel cell power density further, a tetramethylated ferrocene derivative was synthesized and characterized. The tetramethylferrocene (as a mixture of isomers) was then modified with a three-carbon tether and attached to LPEI ($FcMe_4$-$C_3$-LPEI) . When this redox polymer was mixed with glucose oxidase, a precipitate was formed. However, the polymer/enzyme mixture was still able to be crosslinked into a redox hydrogel. The redox potential was again lowered by the predicted 90 mV, however, the performance of bioelectrodes made with $FcMe_4$-$C_3$-LPEI was lower than that of the previous $C_3$ polymers, indicating that the enzyme/polymer precipitate could have a detrimental effect on the morphology of the films. Despite the lesser performance, $FcMe_4$-$C_3$-LPEI was shown to be a better anodic material (relative to $FcMe_2$-$C_3$-LPEI) in a stationary compartment-less biofuel cell due to its lower redox potential. However, when the biocathodes were rotated, $FcMe_2$-$C_3$-LPEI anodes produced higher power densities due to their higher limiting current densities.

*Future Studies*

The possibilities for future studies involving these projects are virtually endless. There are many detailed fundamental studies which could be carried out as well as projects designed to increase the performance of biosensors and biofuel cells made with these materials.

Regarding the original polymer, Fc-$C_1$-LPEI, a study on how electron diffusion changes with increasing substitution percentage should show how electron diffusion correlates with the enzymatic response and this could reveal important information about the nature of the enzyme/polymer interaction as the amount of hydrophobic

ferrocene is increased on the hydrophilic polymer backbone. In addition, a full evaluation should be carried out to determine if Fc-$C_1$-LPEI(100%) is a reliable probe for the direct determination of polymer protonation.

The full mechanism by which these polymers degrade is still unclear. One obvious mechanism which likely occurs is the typical ferrocenium degradation by nucleophilic attack. However, the rapid degradation of Fc-$C_1$-LPEI is likely due to other mechanisms as well, including cleavage of the ferrocene group or some type of irreversible phosphate coordination. Also, all of the 3 and 6-carbon tether films revealed an extended "break-in" period in the electrochemical stability studies. The reason for this break-in is unknown, and the electrochemical cycling tests could be carried out under different pH conditions or in different buffers to determine if dibasic phosphate and/or film collapse is the cause of the extended break-in period.

Another fundamental study which could be useful is an investigation into how the LPEI stabilizes glucose oxidase (GOx). Polymer encapsulation of enzymes is known to increase the stability of enzymes, and this study could reveal yet another favorable property of LPEI and give further reason to broaden the scope of enzymes and mediators used with the polymer.

The full potential of $FcMe_4$-$C_3$-LPEI as a bioanode material has not been realized, possibly due to the precipitate which forms when the polymer is mixed with the enzyme. This precipitate could be due to a large number of oxidized tetramethylferrocenes on the polymer. Possible methods to avoid this interaction could include letting the polymer cross-link for a while before mixing in the enzyme, using different buffer solutions to dissolve the polymer and enzyme, using a reducing agent in

the mixture (glucose, $NaBH_4$, etc.), or gently heating the mixture. If this problem can be solved, the current densities produced with $FcMe_4$-$C_3$-LPEI bioanodes should be as high as those produced with the other $C_3$ polymers and would lead to much more powerful biofuel cells.

If the problems with the $FcMe_4$-$C_3$-LPEI bioanodes can be solved, further methylation of the ferrocene should be investigated as a means to lower the redox potential even further. Two (or four) more methyl groups should allow for a large increase in biofuel cell power and could also result in biosensors which have no ascorbate sensitivity.

Alternatively, other redox mediators for the bioanodes should be investigated as well. If the ability of LPEI to act as a scaffold for immobilization of GOx/mediators is general and does not require that ferrocene derivatives be used, many other redox mediators for the anode could be investigated. These could include lower potential osmium compounds, quinone derivatives, or metals such as copper or nickel.

Further development of the biocathode should also be pursued. Many possibilities exist for making a better biocathode, including using higher potential redox mediators such as ABTS, anthracene, or other osmium compounds. LPEI should be investigated as a scaffold for laccase immobilization using these mediators. Laccases also have the ability to directly transfer electrons to electrode surfaces because of the proximity of the T1 copper site to the surface of the enzyme. Attempts to utilize this property with LPEI as an immobilization scaffold should be investigated as well. One method by which this could be carried out would be to cross-link LPEI in the presence of laccase and a large concentration of carbon nanotubes or nanoparticles. The

development of this type of DET laccase cathode should lead to very high cell voltages due to the removal of any enzyme/mediator overpotential.

Another area which has not been fully investigated with the Fc-LPEI redox polymers is the use of other redox enzymes. Fc-$C_1$-LPEI was shown to work well as a mediator for horseradish peroxidase and preliminary studies (not discussed) showed that Fc-$C_3$-LPEI can effectively mediate electron transfer from laccase to the electrode surface as well. Many other redox enzymes could be investigated and multi-enzyme systems could be developed as well for more complete oxidation of biofuels.

Lastly, the use of nanomaterials to enhance the performance of the previously discussed biofuel cells is largely un-investigated. Some preliminary results (not discussed) showed that carbon nanotubes could significantly enhance the performance of $FcMe_4$-$C_3$-LPEI bioanodes to increase their room-temperature current densities to 1 $mA/cm^2$ (not discussed in this work). This would provide the boost in current needed to fully take advantage of their lower potential in a biofuel cell. $FcMe_4$-$C_3$-LPEI/GOx/CNT electrodes should be fully tested and characterized for use in biosensors and biofuel cells. In addition, any of the other redox polymers being used on the anode or cathode could be mixed with CNT's and tested for improved biofuel cell performance.

# APPENDIX A: $^{1}$H NMR SPECTRA

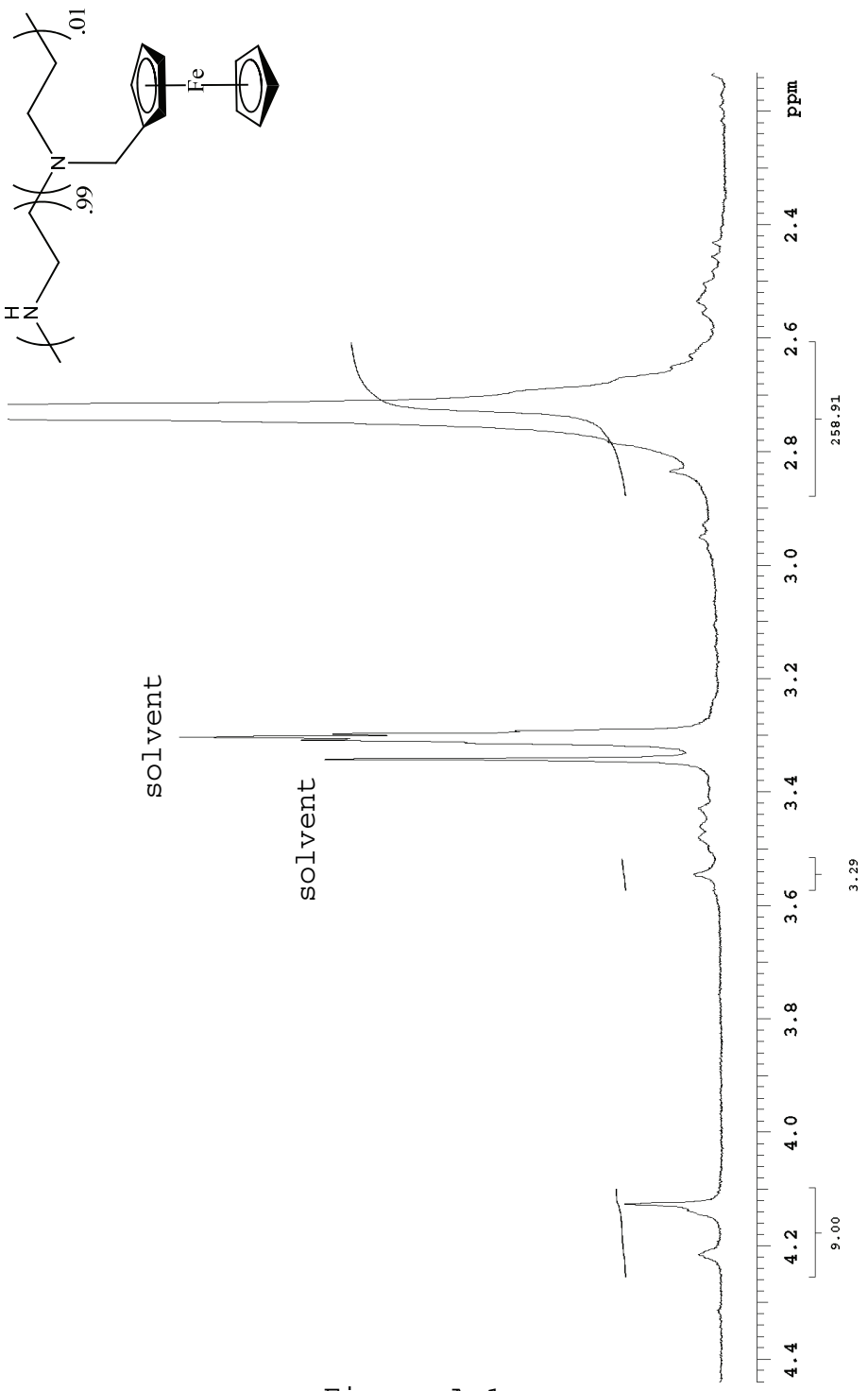


Figure A-1
$H^1$ NMR for Fc-$C_1$-LPEI(1%)

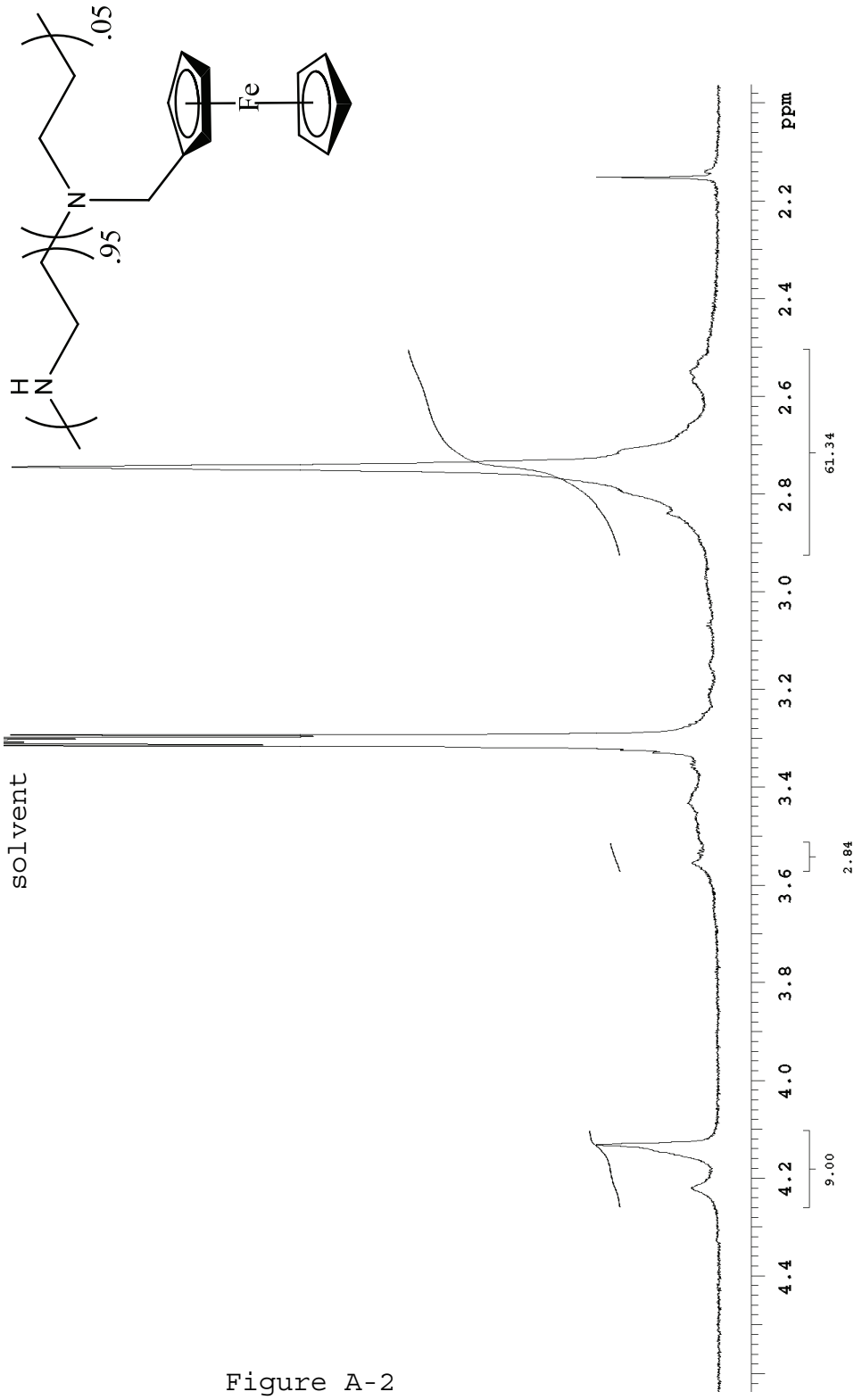


Figure A-2
$H^1$ NMR for Fc-$C_1$-LPEI(5%)

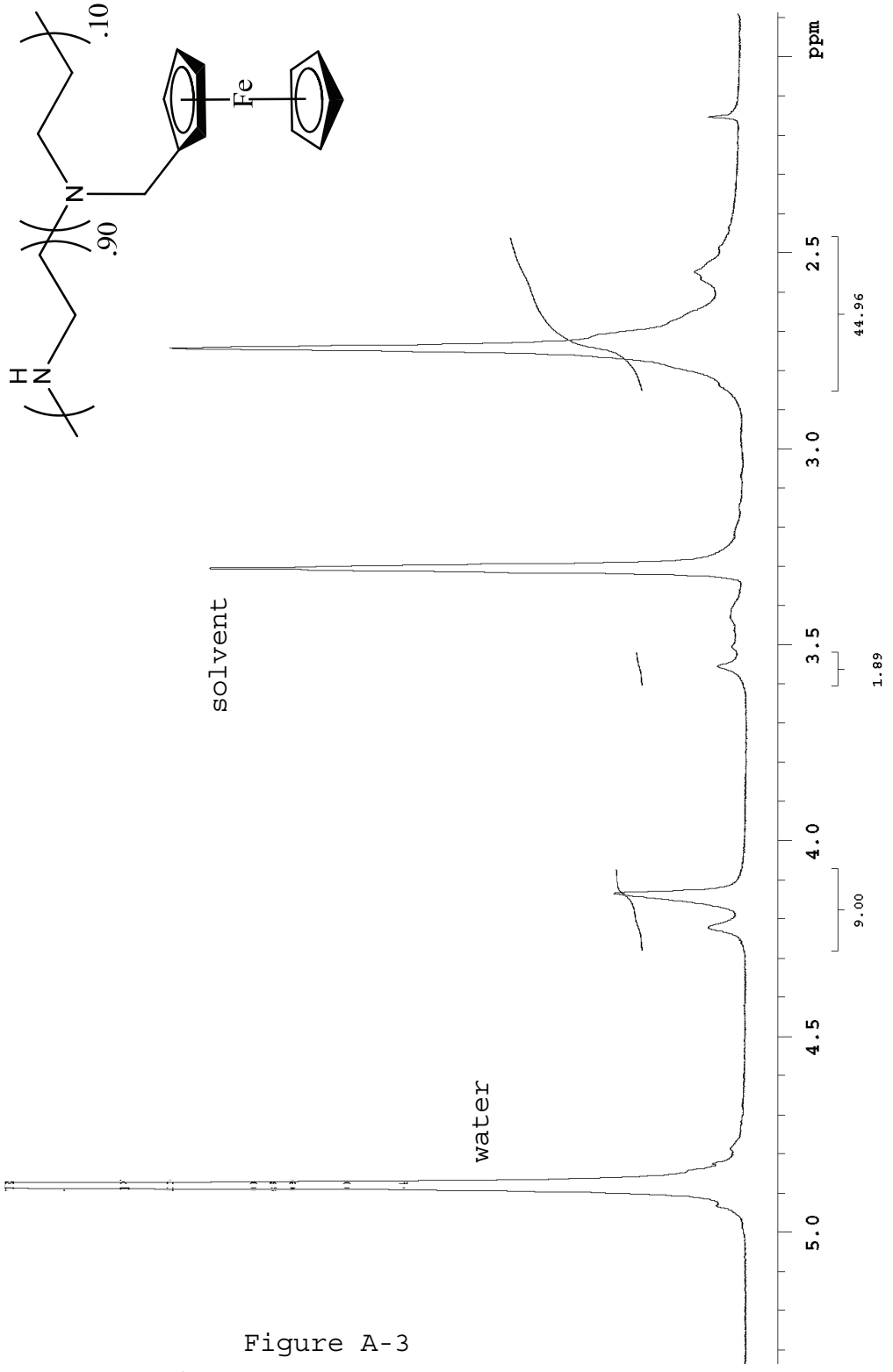


Figure A-3

$H^1$ NMR for Fc-$C_1$-LPEI(10%)

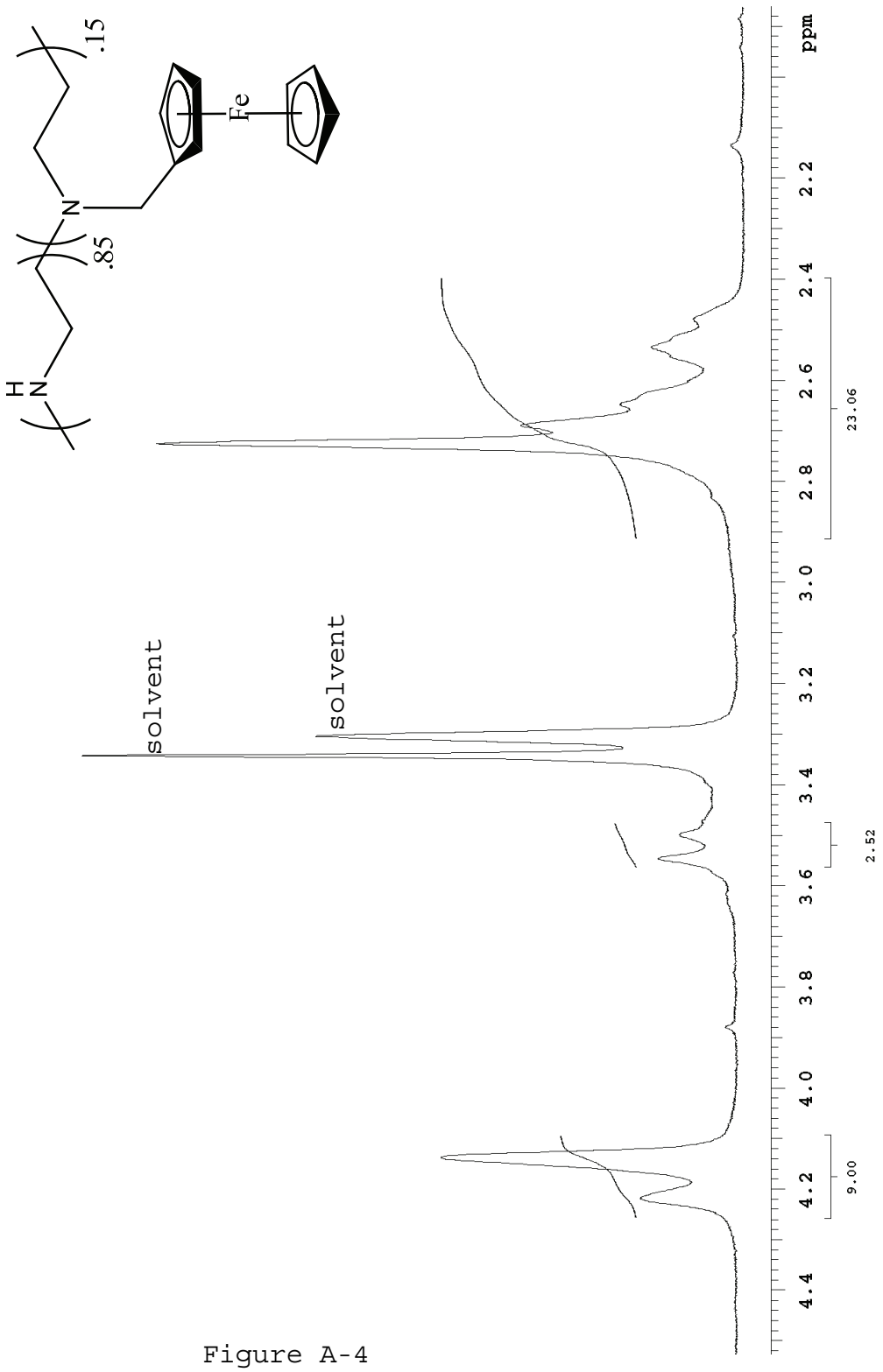


Figure A-4

$H^1$ NMR for Fc-$C_1$-LPEI(15%)

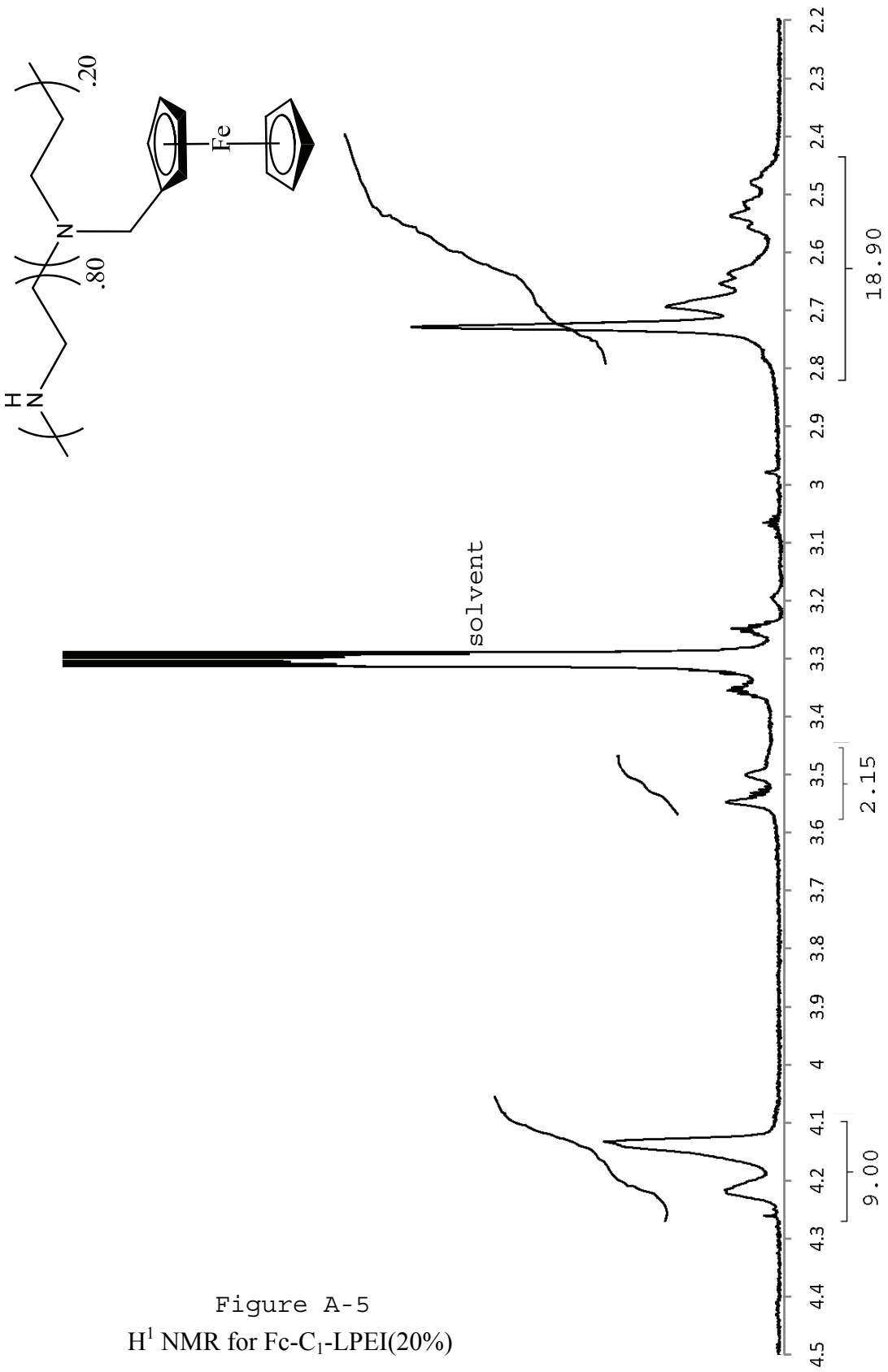


Figure A-5
$H^1$ NMR for Fc-$C_1$-LPEI(20%)

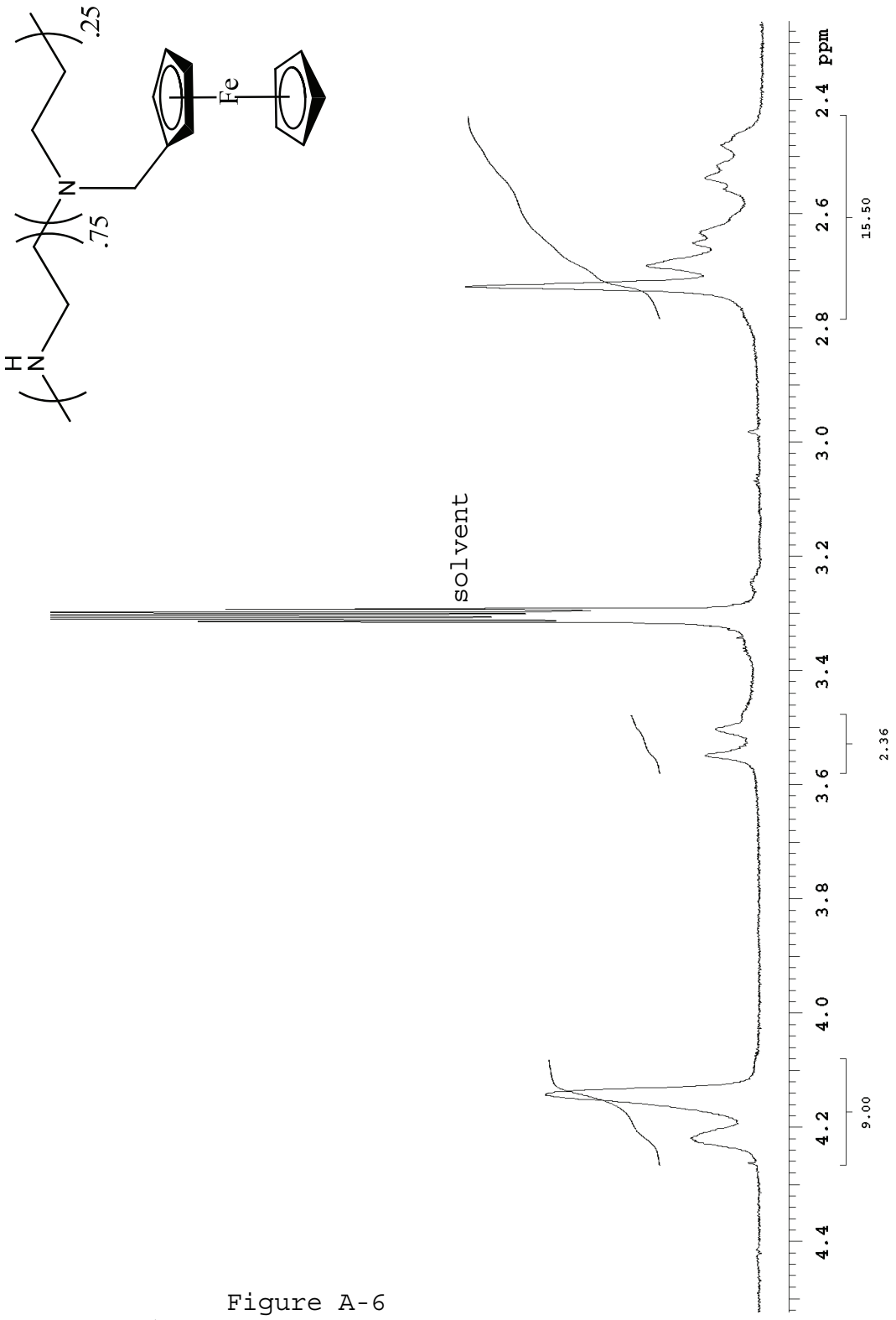


Figure A-6
$H^1$ NMR for Fc-$C_1$-LPEI(25%)

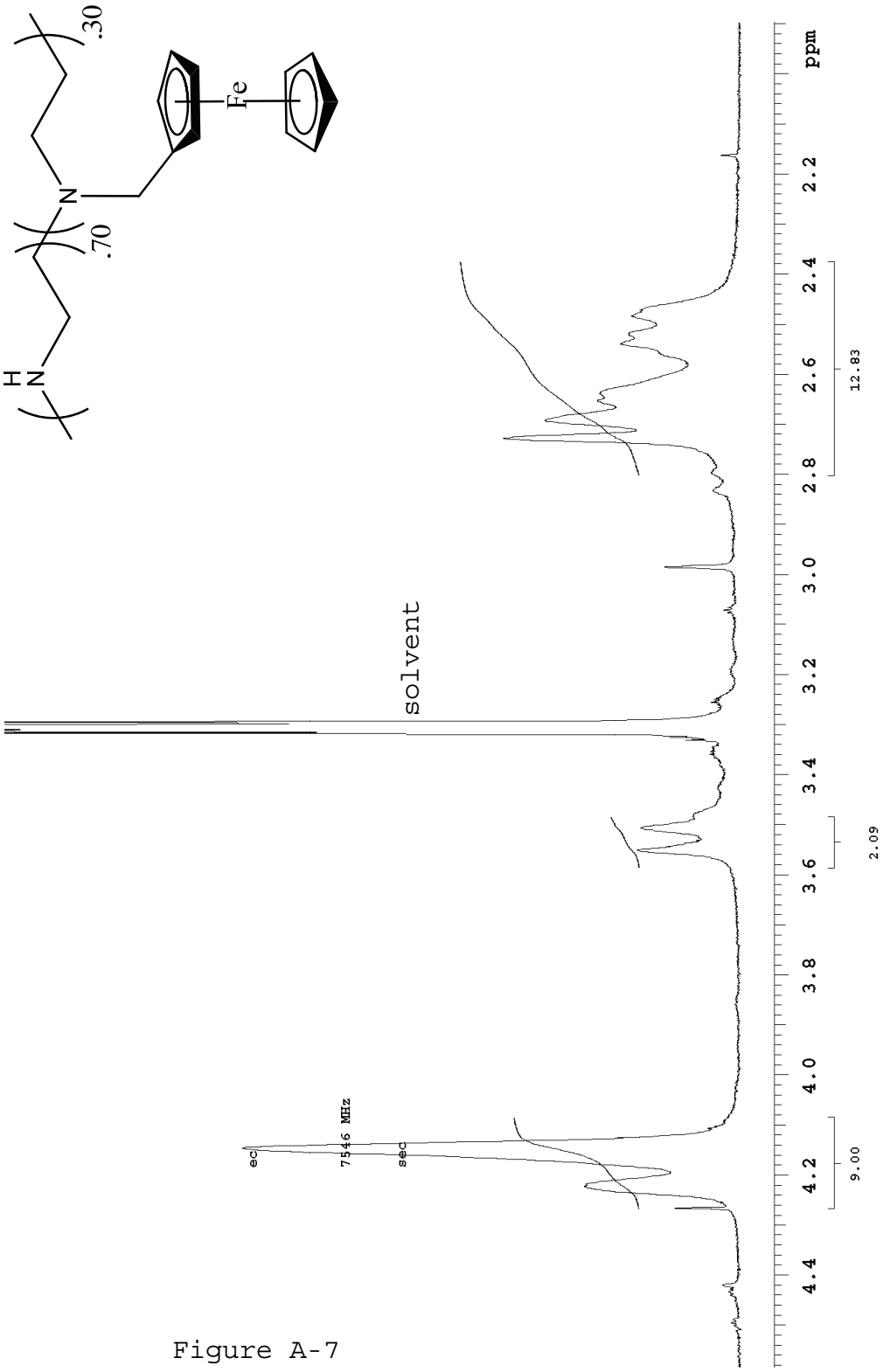


Figure A-7

$H^1$ NMR for Fc-$C_1$-LPEI(30%)

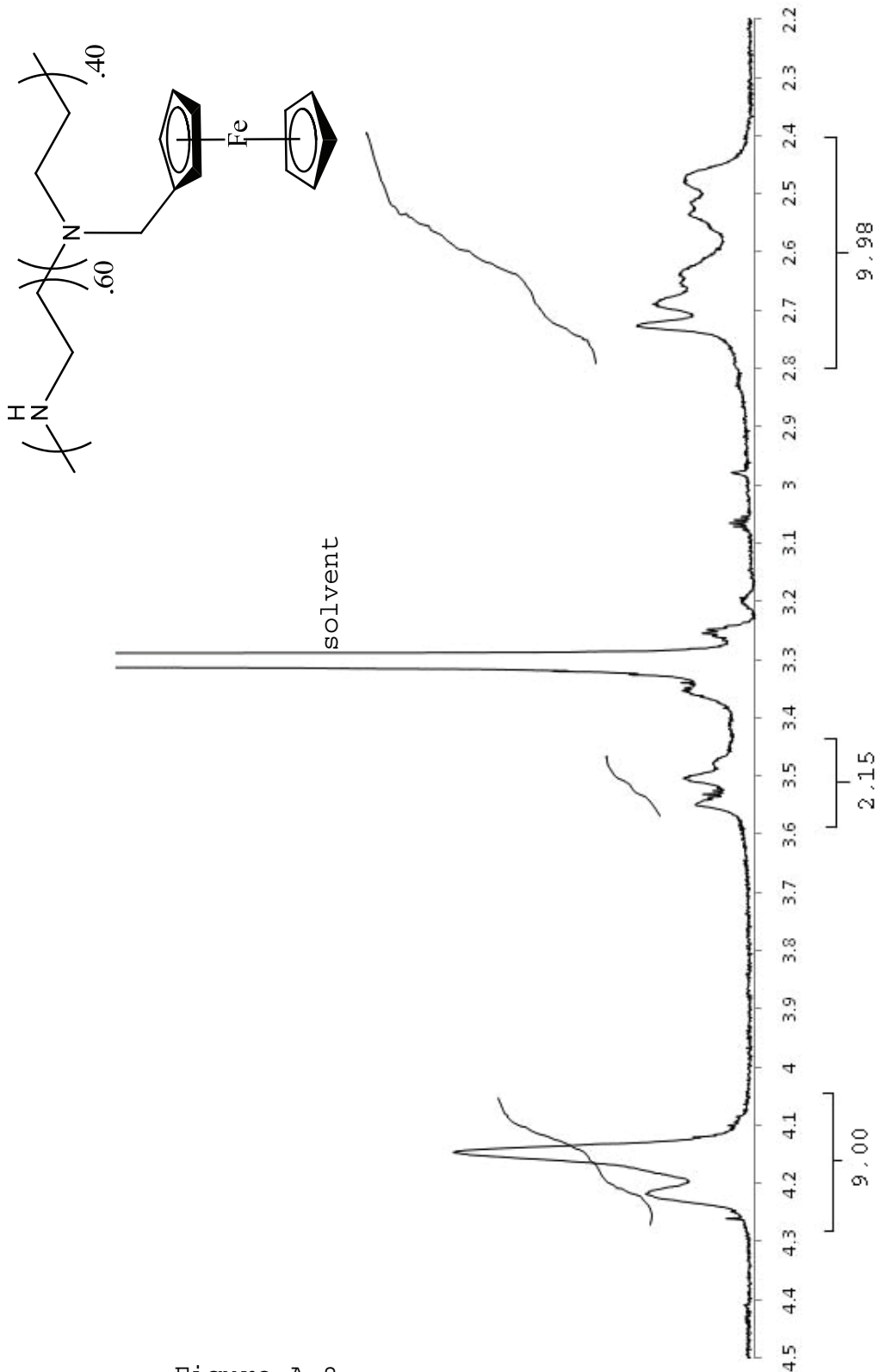


Figure A-8
$H^1$ NMR for Fc-$C_1$-LPEI(40%)

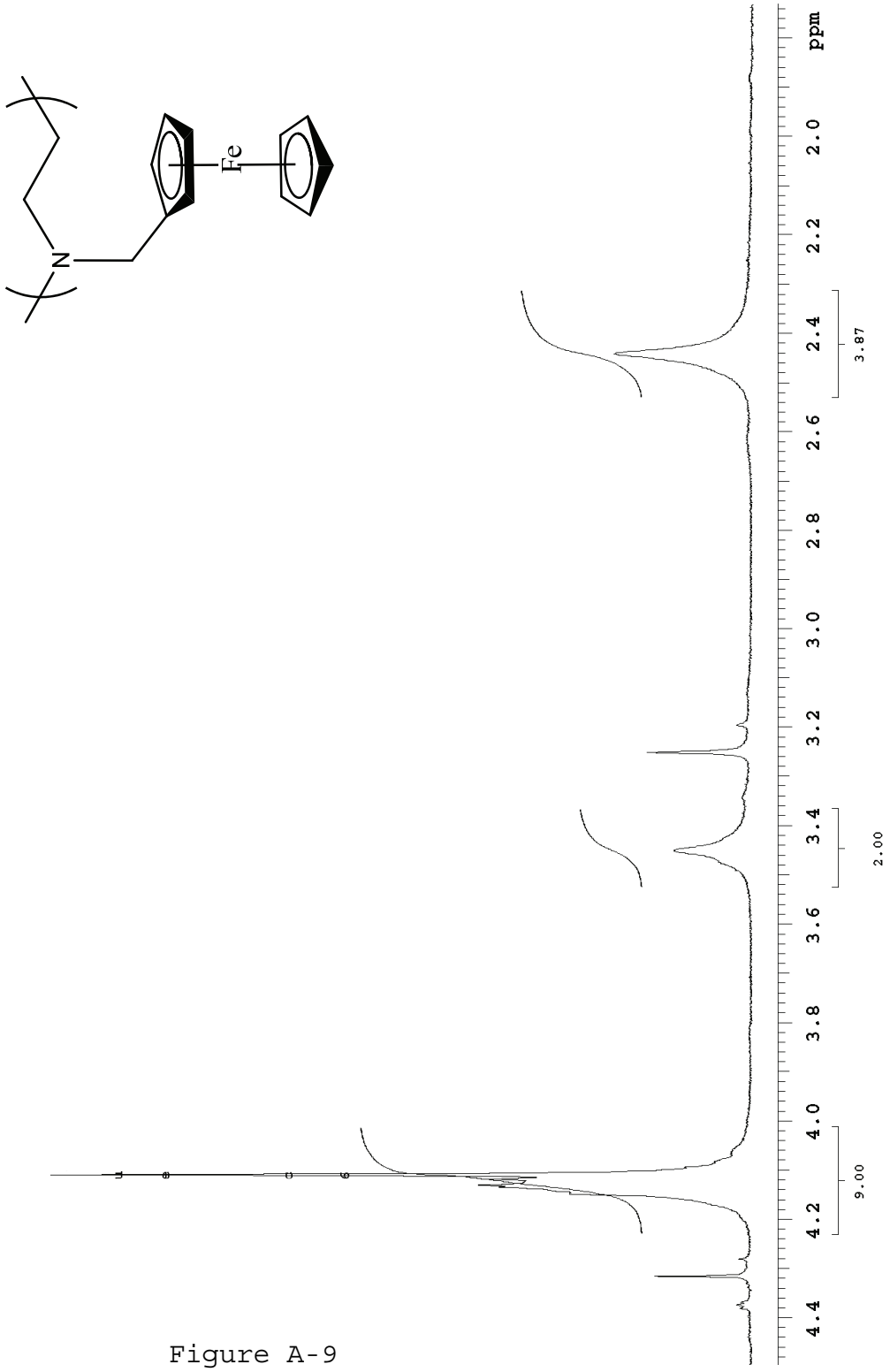


Figure A-9
$H^1$ NMR for Fc-$C_1$-LPEI(100%)

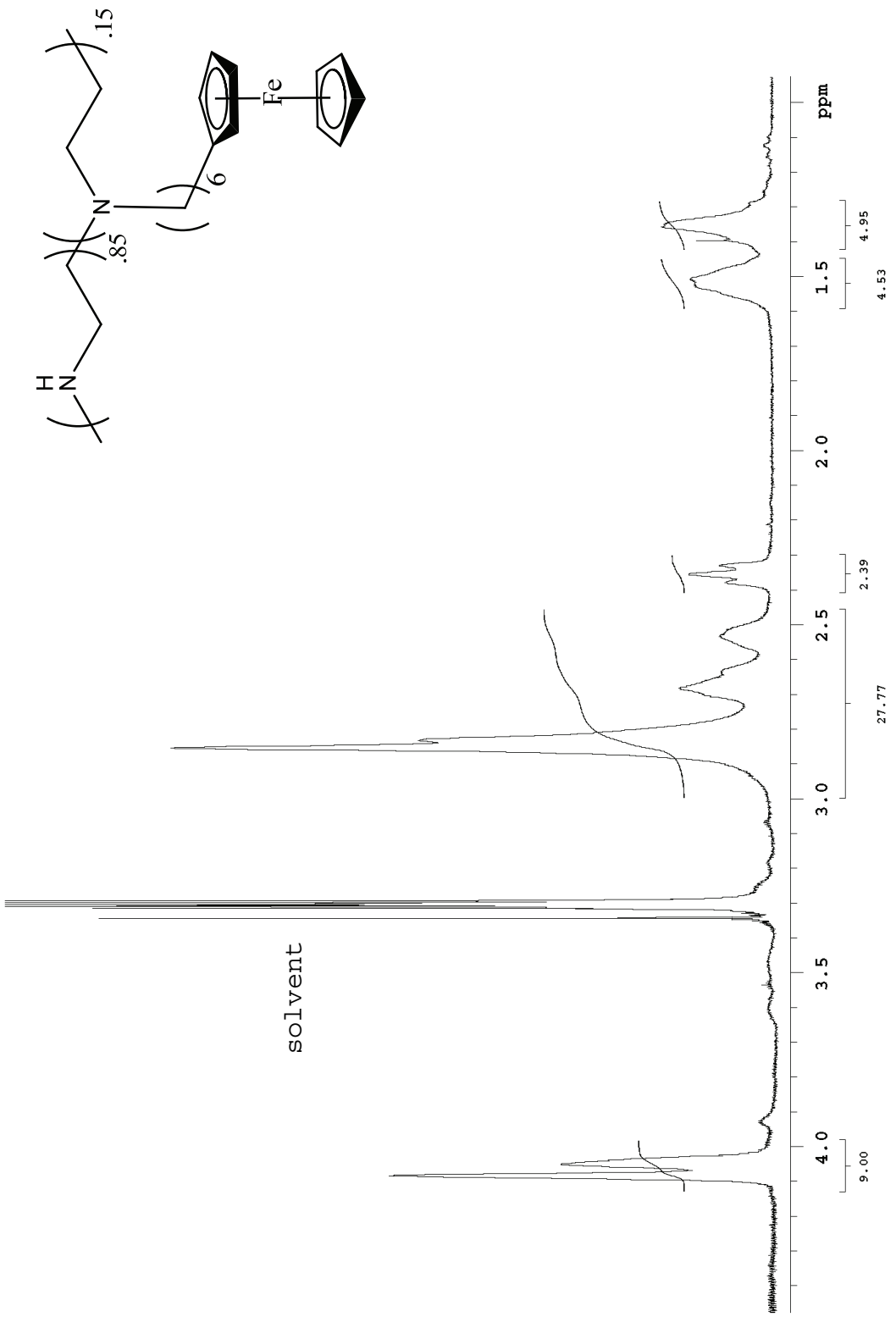


Figure A-10
$H^1$ NMR for Fc-$C_6$-LPEI

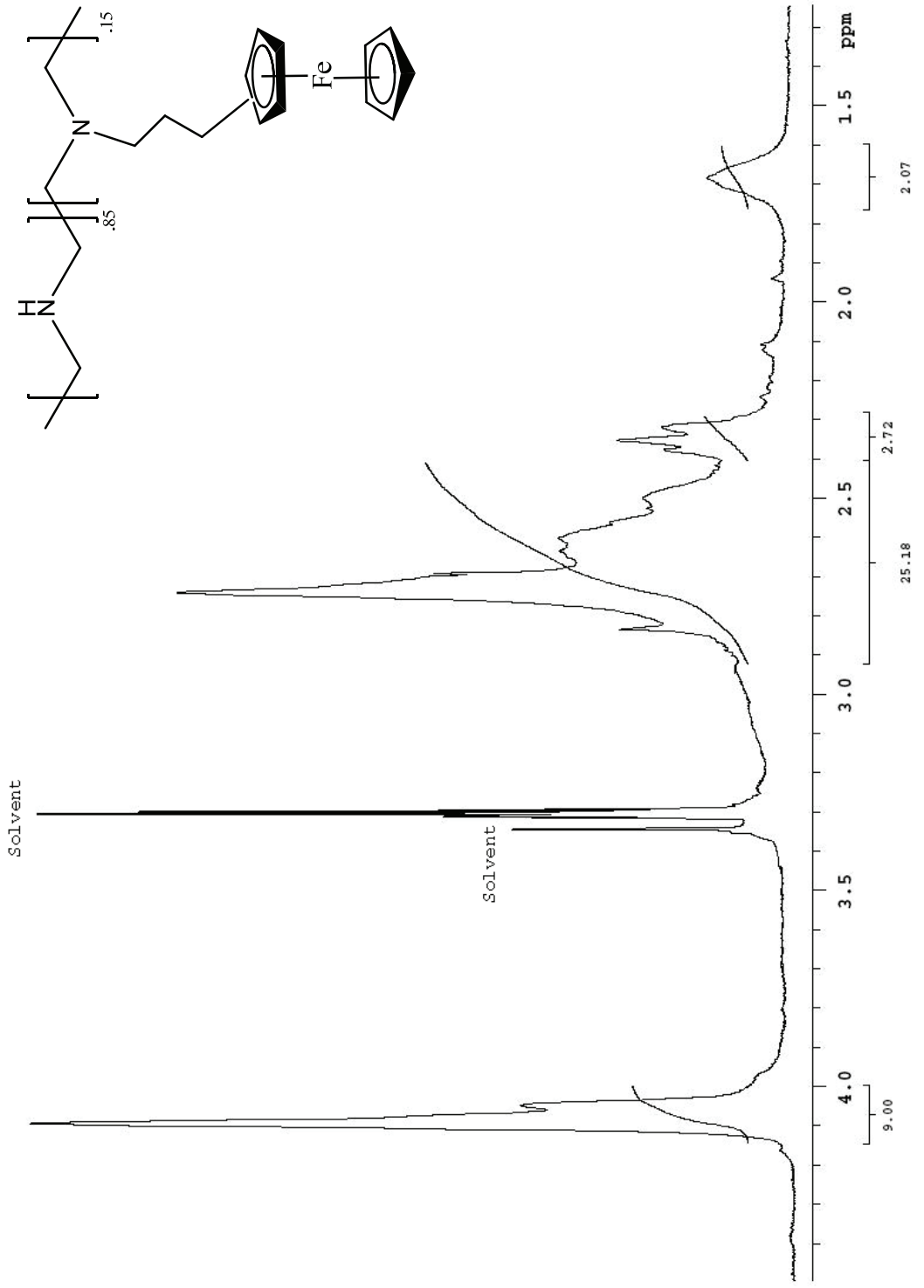


Figure A-11
$H^1$ NMR for Fc-$C_3$-LPEI

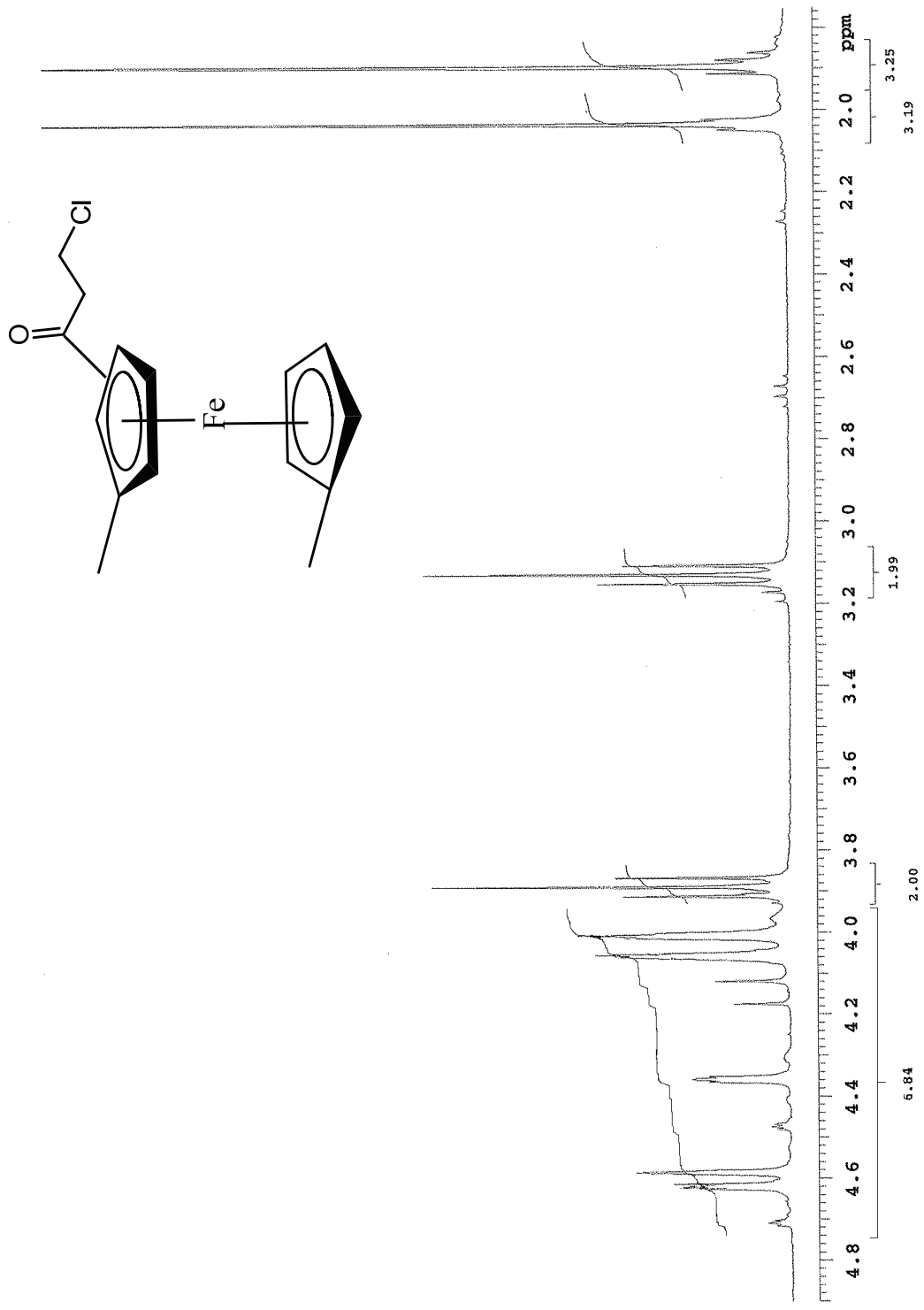


Figure A-12

$H^1$ NMR for mixture of 1-(3-chloropropionyl)-2,1'-dimethylferrocene and 1-(3-chloropropionyl)-3,1'-dimethylferrocene

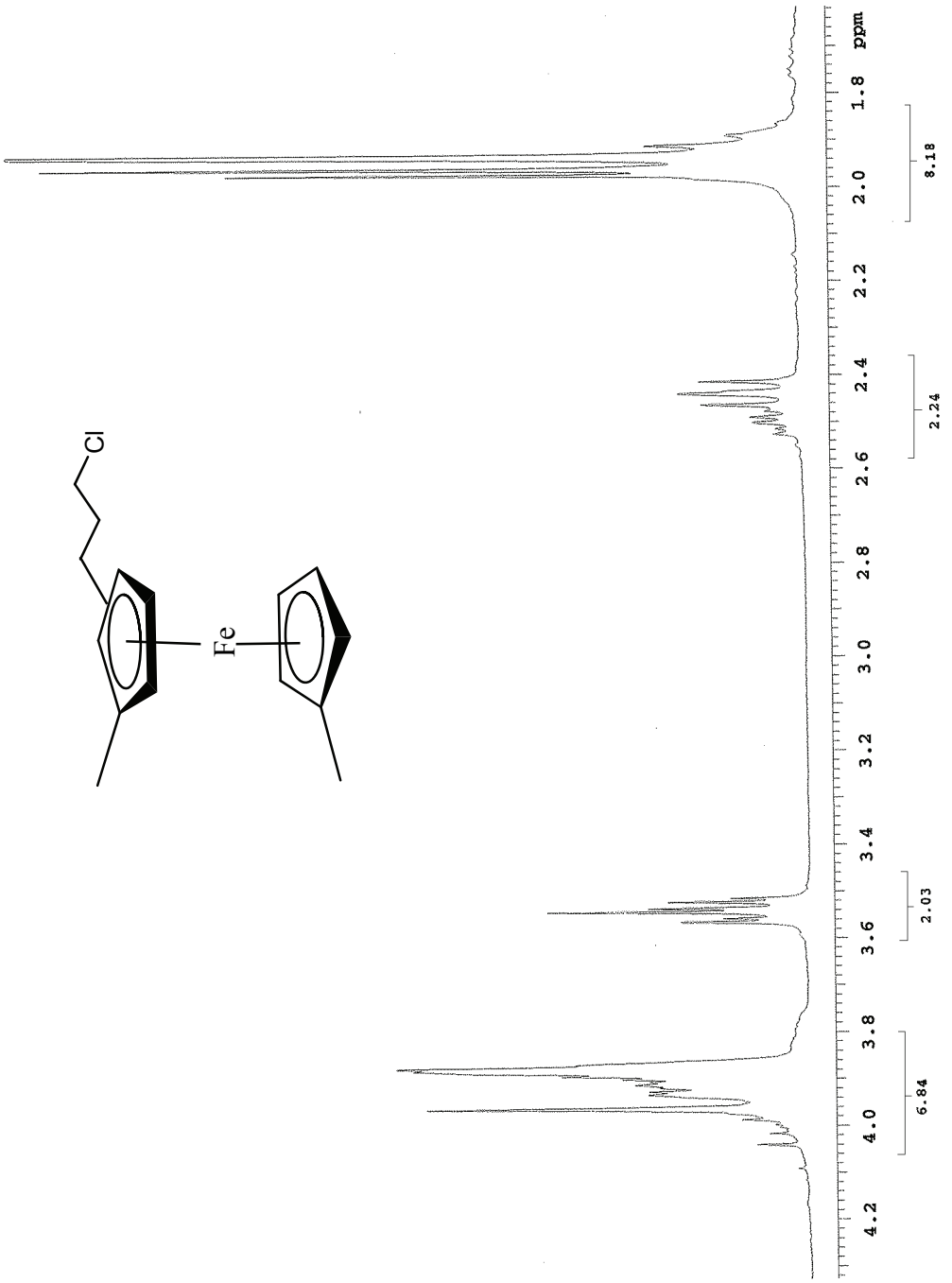


Figure A-13

$H^1$ NMR for mixture of 1-(3-chloropropyl)-2,1'-dimethylferrocene and 1-(3-chloropropyl)-3,1'-dimethylferrocene

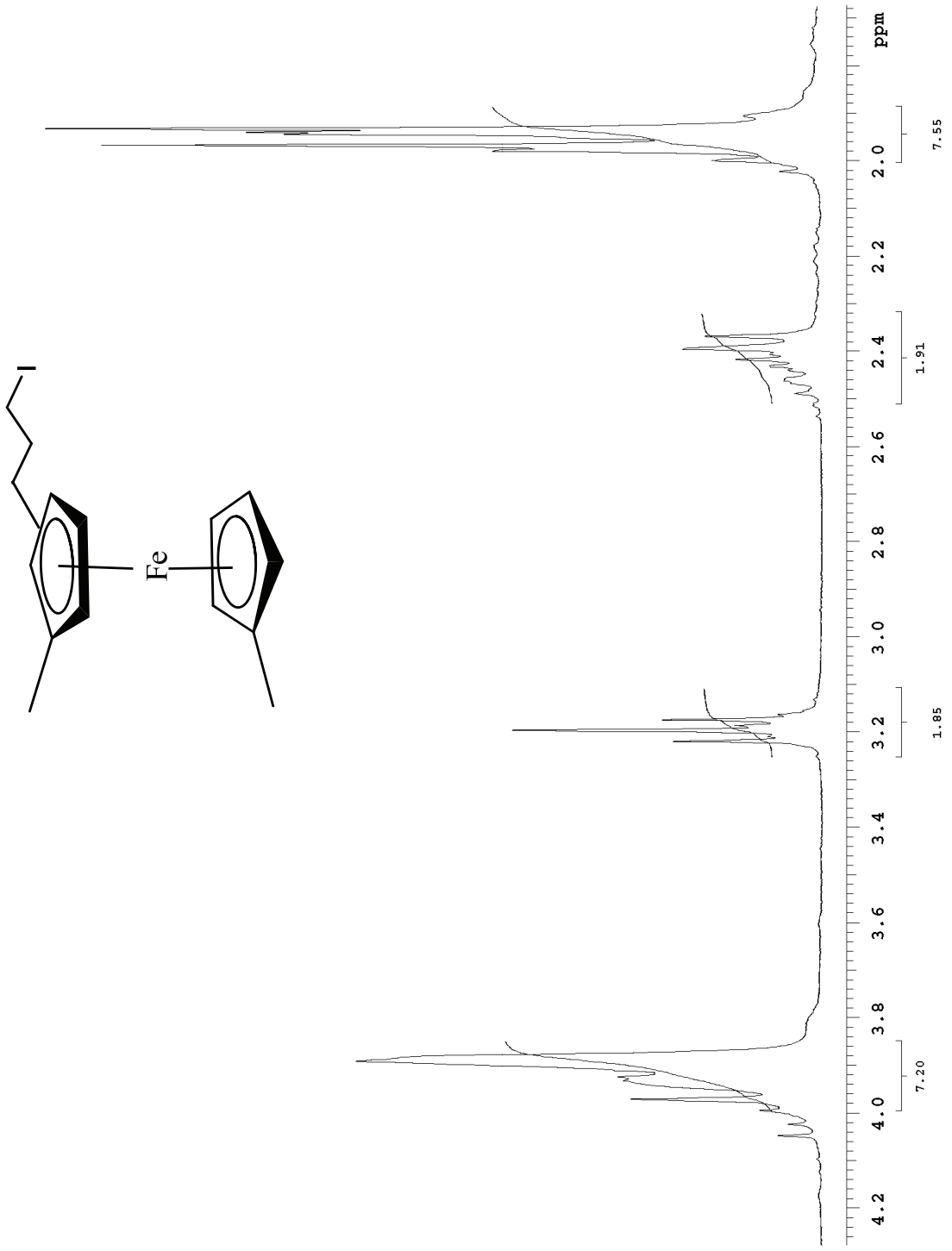


Figure A-14

$H^1$ NMR for mixture of 1-(3-iodopropyl)-2,1'-dimethylferrocene and 1-(3-iodopropyl)-3,1'-dimethylferrocene

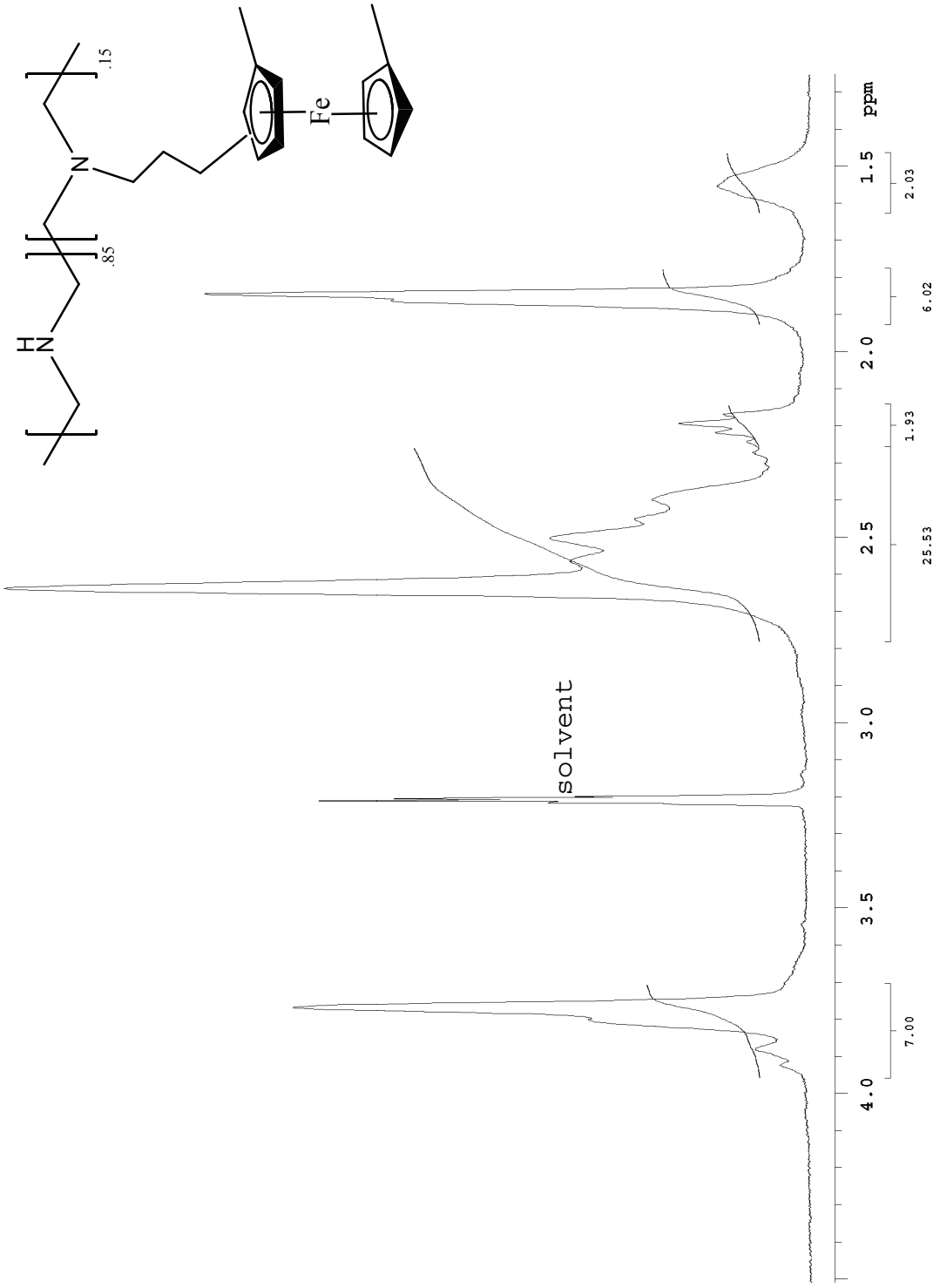


Figure A-15
$H^1$ NMR for $FcMe_2$-$C_3$-LPEI

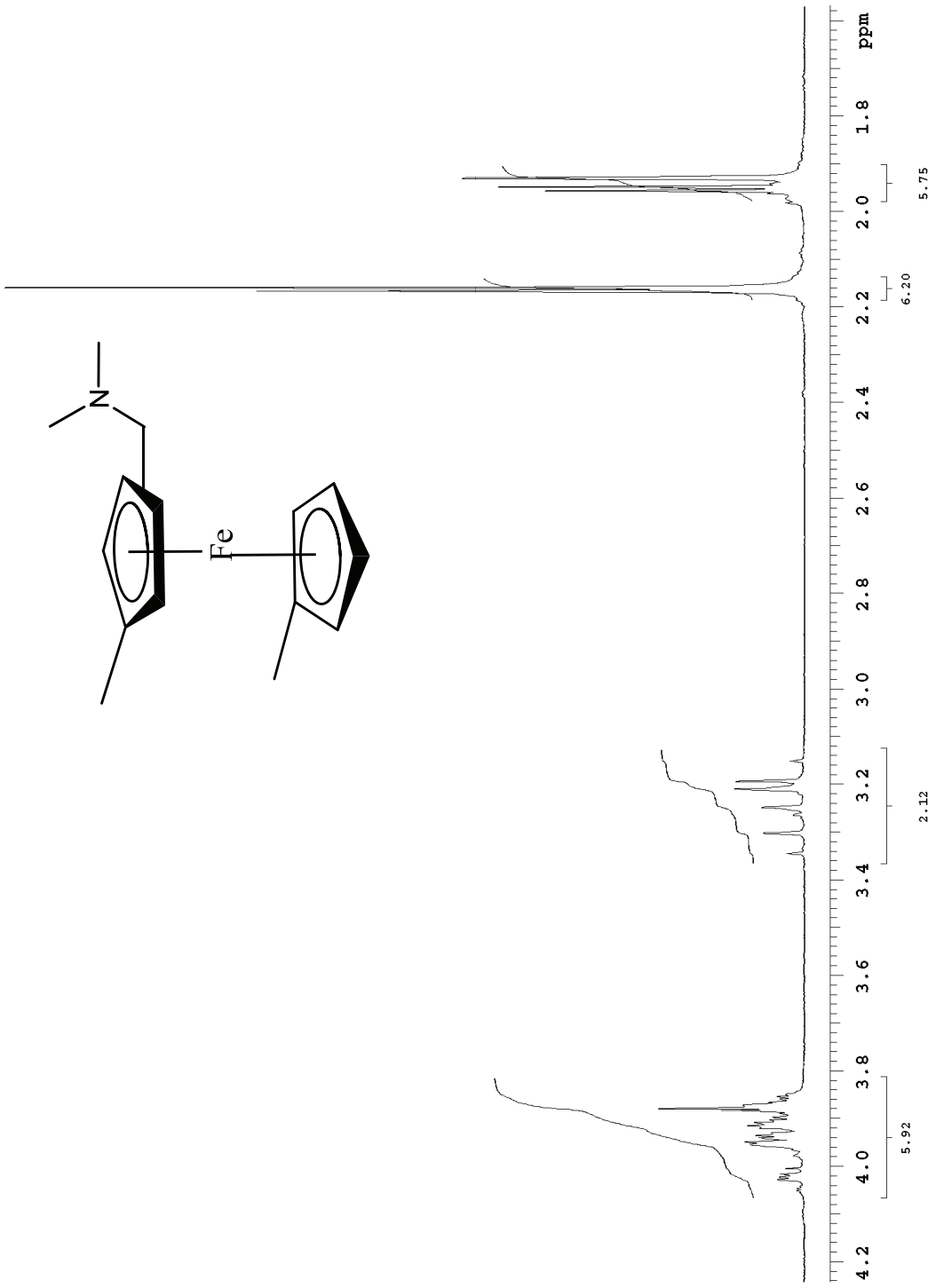


Figure A-16

$H^1$ NMR for compound **2,** a mixture of 1-dimethylaminomethyl-2,1'-dimethylferrocene and 1-dimethylaminomethyl-3,1'-dimethylferrocene

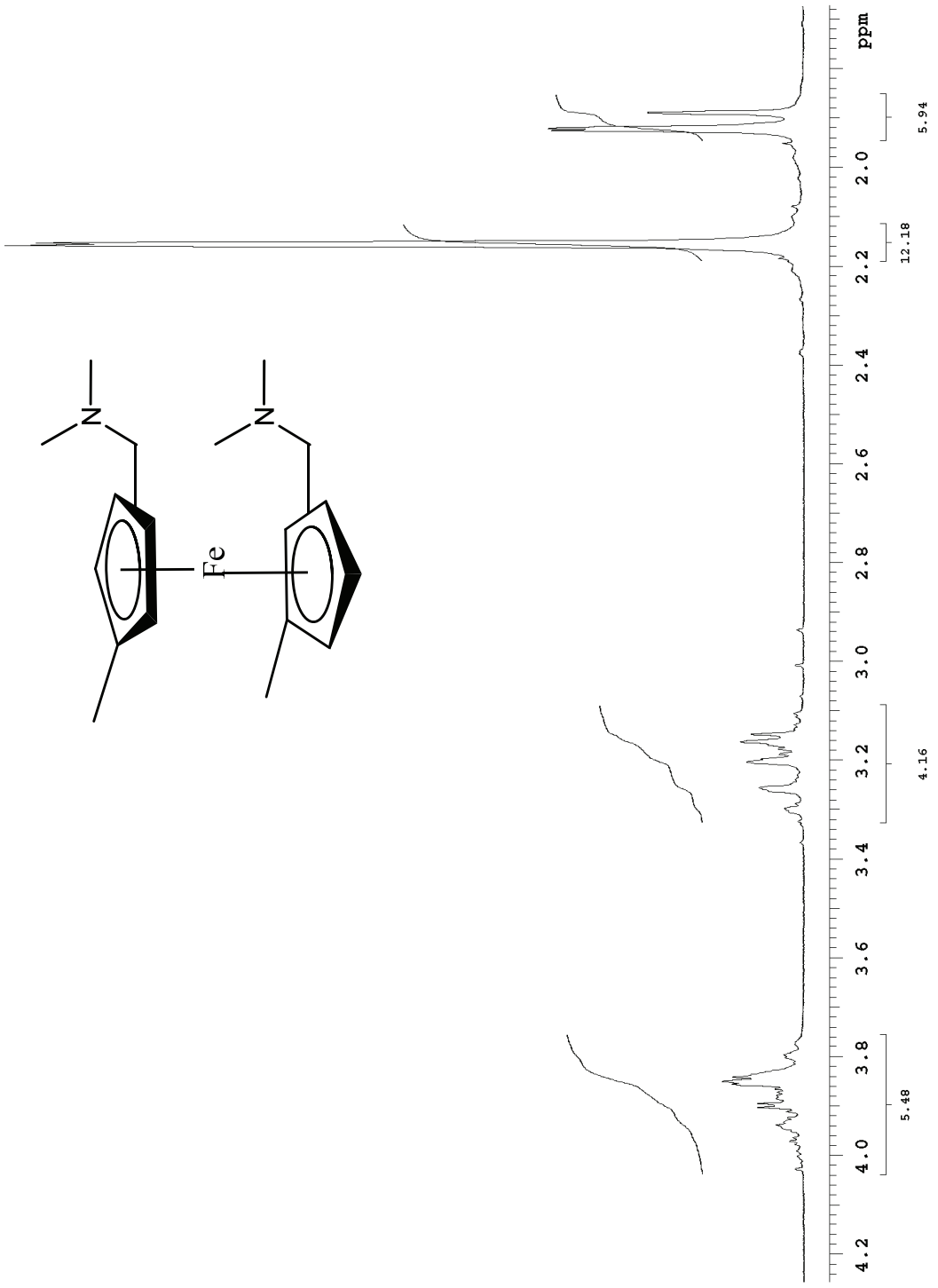


Figure A-17

$H^1$ NMR for compound **3**, a mixture of 1,1'-*Bis*-Dimethylaminomethyl-3,3'-dimethylferrocene, 1,1'-*Bis*-Dimethylaminomethyl-2,2'-dimethylferrocene, and 1,1'-*Bis*-Dimethylaminomethyl-2,3'-dimethylferrocene

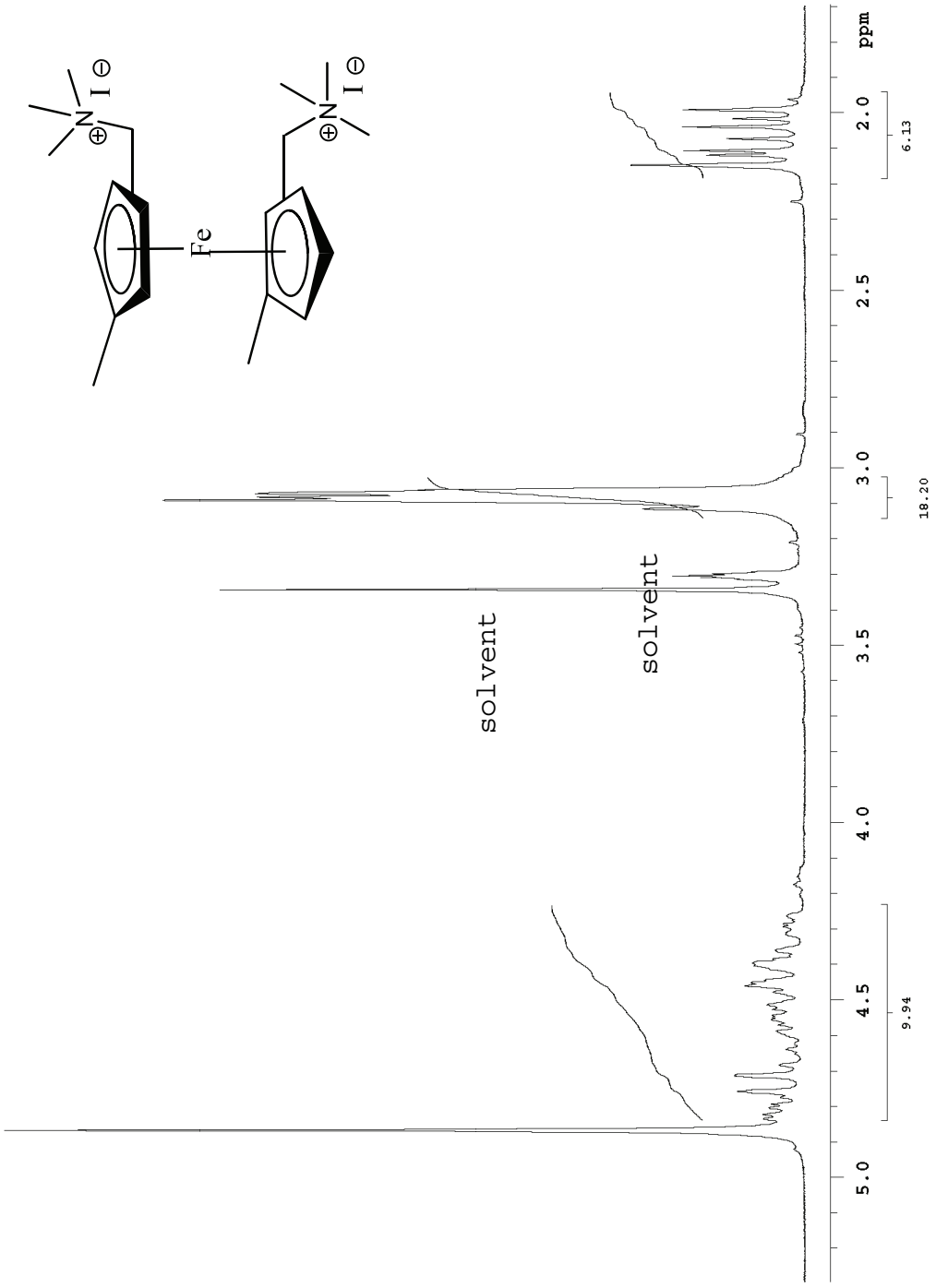


Figure A-18

$H^1$ NMR for compound **4**, a mixture of 1,l'-bis-(NN-dimethylaminomethyl)-2,2'-dimethylferrocene dimethiodide, 1,l'-bis-(NN-dimethylaminomethyl)-2,3'-dimethylferrocene dimethiodide, and 1,l'-bis-(NN-dimethylaminomethyl)-3,2'-dimethylferrocene dimethiodide

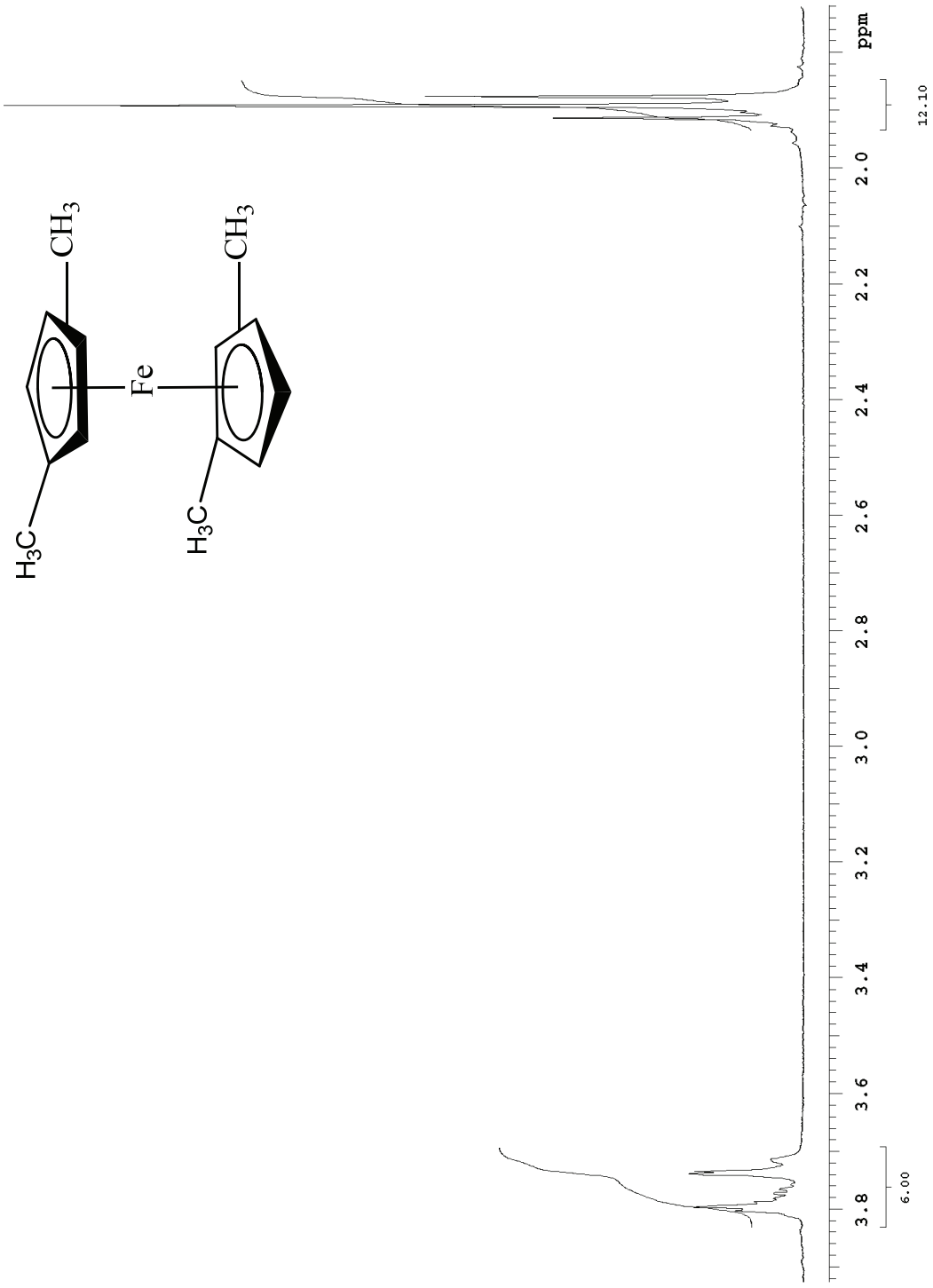


Figure A-19

$H^1$ NMR for compound **1a,** a mixture of 1,2,1',2'-tetramethylferrocene, 1,3,1'-2'-tetramethylferrocene, and 1,3,1',3'-tetramethylferrocene

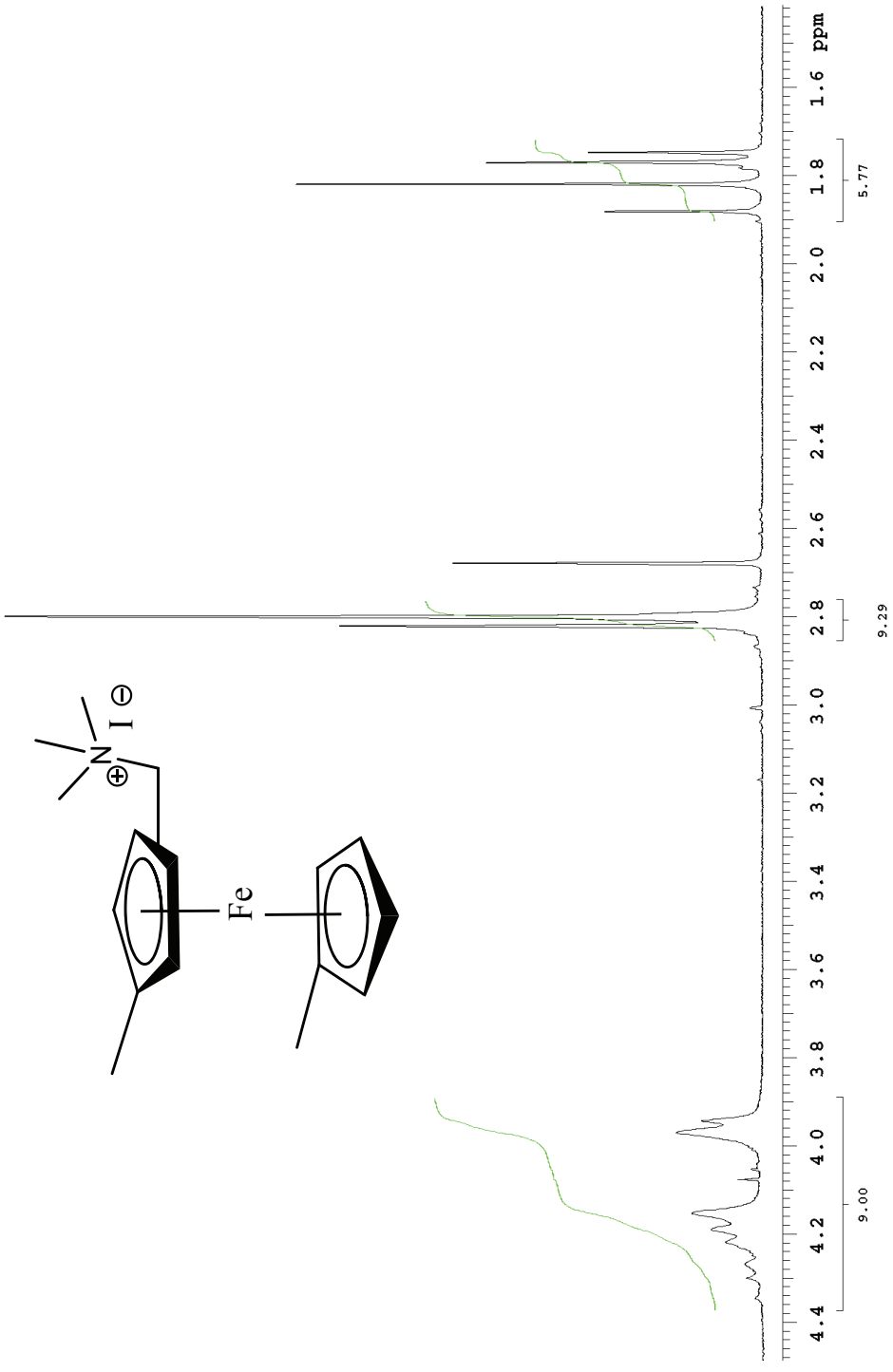


Figure A-20

$H^1$ NMR for compound **5**, a mixture of (2,1'-dimethyl-1-ferrocenylmethyl) trimethylammonium iodide and (3,1'-dimethyl-1-ferrocenylmethyl) trimethylammonium iodide

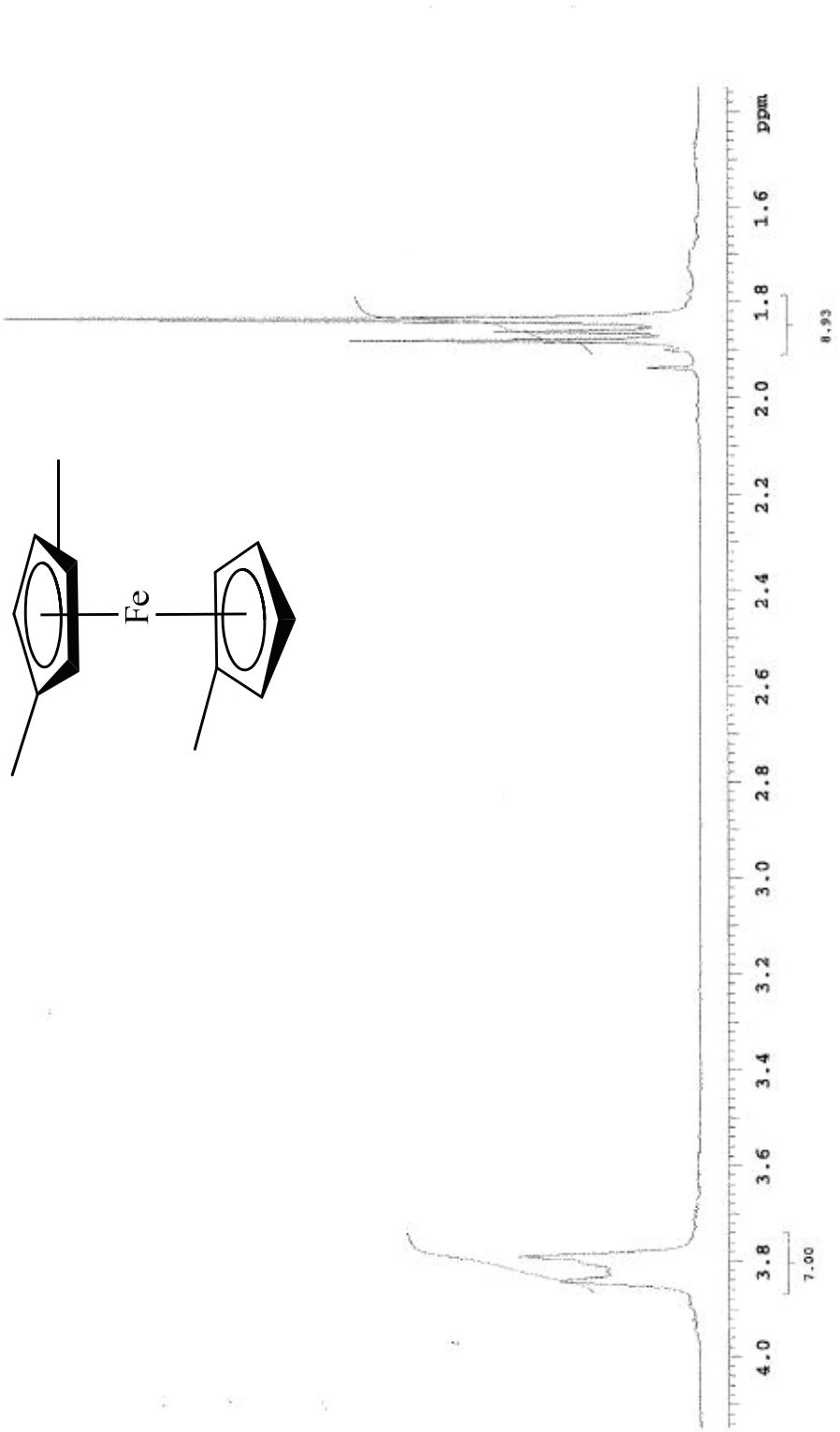


Figure A-21

$H^1$ NMR for compound **6**, a mixture of 1,2,1'-trimethylferrocene, 1,3,1'-trimethylferrocene

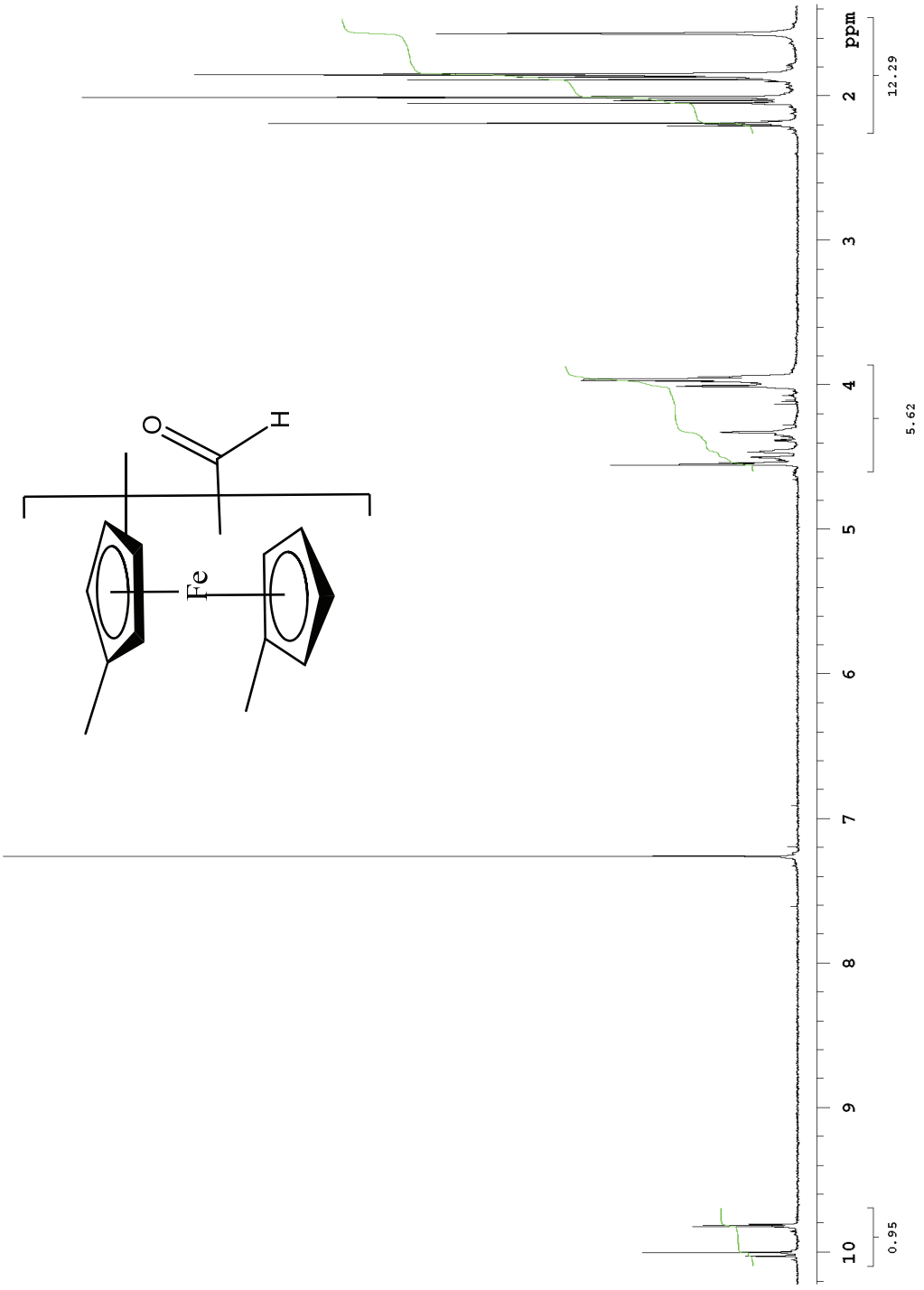


Figure A-22

$H^1$ NMR for compound **7**, a mixture of trimethylferrocenecarboxaldehyde isomers

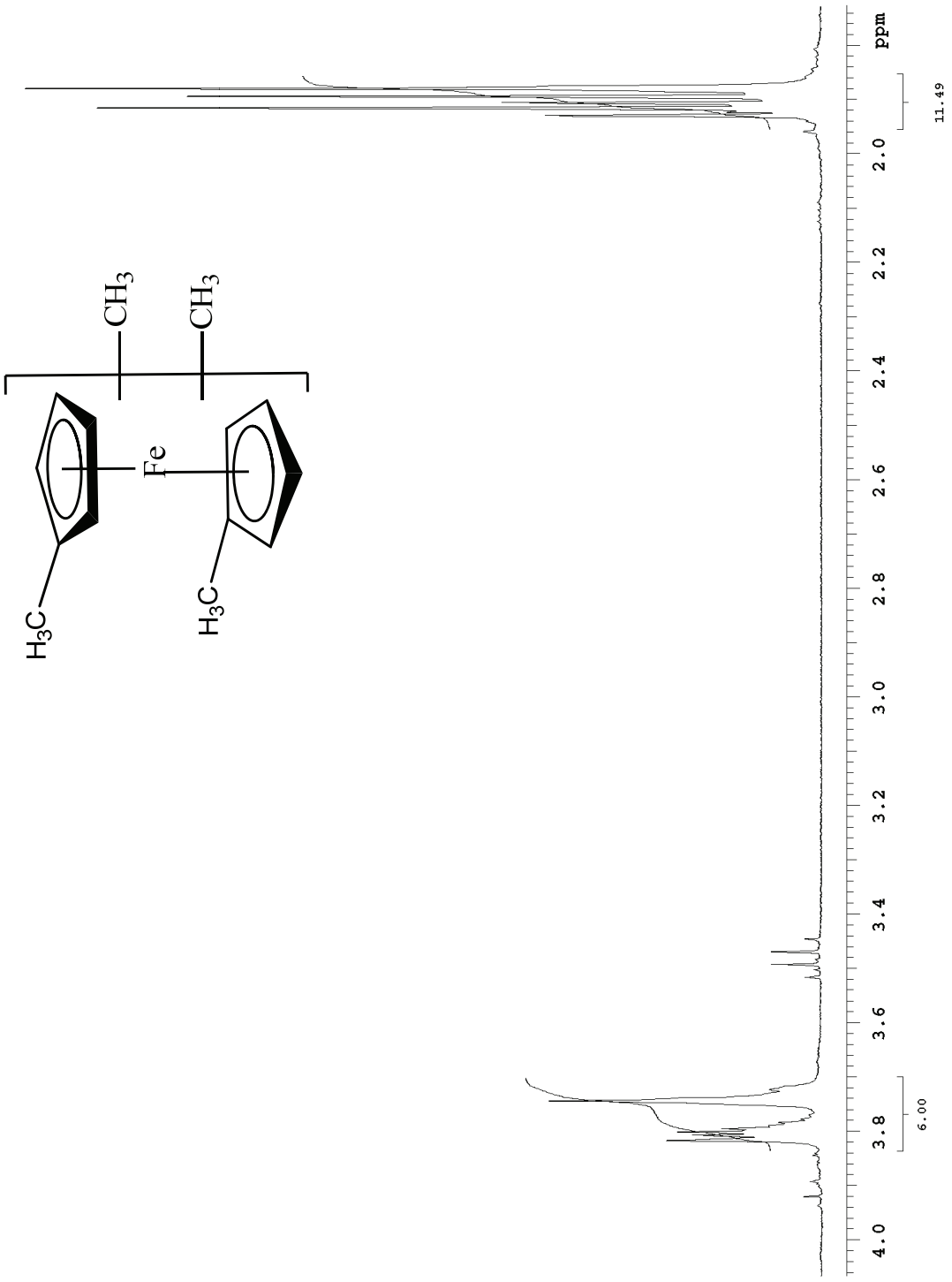


Figure A-23

$H^1$ NMR for compound **1b**, a mixture of tetramethylferrocene isomers synthesized from formylation/reduction of trimethylferrocene

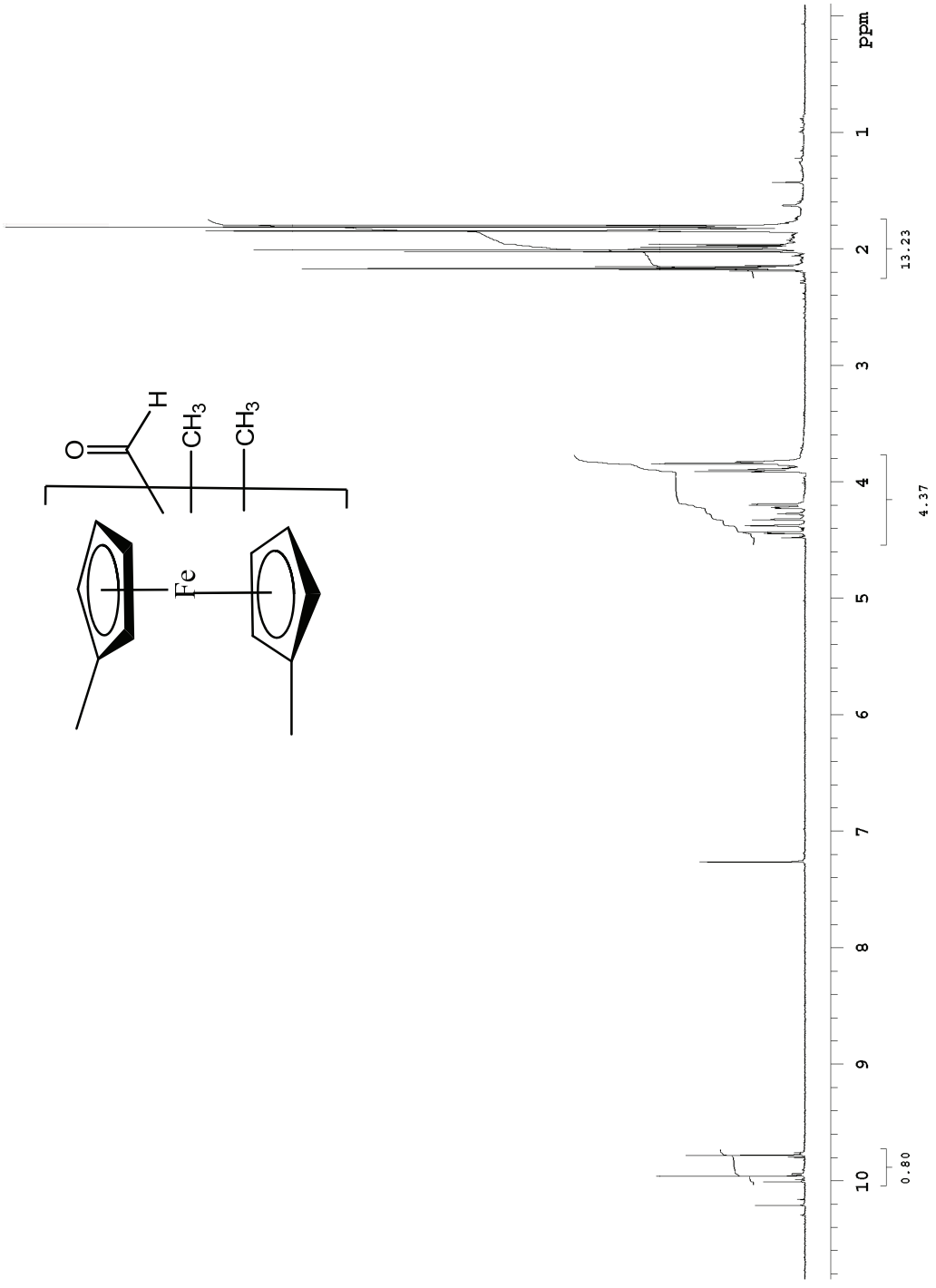


Figure A-24

$H^1$ NMR for compound **8**, a mixture of tetramethylferrocenecarboxaldhyde isomers

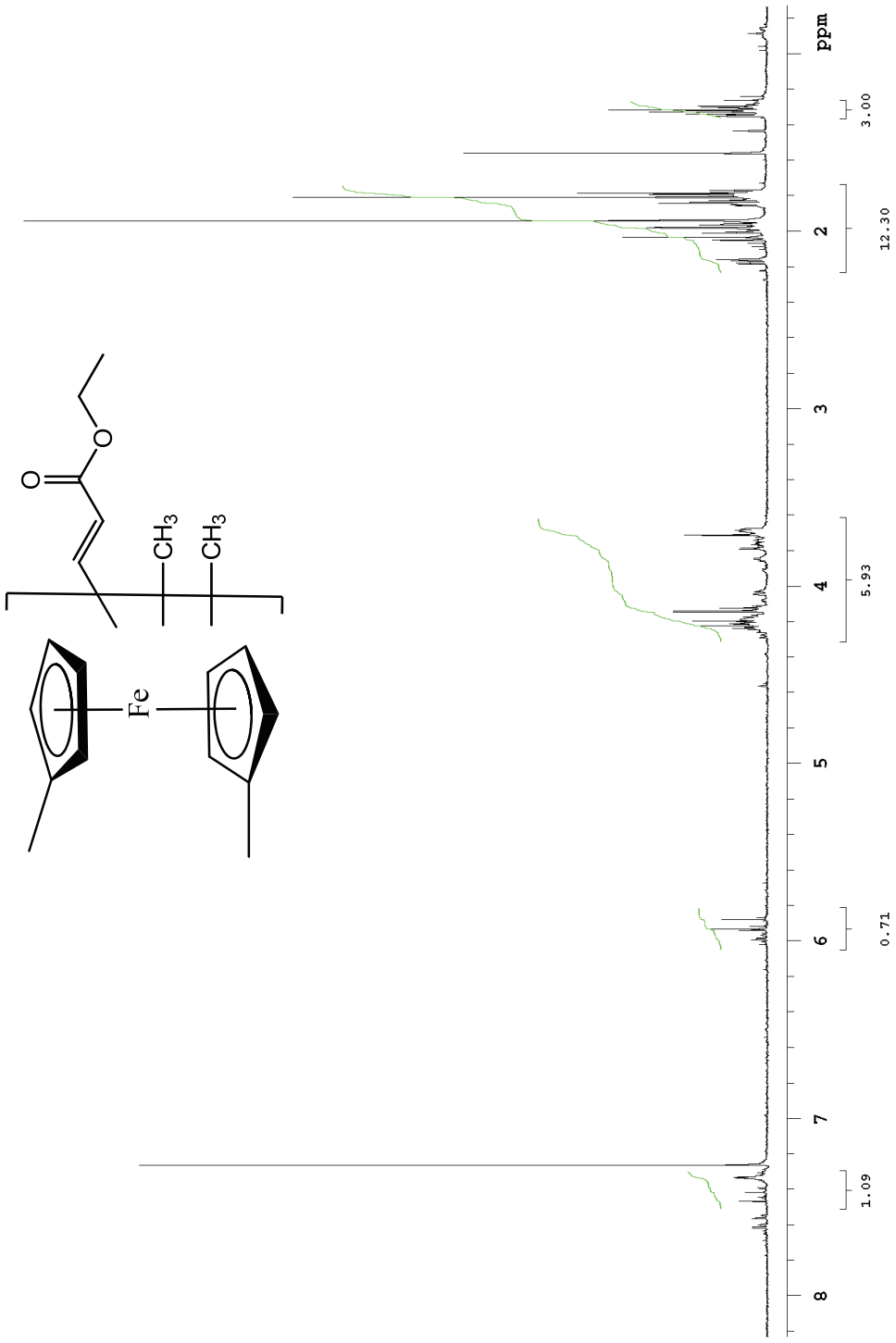


Figure A-25

$H^1$ NMR for compound **9**, a mixture of ethyl 3-tetramethylferrocenylpropenoate isomers

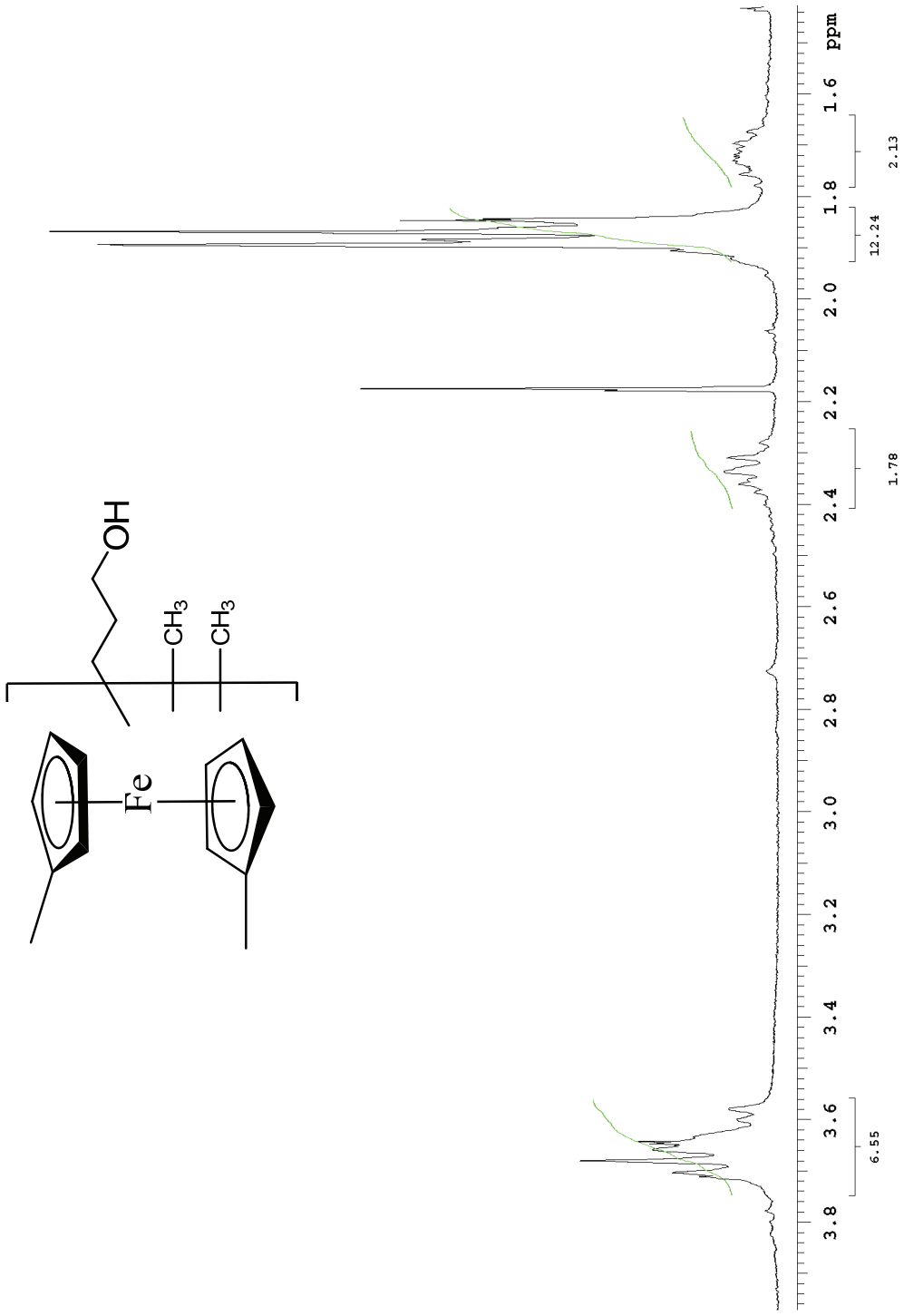


Figure A-26

$H^1$ NMR for compound **10**, a mixture of (3-hydroxypropyl)tetramethylferrocene isomers

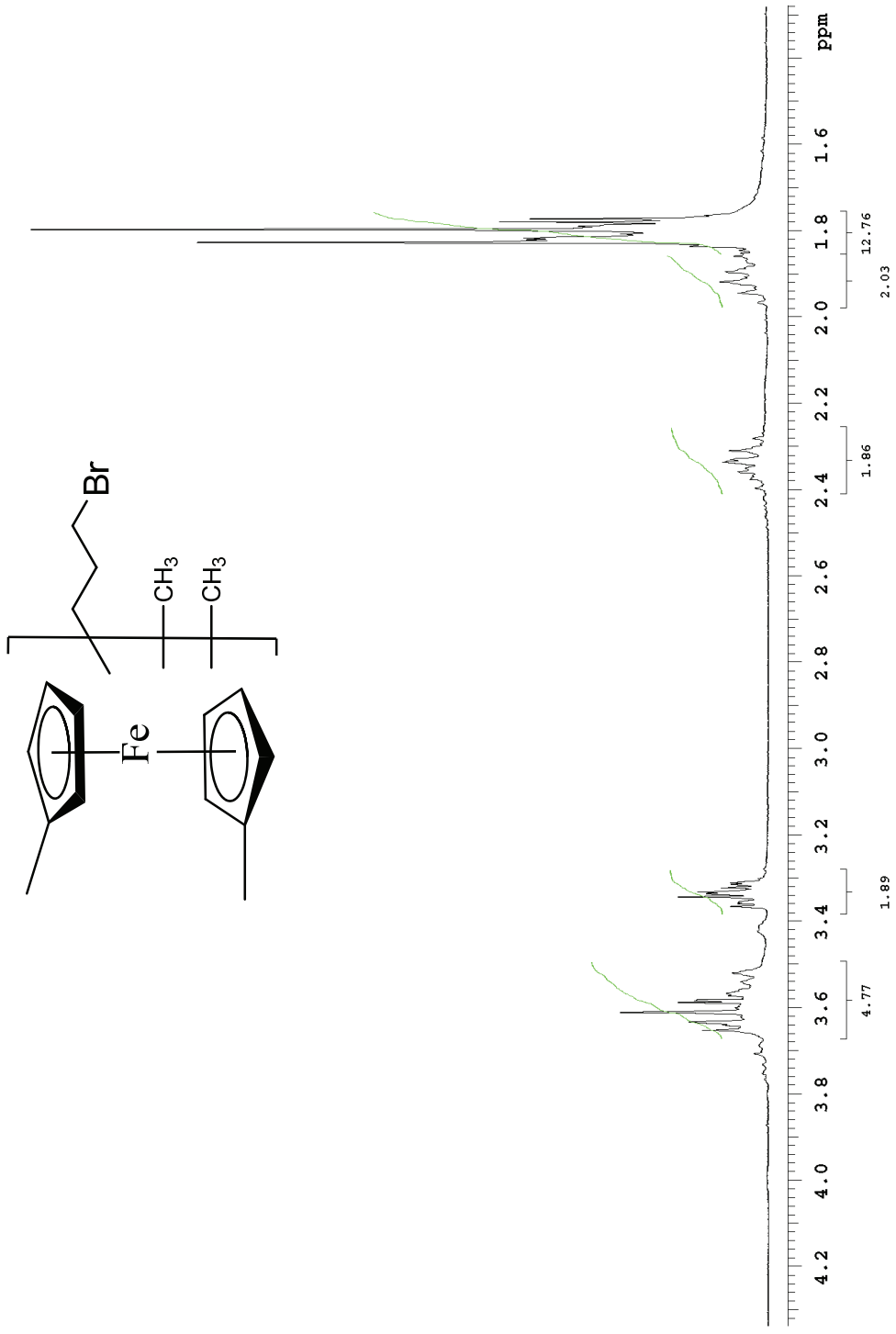


Figure A-27

$H^1$ NMR for compound **11**, a mixture of (3-bromopropyl)tetramethylferrocene isomers

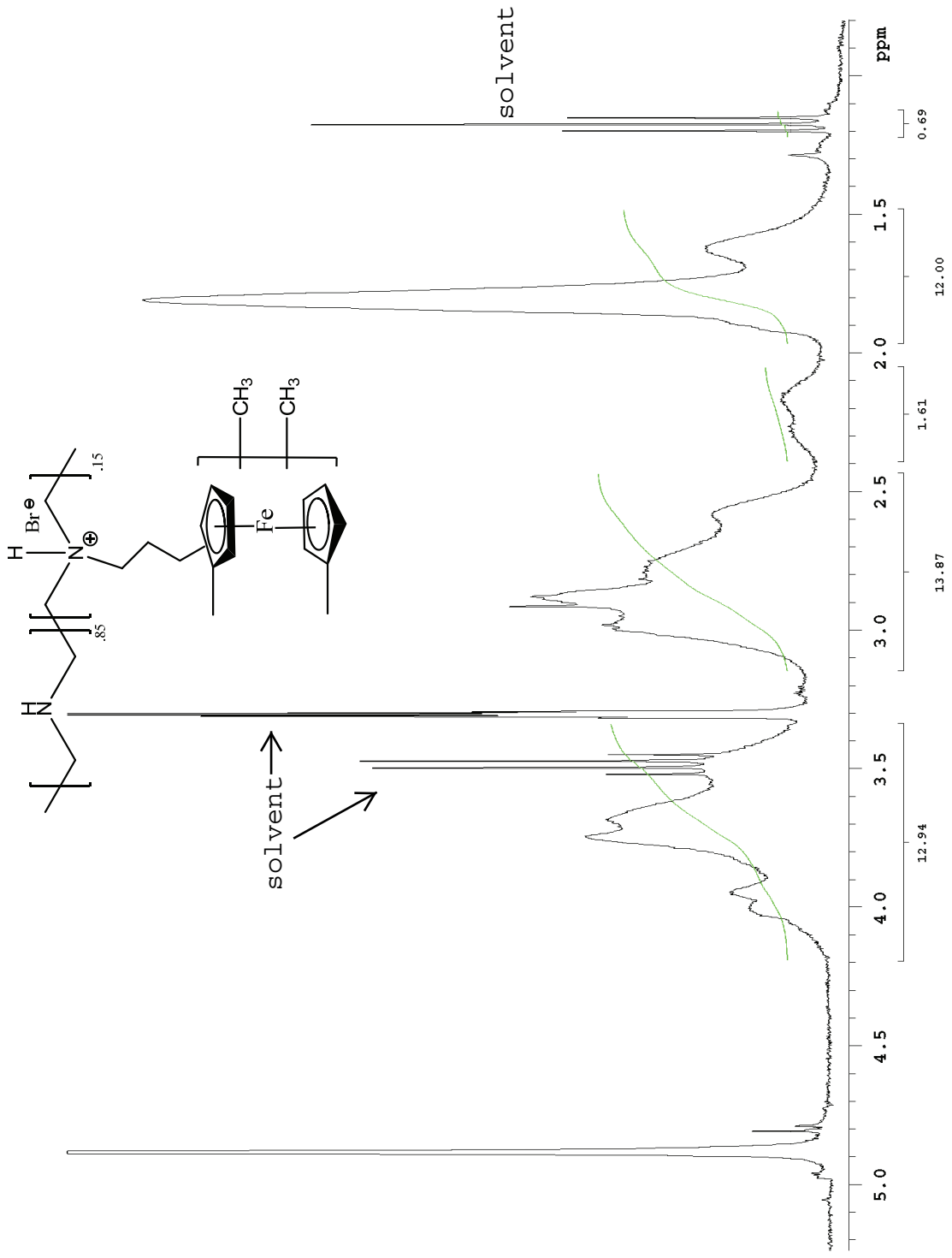


Figure A-28
$H^1$ NMR for $FcMe_4$-$C_3$-LPEI